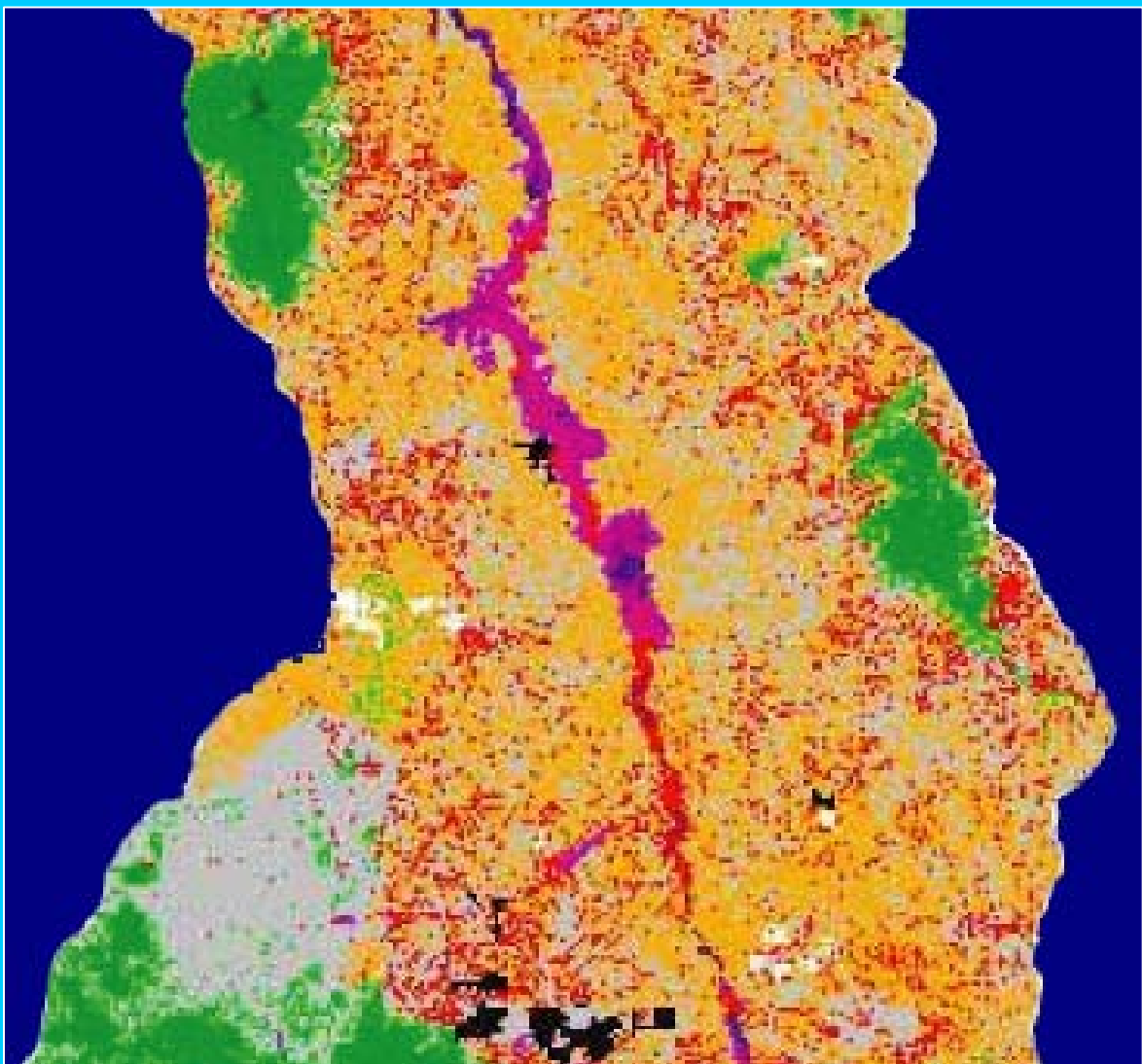


MODELING AND REMOTE SENSING APPLIED TO AGRICULTURE (U.S. AND MEXICO)



Clarence W. Richardson
Alma Delia Baez-Gonzalez
Mario Tiscareño-Lopez



Modeling and Remote Sensing Applied to Agriculture (U.S. and Mexico)

EDITORS

**Clarence W. Richardson
Alma Delia Baez-Gonzalez
Mario Tiscareño-Lopez**

Managing Editor: Maria Elvira Aranda Tabobo

Production Editor: Luis Reyes-Muro

Associate Production Editor: Jose Luis Ramos-Gonzalez

Technical Consultant: James R. Kiniry

COVER

We acknowledge the U.S Environmental Protection Agency, Office of Research and Development, Las Vegas, N.V., and the USDA Agricultural Research Service, Southwest Watershed Research Center, Tucson, AZ, for the San Pedro River 2000 baseline digital data used for the front cover. The image appears in Kepner, W.G., D.J. Semmens, S.D. Bassett, D.A. Mouat, and D.C. Goodrich. 2004. Scenario analysis for the San Pedro River, analyzing hydrological consequences of a future environment. *J. Environ. Monitoring and Assessment* 94:115-127 and in Chapter 9 of this book. Our thanks to M. Hernandez for providing the image file.

2006

USDA Agricultural Research Service
Grassland Soil and Water Research Laboratory
Temple, TX, USA
Instituto Nacional de Investigaciones Forestales, Agrícolas y Pecuarias
Laboratorio Nacional de Modelaje y Sensores Remotos
Aguascalientes, AGS, Mexico
Publishers

Printed in the United States of America

ISBN 1-59971-269-5

Print Run: 500

Parts of this book may be reproduced provided due acknowledgment is made.

FOREWORD

The United States and Mexico share a 3,326 km boundary. Four U.S. States (California, Arizona, New Mexico, and Texas) and six Mexican states (Baja California, Sonora, Chihuahua, Coahuila, Nuevo León, and Tamaulipas) are neighbors. There has long been a close relationship between the two countries. Trading between the countries increased when the North America Free Trade Agreement (NAFTA) was implemented in 1994. Exports from the U.S. to Mexico increased 15% annually, involving agricultural products such as corn, soybeans, wheat, vegetable oils, barley, rice, and meat. At the same time, exports from Mexico to the U.S. increased 12% annually, involving products such as coffee, tomatoes, melons, orange juice, onions, cucumbers, strawberries, grapes, and chilies. These increases in trade between the two countries were made possible, in part, by increases in agricultural production on both sides of the border. Research conducted by the Mexican National Research Institute for Forestry, Agriculture, and Livestock Production (INIFAP) and the U. S. Department of Agriculture, Agricultural Research Service (ARS) has had a major impact on these increases in productivity. Much of the research has been conducted cooperatively between the two research institutions.

In addition to a common border, Mexico and the U.S. share many common problems and challenges. Efficient crop production management and sustainable uses of our soil and water resources are two common areas of interest. INIFAP and ARS have conducted collaborative research in these areas for several years. In a relatively short time, great strides have been made in utilizing models and remote sensing techniques to predict crop yields and in developing farming systems that provide for more efficient crop management and utilization of natural resources.

A joint conference was held in 2003 in Aguascalientes, Mexico in which scientists from ARS, INIFAP and other organizations reported results of both independent and joint research in the area of the application of remote sensing and modeling to agriculture. Subsequently, these research findings have been utilized in developing operational systems for crop yield predictions and efficient crop management systems. This book is based on the 2003 conference and describes some of the research conducted by the two institutions that relate to utilizing crop and hydrologic models and remote sensing technology and to improving crop yield estimates and resource management. The twelve chapters contained herein document the scientific accomplishments of the two international research partners in bringing together remote sensing and modeling into a useful package for agriculture management and policy decisions. The book should be an excellent resource for scientists, students, and others interested in the application and further advancement of crop modeling and remote sensing.

I am pleased that scientists from INIFAP, ARS, and other institutions have collaborated to produce this book. The book serves as an excellent example of the

cooperative spirit and commitment to scientific excellence that exists on the part of scientists from ARS and INIFAP. The cooperative spirit exists not only in the technical areas described in this book, but also in many other research areas. We in ARS are indebted to INIFAP for their excellent collaboration that has led to numerous accomplishments that are important to both of our countries.

Edward B. Knippling
Administrator
USDA Agricultural Research Service

FOREWORD

During the past 10 years, cooperative and collaborative research in agriculture between Mexico and the United States of America has increased as a result of commercial trade agreements that include the trading of agricultural products. This development has been beneficial for both countries in economic and social terms, particularly in addressing food security issues.

However, the exchange of biological agents other than food or fiber commodities, such as seeds, plants, animals and microorganisms required for agricultural production, has its concomitant problems, foremost of which are undesired pests and disease outbreaks in crops and livestock. The increasing traffic of transportation vehicles makes it much more difficult to contain noxious insects that adversely affect the quality of agricultural products or the health of natural resources. These are some of the common problems that require the concerted efforts of the U.S. and Mexican governments.

Fortunately, an excellent inter-institutional relationship, one that mutually benefits Mexico and USA in the solution of agricultural problems, exists between the Agricultural Research Service of the United States Department of Agriculture (USDA-ARS) and the Mexican National Research Institute for Forestry, Agriculture, and Livestock Production (INIFAP). Collaborative scientific investigations aimed at improving food production have been implemented in several areas, such as conservation tillage, agricultural machinery design, best management practices to prevent pests and diseases, plant breeding, simulation modeling of plant growth and pest control, and remote sensing of cropland areas and natural resources.

This book offers ample evidence of the technological outcomes of INIFAP and ARS collaboration. The research studies presented herein are important to us in Mexico as they provide insights and know-how needed for implementing not only large-area, long-term crop monitoring and yield prediction programs but also precision agriculture, considering local soils, climate and land use. It is evident that within just a few years of ARS cooperation with INIFAP, there have been great strides in plant growth and climate modeling for estimating national production of maize, beans, wheat, sorghum, and other crops in Mexico.

This book presents the state-of-the-art in modeling agricultural processes and in applying remote sensing to agriculture. The twelve chapters contain useful material for scientists and students interested in the applications of modeling and remote sensing in a range of areas: climate and crop monitoring, yield prediction, irrigation scheduling, erosion and fire control, watershed management, land-use identification. The book provides comprehensive literature reviews on such topics as radar remote sensing and hydrologic modeling, and numerous governing equations of soil erosion and evapotranspiration models, the conservation of soil and water being an important issue. It addresses such challenges as monitoring crops in real time under climate uncertainty

and predicting yield at national scale to aid governmental decision-making. It also discusses at length a Decision Support System based on decision-making theory, which is useful for selecting management practices when farmers' opinions need to be considered in a trade-off process involving water quality against land productivity.

I am very pleased about this joint publication and grateful to the USDA-ARS and INIFAP scientists and their co-authors from other institutions for their contribution to this book. Their commitment to the important mission of improving agriculture is reflected in the time and effort they generously contributed to this book project. INIFAP is truly indebted to ARS for opening the doors of its laboratories to INIFAP researchers. This book showcases the fruits of that valuable INIFAP-ARS collaboration in agricultural research.

Pedro Brajcich Gallegos
Director General
INIFAP

PREFACE

The simulation of hydrologic and agricultural processes began over 30 years ago as independent endeavors. Early hydrologic process models focused on the distribution and movement of water across the earth's surface and through the soil mantel with little attention to plants, the primary user of water. The earliest agricultural process models simulated crop growth and yield with little attention to the dynamics of hydrologic processes and their influence on plant growth. Eventually, these two types of models came together, resulting in integrated systems capable of simulating hydrologic and crop growth processes in a continuum of soils, crops, and weather. Modern integrated systems can be used to make within-season management decisions and end-of-season yield estimates. In like manner, remote sensing technology has progressed over the last 30 years from simply identifying crops on specific areas to being capable of quantifying crop development. These two areas of technology, simulation models and remote sensing, can be used together to provide a powerful tool for managing crop production and estimating crop yield.

Scientists with the U. S. Department of Agriculture, Agricultural Research Service (USDA-ARS) and the Mexican National Research Institute for Forestry, Agriculture, and Livestock Production (INIFAP) conducted a joint project to evaluate the potential of using remote sensing and crop simulation models for agriculture management and crop yield predictions. This book describes some results of this collaborative effort involving ARS, INIFAP and other organizations.

The first two chapters of the book present models that have been used for crop monitoring and yield prediction. Chapter 1 describes a general plant model developed by the USDA-ARS in Texas, which has been validated for several crops in diverse sites in the U.S. and elsewhere. This field-scale model simulates the growth of a wide range of plant species and can be easily applied to agro/ecological models. This model is implemented in the Agricultural Land Management Alternatives with Numerical Assessment Criteria (ALMANAC) model. The second chapter presents the *Modelo de Simulación para Predicción de Cosechas* (MSPC) of INIFAP, which uses field and remotely sensed data for large-area crop growth monitoring and yield estimation in Mexico. The performance of the model in predicting maize yield in Sinaloa, Mexico is discussed. Related INIFAP-USDA studies are also outlined in Chapter 2.

The third and fourth chapters of the book focus on climate and its impact on agriculture. Chapter 3 presents a study that used a process-based biophysical simulation model to determine the effects of ENSO-related climatic changes on production of basic crops in Mexico. Chapter 4 introduces the reader to the Weekly Weather and Crop Bulletin published by the USDA World Agricultural Outlook Board (WAOB) and the

National Oceanic & Atmospheric Administration (NOAA), and explains the role that modeling and remote sensing play in crop weather assessments. Information is provided on the suite of agrometeorological data and analytical methods that WAOB meteorologists use in preparing assessments.

Chapter 5 discusses how advances in the spatial sciences and internet have led to the use of real-time data in the management of natural resources. Three research products are presented: a wildfire risk assessment index for Texas, a real-time crop monitoring system that was developed with Mexican data, and a runoff prediction map for the state of Texas.

The need for water use efficiency is addressed in Chapter 6 and other chapters of the book. Chapter 6 discusses evapotranspiration modeling for irrigation purposes and explains different methods of computing evapotranspiration.

Chapters 7 through 10 discuss modeling and remote sensing at the watershed scale. Chapter 7 provides a review of approaches for estimating surface soil moisture at the watershed scale, which include physically based approaches using SAR (synthetic aperture radar), with particular emphasis on the use of radar backscatter models. A synthesis is made of the most important research and development issues related to watershed management. Chapter 8 reviews the literature and gives a historical background of watershed models in the U.S. It then describes the Soil Water Assessment Tool (SWAT) model, its applications in the U.S., and Geographic Information System (GIS) interfaces for automation of model input development. The chapter also outlines available U.S. datasets and the requirements for the successful application of watershed models in Mexico. Chapter 9 discusses the Automated Geospatial Watershed Assessment (AGWA) tool and two case studies illustrating its application. The case studies deal with assessing the impact of land-use/cover change on water quantity and quality, and investigating the hydrologic impacts likely to result from a variety of forecasted population growth and development scenarios for a semi-arid basin on the U.S. - Mexico border. Chapter 10 presents a study conducted at Lake Patzcuaro Watershed in Mexico that evaluated runoff and sediment output at watershed scale and compared traditional tillage with conservation tillage.

The application of remote sensing in land use identification is discussed in Chapter 11. Two general approaches and several methods and techniques in using remote sensing imagery in land-use/cover classification are described. The chapter includes examples of land-use/cover classification in Mexico.

The last chapter discusses how research institutions in Mexico can use Decision Support Systems (DSS) to apply remote sensing and modeling to improve agriculture. It also provides some suggestions for lowering the cost of developing DSS.

The resources to conduct the research and publish this book were made available as a special allocation of funds by the leadership of both INIFAP and ARS. The work has proven to be very fruitful to both the U. S. and Mexico. We gratefully acknowledge the

foresight and support provided by the leaders of the two agencies. We also acknowledge the hard work and dedication of the scientists from ARS, INIFAP and other organizations who unselfishly worked together to conduct the research and write the chapters contained herein. The cooperation not only produced results of technical value but also lifelong friendships that span the border between the two countries. Lastly, we would like to thank the numerous support personnel from both ARS and INIFAP who worked tirelessly behind the scenes to make this book possible.

Clarence W. Richardson
USDA-ARS
Temple, TX, USA

Alma Delia Baez-Gonzalez
INIFAP
Aguascalientes, México

Mario Tiscareño-Lopez
INIFAP
Aguascalientes, México

THE EDITORS

Clarence W. Richardson is an agricultural engineer and laboratory director of the USDA-ARS Grassland Soil & Water Research Laboratory in Temple, Texas. He holds B.S. and M.S. degrees in Agricultural Engineering from Texas A&M University and a PhD degree in Civil Engineering from Colorado State University. He has made original research contributions to basic hydrologic relationships, agricultural water quality, erosion, and mathematical modeling of hydrologic processes. Richardson is internationally known for developing models for simulating daily weather variables. His weather simulation models have been used extensively in the U.S. and other countries. He has authored over 120 publications dealing with various aspects of agricultural hydrology. Richardson was elected Fellow in the American Society of Agricultural Engineers in 1997 and has received numerous awards for his research accomplishments.

Alma Delia Baez-Gonzalez is a modeling and systems analysis specialist and head of a national crop modeling project at INIFAP in Mexico. She holds B.S. (Livestock Production) and M.Sc. (Rangeland Management and Ecology) degrees from the Universidad de Chihuahua, Mexico, and a Ph.D. in Agricultural Systems from Reading University, England. She pursued postdoctoral studies in Wageningen, Holland, and had additional training at the USDA-ARS Grassland, Soil & Water Research Laboratory in Temple, Texas. Her major research contributions are in the areas of regional crop yield prediction using modeling with remote sensing, modeling of natural resources using GIS, modeling of livestock production systems, and establishment of sustainability indicators for family farm systems. Baez-Gonzalez has developed several crop models, including the SorModel and the Modelo de Simulacion para Prediccion de Cosechas (MSPC), which has been used for large-area maize yield prediction in Mexico. She has 46 publications and 7 patents. One of her awards, granted by Fundacion Mexicana para la Investigacion in 2002, is for outstanding, high-impact research. Baez-Gonzalez is a member of the Sistema Nacional de Investigadores and the Academia Mexicana de Ciencias.

Mario Tiscareño-López is a hydrologist and national leader of the Modeling and Remote Sensing Research Program of INIFAP in Mexico. He earned his B.S. in Agronomy at the University of Aguascalientes, Mexico, and his M.Sc. and Ph.D in Watershed Management at the University of Arizona, USA. His major research contributions are in the areas of soil erosion and hydrologic modeling, climate studies and modeling of El Niño Southern Oscillation phenomena, and plant growth simulation studies to estimate Mexico's crop grain production. Among his many accomplishments is the establishment of a national network of agroclimatic weather stations in Mexico. Tiscareno-Lopez has published over forty scientific papers related to the use of simulation models in Mexican agriculture.

CONTRIBUTORS

Jeffrey G. Arnold

Grassland, Soil, and Water Research Lab.
USDA-ARS
808 East Blackland Road
Temple, TX 76502
USA
jgarnold@spa.ars.usda.gov

Alma Delia Baez-Gonzalez

Laboratorio Nacional de Modelaje y
Sensores Remotos
INIFAP
Km. 32.5 Carr. Aguascalientes-Zacatecas
Ap. Postal #20 Pabellon de Arteaga
Aguascalientes 20660
Mexico
abaez@labpred.inifap.gob.mx

Ernesto A. Catalan Valencia

CENID RASPA
INIFAP
Km. 6.5 Margen Derecha
Canal de Sacramento
Gomez Palacio, Durango 35150
Mexico
catalan.ernesto@inifap.gob.mx

Gilberto Chavez-León

INIFAP
Av. Latinoamericana 1101
Uruapan, Michoacán 60080
Mexico
calg_mx@yahoo.com

Pei-Yu Chen

Blackland Research and Extension Center
720 E. Blackland Rd.
Temple, TX 76502
USA
pchen@brc.tamus.edu

Mauro DiLuzio

Texas Agricultural Experiment Station
808 East Blackland Road
Temple, TX 76502
USA
diluzio@brc.tamus.edu

J. German Flores-Garnica

Geomatica e Incendios Forestales
INIFAP
Parque Los Colomos S/N
Col. Providencia
Guadalajara, Jalisco 44660
Mexico
flores.german@inifap.gob.mx

David C. Goodrich

Southwest Watershed Research Center
USDA-ARS
2000 East Allen Rd.
Tucson, AZ 85719
USA
dgoodrich@tucson.ars.ag.gov

Philip Heilman

Southwest Watershed Research Center
USDA-ARS
2000 East Allen Rd.
Tucson, AZ 85719
USA
pheilman@tucson.ars.ag.gov

Mariano Hernandez

Southwest Watershed Research Center
USDA-ARS
2000 East Allen Rd.
Tucson, AZ 85719
USA
mhernandez@tucson.ars.ag.gov

Fabián Islas-Gutiérrez

INIFAP
Serapio Rendon 83, 3er Piso
Col. San Rafael
Mexico D.F. 06470
Mexico

Jennifer H. Jacobs

Spatial Sciences Laboratory
Texas A & M University
1500 Research Parkway Suite B223
College Station, TX 77845
USA
jhjacobs@tamu.edu

William G. Kepner

Office of Research and Development
National Exposure Research Laboratory
Landscape Ecology Branch
USEPA
944 E. Harmon Ave.
Las Vegas, NV 89119-6748
USA
kepner.william@epamail.epa.gov

James R. Kiniry

Grassland, Soil, and Water Research Lab.
USDA-ARS
808 East Blackland Road
Temple, TX 76502
USA
Jkiniry@spa.ars.usda.gov

Jaime Macias

Campo Experimental de Valle del Fuerte
INIFAP
Carr. Internal, Mexico-Nogales, Km. 609
Ejido San Jose Rios
Guasave, Sinaloa 81200
Mexico
macias.jaime@inifap.gob.mx

Hilario Macías Rodríguez

CENID RASPA
INIFAP
Km. 6.5 Margen Derecha
Canal de Sacramento
Gomez Palacio, Durango 35150
Mexico
macias.hilario@inifap.gob.mx

Juan R. Manjarrez

Campo Experimental de Culiacán
INIFAP
Culiacán, Sinaloa
Mexico
(Retired)

Roy S. Mann

West National Technical Center
USDA-NRCS
USA
(Retired)

Stephen McElroy

Southwest Watershed Research Center
USDA-ARS
2000 East Allen Rd.
Tucson, AZ 85719
USA

Jose L. Mendoza

Campo Experimental de Valle del Fuerte
INIFAP
Guasave, Sinaloa
Mexico
(Deceased)

Scott N. Miller

Rangeland Ecology and Watershed
Management
University of Wyoming, Department 3354
1000 E. University Ave.
Laramie, WY 82070
USA
snmiller@uwyo.edu

M. Susan Moran

Southwest Watershed Research Center
USDA-ARS
2000 East Allen Rd.
Tucson, AZ 85719
USA
smoran@tucson.ars.ag.gov

Balaji Narasimhan

Spatial Sciences Laboratory
Texas A & M University
1500 Research Parkway Suite B223
College Station, TX 77845
USA
balaji@tamu.edu

Christa D. Peters-Lidard

Hydrological Sciences Branch
NASA Goddard Space Flight Center
Greenbelt, MD 20771
USA
Christa.Peters@nasa.gov

Jose Luis Ramos-Gonzalez

Laboratorio Nacional de Modelaje y
Sensores Remotos
INIFAP
Km. 32.5 Carr. Aguascalientes-Zacatecas
Ap. Postal #20 Pabellon de Arteaga
Aguascalientes 20660
Mexico
ramos.jose@inifap.gob.mx

Luis Reyes-Muro

Laboratorio Nacional de Modelaje y
Sensores Remotos
INIFAP
Km. 32.5 Carr. Aguascalientes-Zacatecas
Ap. Postal #20 Pabellon de Arteaga
Aguascalientes 20660
Mexico
reyes.luis@inifap.gob.mx

Victor Rodríguez-Moreno

Laboratorio Nacional de Modelaje y
Sensores Remotos
INIFAP
Km 32.5 Carr. Aguascalientes-Zacatecas
Ap. Postal #20 Pabellon de Arteaga
Aguascalientes 20660
Mexico
rodriguez.victor@inifap.gob.mx

Ignacio Sanchez Cohen

CENID RASPA
INIFAP
Km. 6.5 Margen Derecha
Canal de Sacramento
Gomez Palacio, Durango 35150
Mexico
sanchez.ignacio@inifap.gob.mx

Darius J. Semmens

Office of Research and Development
National Exposure Research Laboratory
Landscape Ecology Branch
USEPA
944 E. Harmon Ave.
Las Vegas, NV 89119-6748
USA
semmens.darius@epamail.epa.gov

Harlan D. Shannon

World Agricultural Outlook Board
USDA
Room 4441 South Building
1400 Independence Ave. SW
Washington D.C. 20250-3812
U.S.A.
hshannon@oce.usda.gov

Raghavan Srinivasan

Spatial Sciences Laboratory
Texas A & M University
1500 Research Parkway Suite B223
College Station, TX 77845
USA
r-srinivasan@brc.tamus.edu

Jeffry Stone

Southwest Watershed Research Center
USDA-ARS
2000 East Allen Rd.
Tucson, AZ 85719
USA
jstone@tucson.ars.ag.gov

Luis Mario Tapia Vargas

INIFAP
Ave. Latinoamericana 1101
Uruapan, Michoacán 60080
Mexico
tapia.luismario@inifap.gob.mx

Mario Tiscareño-Lopez

Laboratorio Nacional de Modelaje y
Sensores Remotos
INIFAP
Km 32.5 Carr. Aguascalientes-Zacatecas
Apt. Postal #20 Pabellon de Arteaga
Aguascalientes 20660
Mexico
tiscareno.mario@inifap.gob.mx

Ignacio Vidales Fernandez

INIFAP
Av. Latinoamericana 1101
Uruapan, Michoacán 60080
Mexico
vidales.ignacio@inifap.gob.mx

Magdalena Villa Castorena

CENID RASPA
INIFAP
Km. 6.5 Margen Derecha
Canal de Sacramento
Gomez Palacio, Durango 35150
Mexico
villa.magdalena@inifap.gob.mx

Joseph M. Watts

US Army Engineer Research and
Development Center
Topographic Engineering Center
701 Telegraph Rd
Alexandria, VA 22315
USA

CONTENTS

Chapter 1	A General Crop Model	1
James R. Kiniry		
Chapter 2	Combining Modeling and Remote Sensing for Crop Yield Prediction in Mexico	13
Alma Delia Baez-Gonzalez, Mario Tiscareno-Lopez, Victor Rodriguez-Moreno, Jaime Macias, Jose L. Mendoza, and Juan R. Manjarrez		
Chapter 3	Crop Yield Assessment under Climate Uncertainty	29
Mario Tiscareño-Lopez, Alma Delia Baez-Gonzalez, and Jose Luis Ramos-Gonzalez		
Chapter 4	The Weekly Weather and Crop Bulletin: Integrating Agricultural and Meteorological Data for Decision Makers	45
Harlan D. Shannon		
Chapter 5	Real-Time Modeling of Natural Resources Using the Spatial Sciences	51
Balaji Narasimhan, Pei-Yu Chen, Jennifer H. Jacobs, and Raghavan Srinivasan		
Chapter 6	Evapotranspiration Modeling for Irrigation Purposes	71
Ignacio Sanchez Cohen, Ernesto A. Catalan Valencia, and Magdalena Villa Castorena		
Chapter 7	Radar Remote Sensing for Estimation of Surface Soil Moisture at the Watershed Scale	91
M. Susan Moran, Stephen McElroy, Joseph M. Watts, and Christa D. Peters-Lidard		
Chapter 8	Watershed Modeling and GIS Applications in the U.S. Using SWAT and Potential Use in Mexico	107
Jeffrey G. Arnold and Mauro DiLuzio		
Chapter 9	Development and Application of the Automated Geospatial Watershed Assessment Tool	127
Mariano Hernandez, Darius J. Semmens, Scott N. Miller, David C. Goodrich, and William G. Kepner		

Chapter 10	Modeling Runoff and Erosion in the Lake of Patzcuaro Watershed, Michoacan, Mexico	159
	Luis Mario Tapia Vargas, Mario Tiscareño-Lopez, Gilberto Chavez-Leon, Ignacio Vidales Fernandez, and Luis Reyes-Muro	
Chapter 11	Alternative Approaches for Land Use Identification Systems Using Remote Sensing	189
	J. German Flores-Garnica and Fabian Islas-Gutierrez	
Chapter 12	Working Smarter: Research and Decision Support Systems in Mexican Agriculture	211
	Philip Heilman, Jeffry Stone, Ignacio Sanchez Cohen, Hilario Macias Rodriguez, and Roy S. Mann	
Index		237

CHAPTER 1

A General Crop Model

James R. Kiniry

CONTENTS

Introduction	1
Background on Crop Modeling	1
Background on the ALMANAC Crop Model	2
Details of the ALMANAC Crop Model	3
Crop Parameters for the ALMANAC Crop Model	5
Deriving New Crop Parameters or Testing Old Ones.	7
Yield Components: Beyond HI	8
Conclusions	10
References	10

INTRODUCTION

Agricultural and ecosystem simulation models valuable for technology transfer require a realistic, process-oriented plant model that can be easily applied to different crops, grasses, and woody species. User-oriented models help agricultural producers, crop consultants, and policy makers make intelligent decisions based on current scientific knowledge and readily available soils and weather data. Such models integrate information from a wide range of sources into easily applied decision aids. The objective of this chapter was to describe a general plant model that can be easily applied in agro/ecological simulation models.

BACKGROUND ON CROP MODELING

Crops such as maize (*Zea mays* L.) and sorghum [*Sorghum bicolor* (L.) Moench] are grown in a wide range of soils and climatic conditions and can be vulnerable to late-spring freezes, drought, and high temperatures during the growing season. Producers make decisions on planting date,

maturity type, planting rate, and fertilizer rates, attempting to maximize profit and minimize risks associated with unpredictable weather conditions. With delays in planting due to wet spring conditions and with replanting following stand loss, producers must choose between replanting different maturity crops or even shorter duration alternative crops. Crop consultants advising producers on such decisions can use crop models as tools to optimize such management practices and minimize risk. With multiyear weather scenarios, a robust crop model can provide a quantitative means to predict crop yields under different environmental and climatic conditions. Consultants, using accurate soil information and updated weather data, can provide producers with realistic predictions on the outcome of various management alternatives. Likewise, crop advisory information can be linked to soil type and measurements of soil layer depths in individual fields.

Crop models capable of accurately simulating long-term mean crop yields for diverse environments and capable of simulating annual crop yields in extreme climatic conditions would be valuable for risk assessment and management evaluation. Such models can greatly increase confidence in crop modeling.

Canopy-level, single-field models share some common applications with single-plant models, but tend to use more conservative and more general approaches to simulating plants. Leaf growth can be simulated as leaf area index (LAI), and yield can be simulated as harvest index (HI). While not able to describe some of the detailed differences among cultivars of a crop, such models can be readily applied to several crops by deriving realistic crop parameters. For such a model, within-crop species differences that can be simulated include maturity type, leaf angle through the light extinction coefficient, and potential and lower limit of HI. Single-field models can simulate the impact of management systems (crop rotations, tillage, irrigation, manure and fertilizer management, and drainage) on edge-of-field sediments and pollutant loadings.

In this chapter, I describe a general plant model developed by USDA-ARS at Temple, TX, that is implemented in the ALMANAC (Agricultural Land Management Alternatives with Numerical Assessment Criteria) (Kiniry et al., 1992a) model. This field-scale model simulates a wide range of plant species and simulates competition among species. This plant model, in somewhat different forms, is in some other models, including EPIC (erosion/productivity impact calculator) (Williams et al., 1990), SWAT (Soil and Water Assessment Tool) (Arnold et al., 1998), and HUMUS (Hydrologic Unit Model for the United States) (Srinivasan, et al., 1993). The form in ALMANAC is unique in its ability to accurately simulate competition for light, nutrients, and water for several plant species.

BACKGROUND ON THE ALMANAC CROP MODEL

The ALMANAC model simulates the water balance, the nutrient balance, and the interception of solar radiation for one or more plant species. The model includes subroutines and functions from the EPIC model (Williams et al., 1984) and has additional details for plant growth. The model has a daily time step. It can simulate weed impacts on crop yields and intercropping in a reasonable and easily implemented way.

The model has been extensively validated for row crops in a wide range of locations, drought conditions, and plant species. ALMANAC accurately simulated crop yields at sites within Texas (Kiniry and Bockholt, 1998) and in nine states in the U.S. with diverse soils and climate (Kiniry et al., 1997). It accurately simulated spring wheat (*Triticum aestivum* L.) yields with different densities of competing oats (*Avena sativa* L.), oilseed rape (*Brassica napus* L.), and vetch (*Vicia*

sativa L.) in France (Debaeke et al., 1997). ALMANAC realistically simulated grain yields when applied to maize at eleven sites and sorghum at eight sites in Texas for the dry conditions of 1998 (Yun et al., 2001). In that study, the model demonstrated ability to simulate site-to-site differences in grain yields under dry climate conditions, showing it can be valuable for risk assessment of grain production. ALMANAC realistically simulates grasses, both in monoculture and with multiple species growing together. Kiniry et al. (1996) successfully simulated Alamo switchgrass (*Panicum virgatum* L.) at several sites in Texas. In addition, ALMANAC realistically simulated range yields for 20 sites representing the extremes of productivity for Texas (Kiniry et al., 2001a). Recent sensitivity analysis has shown the relative importance of some of ALMANAC's main input variables (Yun et al., 2003).

DETAILS OF THE ALMANAC CROP MODEL

ALMANAC relies on readily available daily weather data and on the extensive USDA-NRCS soils data. Commonly reported values of daily maximum and minimum temperatures, rainfall, and solar radiation are needed. This enables users to apply the models throughout the U.S. and the world by using data from the nearest weather station. In cases where weather data or portions of weather data are not available, realistic values can be generated, usually within the models themselves.

The model uses a daily time step, enabling rapid execution of multiple year runs. It does not have iterative processes such as curve fitting or solving differential equations which can slow down execution. Users can make runs with several years of weather in a few seconds, enabling them to efficiently simulate an extensive range of management, crop, and soil scenarios.

The ALMANAC model simulates processes of crop growth and soil water balance including light interception by leaves, dry matter production, and partitioning of biomass into grain. The model simulates grain yield based on HI, which is grain dry weight as a fraction of total aboveground dry matter at maturity. The HI can be reduced if drought stress occurs near anthesis (from 45 to 60% of the summed degree days to physical maturity). ALMANAC simulates leaf area index (LAI), light interception with Beer's law, and potential daily biomass increase with a species-specific value of radiation use efficiency (RUE). The daily increases in LAI and biomass are reduced when plant available water in the current rooting depth is insufficient to meet potential evapotranspiration. Plant development is temperature driven, with duration of growth stages dependent on degree days. Each plant species has a defined base temperature and optimum temperature. Parameters for describing plant processes are easily derived for a plant species or cultivar.

ALMANAC includes a generic LAI function. The maximum LAI of a crop species at high planting density is a parameter. This potential LAI is reduced as a function of planting density. The development of LAI as a function of fraction of seasonal degree day sum follows an "s" curve, with two input parameters defining the curve. Daily increments of LAI growth can be reduced by water stress. At a defined fraction of the seasonal degree days, grain growth is assumed to begin.

ALMANAC simulates light interception by leaf canopies, using Beer's law (Monsi and Saeki, 1953), and the LAI of the total canopy. For a crop, the fraction of daily incoming solar radiation

intercepted by the leaf canopy is:

$$\text{Fraction} = 1.0 - \exp(-k \times \text{LAI}) \quad [1]$$

where variable k is a species' extinction coefficient (positive value).

ALMANAC can divide intercepted light between competing plant species using the system of Spitters and Aerts (1983). The total interception is calculated with the LAI of each species, weighted by their light extinction coefficients (k). The greater the value of k for a species, the more light that species will intercept at a given LAI value and the more effectively that species will compete for light.

Accurate simulation of light interception depends on realistic values of leaf area for both plant species. This requires that the leaf area be sensitive to population density. Three variables are used in ALMANAC to simulate the potential LAI of each species at different population densities. The first is the potential LAI at high densities. The other two variables are data points used to fit an s-curve function for a zero-to-one factor which reduces potential LAI at different population densities (Fig. 1-1). The same general s-curve function simulates leaf area production as discussed below.

The model generates an s-curve that is forced through the origin and the two points, asymptotically approaching $y = 1.0$. The s-curve function takes the form:

$$F = X / [X + \exp(Y_1 - Y_2 \times X)] \quad [2]$$

where F is the factor for reducing potential LAI, X is the population density, and Y1 and Y2 are the s-curve coefficients generated by ALMANAC.

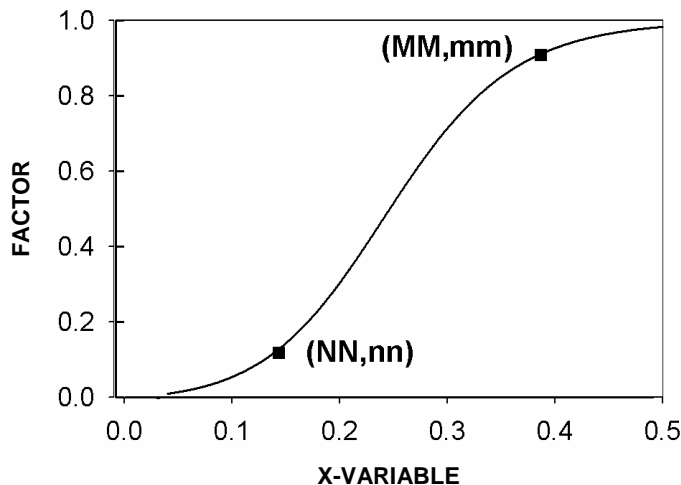


Fig. 1-1. General function for a zero-to-one factor as a function of a variable using an "s" curve. For the factor reducing potential maximum leaf area index (LAI) in the season, the x-variable is the plant population density. For the factor describing potential leaf area each day, the x-variable is fraction of heat units (PHU) which have accumulated between planting and maturity.

Simulation of light competition also requires an accurate description of leaf area production and decline. The model estimates leaf area production, up to the point of maximum leaf area for the growing season, by using a function similar to Eq. [2]. In this case, two data points define an s-curve in which both the X and Y variables are on a zero-to-one scale. For each simulation day, the fraction of total heat units (PHU) that have accumulated is determined, denoted as SYP. The value for PHU is zero at planting and maximum at maturity. The s-curve simulates how LAI can increase, under nonstress conditions, as a function of SYP.

CROP PARAMETERS FOR THE ALMANAC CROP MODEL

Values for radiation-use efficiency (RUE) have been derived for sorghum and maize (Stockle and Kiniry, 1990), soybean (*Glycine max* L. Merr.) (Williams et al., 1989), and wheat and rice (*Oryza sativa* L.) (Kiniry et al., 1989; Kiniry et al., 2001b).

Vapor pressure deficit (VPD) directly affects simulated RUE for biomass growth and potential evapotranspiration. The functions of evapotranspiration are the same for all plant species (Williams et al., 1984). The response function for RUE is based on the work of Stockle and Kiniry (1990), Manrique et al. (1991), and Kiniry et al. (1992b). Values of RUE are constant for a species at a VPD less than the threshold VPD. When VPD exceeds the threshold, RUE decreases linearly with increasing VPD. This form is easily implemented, with a typical value for the threshold 1.0 kPa and typical values for the slope -6.5 to -8.5 units of RUE per kPa increase in VPD for C_4 species (Stockle and Kiniry, 1990), -14.8 for potato (*Solanum tuberosum* L.) (Manrique et al., 1991), and -32.3 for sunflower (*Helianthus annus* L.) (Kiniry et al., 1992b). In ALMANAC, VPD does not affect RUE of rice or wheat.

The sensitivity of RUE to VPD has been supported by recent results of Bunce (2003) for rate of assimilation of CO_2 . For field-grown sorghum, Bunce's assimilation rate and Stockle and Kiniry's RUE showed nearly identical relative responses to VPD. Thus, the whole plant responsiveness as exhibited by RUE was supported by the leaf-level gas exchange responses.

The water balance consists of transpiration calculations, with a crop using the water it needs if sufficient water is present in its current rooting zone. The nutrient balance (N and P) also allows for a crop to acquire sufficient nutrients to meet the demands if adequate quantities are available in its current rooting zone. For a crop, four values are used to define the optimum N concentration and four to define optimum P concentration. The first three are the optimum concentrations of the whole plant at seedling emergence, at midseason (near anthesis), and at maturity. The fourth value is the optimum concentration in the grain at maturity. For each day, based on growth stage, the potential uptake of N and P is calculated. If insufficient nutrient quantities are available in the soil to satisfy this demand, plant growth is reduced.

The base temperature is important in a crop model because the emergence date and rate of development early in the season are critical for simulating how early season climate affects leaf area development. While seedling emergence is not directly simulated, base temperature is assumed to be the same for all growth stages of a crop. Base temperature constrains the initiation of leaf area growth and thus dry matter accumulation. Higher optimum temperature can delay leaf area development until later in the season when temperatures are greater. The sum of degree days from sowing to maturity (PHU) controls duration of crop growth and how late season stresses affect grain yield.

Base temperatures for most crops range from 0 to 11 °C, and optimum temperatures are usually 15 to 25 °C. For most warm-season crops, base temperature ranges from 8 to 11 °C. Base temperature for winter and spring wheat is 0 °C (Kiniry et al., 1991). We use 8 °C for maize (Kiniry and Bonhomme, 1991) and 10 °C for soybean (Kiniry et al., 1991). For many warm-season crops, optimum temperature is 25 °C, whereas optimum temperature for cool-season crops such as wheat is 15 °C.

The sums of degree days from sowing to maturity for the various species are determined by making model runs and estimating dates of maturity based on reported dates of leaf senescence or of cessation of seed growth.

The potential LAI in ALMANAC at high plant populations in the absence of competition with other species is 6.0 for maize, 7.0 for soybean, 5.0 for grain sorghum and wheat, and 4.3 for sunflower. Reasonable values for LAI of these crops at two common population densities are then used to estimate the potential LAI at any density. Potential LAI of maize in ALMANAC is 47% of potential at 4 plants m⁻² and 77% at 7 plants m⁻². Potential LAI of grain sorghum is assumed to be 43% at 5 plants m⁻² and 79% at 15 plants m⁻². Likewise, for wheat, potential LAI is 60% at 125 plants m⁻² and 95% at 250 plants m⁻².

The competitiveness and productivity of plants late in the season are dependent on the rate of decline in leaf area (RLAD), rate of decline in biomass production (RBMD), and the elapsed portion of the growing season when these declines begin (XDLAI) (Fig. 1-2). Maize and soybean are simulated with slow rates of both decline in leaf area and decrease in RUE. Thus, values for RLAD and RBMD are assumed to be 0.1. Leaf photosynthesis of both of these species has been reported to remain high late in the grainfilling period. By the dent stage of maize (about 80% of the time from silking to maturity), the photosynthetic rate is 87% of the value at blister (about 20% of the time from silking to maturity) (Vietor et al., 1977). The CO₂ uptake rate of soybeans reportedly decreases linearly during the last 20% of the season (Boon-Long et al., 1983).

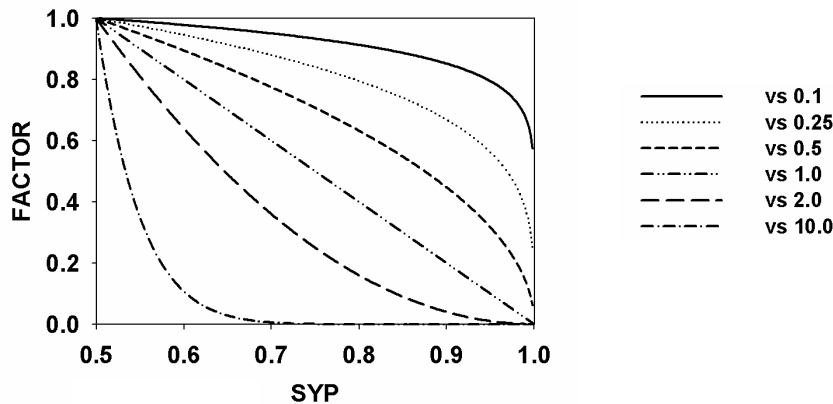


Fig. 1-2. Factor for reducing radiation-use efficiency (RUE) or leaf area index (LAI) late in the season. Variable SYP is the fraction of the season from sowing to maturity. Variable XDLAI (in this case equal to 0.5) is the fraction of the season when RUE and LAI begin to decline. Lines represent declines due to input parameter values varying from 0.1 to 10.0

Loss of leaf area late in the season is described with the LAI decline factor (RLAD). This occurs after the input fraction (XDLAI) of PHU has accumulated. Three equations describe how LAI declines late in the season:

$$XX = \log_{10} [(1.001 - SYP)/(1.0 - XDLAI)] \quad [3]$$

$$RTO = RLAD \times XX \quad [4]$$

where RTO is constrained to be greater than or equal to -10.0, and:

$$LAI_t = \text{Minimum of } (LAI_{t-1} \text{ and } LAIO \times 10^{RTO}) \quad [5]$$

where t is the current day, $t - 1$ is the previous day, and LAIO is the LAI on the day before leaf area begins to decrease. Thus, as SYP goes from XDLAI to 1.0, XX goes from approximately 1.0 to almost zero. The value of RLAD determines the shape of this leaf area decline function. The maximum rooting depth defines the potential depth in the absence of a root-restricting soil layer. Both sorghum (Davis et al., 1967) and maize (Kiesselbach, 1949) have rooting depths of almost 2 m by maturity. Soybean roots are not as deep, with the depth about 80% of that for cocklebur (Monks et al., 1988). Maximum rooting depths for soybeans ranged from 1.6 m to 1.9 m in an Iowa field in August (Kaspar et al., 1984). The value for soybean, based on the field measurements in Iowa, are assumed to be 1.7 m. Further applications of the model, especially in moisture-limited conditions, may require more accurate values for this depth.

Harvest index is the dry weight of the seed divided by the dry weight of the total above-ground plant at maturity. Harvest index can be reduced when stress occurs near anthesis. Values for the crops are often reported in the literature and are easily derived with field experiment.

As previously discussed, light interception by the leaf canopy is based on the LAI at the given plant spacings and the k of the plant species. Values for maize, sorghum, soybean, and sunflower at different row spacings were derived by Flenet et al. (1996). Values have recently been reported for rice (Kiniry et al., 2001b) and for several warm-season grasses by Kiniry et al. (1999).

The equation for k is a linear function of row spacing for maize and sorghum (Flenet et al., 1996):

$$k = 0.685 - 0.209 \times \text{ROWS}, \quad [6]$$

where ROWS is the row spacing for maize and sorghum in meters.

DERIVING NEW CROP PARAMETERS OR TESTING OLD ONES

When measuring fraction of light interception, we measure photosynthetically active radiation (PAR) interception during the season with a 0.8-m-long Sunfleck Ceptometer (Decagon, Pullman, WA 99163). In each replication, we take three series of measurements in rapid succession. Likewise, we express RUE in units of g of biomass per MJ of intercepted PAR. Consistency in using PAR for light interception measurement, k calculation, and RUE calculation is vital. As discussed by Kiniry (1999), incident total solar radiation is easily converted to PAR above the plant canopy by multiplying by a factor of 0.45 (Monteith, 1965; Meek et al., 1984). Recently, Lizaso et al. (2003) reported a similar conversion factor of 0.43 in Iowa. PAR is the definitive

band of wavelengths pertinent to photosynthetic responses inherent in the RUE approach. Differences between PAR and total solar radiation, in fraction intercepted by leaves (as discussed by Jovanovic and Annandale, 1998; and Kiniry, 1999), are avoided by making the total solar radiation to PAR conversion for the incident light above the plant canopy before interception by leaves.

A series of measurements can consist of 10 PAR measurements above the canopy, 10 below the canopy, and 10 more above the canopy. The fraction of PAR intercepted is calculated with the mean of the measurements above and below the canopy. While taking the readings below the canopy, the light meter is moved across the plant rows. Measurements are taken within 1.5 h of solar noon, during times with relative stable incident solar radiation (without intermittent clouds).

Whole plants are harvested for measuring LAI and dry weight on each day the light interception is measured. Samples can consist of 0.5 to 1.0 m of row per replication per cultivar. Leaf areas of the samples can be measured with a LiCor LI-3100 leaf area meter (LiCor Inc., Lincoln, Nebraska). Weights of the total above-ground plant and the panicle are measured after drying in a forced-air drying oven until the weight stabilizes. Depending on the plant type and the planting density, a sample of at least 0.5 to 1.0 m of row from each plot should be harvested after maturity for determining HI. Grain should be separated from a subsample of plants from each replication, and the fraction of the panicle which is grain should be measured. Plant N concentrations can be determined by the total Kjehdal Digest procedure.

Regressions can be fit with the treatment means for each replication. The RUE is the slope of the regression for above-ground plant dry weight (g m^{-2}) as a function of PAR intercepted (MJ m^{-2}). Significance of the regression parameter for a cultivar can be tested, using indicator variables, for significantly different slope or the intercept compared to other cultivars or crops (Neter et al., 1985).

The light extinction coefficient (k) for Beer's law (Monsi and Saeki, 1953) is calculated from the fraction of PAR intercepted (FIPAR) and the LAI. Values for k are calculated for each harvest date of each cultivar as:

$$k = [\log(1 - \text{FIPAR})] / \text{LAI} \quad [7]$$

Using the measured values for each replication of each cultivar, means and SD values can be calculated for LAI, k , grain yield, and HI.

YIELD COMPONENTS: BEYOND HI

While this study described yield simulation with HI, crop yield variability due to HI differences remains an important area for research on crop modeling. Simulation of environmental aspects of crop production relies heavily on realistic description of plant biomass production and nutrient uptake. On the other hand, yield variability among many crop cultivars is highly dependent on HI. In a study on grain legumes, Jeuffroy and Ney (1997) stated: "Little increase is to be expected in potential RUE... [whereas] partitioning of growth in harvested yield ... could be improved. Harvest index remains widely variable [for] some species." In a rice study (Kiniry et al., 2001b), the earliest cultivar studied, Jefferson, had the largest HI in three of the four seasons and had the greatest yield those seasons. Crop models need better description of why HI varies to improve the accuracy in grain yield simulation. Accurate description of the processes describing

panicle development, the determination of number of seeds per panicle, and the weight per seed should be vigorously pursued to quantify the differences in HI observed among cultivars and among environmental conditions.

Future high-yielding cultivars will likely come from increases in such yield components contributing to the aforementioned increased HI and not from increased RUE. In the above-mentioned rice study, cultivars showed large differences in grain yield while having similar RUE values. For the 1999 main crop, RUE of Jefferson was not significantly different from Cocodrie, but Jefferson had much smaller yield. For the ratoon crop of 2000, Jefferson and Cypress had similar RUE values, but Jefferson had 79% greater yield. These yield differences among cultivars were largely related to differences in HI.

Simulation of yield components, especially seeds per plant, can be based on some general principles of crop physiology. Kiniry et al. (2002) reported that when maize plants received adequate moisture and nutrients, responses of seed number per plant to intercepted light and to ear growth rate were linear, with y-intercepts not significantly different from zero. This implies that plants set seeds in direct proportion to the amount of assimilate (carbohydrate) available in the ear following silking. Seeds require this carbohydrate to continue to develop after ovule fertilization. The amount of light intercepted per plant required to support each seed is remarkably stable for several sites in this study.

Thus, a potentially useful approach to understanding maize yields in many environments is the assumption that the number of seeds that develop on a plant is proportional to the available nonstructural carbohydrate (NCO) in the ear during early seed development following pollination. During the first 10 to 11 d after silking, maize plants can abort seeds if drought or interplant competition for light reduces NCO supply to the ear (Westgate and Boyer, 1986). This has been supported by shading and drought stress studies (Kiniry and Ritchie, 1985; Grant et al., 1989) and with supplemental NCO fed into plants under drought stress (Boyle et al., 1991; Zinselmeier et al., 1995).

If seeds each require the same amount of NCO to support their early development, the responsiveness of seed number to amount of NCO in the ear soon after pollination would be linear. Growth per plant and light intercepted per plant have been used as surrogates for NCO in the ear. Linear seed number responses have been demonstrated for sorghum [*Sorghum bicolor* (L.) Moench] growth rate by Vanderlip et al. (1984), for wheat (*Triticum aestivum*) incident solar radiation by Fisher (1985), and for wheat photothermal quotient by Abbate et al. (1995) when nitrogen supply was adequate.

Likewise, many maize data sets show linear seed number responses. Hawkins and Cooper (1981) analyzed results from a wide range of experiments in Kenya, including planting densities of 1.7 and 11.1 plants m⁻². They found a linear relationship between seeds per plant and growth rate per plant from spikelet initiation to silking. Barbieri et al. (2000) reported a linear response of seeds m⁻² to intercepted PAR m⁻² with different nitrogen and row spacing treatments. Kiniry and Knievel (1995) found linear relationships for a wide range of population studies in the literature. With data of Whigham and Wooley (1974) in Iowa, they showed linear seed number responses to intercepted light per plant for all their plant density data, from 4.0 to 8.5 plants m⁻². Using all the seed number data of Iremiren and Milbourn (1980) in Britain, they also showed a linear response of seed number to intercepted light. These treatments were plant densities of 8 to 32 plants m⁻². There was also a linear seed number response for the data of Muleba et al. (1983) in a maize study in Zaire. These treatments were 4 to 10 plants m⁻². The seed number response was linear for

shaded plant values at 3 to 12 plants m^{-2} pooled with unshaded plant values at 7.5 and 12 plants m^{-2} for data in Massachusetts (Hashemi-Dezfouli and Herbert, 1992). Only the 3 plants m^{-2} unshaded treatment failed to be close to the response line. Using shading treatments and variable N treatments, Uhart and Andrade (1995) derived linear equations for seed number as a function of intercepted PAR. They derived linear equations with a plateau for seed number as a function of crop growth rate and ear growth rate. Finally, the response of seed number to light intercepted per plant was linear, with a positive y-intercept for data collected in Texas and Pennsylvania (Kiniry and Knievel, 1995). A general linear function was adequate for 10 hybrids with population densities ranging from 2.5 to 10 plants m^{-2} .

CONCLUSIONS

A general crop model was described that has functions easily applied to any crop species. It has been validated for several common crops in diverse sets of sites. The input parameters for growth and development can be easily derived in field experiments where there are adequate soil moisture and soil nutrients. Areas for future model development are described, especially related to yield components as contributing to differences in harvest index.

REFERENCES

- Abbate, P.E., F.H. Andrade, and J.P. Culot. 1995. The effects of radiation and nitrogen on number of grains in wheat. *J. Agric. Sci. (Cambridge)* 124:351-360.
- Arnold, J.G., R. Srinivasan, R.S. Muttiah, and J.R. Williams. 1998. Large area hydrologic modeling and assessment part I: Model development. *J. Am. Water Resour Assoc.* 34(1):73-89.
- Barbieri P.A., H.R. Sainz Rozas, F.H. Andrade, and H.E. Echeverria. 2000. Row spacing effects at different levels of nitrogen availability in maize. *Agron. J.* 92:283-288.
- Boon-Long, P., D.B. Egli, and J.E. Leggett. 1983. Leaf N and photosynthesis during reproductive growth in soybeans. *Crop Sci.* 23:617-620.
- Boyle M.G., J.S. Boyer, and P.W. Morgan. 1991. Stem infusion of liquid culture medium prevents reproductive failure of maize at low water potential. *Crop Sci.* 31:1246-1252.
- Bunce, J.A. 2003. Effects of water vapor pressure difference on leaf gas exchange in potato and sorghum at ambient and elevated carbon dioxide under field conditions. *Field Crops Research* 82: 37-47.
- Davis, R.G., W.C. Johnson, and F.O. Wood. 1967. Weed root profiles. *Agron. J.* 59:555-556.
- Debaeke, P., J.P. Caussanel, J.R. Kiniry, B. Kafiz, and G. Mondragon. 1997. Modeling crop:weed interactions in wheat with ALMANAC. *Weed Research* 37:325-341.
- Debaeke, P., J.P. Caussanel, J.R. Kiniry, B. Kafiz, and G. Mondragon. 1997. Modeling crop:weed interactions in wheat with ALMANAC. *Weed Research* 37:325-341.
- Fischer, R.A. 1985. Number of kernels in wheat crops and the influence of solar radiation and temperature. *J. Agric. Sci. (Cambridge)*. 105: 447-461.
- Flenet F., J.R. Kiniry, J.E. Board, M.E. Westgate, and D.C. Reicosky. 1996. Row spacing effects on light extinction coefficients of corn, sorghum, soybean, and sunflower. *Agron. J.* 88:185-190.
- Grant R.F., B.S. Jackson, J.R. Kiniry, and G.F. Arkin. 1989. Water deficit timing effects on yield components in maize. *Agron. J.* 81:61-65.
- Hashemi-Dezfouli, A. and S.J. Herbert. 1992. Intensifying plant density response of corn with artificial shade. *Agron. J.* 84:547-551.

- Hawkins, R.C. and P.J.M. Cooper. 1981. Growth, development and grain yield of maize. *Exp. Agric.* 17:203-207.
- Iremiren, G.O. and G.M. Milbourn. 1980. Effects of plant density on ear barrenness in maize. *Exp. Agric.* 16:321-326.
- Jeuffroy, M.H. and B. Ney. 1997. Crop physiology and productivity. *Field Crops. Res.* 53:3-16.
- Jovanovic , N.Z. and J.G. Annandale. 1998. Measurement of radiant interception of crop canopies with the LAI-2000 plant canopy analyzer. *S. Afr. Tydskr. Plant Grond.* 15(1):6-13.
- Kaspar, T.C., H.M. Taylor, and R.M. Shibles. 1984. Taproot-elongation rates of soybean cultivars in the glasshouse and their relation to field rooting depth. *Crop. Sci.* 24:916-120.
- Kiesselbach, T. A. 1949. The Structure and Reproduction of Corn. University of Nebraska Research Bulletin 161, University of Nebraska College of Agriculture. Agricultural Experiment Station, Lincoln, NE.
- Kiniry, J.R. and J.T. Ritchie. 1985. Shade-sensitive interval of kernel number of maize. *Agron. J.* 77:711-715.
- Kiniry, J.R., C.A. Jones, J.C. O'Toole, R. Blanchet, M. Cabelguenne, and D.A. Spanel. 1989. Radiation-use efficiency in biomass accumulation prior to grain-filling for five grain-crop species. *Field Crops Res.* 20:51-64.
- Kiniry, J.R. and R. Bonhomme. 1991. Predicting maize phenology. p. 115-131. In Hodges, T. (ed.) *Physiological Aspects of Predicting Crop Phenology*. CRC Press, Boca Raton, FL.
- Kiniry, J.R., W.D. Rosenthal, B. S. Jackson, and G. Hoogenboom. 1991. Predicting leaf development of crop plants. p. 29-42. In Hodges, T. (ed.) *Physiological Aspects of Predicting Crop Phenology*. CRC Press, Boca Raton, FL.
- Kiniry, J.R., J.R. Williams, P.W. Gassman, and P. Debaeke. 1992a. A general, process-oriented model for two competing plant species. *Trans. ASAE* 35:801-810.
- Kiniry, J. R., R. Blanchet, J.R. Williams, V. Texier, C. A. Jones, and M. Cabelguenne. 1992b. Simulating sunflower with the EPIC and ALMANAC models. *Field Crops Res.* 30:403-423.
- Kiniry, J.R. and D.P. Knievel. 1995. Response of maize seed number to solar radiation intercepted soon after anthesis. *Agron. J.* 87:228-234.
- Kiniry, J.R., M.A. Sanderson, J.R. Williams, C.R. Tischler, M.A. Hussey, W.R.Ocumpaugh, J.C. Read, G. VanEsbroeck, and R.L. Reed. 1996. Simulating Alamo switchgrass with the ALMANAC model. *Agron J.* 88:602-606.
- Kiniry, J.R., J.R. Williams, R.L. Vanderlip, J.D. Atwood, D.C. Reicosky, J. Mulliken, W.J. Cox, H.J. Mascagni Jr., S.E. Hollinger, and W.J. Wiebold. 1997. Evaluation of two maize models for nine U.S. locations. *Agron. J.* 89:421-426.
- Kiniry, J.R. and A.J. Bockholt. 1998. Maize and sorghum simulation in diverse Texas environments. *Agron. J.* 90:682-687.
- Kiniry, J.R., C.R. Tischler, and G.A. VanEsbroeck. 1999. Radiation use efficiency and leaf CO₂ exchange for diverse C₄ grasses. *Biomass and Bioenergy* 17:95-112.
- Kiniry, J.R. 1999. Response to questions raised by Sinclair and Muchow. *Field Crops Res.* 62:245-247.
- Kiniry, J.R., H. Sanchez, J. Greenwade, E. Seidensticker, J.R. Bell, F. Pringle, G. Peacock, Jr., and J. Rives. 2001a. Simulating range productivity on diverse sites in Texas. *J. Soil Water Conserv.* 57:144-150.
- Kiniry, J.R., G. McCauley, X. Yun, and J.G. Arnold. 2001b. Rice parameters describing crop performance for four U.S. cultivars. *Agron. J.* 93:1354-1361.
- Kiniry, J.R., X Yun, and T.J. Gerik. 2002. Similarity in maize seed number responses for a diverse set of sites. *Agronomie (Paris)* 22:265-272.

- Lizaso, J.I., W.D. Batchelor, M.E. Westgate, and L. Escharte. 2003. Enhancing the ability of CERES-Maize to compute light capture. *Agric. Syst.* 76:293-311.
- Manrique, L.A., J.R. Kiniry, T. Hodges, and D.S. Axness. 1991. Dry matter production and radiation interception of potato. *Crop Sci.* 31:1044-1049.
- Meek, D.W., J.L. Hatfield, T.A. Howell, S.B. Idso, and R.J. Reginato. 1984. A generalized relationship between photosynthetically active radiation and solar radiation. *Agron. J.* 76:939-945.
- Monks, D.W., L.R. Oliver, and R.C. Bozsa. 1988. Seedling growth of soybeans and selected weeds. *Weed Sci.* 36: 167-171.
- Monsi, M. and T. Saeki. 1953. Über den lichtfaktor in den pflanzengesellschaften und seine bedeutung fur die stoffproduktion. *Jpn. J. Bot.* 14:22-52.
- Monteith, J.L. 1965. Radiation and crops. *Exp. Agric.* 1:241-251.
- Muleba, N., T.G. Hart, and G.M. Paulsen. 1983. Physiological factors affecting maize (*Zea mays* L.) yields under tropical and temperate conditions. *Trop. Agric. (Trinidad)* 60:3-10.
- Neter, J., W. Wasserman, and M.H. Kutner. 1985. Applied Linear Statistical Models. Irwin Press, Homewood, IL.
- Spitters, C.J.T. and R. Aerts. 1983. Simulation of competition for light and water in crop-weed associations. *Aspects of Appl. Biol.* 4:467-483.
- Srinivasan, R., J.G. Arnold, R. S. Muttiah, C. Walker, and P.T. Dyke. 1993. Hydrologic Unit Model for United States (HUMUS). p. 451-456. In Proc. of Advances in Hydro Science and Engineering, Washington, D.C. 7-11 June 1993. University of Mississippi, Oxford, MS.
- Stockle, C.O. and J.R. Kiniry. 1990. Variability in crop radiation use efficiency associated with vapor pressure deficit. *Field Crops Res.* 21:171-181.
- Uhart, S.A. and F.H. Andrade. 1995. Nitrogen deficiency in maize: II. Carbon-nitrogen interaction effects on kernel number and grain yield. *Crop Sci.* 35:1384-1389.
- Vanderlip, R.L., D.A. Charles-Edwards, M.A. Foale, and R. Ferraris. 1984. Predicting tiller number and seed number in grain sorghum. *Agron. Abstr.* 138.
- Vietor, D.M., R.P. Ariyanayagam, and R.B. Musgrave. 1977. Photosynthetic selection of *Zea mays* L. I. Plant age and leaf position effects and a relationship between leaf and canopy rates. *Crop Sci.* 17:567-573.
- Westgate, M.E., and J.S. Boyer. 1986. Reproduction at low silk and pollen water potentials in maize. *Crop Sci.* 26:951-956.
- Whigham, D.K., and D.G. Woolley. 1974. Effect of leaf orientation, leaf area, and plant densities on corn production. *Agron. J.* 66:482-486.
- Williams, J.R., C.A. Jones, and P.T. Dyke. 1984. A modeling approach to determining the relationship between erosion and soil productivity. *Trans. ASAE* 27(1):129-144.
- Williams, J.R., C.A. Jones, J.R. Kiniry, and D.A. Spanel. 1989. The EPIC crop growth model. *Trans. ASAE* 32(2):497-511.
- Williams, J.R., P.T. Dyke, W.W. Fuchs, V.W. Benson, O.W. Rice, and E.D. Taylor. 1990. EPIC- erosion/productivity impact calculator: 2. User manual. In A.N. Sharpley and J.R. Williams (ed.) USDA Tech. Bulletin No. 1768.
- Yun, X., J.R. Kiniry, V. Nedbalek, and W.D. Rosenthal. 2001. Maize and sorghum simulations with CERES-Maize, SORKAM, and ALMANAC under water-limiting conditions. *Agron. J.* 93:1148-1155.
- Yun, X., J.R. Kiniry, and J.R. Williams. 2003. The ALMANAC model's sensitivity to input variables. *Agric. Syst.* 78:1-6.
- Zinselmeier, C., M.J. Lauer, and J.S. Boyer. 1995. Reversing drought-induced losses in grain yield: Sucrose maintains embryo growth in maize. *Crop Sci.* 35:1390-1400.

CHAPTER 2

Combining Modeling and Remote Sensing for Crop Yield Prediction in Mexico

Alma Delia Baez-Gonzalez, Mario Tiscareno-Lopez, Victor Rodriguez-Moreno,
Jaime Macias, Jose L. Mendoza, and Juan R. Manjarrez

CONTENTS

Introduction	13
Yield Forecasting	14
Crop Modeling	14
Remote Sensing	15
Combining Remote Sensing and Modeling	15
A Mexican Study: The MSPC Model	16
Variables	17
Model Input	18
Satellite Data	18
Field Data	18
Model performance in Sinaloa	19
Conclusions	22
Related Studies	22
Acknowledgments	23
References	24

INTRODUCTION

The early assessment of crop yield at large scale is essential for food security and agricultural decision-making in Mexico. However, traditional methods of estimation, such as field surveys, are costly and time-consuming. The use of imported yield prediction technology is often not viable because of complex operational requisites, such as databases that are not readily available in the country. Also, with the great variability in the country's agricultural regions, the use nationwide of

a uniform tool is often not practicable. Thus, Mexican scientists need to develop efficient yield prediction tools that meet the demands of the country's diverse agricultural regions.

This chapter presents the Modelo de Simulacion para Prediccion de Cosechas (MSPC) or Simulation Model for Crop Yield Prediction. This model is an output of the Proyecto Nacional de Prediccion de Cosechas (National Crop Yield Prediction Project) established by the Instituto Nacional de Investigaciones Forestales, Agricolas y Pecuarias (INIFAP), or National Research Institute for Forestry, Agriculture, and Livestock Production, with the support of the U.S. Department of Agriculture-Agricultural Research Service (USDA-ARS) and the Spatial Sciences Laboratory of Texas A & M University (TAMU). The MSPC is a tool for large-area crop growth monitoring and yield estimation that uses satellite and field data with crop growth modeling (Baez-Gonzalez et al., 2002). This chapter describes the model and discusses its performance with maize (*Zea mays* L.) in Sinaloa, one of the 11 Mexican states in the national project network. Related ongoing research is likewise presented.

Yield Forecasting

Yield forecasting, or determining yield in advance of harvest, has been done in many parts of the world to assess national food security and provide early food shortage warning (Thornton et al., 1997; Pierre et al., 2000; Snijders, 2000; Tychon et al., 2000). In Mexico, it is essential for determining such matters as import-export policies, government aid for farmers, and allocation of subsidies for regional agricultural programs. For farmers worldwide, yield assessments during crop production can aid in crop management decision-making (e.g., in application of chemicals, irrigation, marketing of products) (Horie et al., 1992; Boote et al., 1996).

Yield forecasting is done at different scales in space and time. Forecasting for crop management is usually on a farm or regional scale while forecasting for national food security and agricultural policies involves larger scales in space and time. A review of methods used in yield forecasting, including those by means of modeling and remote sensing technology, is provided by Horie et al. (1992).

In Mexico, INIFAP forecasts for maize at regional scale are made thrice each autumn-winter and spring-summer season: 1) before the growing season, with an agro-meteorological model; 2) mid-season, with a model based on the empirical relationship between yield and maximum leaf area index (LAI) gathered from the field; and 3) towards the end of the season, with the MSPC model, using field and satellite data with crop growth modeling. The forecasts are submitted to the Mexican Secretary of Agriculture.

Crop Modeling

A crop growth model is a quantitative scheme for predicting the growth, development, and yield of a crop, given a set of genetic coefficients and relevant environmental variables (Monteith, 1996). Crop modeling involves the dynamic simulation of crop growth by numerical integration of constituent processes with the aid of computers (Sinclair and Seligman, 1996). It evolved in the 1960s as a means of integrating biophysical processes in order to improve understanding of crop behavior. Later, there was a shift in modeling emphasis, from the search for scientific insights to putting insights into practical use. Bouman et al. (1996) and Sinclair and Seligman (1996) provide an extensive review of the development of crop simulation modeling.

Crop modeling has three primary uses: research knowledge synthesis, crop system decision management, and policy analysis (Bouman et al., 1996). The heuristic value of crop models has long been recognized; models are important interdisciplinary tools that promote understanding of the interactions of genetics, physiology and the environment, and facilitate hypotheses-testing (Hanks and Ritchie, 1991; Boote et al., 1996; Sinclair and Seligman, 1996). The use of models in agricultural decision-making and policy formulation has recently been increasingly explored, and this has resulted in the design of models to aid in such matters as water and fertilizer management, evaluation of consequences of changes in climate and rainfall patterns, crop monitoring, and yield prediction (Weigand and Richardson, 1984; Maas et al., 1985; Boote et al., 1996; Bouman et al., 1996; Sinclair and Seligman, 1996; Irmak et al., 2001; Paz et al., 2001). A review of the applications of crop growth models in semi-arid areas such as Mexico is provided by Sivakumar and Glinni (2002).

Remote Sensing

Remote sensing, generally known as the acquisition of information about an object or phenomenon by a device that is not in physical contact with it, involves the use at a distance, as from an aircraft or spacecraft, of cameras, lasers, radar systems, seismographs, and other devices for measuring force fields, acoustic energy, or electromagnetic radiation.

In crop modeling, remotely sensed information usually refers to a quantification of a plant community attribute (e.g., LAI) obtained through noncontact instruments. This involves the measurement of electromagnetic radiation in specific wavelengths reflected or emitted by the plants (Maas, 1988a). Satellite imagery has been used to measure crop parameters such as photosynthetic rate, intercepted photosynthetically active radiation (IPAR), biomass, photosynthetic size of canopy, net primary productivity (NPP), and LAI (Weigand et al., 1979; Weigand and Richardson, 1984; Sellers, 1985, 1987; Baret and Guyot, 1991; Ochi et al., 2000; Aparicio et al., 2002).

Remote sensing technology can provide observations over large areas at even times; hence, it is useful in crop modeling at regional scale (Moulin et al., 1998). It has been used to assess crop growth and yield at regional and national levels in various parts of the world (Prince, 1991; Supit, 1997; Thornton et al., 1997; Fueller, 1998; Sannier et al., 1998; Seiler et al., 1998; Bingfeng and Chenglin, 2000; Bochenek, 2000; Denore et al., 2000; Kuittinen et al., 2000; Reynolds et al., 2000; Snijders, 2000; Wouters et al., 2000; Lobell et al., 2003). Its use in precise crop management (PCM) has also been explored (Moran et al., 1997; Jones and Barnes, 2000).

Combining Remote Sensing and Modeling

It is believed that the use of remotely sensed information might improve the accuracy of agricultural crop modeling (Wiegand et al., 1979; Arkin et al., 1980; Maas, 1988a, 1988b). A review of how satellite observations are used to improve the capability of crop models to predict yield from field to regional scales is provided by Moulin et al. (1998).

Crop models and satellite data may be combined in several ways. One way is to use satellite data as model input to evaluate one or more driving variables. Another is to use satellite data to update a state variable of the model (e.g., LAI). Remotely sensed data may also be used for the re-initialization of the model (i.e., the adjustment of an initial condition to obtain a simulation in

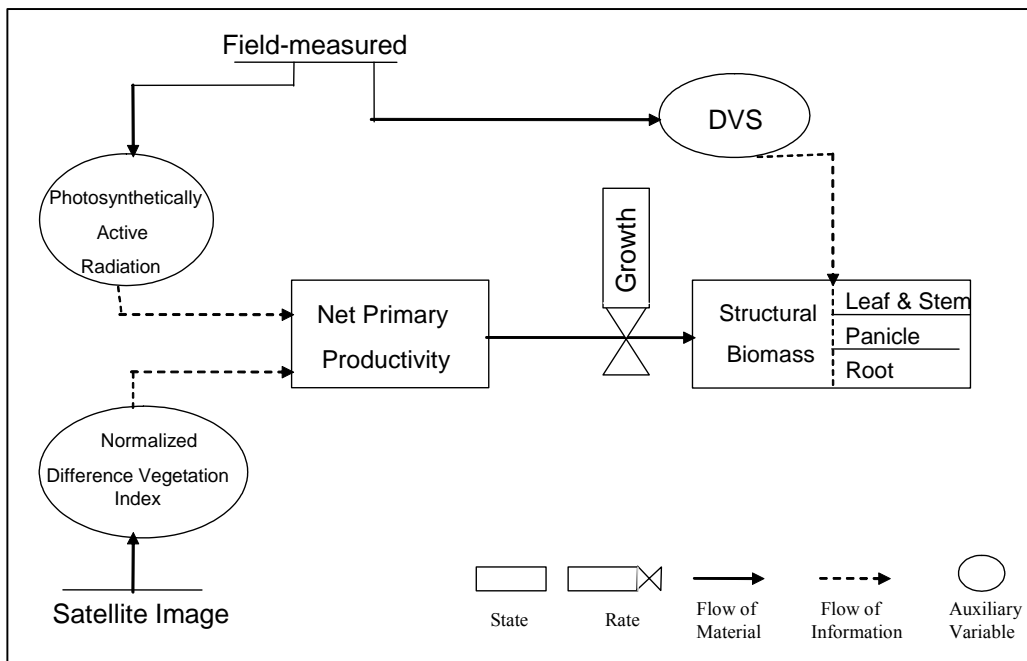


Fig. 2-1. Schematic presentation of the yield prediction model MSPC (Modelo de Simulacion para Prediccion de Cosechas).

agreement with the remotely sensed derived observations) and for model re-calibration (e.g., the adjustment of model parameters to obtain a simulation in agreement with LAI derived from the observations) (Maas, 1988a; Moulin et al., 1998).

For the coupling of satellite data with crop models to be useful, it is essential that satellite observations be correctly processed. Also, the low spatial resolution signal, if used, must be correctly interpreted (Moulin et al., 1998).

A MEXICAN STUDY: THE MSPC MODEL

The National Crop Yield Prediction Project of the Laboratorio Nacional de Modelaje y Sensores Remotos (National Laboratory of Modeling and Remote Sensing) of INIFAP aims to develop approaches for monitoring crop growth and assessing crop yield at large scale by means of modeling and remote sensing. One project study has resulted in the development and validation of the crop yield prediction model now known as the MSPC (Modelo de Simulacion para Prediccion de Cosechas), which can be used to predict yield of corn under irrigated and non-irrigated conditions in the important agricultural regions of Mexico (Baez-Gonzalez et al., 2002).

In the MSPC framework, the systems approach (Spedding, 1979) is applied to integrate information and mimic the behavior of the crop. The corn crop is considered the system under study. The simulation model is the main tool used to mimic the behavior of the corn crop and to integrate satellite and ground-based data. Figure 2-1 shows a schematic representation of the MSPC. This crop growth model has been developed to estimate biomass among the different plant

organs at a 15-d time step and to predict yield when the crop reaches the reproductive stage called anthesis.

Variables

Crop growth simulation models usually consist of the following: 1) state variables (e.g., leaf area, dry mass), which describe the state of the crop at a given time; 2) input or driving variables (e.g., temperature, intercepted solar radiation), which provide the basis for change in the modeled crop; and 3) parameters, which determine the response of the state variables to the driving variables (de Wit, 1982). In the case of the MSPC, the variables are the net primary productivity (NPP), structural biomass, Normalized Difference Vegetation Index (NDVI), photosynthetically active radiation (PAR), and development stage (DVS) of the crop. The parameters are the partitioning coefficients.

Net primary productivity (NPP) is a fundamental variable that provides information about the health and status of vegetation communities (Markon and Peterson, 2002). It is defined and measured in terms of either biomass or CO₂ exchange (Field et al., 1995). Terrestrial NPP is the rate of atmospheric carbon uptake by vegetation through the process of net photosynthesis minus dark respiration. Instantaneous NPP is a fraction of the incoming solar energy stored into organic matter (Ruimy et al., 1994). The NPP has various applied and theoretical uses and has been modeled from different perspectives (Potter et al., 1993; Ruimy et al., 1994; Field, et al., 1995; Malmström et al., 1997; Ochi et al., 2000; Lobell et al., 2002; Markon and Peterson, 2002; Matsushita and Tamura, 2002).

It is possible to measure NPP directly or indirectly (Markon and Peterson, 2002). In this study, the NPP is calculated following the approach of Goward and Huemmrich (1992) and Ruimy et al. (1994) and adapting the equation of Ochi et al. (2000):

$$\text{NPP} = \{0.5[(-0.08 + 1.075)\text{NDVI}]\text{PAR}\} \quad [1]$$

where NPP = net primary productivity, NDVI = Normalized Difference Vegetation Index, and PAR = Photosynthetically Active Radiation.

The connection between NPP and NDVI is based on the view that plant production of organic matter is proportionally related to both the absorbed radiation and reflected radiation by green vegetation, primarily leaves (Markon and Peterson, 2002). The NDVI derived from satellite data has been linked to vegetation condition and plant biomass on the land surface (Goward and Huemmrich, 1992; Groten, 1993; Delecolle and Guerif, 1995; Tan and Shih, 1997; Ochi and Murai, 1999; Hill and Donald, 2003). High NDVI values indicate that the land surface is covered with dense healthy vegetation, while negative values indicate the presence of clouds, snow, water, or a bright non-vegetated surface (Yin and Williams, 1997).

Photosynthetically active radiation (PAR) refers to the radiation in the 400- to 700-nm waveband. It represents the portion of the solar spectrum that plants use for photosynthesis (Hay and Walker, 1989; Daughtry et al., 1992). The amount of PAR absorbed by green vegetation is an important determinant of photosynthesis and growth (Hanan et al., 1995).

Development stage (DVS) is defined as progress from germination to maturity; major phases can be distinguished by well-defined events such as flower initiation and anthesis (Ong and Squire, 1984). Growth implies the conversion of primary photosynthesis into structural plant material (Hay and Walker, 1989). In the MSPC, the total growth of the crop (kg ha⁻¹ d⁻¹) is

partitioned among the plant organs according to partitioning coefficients adapted from Penning de Vries, et al. (1989) and introduced as forcing functions. The values of the partitioning coefficients change with the development stage of the crop, which is reported from field observation with the decimal code for description (Tottman et al., 1979). The MSPC considers leaves and stems as one plant organ.

Model Input

Satellite Data

The MSPC uses satellite-derived NDVI data. Advanced Very High Resolution Radiometer (AVHRR) High Resolution Picture Transmission (HRPT) data are downloaded daily from the NOAA-16 satellite to the receiving station at the Blackland Research Center in College Station, Texas. Each AVHRR scan line contains 2048 pixels with a resolution of 1.1 km, and every AVHRR scene extends from the U.S.-Canadian border down to southern Mexico.

The NOAA AVHRR images used by the model have low spatial but high temporal resolution. It is believed that the dynamism of corn crop development cannot be assessed as well by high spatial resolution images whose low temporal resolution limits the number of observations provided during the growing season (Moulin et al., 1995).

The NDVI values are derived as (NIR-VIS)/(NIR+VIS) based on surface reflectance. Due to the problem of cloud-contaminated images, 15-d NDVI composites are created using the Maximum Value Composite (MVC) procedure (Holben, 1986). Pixels having a solar zenith angle greater than 80 are not used in the study. A full description of the methodology for processing satellite data is provided in Baez-Gonzalez et al. (2002).

Field Data

The model uses the following field data: date of planting, PAR above and below the canopy of the crop, and DVS. Due to the low spatial resolution of the satellite images used in the study, it is necessary to gather field data from areas with homogenous (90%) corn cover and an extension of 300 ha. Every 15 d during the growing season, the following crop data are gathered: PAR, LAI (mainly for use in a related study), and DVS. A linear PAR/LAI ceptometer is used to sample PAR and LAI in each site. The Global Positioning System (GPS) is used to locate the sampling sites, and the planting dates are reported. In order that a comparison between simulated and actual yield can be made, at the end of the growing season, grain yield ($Mg\ ha^{-1}$) is measured in the field by destructive methods on the same day that the farmers harvest the fields. Each sampled area is 8 m^2 . Grain weight is reported at 14% of moisture.

Table 2-1. Planting dates of corn in irrigated sites in Sinaloa, Mexico, during autumn-winter 2001-2002.

Site	Planting date	Site	Planting date
1	18 Nov. 2001	18	1 Dec. 2001
2	15 Nov. 2001	19	12 Nov. 2001
3	17 Nov. 2001	20	24 Nov. 2001
4	2 Nov. 2001	21	11 Nov. 2001
5	2 Nov. 2001	22	21 Nov. 2001
6	5 Nov. 2001	23	12 Nov. 2001
7	7 Nov. 2001	24	3 Nov. 2001
8	21 Nov. 2001	25	30 Nov. 2001
9	21 Nov. 2001	26	18 Nov. 2001
10	14 Nov. 2001	27	10 Dec. 2001
11	1 Nov. 2001	28	28 Dec. 2001
12	9 Nov. 2001	29	29 Dec. 2001
13	12 Nov. 2001	30	10 Dec. 2001
14	15 Nov. 2001	31	4 Dec. 2001
15	11 Nov. 2001	32	25 Nov. 2001
16	11 Nov. 2001	33	20 Nov. 2001
17	30 Nov. 2001		

Model Performance in Sinaloa

The MSPC has been used for several years to predict corn yield in several agricultural regions in Mexico. This section focuses on its performance under irrigated conditions in the northern and central agricultural areas of the state of Sinaloa. High spatial resolution images (Landsat ETM+) were used determine the total size of agricultural areas in the valleys under study. During the growing season of 2001-2002, a mosaic of four Landsat ETM+ images covering corn valleys in northern and central Sinaloa was processed. The total area planted to corn during that season was 348,208 ha.

Thirty-three irrigated sites in Guasave, Ahome, El Carrizo, Culiacan, and Navolato valleys that had been planted to corn (Table 2-1) during autumn-winter 2001-2002 were monitored from February to April 2002. Guasave, Ahome, and El Carrizo are in the north while Culiacan and Navolato are in the central part of the state. The study sites were chosen at random from farmers' fields.

Table 2-2. Measured and simulated corn yield in irrigated sites in Sinaloa, Mexico, during autumn - winter 2001-2002.

Site	Measured yield	Simulated yield	Difference	—
				Mg ha ⁻¹
1	10.9	11.0	0.1	
2	7.3	8.0	0.7	
3	8.6	8.3	-0.3	
4	10.5	10.9	0.4	
5	10.9	10.7	-0.2	
6	9.9	10.2	0.3	
7	10.8	11.2	0.4	
8	7.7	7.9	0.2	
9	12.3	11.5	-0.8	
10	9.0	8.6	-0.4	
11	11.6	12.9	1.3	
12	10.1	10.5	0.4	
13	7.9	7.9	0.0	
14	10.4	10.6	0.2	
15	11.8	13.1	1.3	
16	9.9	9.2	-0.7	
17	8.1	8.9	0.8	
18	5.9	7.3	1.4	
19	6.4	5.2	-1.2	
20	10.1	11.3	1.2	
21	9.2	8.9	-0.3	
22	12.0	13.0	1.0	
23	12.3	11.4	-0.9	
24	9.0	10.4	1.4	
25	10.7	10.3	-0.4	
26	8.3	9.9	1.6	
27	10.7	10.0	-0.7	
28	9.6	9.0	-0.6	
29	10.7	11.9	1.2	
30	10.5	11.8	1.3	
31	12.0	11.0	-1.0	
32	10.0	11.2	1.2	
33	10.2	11.1	0.9	

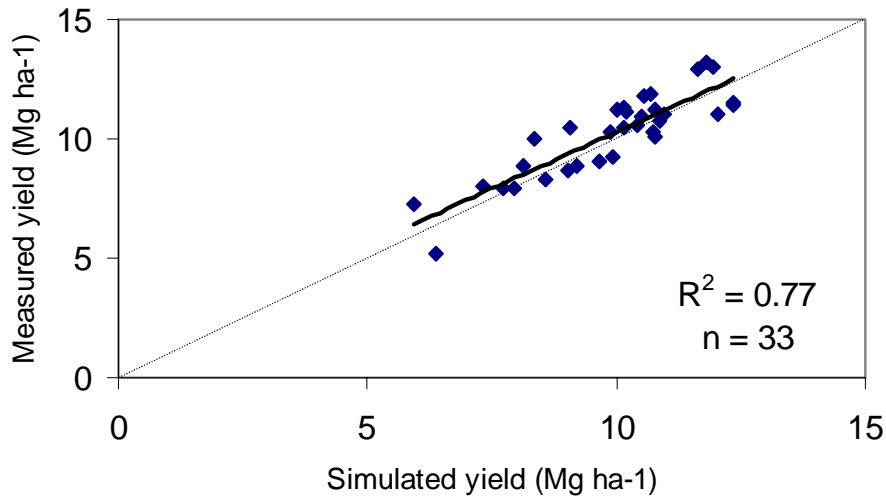


Fig. 2-2. Measured and simulated corn grain yield in irrigated sites in Sinaloa, Mexico, during autumn-winter 2001-2002. The solid line is the fitted regression line and the dashed line is the 1:1 fit.

Since the objective was to determine if the MSPC could reliably predict yield at large scale in Sinaloa, a comparison was made of the simulated yield versus the measured yield at regional level. The simulation of grain yield in the five valleys showed a mean error (simulated minus measured) of 0.23 Mg ha⁻¹. The growth model accounted for 77% of the variability in measured yields (Table 2-2 and Fig. 2-2). A paired t-statistic analysis (Steel and Torrie, 1980) showed that the simulated and measured yield were statistically similar at 0.01 level of significance.

Table 2-3 presents a comparison of measured yield and simulated yield in the northern and central valleys of Sinaloa. It also shows the mean measured yield of the five valleys, which is reported as the mean corn production of the state. The model over-estimated by 11% corn production in valleys in northern Sinaloa (10.2 ± 0.6 versus 9.2 ± 0.7). For the central part, the over-estimation was 7% (10.8 ± 0.7 versus 10.1 ± 0.5). A comparison of measured and simulated yield at state level showed that the MSPC over-estimated production by 3%.

Table 2-3. Measured and simulated corn grain yield in different parts of Sinaloa, Mexico, during the growing season autumn-winter 2001-2002.

Location in Sinaloa	Measured yield* during May to June 2002 Mg ha ⁻¹	Simulated yield* during May 2002 Mg ha ⁻¹
North	9.2 ± 0.7	10.2 ± 0.6
Central	10.1 ± 0.5	10.8 ± 0.7
Mean at State level	9.7 ± 0.4	10.0 ± 0.3

*Confidence at 0.05 significance level

The accuracy of the model in simulating grain yield seemed to have been affected by the time the crop was monitored. It was possible to assess with higher accuracy when the field data (PAR, DVS) were gathered at the initial stage of plant development. One reason for this higher accuracy is that NDVI is sensitive to low LAI (>3), and therefore suitable for assessing crop growth at the initial stages (Serrano et al., 2000). In contrast, a high degree of over- or under-estimation was observed when data were gathered at the reproductive stage of the crop. The simulation error may have been partly due to the partitioning coefficients used by the model when the plant reaches the reproductive stage. During this stage, the NPP calculated by the model is assigned fully to the panicle of the plant.

The INIFAP yield prediction report for Sinaloa is done in two ways: 1) in Mg ha^{-1} and 2) in volume (Mg) predicted for the total agricultural areas of the state. An analysis of the performance of the MSPC in 2001-2002 shows an over-estimation error of 3% at state level or 101,328 Mg out of a total production of 3,528, 554 Mg. This is minimal, considering the large areas involved.

On the whole, the use of the MSPC for assessing yield at regional level is feasible because the model can predict yield at pre-harvesting time (at least one month ahead of the harvesting period) with acceptable accuracy. The model can serve the needs of decision-makers. Moreover, even if the MSPC needs field and satellite data to make the predictions, the use of the model with these data at regional scale is less costly than traditional methods involving large numbers of technicians assessing yield at farm level.

Conclusions

The approach of predicting yield by combining modeling and remote sensing, such as by means of the MSPC, is viable for large-scale assessment of corn yield in the Mexican state of Sinaloa. However, further research is needed to improve the MSPC and to develop other models for use in irrigated and non-irrigated agricultural areas in the country. Research efforts in remote sensing must be strengthened in order to lessen reliance on field data. It is necessary to solve problems related to the use of coarse spatial resolution sensors (e.g., AVHRR) and to explore other types of remote sensing technology.

RELATED STUDIES

The following are related INIFAP-USDA (ARS) research studies:

1. Incorporating weather and soil information into the MSPC model

The objective of this study is to increase the accuracy of the MSPC in estimating yield under non-irrigated conditions while reducing the amount of input data gathered from the field (e.g., DVS and LAI). This involves the use of low and high spatial resolution images and the incorporation of the water stress factor. The growth submodel of the MSPC will be modified to calculate DVS from growing degree days. A soil-water submodel has already been adapted (Baez and Jones, 1995). This submodel considers soil texture and the processes of infiltration, evaporation, transpiration, and drainage. The required weather data, which are available for most areas of Mexico, are precipitation, maximum and minimum temperature, and pan evaporation.

2. Incorporating high spatial resolution imagery data into an empirical model

This study involves the direct use of a driving variable (LAI) estimated from high spatial resolution images (Landsat ETM+) in an empirical yield prediction model. An equation considering field-measured LAI at silking stage and yield at farmer's plot level has been developed and used in yield prediction for four consecutive years with high accuracy (Baez-Gonzalez et al., 2005). It is being adjusted to respond to LAI gathered from high spatial resolution satellite data, such as from SPOT. This approach has certain limitations (e.g., low temporal frequency of high spatial resolution images, wide range of sowing dates resulting in crop reaching maximum LAI at different times), which will make it difficult to use for large-scale estimation. However, it will provide a precise monitoring tool at farmer's plot level that will complement techniques for yield estimation at regional scale.

3. Expanding the capability of the ALMANAC (Agricultural Land Management Alternatives with Numerical Assessment Criteria) model to use remotely sensed information

The USDA-ARS ALMANAC model, which was developed from EPIC version 1319, predicts the effects of management decisions on soil and water resources and crop production for field-size areas (Kiniry et al., 1992). Its use in large areas in Mexico is being explored. The following approaches have been developed to enable the ALMANAC to use remotely sensed information from images of high and low spatial resolution for updating some of its driving variables:

- 1) Calculating leaf area index (LAI) as a function of NDVI and then updating the simulated LAI of the model (Approach 1).
- 2) Calculating FIPAR (fraction of incident photosynthetic active radiation) as a function of NDVI and then updating the simulated LAI (Approach 2).
- 3) Calculating LAI as a function of NDVI and IPAR (intercepted photosynthetically active radiation) and updating the simulated LAI and DM (dry matter) of the model (Approach 3).

The approaches will be tested for use in both irrigated and non-irrigated areas in Mexico. They are expected to strengthen the capabilities of INIFAP to deliver reliable and efficient yield forecasts.

ACKNOWLEDGMENTS

The authors thank Juan A. Reyes, Magdalena Ferrel, and Gloria Martinez for providing technical support and Elvira Aranda Tabobo for editing the manuscript. They are grateful to Dr. W.A. Dugas, Dr. R. Srinivasan, and Dr. P.Y. Chen of TAMU for the NOAA AVHRR satellite images and other forms of logistical support. A USDA grant enabled Dr A. Baez to do the related research in Temple, Texas; she extends her special thanks to Dr. C. Richardson, Director of the USDA-ARS Grassland Soil and Water Research Laboratory. She also thanks Dr. J. Kiniry for his collaboration and D. Spanel for technical assistance.

REFERENCES

- Aparicio, N., D. Villegas, J.L. Araus, J. Casadesus, and C. Royo. 2002. Relationship between growth traits and spectral vegetation indices in durum wheat. *Crop Sci.* 42:1547-1555.
- Arkin, G.F., S.J. Maas, and C. Richardson. 1980. Forecasting grain sorghum yields using simulated weather data and updating techniques. *Trans. ASAE.* 23:676-680.
- Baez-Gonzalez, A.D., J.R. Kiniry, S.J. Maas, M.L. Tiscareño, J.C. Macias, J.L. Mendoza, C.W. Richardson, J.G. Salinas, and J. R. Manjarrez. 2005. Large-area maize yield forecasting using leaf area index based yield model. *Agron. J.* 97:418-425.
- Baez-Gonzalez, A.D., P. Chen, M. Tiscareno-Lopez, and R. Srinivasan. 2002. Using satellite and field data with crop growth modeling to monitor and estimate corn yield in Mexico. *Crop Sci.* 42:1943-1949.
- Baez-Gonzalez, A.D., and J.G. Jones. 1995. Models of sorghum and of pearl millet to predict forage dry matter in semi-arid Mexico. I. Simulation models. *Agric. Syst.* 47:133-145.
- Baret, F., and G. Guyot. 1991. Potentials and limits of vegetation indices for LAI and APAR assessment. *Remote Sens. Environ.* 35:161-173.
- Bingfeng, W., and L. Chenglin. 2000. Crop growth monitor system with coupling of AVHRR and VGT data. In Proc. Vegetation 2000 Conf., Lake Maggiore, Italy. 3-6 Apr. 2000 [Online]. Available at <http://vegetation.cnes.fr/vgtprep/vgt2000/bingfeng.html> (accessed 15 Nov. 2003; verified 26 Oct. 2004).
- Bochenek, Z. 2000. Operational use of NOAA data for crop condition assessment in Poland. p. 387-392. In J.L. Casanova (ed.). *Remote sensing in the 21st century: Economic and environmental applications*. Balkema, Rotterdam, the Netherlands.
- Boote K.J., J.W. Jones, and N.B. Pickering. 1996. Potential uses and limitations of crop models. *Agron. J.* 88:704-716.
- Bouman, B.A.M., H. van Keulen, H.H. van Laar, and R. Rabbinge. 1996. The “School of de Wit” crop growth models: A pedigree and historical overview. *Agric. Syst.* 52:171-198.
- Daughtry, C.S.T., K.P. Gallo, S.N. Goward, S.D. Prince, and W.P. Kustas. 1992. Spectral estimates of absorbed radiation and phytomass production in corn and soybean canopies. *Remote Sens. Environ.* 39:141-152.
- Delecolle, R., and Guerif, M.O. 1995. Regional calibration of crop model using remote sensing data. p.302-310. In Harrison, P.A., R.E. Butterfield, and T.E. Downing (ed.) *Climate change and agriculture in Europe. Assessment of impacts and adaptations*. Research Report No. 9. Environmental Change Unit, University of Oxford, Oxford, U.K.
- Denore, B.J., J.L. Meilan, J.M. Williams, M. Cole, K.I. de Koeijer, and J.J. Colls. 2000. Estimation of cereal yields combining crop growth models and remotely sensed vegetation indices. p. 371-378. In J.L. Casanova (ed.) *Remote sensing in the 21st century: Economic and environmental applications*. Balkema, Rotterdam, the Netherlands.
- Field, C.B., J.T. Randerson, and C.M. Malmstrom. 1995. Global net primary production: Combining ecology and remote sensing. *Remote Sens. Environ.* 51:74-88.
- Fueller, D.O. 1998. Trends in NDVI series and their relation to rangeland and crop production in Senegal, 1987-1993. *Int. J. Remote Sens.* 19:2013-2018.
- Goward, S.N., and K.F. Huemmrich. 1992. Vegetation canopy PAR absorptance and the normalized difference vegetation index: An assessment using the SAIL Model. *Remote Sens. Environ.* 39:119-140.
- Grotens, S.M.E. 1993. NDVI-crop monitoring and early yields assessment of Burkina Faso. *Int. J. Remote Sens.* 14:1495-1515.

- Hanan, N.P., S.D. Prince, and A. Begue. 1995. Estimation of absorbed photosynthetically active radiation and vegetation net production efficiency using satellite data. *Agric. Forest Meteorol.* 76:259-276.
- Hanks, J., and J.T. Ritchie. 1991. Modeling plant and soil systems. *Agron. Monogr.* 31. ASA, Madison, WI.
- Hay, K.M.R., and A.J. Walker. 1989. An introduction to the physiology of crop yield. Longman Scientific & Technical, Essex, England.
- Hill, J.M., and G.E. Donald. 2003. Estimating spatio-temporal patterns of agricultural productivity in fragmented landscape using AVHRR NDVI time series. *Remote Sens. Environ.* 84(3):367-384.
- Holben, B.N. 1986. Characteristics of maximum-values composite images from temporal AVHRR data. *Int. J. Remote Sens.* 7:1417-1434.
- Horie T., M. Yajima, and H. Nakagawa. 1992. Yield Forecasting. *Agric. Syst.* 40:211-236.
- Irmak A, J.W. Jones, W.D. Batchelor, and J.O. Paz. 2001. Estimating spatially variable soil properties for application of crop models in precision farming. *Trans. ASAE.* 44(5):1343-1353.
- Jones, D., and E.M. Barnes. 2000. Fuzzy composite programming to combine remote sensing and crop models for decision support in precision crop management. *Agric. Syst.* 65:137-158.
- Kiniry, J.R., J.R. Williams, P.W. Gassman, and P. Debaeke. 1992. A general, process-oriented model for two competing plant species. *Trans. ASAE.* 35(3): 801-810.
- Kuittinen, R., L. Matikainen, V. Keskkisarja, and E. Parmes. 2000. Integration of satellite data and administrative information in crop yield monitoring. p. 379-385. In J.L. Casanova (ed.) *Remote sensing in the 21st century: Economic and environmental applications*. Balkema, Rotterdam, the Netherlands.
- Lobell, D.B., G.P. Asner, J.I. Ortiz-Monasterio, and T.L. Benning. 2003. Remote sensing of regional crop production in the Yaqui Valley, Mexico: Estimates and uncertainties. *Agric. Ecosyst. Environ.* 94(2):205-220.
- Lobell, D.B., J.A. Hicke, G.P. Asner, C.B. Field, C.J. Tucker, and O. Los. 2002. Satellite estimates of productivity and light use efficiency in United States agriculture, 1982-98. *Global Change Biol.* 8:722-735.
- Maas, S.J. 1988a. Use of remotely-sensed information in agricultural crop growth models. *Ecol. Modell.* 41:247-268.
- Maas, S.J. 1988b. Using satellite data to improve model estimates of crop yield. *Agron. J.* 80:655-662.
- Maas, S.J., A.J. Richardson, C.L. Wiegand, and P.R. Nixon. 1985. Use of plant spectral and weather data in modeling corn growth. p.167-186. In Proc. Int. Symp. Remote Sens. Environ. 19th. 21-25 Oct. 1985. Environ. Res. Inst. Ann Arbor, MI.
- Malmström, C.L., M.V.Thompson, G.P. Juday, S.O. Los, J.T. Randerson, and C.B. Field. 1997. Interannual variation in global-scale net primary production: Testing model estimates. *Global Biogeochem. Cycles* 11(3):367-392.
- Markon, C.J., and K.M. Peterson. 2002. The utility of estimating net primary productivity over Alaska using baseline AVHRR data. *Int. J. Remote Sens.* 23:4571-4596.
- Matsushita, B., and M. Tamura. 2002. Integrating remotely sensed data with an ecosystem model to estimate net primary productivity in East Asia. *Remote Sens. Environ.* 8:58-66.
- Monteith, J.L. 1996. The quest of balance in crop modeling. *Agron. J.* 88:695-697.
- Moran, M.S., Y. Inoue, and E.M. Barnes. 1997. Opportunities and limitations for image-based remote sensing in precision crop management. *Remote Sens. Environ.* 61:319-346.
- Moulin, S., A. Bondeau, and R. Delecolle. 1998. Combining agricultural crop models and satellite observations from field to regional scales. *Int. J. Remote Sens.* 19:1021-1036.

- Moulin, S., A. Fischer, G. Dedieu, and R. Delecolle. 1995. Temporal variations in satellite reflectance at field and regional scales compared with values simulated by linking crop growth and SAIL models. *Remote Sens. Environ.* 54:261-272.
- Ochi, S., and S. Murai. 1999. Analysis of relationship between NPP and population carrying capacity for major river basins in Asia. p. 258-262. *In Proc. SEIKEN Forum "Global Environment Monitoring from Space", 9th.*
- Ochi, S., R. Shibasaki, and S. Murai. 2000. Modeling and assessment of NPP/crop productivity in Asia by GIS combined with remote sensing data. *In Proc. 5th Gisdeco Seminar on GIS and Developing Countries [CD-ROM]. IRRI, Los Baños, Philippines.*
- Ong, C.K., and G.R. Squire. 1984. Response to temperature in a stand of pearl millet (*Pennisetum typhoides* S. & H.). 7. Final number of spikelets and grains. *J. Exp. Bot.* 35:1233-1240.
- Paz , J.O., W.D. Batchelor, G.L.Tylka, and R.G. Hartzler. 2001. A modeling approach to quantify the effects of spatial soybean yield limiting factors. *Trans. ASAE.* 44:1329-1334.
- Penning de Vries, F.W.T., D.M. Jansen, H.F.M. Gen Berge, and A. Bakema. 1989. Simulation of ecophysiological process of growth in several annual crops. *Simulation Monogr. PUDOC, Wageningen, the Netherlands.*
- Pierre, G., C. Crepeau, P. Bicheron, T. Bennouna, and V. Caldairou. 2000. The contribution of VEGETATION/SPOT4 products to remote sensing applications for food security, early warning and environmental monitoring in the IGAD sub region. *In Proc. Vegetation 2000 Conf., Lake Maggiore, Italy. 3-6 Apr. 2000[Online]. Available at <http://vegetation.cnes.fr/vgtprep/vgt2000/pierre.html> (accessed 15 Nov. 2000; verified 26 Oct. 2004).*
- Potter, C.S., J.T. Randerson, C.B. Field, P.A. Matson, P.M. Vitousek, H.A. Mooney, and S.A. Klooster. 1993. Terrestrial ecosystem production: A process model based on global satellite and surface data. *Global Biogeochem. Cycles* 7(4):811-841.
- Prince, S.D. 1991. A model of regional primary production for use with coarse resolution satellite data. *Int. J. Remote Sens.* 12:1313-1330.
- Reynolds, C.A., M. Yitayew, D. Slack, C.F. Hutchinson, A. Huete, and M.S. Peterson. 2000. Estimating crop yields and production by integrating the FAO Crop Specific Water Balance model with real-time satellite data and ground-based ancillary data. *Int. J. Remote Sens.* 21: 3487-3508.
- Ruimy A., B. Saugier, and G. Dedieu. 1994. Methodology for the estimation of terrestrial net primary production from remotely sensed data. *J. Geophys. Res.* 99:5263-5283.
- Sannier, C.A.D., J.C. Taylor, W. Du Plessis, and K. Campbell. 1998. Real-time vegetation monitoring with NOAA-AVHRR in Southern Africa for wildlife management and food security assessment. *Int. J. Remote Sens.* 19: 621-639.
- Seiler, R.A., F. Kogan, and J. Sullivan. 1998. AVHRR-based vegetation and temperature condition indices for drought detection in Argentina. *Adv. Space Res.* 21:481-484.
- Sellers, P.J. 1985. Canopy reflectance, photosynthesis, and transpiration. *Int. J. Remote Sens.* 6:1335-1372.
- Sellers, P.J. 1987. Canopy reflectance, photosynthesis, and transpiration. II. The role of biophysics in the linearity of their interdependence. *Remote Sens. Environ.* 21:143-183.
- Serrano, L., I. Filella, and J. Penuelas. 2000. Remote sensing of biomass and yield of winter wheat under different nitrogen supplies. *Crop Sci.* 40:723-731.
- Sinclair, T.R., and N.G. Seligman. 1996. Crop modeling: From infancy to maturity. *Agron. J.* 88:698-703.
- Sivakumar, M.V.K., and A.F. Glinni. 2002. Applications of crop growth models in the semiarid regions. p. 177-205. *In L.R. Ahuja, L. Ma, and T.A. Howell (ed.). Agricultural systems models in field research and technology transfer. Lewis Publ., Washington, D.C.*

- Snijders, F.L. 2000. Incorporating the use of vegetation data in FAO's programmes. *In Proc. Vegetation 2000 Conf.*, Lake Maggiore, Italy. 3-6 Apr. 2000 [Online]. Available at <http://vegetation.cnes.fr/vgtprep/vgt2000/snijders.html> (accessed 15 Nov. 2003; verified 26 Oct. 2004).
- Spedding, C.R.W. 1979. An introduction to agricultural systems. Applied Science Publ., UK.
- Steel, R.G.D., and J.H. Torrie. 1980. Principles and procedures of statistics: A biometrical approach. 2nd ed. McGraw-Hill, New York.
- Supit, I. 1997. Predicting national wheat yields using crop simulation and trends models. *Agric. For. Meteorol.* 88:199-214.
- Tan, C.H. and S.F. Shih. 1997. Using NOAA satellite thermal infrared data for evapotranspiration estimation in South Florida. *Soil Crop Sci. Soc. Fla. Proc.* Vol. 56.
- Thornton, P.K., W.T. Bowen, A.C. Ravelo, P.W. Wilkens, G. Farmer, J. Brock, and J.E. Brink. 1997. Estimating millet production for famine early warning: An application of crop simulation modeling using satellite and ground-based data in Burkina Faso. *Agric. For. Meteorol.* 83:95-112.
- Tottman, D.R., R.J. Makepeace, H. Broad. 1979. An explanation of the decimal code for the growth of cereals, with illustration. *Ann. Appl. Biol.* 93:221-34.
- Tychon B., P. Ozer, and S. Toure. 2000. VEGETATION potentialities in food early warning systems in the Sahelian region. *In Proc. Vegetation 2000 Conf.*, Lake Maggiore, Italy. 3-6 Apr. 2000 [Online]. Available at <http://vegetation.cnes.fr/vgtprep/vgt2000/tychon.html> (accessed 15 Nov. 2003; verified 26 Oct. 2004).
- Weigand C.L. and A.J. Richardson. 1984. Leaf area, light interception, and yield estimates from spectral components analysis. *Agron. J.* 76:543-548.
- Weigand C.L., A.J. Richardson, and E.T. Kanemasu. 1979. Leaf area index estimates for wheat from LANDSAT and their implications for evapotranspiration and crop modeling. *Agron. J.* 71:336-342.
- de Wit, C.T. 1982. Simulation of living systems. p. 3-7. *In* F.W.T. Penning de Vries et al. (ed.) *Simulation of plant growth and crop production. Simulation Monogr.* PUDOC, Wageningen, the Netherlands.
- Wouters K., H. Eerens, D. Dehem, B.T. Tychon, D. Buffet, and B. Oger 2000. Use of medium resolution imagery in the Belgian crop growth monitoring system (B-CGMS). *In Proc. Vegetation 2000 Conf.*, Lake Maggiore, Italy. 3-6 Apr. 2000 [Online]. Available at <http://vegetation.cnes.fr/vgtprep/vgt2000/wouters.html> (accessed 15 Nov. 2003; verified 26 Oct. 2004).
- Yin, Z., and T.H.L. Williams. 1997. Obtaining spatial and temporal vegetation data from Landsat MSS and AVHRR/NOAA satellite images for a hydrologic model. *Eng. Remote Sens.* 63:69-77.

Page blank

28

CHAPTER 3

Crop Yield Assessment under Climate Uncertainty

Mario Tiscareño-Lopez, Alma Delia Baez-Gonzalez, and Jose Luis Ramos-Gonzalez

CONTENTS

Introduction	29
ENSO Background	30
ENSO Scenarios	32
Plant Growth Simulation	32
Assessing Changes in Crop Yield	33
Results and Discussion	35
Climate Deviations	35
Crop Yield Changes	41
Conclusions	43
References	43

INTRODUCTION

Agricultural production in Mexico is largely driven by the amount of precipitation and temperature occurring during the summer and winter months. It is estimated that nearly 75% of grain crops are rain-fed produced in marginal lands. However, only 14 million tons of maize - the major staple crop in Mexico – is produced annually under rain-fed conditions in low-fertility, high-salinity soils or under steep-slope agriculture in central and southern Mexico. Eventual changes or departures of climate from its regular pattern cause reductions in crop yield, thereby affecting national food security. These climatic changes include not only precipitation reductions but also high variability in air temperature, resulting in warm winters and cold summers due to unusual extreme-minimum and extreme-maximum temperature values that affect plant growth.

In addition, significant climate change has been identified in regions subject to desertification processes; this is based on analyses of long-term historical weather records. Thus, global environmental changes undoubtedly affect agriculture in drylands, but these changing climate conditions seem to affect most the very vulnerable mid-latitude temperate and tropical regions throughout the world that are in a process of desert expansion. Mexico is one of these countries, and the recently observed climatic stresses have severe negative impacts on the country's economy and natural resources.

During the last two decades, scientific research has been directed at identifying major causes of drought and floods and understanding their inherent cyclical patterns in most parts of the world. It is envisioned that water stress forecasts made a few months in advance of the growing season could alleviate the impact of extreme climatic phenomena by altering crop decisions. For instance, farmers could plant alternative crops that are resistant to water stresses. Also, growing low water consumption varieties with a minimum amount of water collected by irrigation dams could help grain production.

Studies have shown that the interannual variability of ocean surface temperatures in the equatorial central and eastern Pacific is linked to persistent regional and global atmospheric anomalies. Uncommon dry and wet conditions over North America can result from abnormal warming in the equatorial Pacific and low atmospheric pressure in the South Pacific. This warming of the sea water, called El Niño by the Peruvians, results when the normal pattern of global precipitation becomes disrupted (Ropelewsky and Halpert, 1986).

This chapter presents the results of simulating plant growth for several species of grain and vegetable crops grown under rain-fed and irrigated conditions in five states of Mexico in order to determine the effects of ENSO scenarios. The baseline of this study is the application of a process-based model parameterized with climate information related to El Niño, La Niña, and Neutral episodes in Mexico.

ENSO BACKGROUND

El Niño Southern Oscillation (ENSO) is a coined term referring to the sea surface water temperature increase in the tropical Pacific Ocean associated with changes in wind direction due to barometric pressure oscillations in the Southern Pacific, which trigger climate anomalies in most parts of the American continent and other regions of the world. The ENSO-related atmospheric and oceanic processes cause a nutrimental content decrease in sea water (plankton) along the South American coast and, consequently, a diminution of important marine species (Rasmusson, 1985; Glantz, 1996).

Meteorological information registered since the beginning of the 20th century in various sites of the American continent has enabled scientists to identify the recurrence of dry and wet periods that coincide with periods of heating and cooling of sea surface waters of the Pacific Ocean. However, it was only recently that a teleconnection between the atmospheric and oceanic conditions of the region 4°S - 4°N, 150°W - 90°W of the Tropical Pacific and the prevailing climate in various parts of the world was identified. The intensive meteorological and marine monitoring of the Pacific Ocean expedited the description of El Niño events registered in the decades of the 80s and 90s with a high degree of reliability (Trenberth and Brandstadter, 1992; Izaurrealde et al., 1998).

Regarding Mexico, it is well-documented that the drought that affected a large extent of the country at the end of 1982 and during 1983, with damages approximating 600 million U.S. dollars, was caused mainly by the presence of El Niño 1982-83 (Canby, 1984). It is believed that the national decline of maize production and the abandonment of cropland fields by farmers were triggered by the El Niño phenomena. At least six of nine El Niño events that occurred after 1960 caused significant slumps in national maize production (Fig. 3-1).

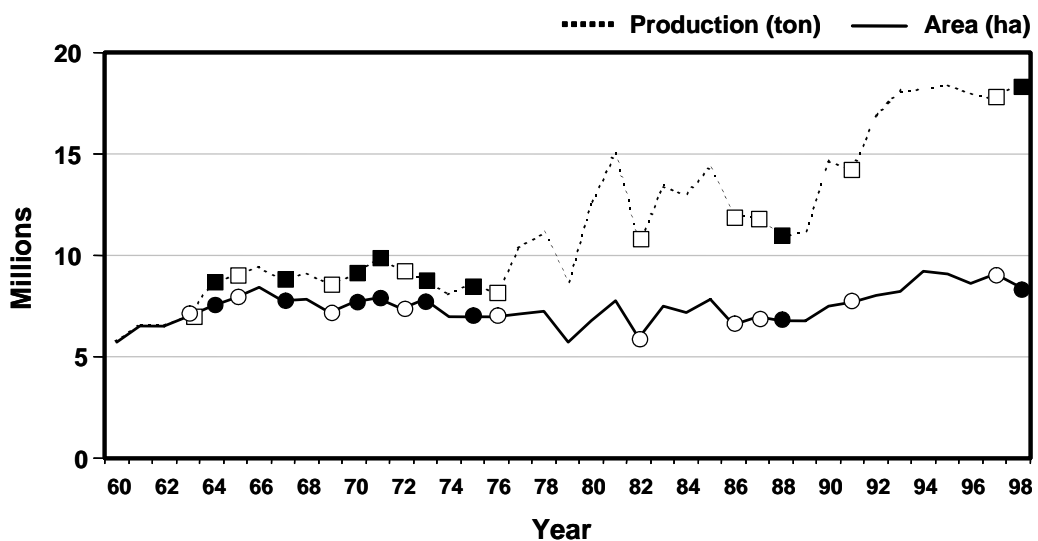


Fig. 3-1. Land use with maize and national maize production in Mexico. White squares and circles represent El Niño years. Black squares and circles represent La Niña years.

Due to the importance of the ENSO phenomena, scientific studies on climate have focused on exploring their impact on agricultural productivity. For example, Cane et al. (1994) identified crop yield reductions in rain-fed areas in Africa during warm phases of ENSO in the Pacific Ocean. This development has led financial analysts of agricultural markets to consider ENSO as an indicator for fixing crop prices, taking into account continental precipitation variations that affect the yield of rain-fed crops. This has raised expectations about the economic value of predictions of climate under the influence of ENSO as they are related to agricultural activities. Solow et al. (1998) estimate that recent improvements of climatic predictions in the United States of America have benefited US agriculture by more than US\$ 200 million per year.

Adams et al. (2003) studied the benefits of establishing an ENSO early warning system for Mexico, as represented by the states of Guanajuato, Jalisco, Mexico, Michoacan, and Tamaulipas. Based on a 51-yr period of El Niño event frequencies (25.5%) and when a forecast skill of 70% is assumed, the benefit approximates US\$ 10 million annually. This value translates into an internal rate of return of approximately 30% for such an early warning system. The values for higher skill levels are correspondingly higher. The present net value of the ENSO early warning system of 70% accuracy ranges from US\$ 36 to 55 million, depending on the frequency of ENSO events that is assumed for the system.

ENSO SCENARIOS

To model the ENSO phenomena, based on the concept of teleconnections, it was necessary to identify ENSO scenarios and to establish their relationship with the prevailing climate in different regions of the country. For this purpose, the Thermal Abnormality Index (τ) developed by the Japan Meteorological Agency was used; it is the sea surface water temperature (SST) of the 90°-150° W and 4° N at 4° S geographically delimited region in the Pacific Ocean. τ is the 5-month running mean of SST anomalies over this region. An ENSO year covers the period from 1 October to 30 September. An El Niño (EN) year occurs when $0.5 \leq \tau < 2.0$ °C during six consecutive months, starting 1 October. An El Viejo (EV) year occurs when $\tau \leq -0.5$ °C. A year is Neutral (N) when $-0.5 < \tau < 0.5$ °C. A fourth category is Strong El Niño (SEN), assigned to those years when $\tau > 2.0$ °C for two consecutive months, instead of six consecutive months as in other scenarios. Considering a period with complete meteorological data from 1960 to 1989, six events have been classified as EN (1963, 1965, 1969, 1976, 1986 and 1987), two as SEN (1972 and 1982), seven as EV (1964, 1967, 1970, 1971, 1973, 1975 and 1988), and the rest as Neutral years.

PLANT GROWTH SIMULATION

Plant growth was simulated with the Erosion Productivity Impact Calculator (EPIC) model developed by Williams (1995). EPIC is a process-based continuous simulation model that uses basic information of soils, climate, and crop management to estimate crop yield and hydrologic responses such as soil water erosion. Major components of the model are stochastic weather generation, surface and subsurface hydrology, erosion-sedimentation processes, nutrient cycling, plant growth, cultivation practices, and accounts of the effects of pests and diseases on the simulated plant biomass. Governing equations of major processes simulated by EPIC are given by Tiscareño et al. (2004).

The climate component of EPIC is a stochastic weather generator that applies a Markov chains scheme to produce series of daily precipitation (Nicks, 1974) and maximum and minimum air temperature correlated with solar radiation (Richardson, 1981). For the generation of synthetic series of EN, EV, SEN, and N scenarios, the stochastic dependence of wet and dry days within the actual climate series obtained from each meteorological station was calculated. This made it possible to estimate the transition probabilities of rainy days and dry days for the generation of rainy events. Rainfall depth was generated with a normal asymmetric function (Sharpley and Williams, 1990).

The EPIC model calculated daily potential plant growth as a function of a crop-specific radiation-use efficiency and canopy-intercepted photosynthetically active radiation. Vapor-pressure deficit and CO₂ influenced the conversion of solar energy into plant biomass (Stockle et al., 1992). Average daily air temperature determined the rate of photosynthesis, respiration, transpiration, and the phenology of plant development. The level of nitrogen and phosphorus available in the soil also influenced the rate of plant growth. The crop yield is thus a result of the accumulated plant biomass multiplied by a harvest efficiency index that utilizes a non-linear function of accumulated heat units, from zero in the moment of seeding up to the highest production value at crop maturity (Sharpley and Williams, 1990).

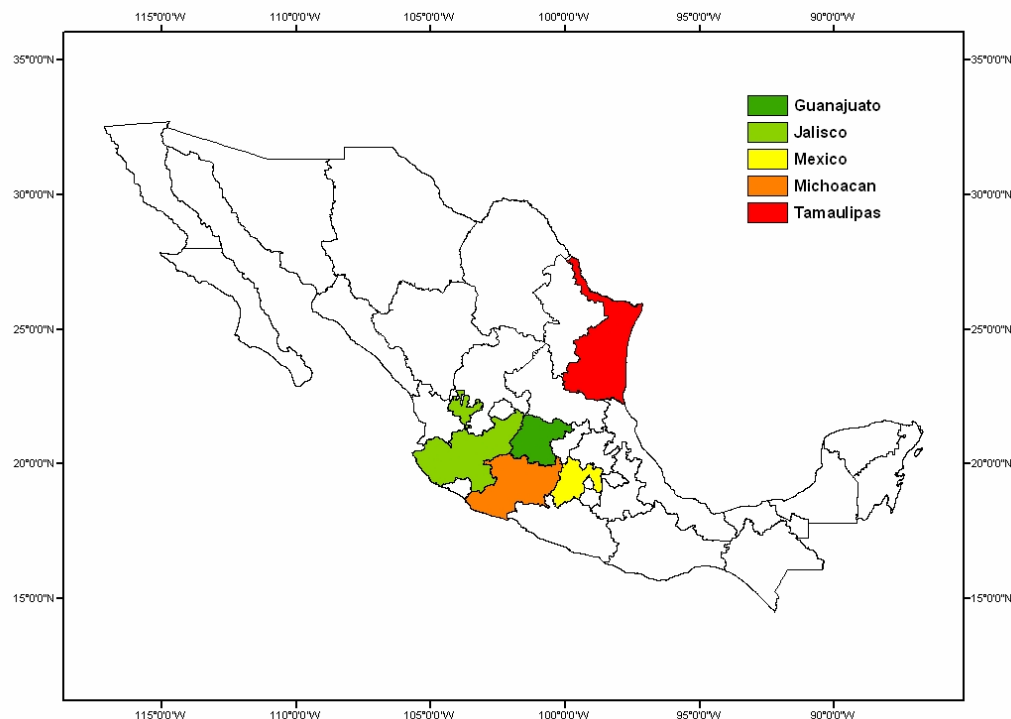


Fig. 3-2. Location of the Mexican states of Guanajuato, Jalisco, Mexico, Michoacan, and Tamaulipas.

Potential evapotranspiration (PET) and actual evapotranspiration (AET) were other variables of interest in the study because the changes in the patterns of precipitation and temperature affect water usage by the crop. PET was calculated using the Priestley-Taylor method (Priestly and Taylor, 1972) since there was a lack of daily data on solar radiation and wind velocity, while AET was computed using a procedure developed by Ritchie (1972), where plant transpiration is a function of PET and the leaf-area index of the crop. Direct evaporation of water from the soil was determined by the soil water content, the canopy cover that determines the amount of direct solar radiation reaching the soil, and the wind velocity (Sharpley and Williams, 1990).

ASSESSING CHANGES IN CROP YIELD

Yields of seven rain-fed and nine irrigated crops were simulated with EPIC for the effects of El Niño, La Niña, and Neutral years in the states of Guanajuato, Jalisco, Michoacan, Mexico, and Tamaulipas (Table 3-1 and Fig. 3-2). These crops account for 95 to 98% of the state's agricultural production under rain-fed and irrigated conditions. Previous ENSO research by Tiscareno et al. (1998) and Izaurrealde et al. (1998) identified variable sensitivity to warm/cold ENSO episodes in regions of Mexico for corn, wheat, and bean crops following the methodology developed by the Center for Ocean-Atmospheric Predictions Studies of the Florida State University for classifying El Niño, La Niña, and Neutral years.

Table 3-1. Simulated crops (by growing season) in five states of Mexico.

Crop	Guanajuato	Jalisco	Michoacan	Mexico	Tamaulipas
Silage Oat		s-s / f-w		s-s / f-w	
Barley	s-s / f-w				
Bean	s-s	s-s	s-s		s-s / f-w
Silage Corn	s-s	s-s		s-s	
Grain Corn	s-s	s-s	s-s	s-s	s-s / f-w
Potato	s-s / f-w	s-s	s-s / f-w	s-s / f-w	f-w
Silage Sorghum		s-s			
Grain Sorghum	s-s	s-s	s-s		f-w
Soybean					s-s
Grain Wheat	f-w	f-w	f-w		

s-s = spring-summer, f-w = fall-winter

A database of climate, soils and crop management information of representative farms in the states was used to build the EPIC input files (Table 3-2). Daily weather records obtained from 67 meteorological stations in the states were used to compute the following monthly climate parameters: mean and standard deviation of maximum and minimum air temperature, total and standard deviation of monthly precipitation, skewness coefficient of the precipitation normal distribution, transition probabilities for the occurrence of rain, and number of rainy days within the month.

Table 3-2. Geographical location and soil and climate characteristics of sites for the simulation of crop growth.

STATE	Latitude	Longitude	Elevation	Soil type	TEMPERATURE				PRECIPITATION				
					DJF	MAM	JJA	SON	DJF	MAM	JJA	SON	
Jalisco	20° 33'	102° 41'	1420	Regosol	17.8	22.7	23.2	21.5	42	43	567	211	863
Michoacan	20° 05'	101° 30'	1848	Vertisol	15.6	20.9	20.3	18.5	35	59	501	219	814
Guanajuato	23° 32'	100° 49'	1765	Vertisol	13.6	19.2	20.1	17.4	44	71	394	156	665
Tamaulipas	25° 59'	98° 06'	28	Vermudoll	15.0	23.2	28.3	24.2	109	153	160	192	615
Mexico	19° 29'	98° 53'	2250	Vertisol	13.0	17.5	17.5	15.6	25	101	334	149	610

†Months of the year

RESULTS AND DISCUSSION

The identification of changes in precipitation and temperature from their regular patterns resulting from different ENSO phases was an important aspect of this study. Variations in precipitation and air temperature throughout the year affected crop development, mainly under rain-fed conditions. The following is a description of the major climate deviations during the ENSO phases.

Climate Deviations

Mexico State (Fig. 3-3a, Fig. 3-3b, Fig. 3-3c): Colder years under EN and LN conditions were detected in the state of Mexico. Reductions in maximum temperature were found during summer and winter months during both EN and LN. Also a decrease in minimum temperature was detected for LN years. However, there were warmer winters (Dec.-Mar.) during EN since minimum temperature increases were above those of normal neutral conditions. There was a tendency toward hot and dry spring months. May and June appeared to have above-normal maximum temperature, and rainfall reductions were up to 40% from March to June. In addition, summer precipitation was quite variable under EN.

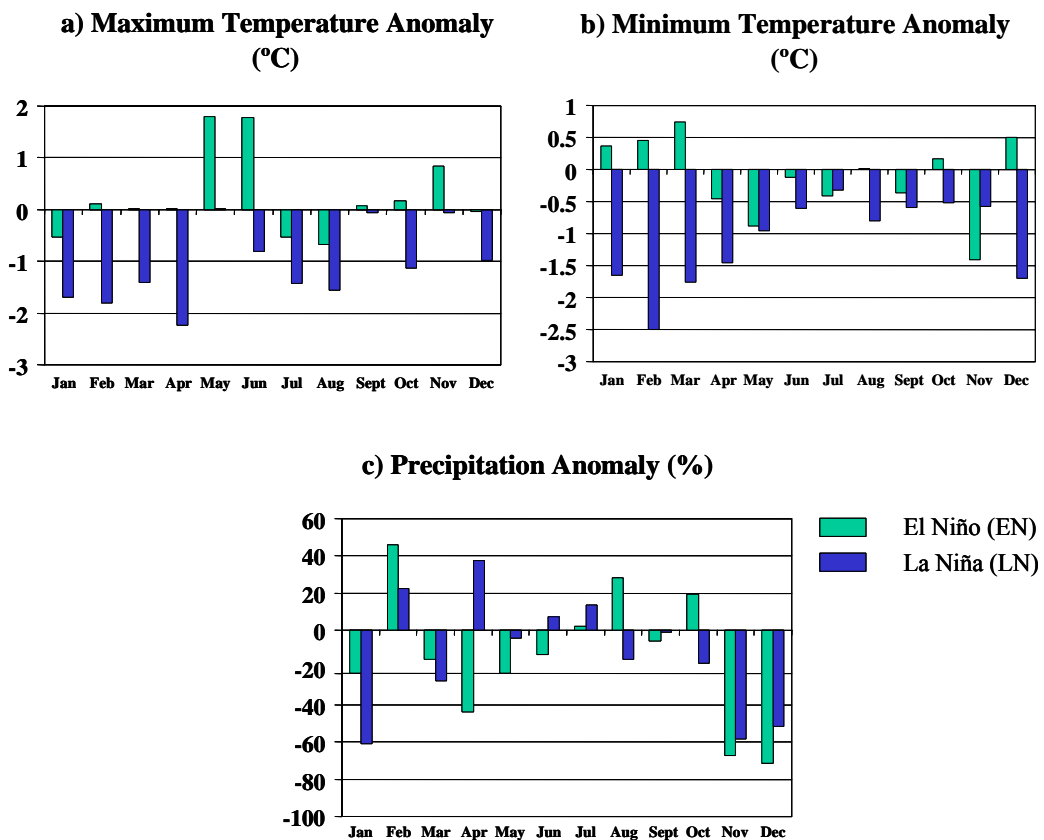


Fig. 3-3. Climate variations during EN and LN years in Mexico State.

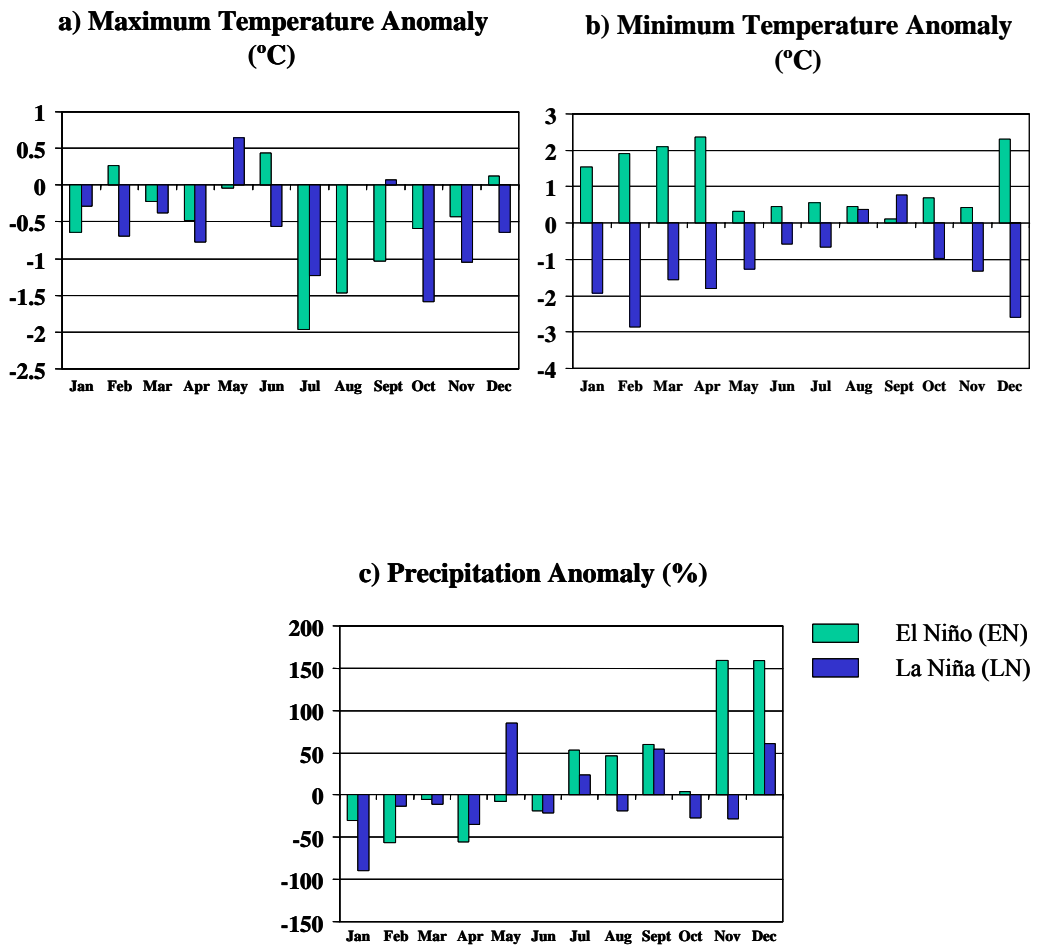


Fig. 3-4. Climate variations during EN and LN years in Guanajuato State.

Guanajuato State (Fig. 3-4a, Fig. 3-4b, Fig. 3-4c): Mild temperature tended to occur in Guanajuato during EN years. A reduction in maximum temperature and an increase in minimum temperature were observed throughout the EN year. On the other hand, colder conditions were more likely to develop in LN years since both maximum temperature and minimum temperature decreased. The amount of precipitation could rise up to 50% in EN summers, and such increase could last until December. But rainfall during LN years was very variable, resulting in a severe reduction in precipitation during the “La Canícula” period (from 15 July to 15 August).

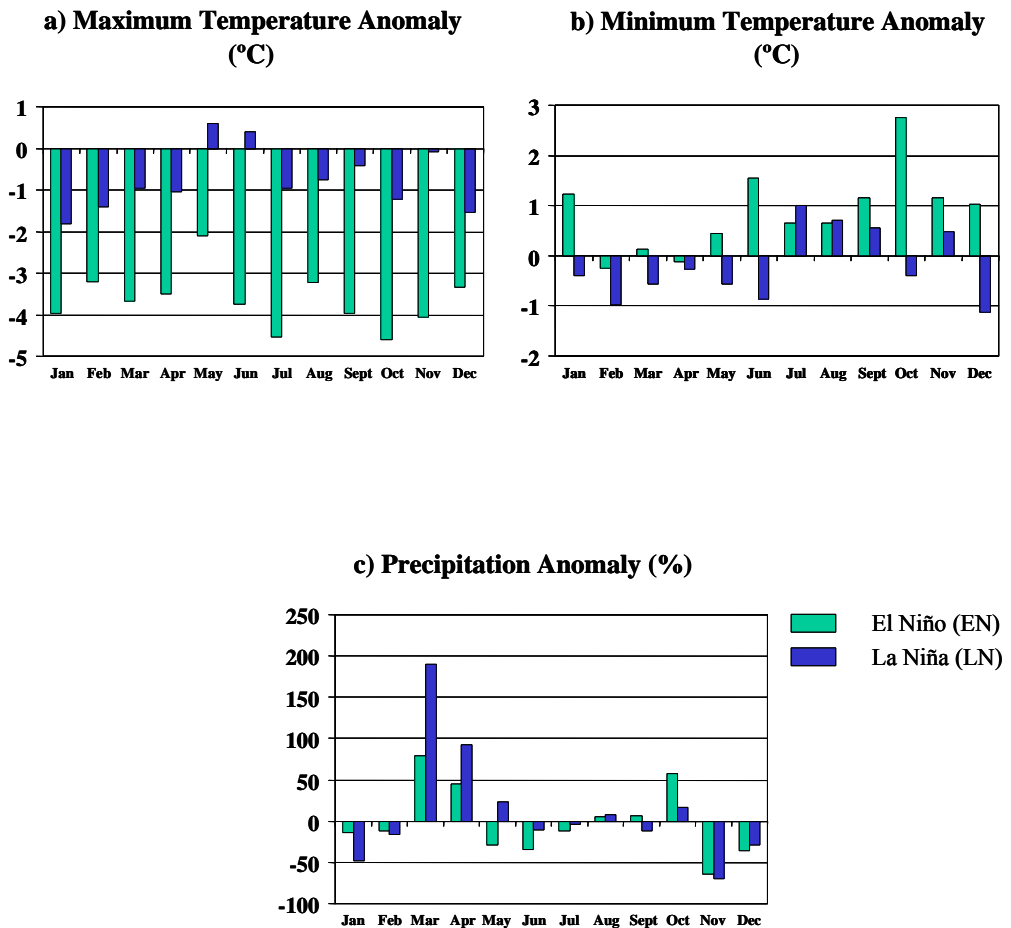


Fig. 3-5. Climate variations during EN and LN years in Jalisco State.

Jalisco State (Fig. 3-5a, Fig. 3-5b, Fig. 3-5c): Maximum temperature decreased during both EN and LN years in Jalisco. EN and LN summers experienced warmer conditions due to an increase in minimum temperature, but during winter and spring months, minimum temperature tended to be below its normal monthly mean. Because of the slight deviations of rainfall from its normal pattern during EN and LN summers, Jalisco appeared insensitive to the ENSO phenomena in terms of precipitation during the wet season of the year. It is remarkable that precipitation rose during EN and LN springs.

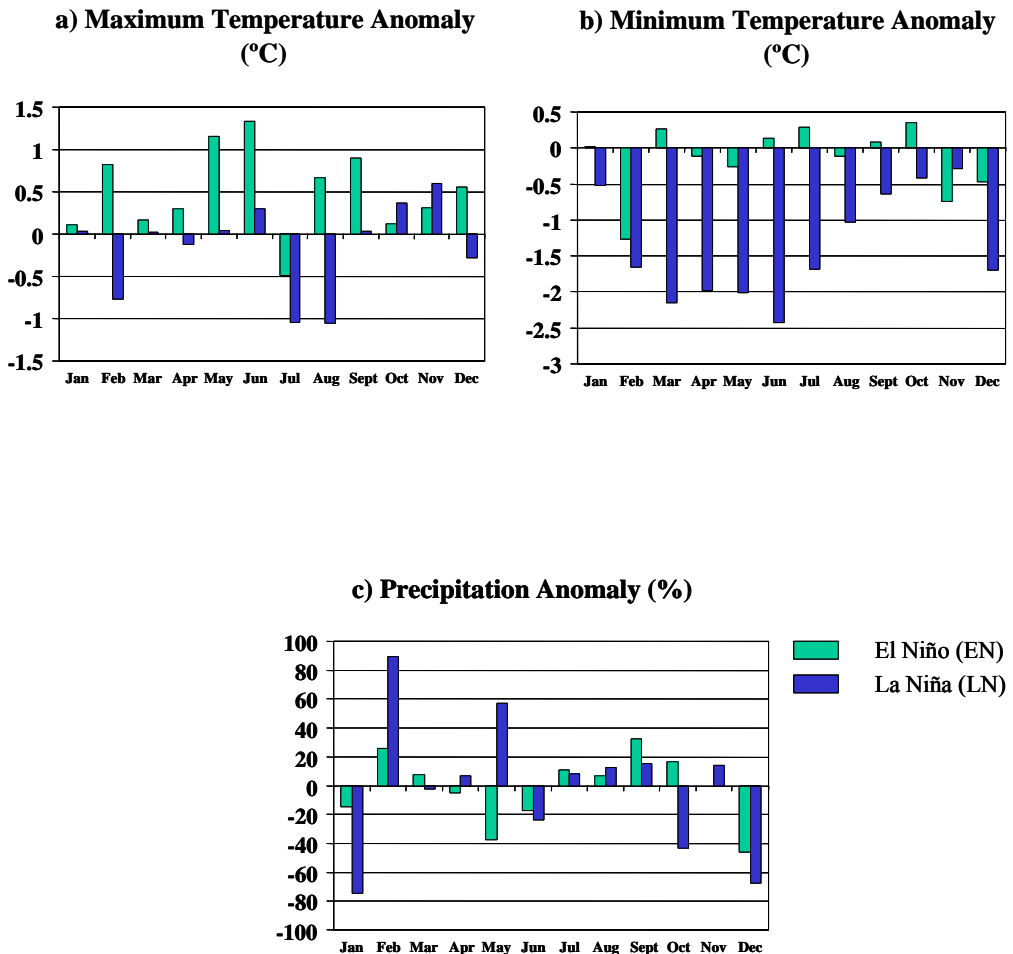


Fig. 3-6. Climate variations during EN and LN years in Michoacan State.

Michoacan State (Fig. 3-6a, Fig. 3-6b, Fig. 3-6c): In Michoacan, maximum temperature increased throughout EN years, and a drop in minimum temperature was observed during LN years. Rainfall had a tendency to increase from July to August during both EN and LN years; however, winter precipitation was reduced by nearly 70% during LN and 50% during EN events.

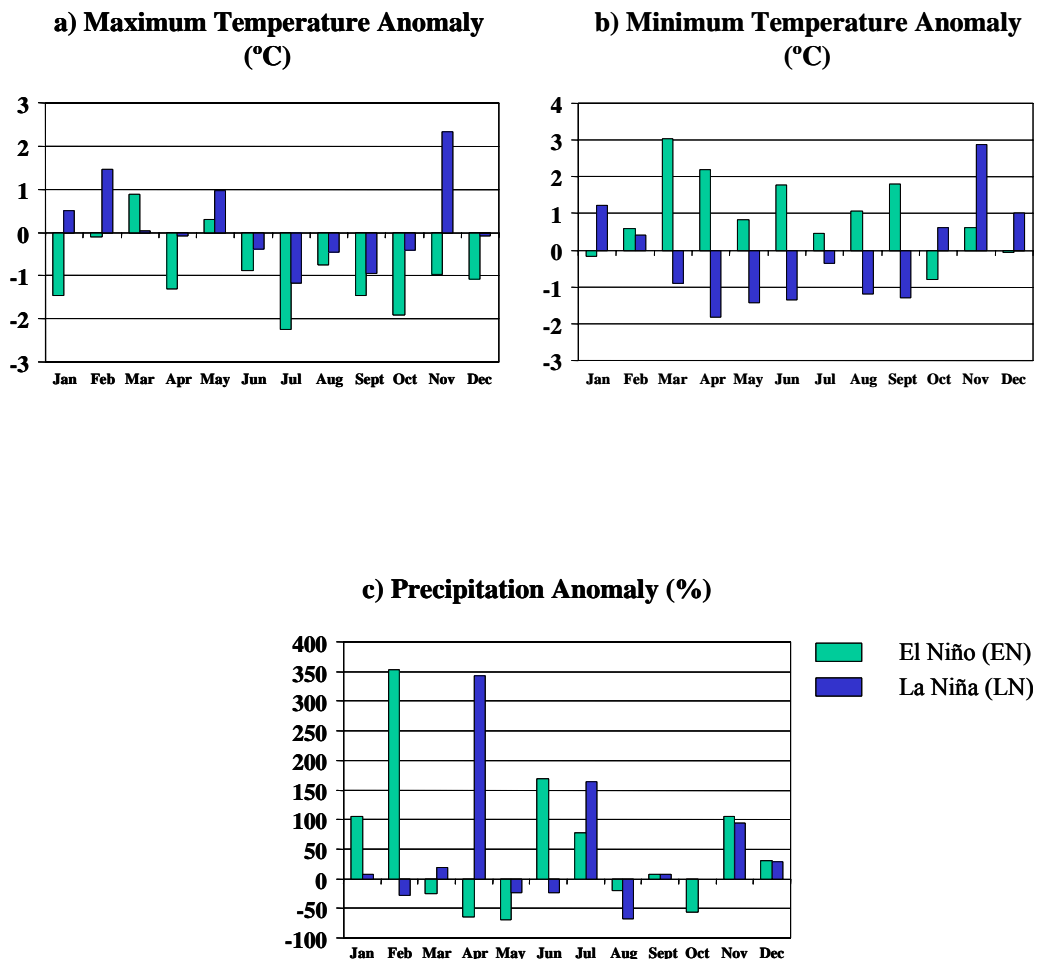


Fig. 3.7. Climate variations during EN and LN years in Tamaulipas State.

Tamaulipas State (Fig. 3-7a, Fig. 3-7b, Fig. 3-7c): Summers under EN and LN conditions in Tamaulipas showed a reduction in maximum temperature for both EN and LN, while minimum temperature increased during most of the months during EN years. Wet winters followed by warm springs were detected during EN years because minimum temperature and rainfall amount increased from October to February. An irregular deviation pattern of summer precipitation was identified for both EN and LN years; increments were detected in June and July, as well as rainfall reduction in August and October.

Table 3-3. Deviations of yield of rain-fed crops, actual and potential evapotranspiration in 30-yr crop growth simulation for El Niño (EN) and La Niña (LN) phases in Mexico.

	Season	Yield			Actual Evapotranspiration			Potential evapotranspiration					
		Deviation		Neutral	Deviation		Neutral	Deviation					
		Neutral	El Niño		La Niña	El Niño		Neutral	El Niño	La Niña			
									ton ha ⁻¹	mm			
										mm			
CORN													
Guanajuato	s-s	2.5	0.2	0.2	606	42	-36	2,580	-169	55			
Jalisco	s-s	6.2	0.5	-0.1	736	-29	-25	2,852	-106	-88			
Mexico	s-s	3.6	0.7	-0.5	610	-24	-2	2,596	10	-36			
Michoacan	s-s	7.1	-0.1	0.2	703	-6	-23	2,501	29	117			
Tamaulipas	s.s	3.2	-0.7	-0.4	535	175	54	2,340	-34	39			
SORGHUM													
Guanajuato	s-s	4.1	-0.5	0.1	616	-93	39	2,586	-180	10			
Jalisco	s-s	6.1	0.0	0.3	764	-42	52	2,843	-61	-89			
Michoacan	s-s	4.5	-1.5	-0.9	624	-150	5	2,491	-16	113			
Tamaulipas	f-w	2.6	-1.2	0.5	534	102	82	2,352	-50	31			
BEAN													
Guanajuato	s-s	1.8	-0.1	-0.1	556	48	-2	2,628	-168	-3			
Jalisco	s-s	1.2	0.1	0.0	640	84	46	2,849	-52	-94			
Michoacan	s-s	1.0	0.1	-0.2	581	35	7	2,525	43	101			
Tamaulipas	f-w	1.2	-0.1	0.0	516	57	48	2,375	-44	37			
BARLEY													
Guanajuato	s-s	3.2	0.2	0.1	592	48	-3	2,613	-63	13			
SILAGE CORN													
Guanajuato	s-s	26.6	0.7	-1.3	593	63	0	2,621	-66	11			
Jalisco	s-s	37.7	2.3	2.3	718	76	38	2,831	-58	-96			
Mexico	s-s	42.6	7.4	-2.6	598	-18	-24	2,535	-59	-107			
SILAGE SORGHUM													
Jalisco	s-s	51.0	2.6	4.6	764	42	55	2,845	-60	-97			
SILAGE OAT													
Jalisco	s-s	8.3	3.3	2.1	445	96	64	2,839	-58	-94			
Mexico	s-s	20.4	0.4	-0.4	594	-44	-38	2,519	-7	-75			
ONION													
Michoacan	s-s	22.5	0.0	0.0	698	-64	-95	2,526	44	100			
Guanajuato	s-s	22.0	-2.0	1.0	525	41	-3	2,625	-64	13			
Tamaulipas	f-w	14.5	8.5	2.5	511	58	50	2,373	-44	35			

Crop Yield Changes

Model results in simulating yields for eight crops under rain-fed conditions are presented in Table 3-3. Actual evapotranspiration (AET) and potential evapotranspiration (PET) were calculated as total annual losses under ENSO climate scenarios EN and LN. It is important to recall that dryland agriculture is established during the rainy season of the year, which goes from June to October; however, differences in amount and distribution of precipitation exist among the geographical locations of the states. Only in Tamaulipas does rain-fed agriculture occur during the fall-winter season.

In the case of rain-fed corn, Tamaulipas appeared as the most sensitive state for EN and LN conditions; crop yield was reduced by 700 and 400 kg ha⁻¹ from the average crop yield of Neutral years (3.2 ton ha⁻¹) during EN and LN, respectively. On the other hand, Michoacan and Jalisco were the states most insensitive to the ENSO phases for corn production. Important differences in corn yield were observed among the states during Neutral conditions; these were closely related to the average climatic conditions of each state.

Sorghum was not affected by EN and LN conditions in Jalisco, but it was affected in Michoacan, where yield could decrease by 1500 and 900 kg ha⁻¹ during EN and LN years, respectively. Yield of rain-fed sorghum diminished in Tamaulipas during EN years by 1200 kg ha⁻¹, so expected yield is approximately 1400 kg ha⁻¹.

In general, rain-fed beans were not very sensitive to EN or LN conditions, while barley yield in Guanajuato could be diminished by 200 kg ha⁻¹.

Silage crops, corn, sorghum and oat improved their yield under EN conditions in all the studied states of Mexico. However, reductions in yield were detected in the case of corn and oat during LN years. This indicates that water deficits resulting from ENSO phases tend to affect grain development, probably mainly during the flowering stage.

On the other hand, irrigated crops were simulated by fixing water application parameters for crop growth under no water stress. It is important to mention that irrigation amount does not account for the water application efficiency of a given farm located in an irrigation district of any state. Practically speaking, the effects of climate on irrigated crops are mostly observed on water demand, not on crop yield that is more related to management practices. Results of irrigated crops are presented in Table 3-4.

Results indicated that corn demanded much more water (32 to 84 mm) during EN years for Guanajuato, Tamaulipas, Mexico, and Michoacan, but not for Jalisco, where irrigated water was reduced by 73 mm. Also, Jalisco during LN years required 103 mm less water, while water demand increased in Tamaulipas by 92 mm. Corn for silage required less water during both EN and LN, with the exception of Mexico State under EN, which required an additional 19 mm of water. The insensitivity of Jalisco to ENSO phenomena is reflected in much less water demand for corn. As for Tamaulipas, it was sensitive to both EN and LN since water demand by corn increased.

Sorghum was much more variable in relation to the effects of ENSO on water demand. It required less water in Guanajuato and more water in Tamaulipas during both EN and LN. About one additional water application in Tamaulipas for EN and LN years was required to grow sorghum. Silage sorghum in Jalisco was insensitive to EN years in terms of water demand, but positively sensitive during LN years because it required 31 mm less water.

Table 3-4. Deviations of yield of irrigated crops, evapotranspiration, and water demand (irrigation) in 30-yr crop growth simulation for El Niño (EN) and La Niña (LN) phases in Mexico.

	Yield			Actual Evapotranspiration			Potential Evapotranspiration			
	Season	Deviation		Neutral	Deviation		Neutral	Deviation		
		Neutral	El Niño	La Niña	Neutral	El Niño	La Niña	Neutral	El Niño	La Niña
ton ha ⁻¹										
CORN										
Guanajuato	s-s	9.1	0.1	0.1	860	10	-19	2,612	14	-5
Jalisco	s-s	10.7	-1.6	-0.6	1330	20	-17	2,851	20	78
Mexico	s-s	9.0	0.1	0.1	1107	-6	-59	2,538	-42	-91
Michoacan	s-s	9.3	0.0	0.9	1131	21	52	2,489	29	115
Tamaulipas	s-s	4.8	0.7	0.3	925	104	72	2,330	-35	40
Jalisco	s-s	9.1	0.1	0.1	860	10	-19	2,612	14	-5
SORGHUM										
Guanajuato	s-s	9.0	-0.2	-0.1	1482	31	30	2,578	-65	4
Jalisco	s-s	8.0	-1.0	-0.5	1572	25	-42	2,823	-42	93
Michoacan	s-s	8.6	-0.2	0.4	1654	46	49	2,480	44	97
Tamaulipas	f-w	7.7	0.3	0.2	1513	15	20	2,346	-51	11
WHEAT										
Guanajuato	f-w	5.3	0.0	0.1	950	62	127	2,609	13	-22
Jalisco	f-w	3.6	1.0	0.3	763	186	123	2,909	-453	94
Michoacan	f-w	4.2	-0.2	-0.3	1118	10	-7	2,490	68	106
BEAN										
Guanajuato	s-s	2.5	0.0	0.1	634	21	-14	2,609	-166	-2
Jalisco	s-s	2.9	0.1	-0.1	1933	10	-80	2,821	-54	-93
Michoacan	s-s	2.5	-0.1	-0.2	1997	-8	86	2,498	41	100
Tamaulipas	f-w	2.2	0.2	0.2	1396	-5	25	2,555	-242	-163
POTATO										
Guanajuato	s-s	20.5	0.1	-0.4	1687	-50	6	2,574	-61	15
Jalisco	s-s	13.9	2.2	0.7	1837	-6	-94	2,928	-36	-113
Mexico	s-s	18.7	1.1	1.9	1629	-53	-21	2,518	-68	111
Michoacan	s-s	19.8	-0.8	1.2	1929	0	54	2,478	44	99
Tamaulipas	f-w	9.5	-0.2	1.0	927	15	33	2,358	-44	33
Guanajuato	f-w	17.6	-0.7	-0.2	1605	12	28	2,566	-65	12
Mexico	f-w	19.9	0.0	0.7	1610	-17	-117	2,500	-68	-136
Michoacan	f-w	16.2	-2.1	1.5	1752	25	98	2,451	45	132
BARLEY										
Guanajuato	f-w	6.7	0.2	0.7	1128	98	41	2,591	-66	-2
SILAGE CORN										
Guanajuato	s-s	88.0	-1.4	-0.7	886	40	-6	2,587	-64	12
Jalisco	s-s	86.6	-12.2	-5.3	1331	40	-8	2,851	-32	-84
Mexico	s-s	78.0	1.0	1.5	1122	-15	-77	2,533	-68	-114
SILAGE SORGHUM										
Jalisco	s-s	66.0	-9.4	-4.7	1598	16	-34	2,824	-42	-85
SILAGE OAT										
Jalisco	f-w	18.3	11.3	6.3	697	152	127	2,822	-418	-80
Mexico	f-w	43.3	-1.3	0.8	1188	-20	-22	2,500	-6	-78
Mexico	s-s	18.3	-5.4	2.5	998	-56	-2	2,522	-1	-75

Wheat, which is grown during the fall-winter season, required more water in Guanajuato, Jalisco, and Michoacan during both EN and LN years. This is related to the reduction in rainfall during winter months and warming conditions close to spring. In the case of barley, which, along with wheat, is largely cultivated in Guanajuato, water demand increased for both EN and LN.

Beans produced in the states of Guanajuato, Jalisco, and Michoacan during the spring-summer season required less water (26 to 46 mm) during EN and LN years than during Neutral years. Also, beans grown in Tamaulipas during the fall-winter season needed less water during EN and LN years.

Potato grown during both spring-summer and fall-winter seasons required less water in most of the states during EN and LN years. An exception was in the state of Mexico during EN fall-winter seasons since water demand increased by 32 mm. Finally, silage oat required less water in the states of Jalisco and Mexico when it was grown during the fall-winter months.

CONCLUSIONS

Based on the results of this research, which aimed to use a process-based biophysical simulation model to identify the impact of the ENSO climate phenomena on agricultural production of basic crops, it is evident that ENSO-derived climate scenarios induce crop yield changes which have impacts on regional and national agricultural productivity.

Alterations in precipitation and temperature patterns vary among regions, depending on the ENSO phase and its intensity. At regional scale, the study identified drier winters under the influence of La Niña (LN), more humid winters during El Niño (EN) years, dry summers in EN years, and humid summers in LN years. The identification of such patterns of precipitation due to ENSO phenomena is an outcome of this research that is relevant for decision-making on crop management in Mexico.

REFERENCES

- Adams, R.M., L.L. Houston, B.A. McCarl, M. Tiscareño L., J. Matus G., and R.F. Weiher. 2003. The benefits to Mexican agriculture of an El Niño-Southern Oscillation (ENSO) early warning system. *J. Agric. For. Meteorol.* 115:183-194.
- Canby, T.Y. 1984. El Niño's ill wind. *National Geographic*, Feb. 144-183.
- Cane, M.A., G. Eshel, and R.W. Buckland. 1994. Forecasting Zimbabwean maize yield using eastern equatorial Pacific sea surface temperature. *Nature* 370:204-205.
- Glantz, M.H. 1996. Currents of change: El Niño's impact on climate and society. Cambridge University Press, Cambridge.
- Izaurralde, R.C., N.J. Rosenberg, R.A. Brown, D.M. Legler, M.Tiscareño L., and R. Shrinivasan. 1998. Modeled effects of moderated and strong "Los Niños" on crop productivity in North America. *J. Agric. For. Meteorol.* 94:259-268.
- Nicks, A.D. 1974. Stochastic generation of the occurrence, pattern, and location of maximum amount of daily rainfall. p. 154-171. *In Proc. Symp. Statistical Hydrology*, Tucson, AZ. Aug.-Sept. 1971. USDA Misc. Publ. No. 1275.
- Priestley, C.H.B. and R.J. Taylor. 1972. On the assessment of surface heat flux and evaporation using large-scale parameters. *Monthly Weather Rev.* 100:81-92.

- Rasmusson, E.M. 1985. El Niño and variations in climate. *American Scientist* 73:168-173.
- Richardson, C.W. 1981. Stochastic simulation of daily precipitation, temperature, and solar radiation. *Trans. ASAE* 25(3): 735-739.
- Ritchie, J.T. 1972. A model for predicting evaporation from a row crop with incomplete cover. *Water Resources Research* 8:1204-1213.
- Ropelewsky, C.F., and M.S. Halpert. 1986. North American precipitation and temperature patterns associated with the El Niño-Southern Oscillation (ENSO). *Monthly Weather Rev.* 423: 52-62.
- Sharpley, A.N., and J.R. Williams. 1990. The nutrient component of EPIC. p. 152-166. *In* A.N. Sharpley and J.R. Williams (ed.) EPIC – Erosion/Productivity Impact Calculator: 1. Model Documentation. USDA Tech. Bull. No. 1768.
- Solow, A.R., R.M. Adams, K.J. Bryant, D.M. Legler, J.J. O'Brien, B.A. McCarl, and W.I. Nayda. 1998. The value of improved ENSO prediction to U.S. agriculture. *Climatic Change* 39:47-60.
- Stockle, C.O., P.T. Dyke, J.R. Williams, C.A. Jones, and N.J. Rosenberg. 1992. A method for estimating direct and climatic effects of rising atmospheric carbon dioxide on growth and yield of crops: Part II Sensitivity analysis at three sites in the Midwestern USA. *Agric. Syst.* 38:239-256.
- Tiscareño Lopez, M., N.J. Rosenberg, D.M. Legler, A. Ruiz Coral, R. Shrinivasan, R.A. Brown, G. Garcia Medina, M.A. Velazquez , and C. Izaurrealde. 1998. Algunos efectos del fenomeno climatico El Niño en la agricultura mexicana. *Ciencia y Desarrollo* 139:5-13.
- Tiscareño Lopez, M., A.D. Baez G., N.J. Rosenberg and C. Izaurrealde. 2004. Modeling El Niño Southern Oscillation climate anomalies to assess their impacts on Mexican agriculture. *J. Geofisica Internacional* 42:331-339.
- Trenberth, K.E., and G.W. Brandstadter. 1992. Issues in establishing causes of the 1988 drought over North America. *J. Climate* 5:159-172.
- Williams, J.R. 1995. The EPIC model. p. 909-1000. *In* V.P. Singh (ed.) Computer models of watershed hydrology. Water Resour. Res. Public. Highlands Ranch, CO.

CHAPTER 4

The Weekly Weather and Crop Bulletin: Integrating Agricultural and Meteorological Data for Decision Makers

Harlan D. Shannon

CONTENTS

Introduction	45
Weekly Weather and Crop Bulletin	46
Agrometeorological Data	47
Analytical Methods	47
Discussion	50
References	50

INTRODUCTION

The United States Department of Agriculture (USDA), World Agricultural Outlook Board (WAOB) is responsible for preparing official government forecasts of agricultural supply and demand for major crop-producing countries worldwide. Because weather has a significant impact on crop progress, conditions, and ultimately production, WAOB employs several meteorologists who prepare agrometeorological assessments in support of agency commodity estimates. Each week, these assessments are disseminated via the *Weekly Weather and Crop Bulletin* (WWCB), a joint publication of the National Oceanic and Atmospheric Administration (NOAA) and USDA intended to keep senior government officials, commercial entities, and the general public abreast of weather impacts on global crop development. This chapter introduces the WWCB and the suite of agrometeorological data and analytical methods that WAOB meteorologists use in preparing these crop weather assessments.

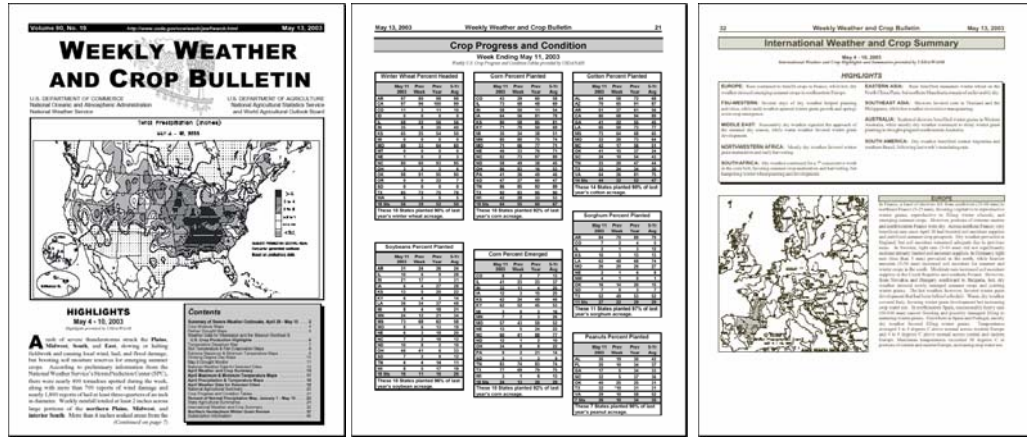


Fig. 4-1. Excerpts from the WWCB, illustrating some of the text, tables, and maps typically published each week.

WEEKLY WEATHER AND CROP BULLETIN

The WWCB is the product of over a century of evolution (Puterbaugh and Rippey, 2002). Initially published in 1872 by the U.S. War Department, the *Weekly Weather Chronicle* provided a brief summary of domestic weather each week. In 1888, the War Department changed the name of this publication to the *Weather Crop Bulletin* and began providing basic crop weather analyses for the United States. Since then, the bulletin has undergone several additional name, content, and management changes, eventually becoming the WWCB in 1924. Despite these changes, the primary goal of the bulletin has remained the same: to provide a comprehensive summary of weather impacts on crop development.

In recent decades, the WWCB has grown into a comprehensive collection of text, tables, and maps describing weather impacts on domestic and international crop production. Several text products appear weekly in the WWCB, including the “U.S. Weather Highlights”, “State Summaries of Weather and Agriculture”, and “International Weather and Crop Summary” (Fig. 4-1a). As companions to these written summaries, tables of weather and crop data are published regularly. For example, tables of precipitation and temperatures for selected cities are published weekly, while crop progress and condition tables for selected crops are published during the growing season (Fig. 4-1b). Maps depicting precipitation and temperatures in major domestic and international crop-producing regions are included as well (Fig. 4-1c). Several maps are included periodically to provide a more detailed description of crop weather in the United States, including maps of soil temperatures, growing degree days, and various drought indices.

The WWCB has become an important source of information for decision makers because it consolidates a wide array of agricultural and meteorological data into a single volume of value-added text and products. Nevertheless, the effectiveness of the WWCB hinges on the accuracy and reliability of raw data that are often not published in the bulletin. Following is a description of the data used in preparing these agrometeorological assessments.

AGROMETEOROLOGICAL DATA

Surface weather observations from point locations have served as an important source of data for conducting agrometeorological analyses because of the close proximity of these weather stations to major growing areas. In international growing areas, the impact of weather on crop progress and conditions is assessed using weather data obtained from the World Meteorological Organization (WMO). Similarly, domestic crop development is monitored using synoptic and cooperative observer data compiled by NOAA. All of these data are archived in the WAOB agricultural weather database to maintain a comprehensive historical record of weather data in major crop-producing regions and thus enable comparisons among the current growing season and prior years (Morris, 2002).

In contrast to these WMO and NOAA data, which are downloaded daily, other meteorological data are obtained less frequently. Nevertheless, these data often play a significant role in assessing weather impacts on crops when extreme weather is observed. For example, data describing the location and intensity of tropical cyclones are often examined when such systems threaten important growing areas. Likewise, data from various mesonetworks (e.g., Florida Automated Weather Network) are used to assess the damage to citrus when freezes are observed.

Remote sensing data complement these surface weather measurements by providing information for areas where surface observations are either sparse or not available. For example, weekly and monthly maps of wetness and temperature anomalies, as derived from the Special Sensor Microwave Imager, help meteorologists determine weather impacts on crop development in parts of the Middle East, Africa, and South America. Similarly, satellite-derived snow cover maps help meteorologists assess the threat of winterkill in areas affected by extreme cold.

Historical crop production and area data are also obtained to identify the major crop producing areas worldwide. These data help staff meteorologists focus their crop weather monitoring efforts on those regions that are agriculturally important and adjust their areas of coverage as cropping patterns change over time. Weekly crop progress and condition data form another important segment of this agrometeorological database. Domestic data are obtained directly from the USDA National Agricultural Statistics Service, while international data are gleaned from news wires and reports issued by various foreign agricultural and statistical agencies.

ANALYTICAL METHODS

Several analytical methods are applied to these agricultural and meteorological data to assess weather impacts on domestic and international crop development. Historical rankings are computed during the growing season (e.g., monthly, seasonally) to determine how precipitation and temperatures in selected regions compare with those in prior years. Similarly, time series analyses are generated to examine how temperature and precipitation patterns vary relative to the stages of crop development, enabling meteorologists to determine how favorable the weather is during critical times of the growing season (Fig. 4-2a). Spatial analyses are valuable in assessing agrometeorological conditions as well (Fig. 4-2b). NOAA meteorologists provide WAOB staff with numerous weekly, monthly, and seasonal maps depicting the weather in important domestic and international growing areas. These and other spatial analyses have been very instrumental in determining the crop acreage affected by favorable and unfavorable weather.

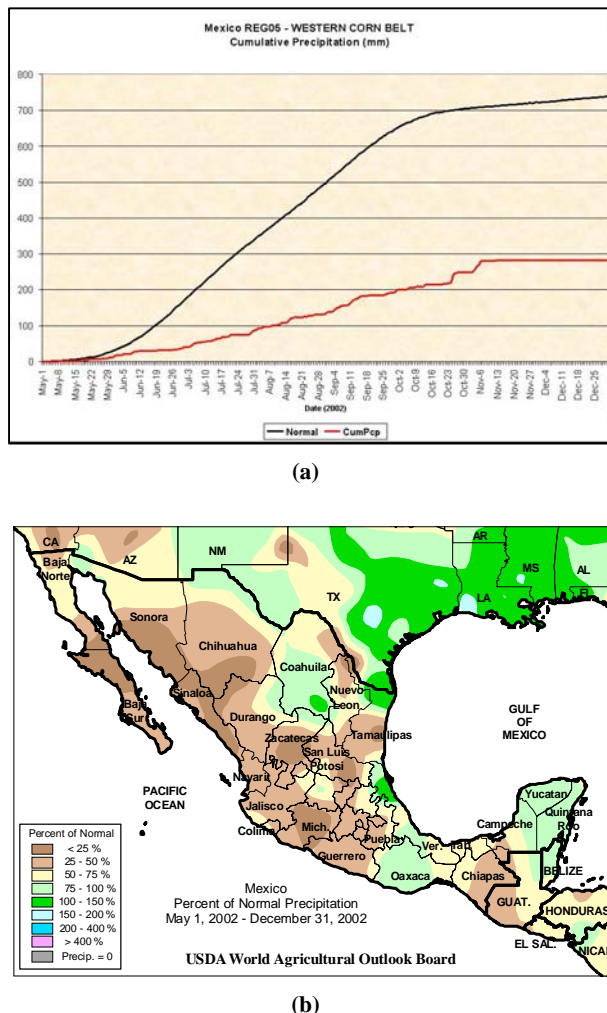


Fig. 4-2. Time series analysis (a) and spatial analysis (b) depicting below-normal rainfall in the Western Corn Belt.

During the past four years, WAOB meteorologists have implemented a geographical information system (GIS) to better analyze these spatial data (Shannon, 2002). Several ArcView 3.2 and ArcGIS 8.2 applications have been developed to facilitate and automate data processing and display, improving staff capabilities to identify and delineate crop areas of concern. Examples of these applications include a fully automated program that plots daily maximum and minimum temperatures and precipitation on regional maps, a semi-automated application that generates weekly, monthly, and seasonal color contour analyses of numerous meteorological variables (Fig. 4-2b), and a semi-automated program that plots weekly crop progress and conditions for various crops in each state.

In addition to these semi-automated applications, GIS has been used to generate products that require more user interaction. For example, each month WAOB meteorologists coordinate with

other drought experts from within the United States, Mexico, and Canada to create the North American Drought Monitor product in ArcGIS (Fig. 4-3). When extreme weather is observed, GIS is often used to generate special products for the U.S. Secretary of Agriculture and top staff. For example, when flooding rains, droughts, freezes, or extreme heat are observed, WAOB meteorologists overlay agricultural and meteorological data layers in the GIS to study weather impacts on agriculture. This capability has enabled WAOB meteorologists to obtain a more comprehensive understanding of the situation because these impacts can be quantified using the underlying spatial data.

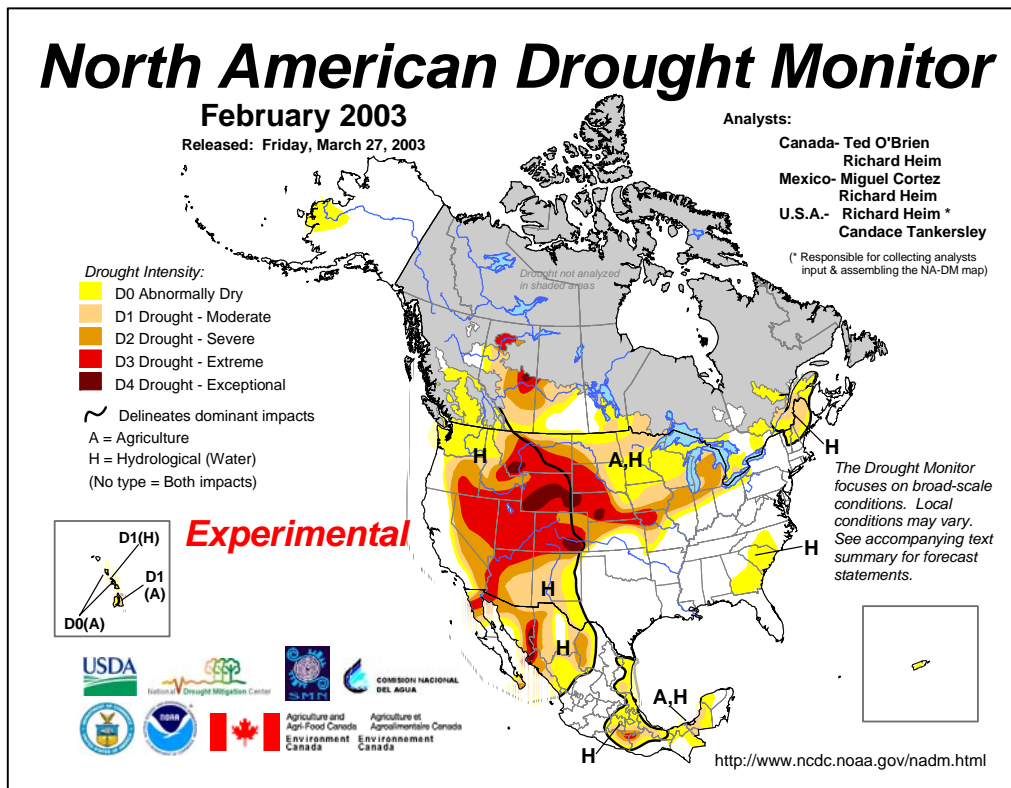


Fig. 4-3. The North American Drought Monitor is a collaborative effort among Mexican, Canadian, and U.S. government agencies.

Several models have also been developed to assist WAOB meteorologists while preparing agricultural weather assessments. Growing degree day models have been implemented for several crops and regions worldwide to estimate crop progress throughout the growing season. Regression models have been developed to study the effects of weather and climate anomalies on crop yields. Examples of these regression models include a model that relates Australian wheat production to the harvested area and monthly rainfall in five regions, a model that predicts South African corn yields based upon a stress index derived from soil moisture estimates, and a model that relates Canadian spring wheat yields to regionally averaged temperature and precipitation data.

DISCUSSION

Although numerous data and tools are currently available to facilitate agricultural weather assessments, continued research into weather impacts on crop development is needed to improve our understanding of these processes. Research that leads to the development of improved, quantitative crop and weather models, and hence better crop production and yield forecasts, would be especially welcomed. The value of model output, however, is intimately related to the quantity and quality of data used to initialize these models. Improvements in surface weather observations can be achieved by increasing station density and by deploying newly developed instruments to sample atmospheric and soil properties. Given that such improvements are difficult to implement on global or even regional scales, remote sensing data are increasingly being considered as an alternative. Remote sensing platforms can measure various atmospheric and surface properties over large areas, making this data collection method particularly attractive. The value of remote sensing data will continue to improve as new sensors are developed and deployed.

In summary, the current suite of agrometeorological data and analytical methods has been very beneficial in conducting agricultural weather assessments. Significantly, the success of the WWCB can be directly attributed to the value-added text and products derived from these data and methods. Further improvements in these products are desired, however, to enhance the ability of senior government officials, commercial entities, and the public in general to make informed decisions based upon observed and modeled agrometeorological conditions.

REFERENCES

- Morris, B.P. 2002. Meteorological database management system at the USDA. p. J284-J285. *In Proc. Int. Conf. Interactive Information and Processing Systems (IIPS) for Meteorology, Oceanography, and Hydrology, 18th, Orlando, FL. 13-17 Jan. 2002. Amer. Meteor. Soc., Boston, MA.*
- Puterbaugh, T.L., and B.R. Rippey. 2002. The weekly weather and crop bulletin - Serving U.S. agriculture. p. 211-223. *In M.V.K. Sivakumar (ed.) Improving agrometeorological bulletins, Proc. Inter-Regional Workshop, Bridgetown, Barbados. 15-19 Oct. 2001. World Meteor. Org., Geneva, Switzerland.*
- Shannon, H.D. 2002. ArcView applications in USDA crop weather analysis. p. J282-J283. *In Proc. Int. Conf. Interactive Information and Processing Systems (IIPS) for Meteorology, Oceanography, and Hydrology, 18th, Orlando, FL. 13-17 Jan. 2002. Amer. Meteor. Soc., Boston, MA.*

CHAPTER 5

Real-Time Modeling of Natural Resources Using the Spatial Sciences

Balaji Narasimhan, Pei-Yu Chen, Jennifer H. Jacobs, and Raghavan Srinivasan

CONTENTS

Introduction	51
Real-Time Wildfire Risk Assessment	53
Keetch-Byram Drought Index	53
Current Practice	54
Real-Time Methodology	54
Development of Real-Time System	56
Summary	56
Real-Time Crop Monitoring	59
Crop Monitoring Study	59
Results and Discussion	60
Summary	63
Real-Time Runoff Estimation	63
Methodology	63
Results and Discussion	66
Real-Time Runoff Estimation Maps	66
Summary	66
Conclusions	67
Acknowledgments	67
References	67

INTRODUCTION

The spatial sciences, including geographic information systems (GIS), remote sensing, and global positioning systems (GPS), have become an invaluable tool across all science and

engineering disciplines, especially in natural resource modeling. Furthermore, with the recent advancements in data collection and dissemination via the internet, there is an increasing opportunity to provide information on a real-time basis which would aid in the decision-making process for natural resource managers. Both raw and processed data can be provided to modelers for use in various applications. In natural resource modeling, elevation, soils, land use, and weather are considered to be the factors that define various processes and interactions. Of these, land use and weather are the most dynamic variables and are closely dependent on each other. Providing near real time access to dynamic resources such as vegetation and weather would greatly improve model results, and thereby management of natural resources. The Advanced Very High Resolution Radiometer (AVHRR) sensor aboard the National Oceanic and Atmospheric Administration (NOAA) series of polar-orbiting satellites, the Moderate Resolution Imaging Spectroradiometer (MODIS) instrument aboard the Terra and Aqua satellites, and the NEXt generation weather RADar (NEXRAD) of the National Weather Service (NWS) are three of the systems currently gathering near real time data.

The NOAA series of Polar Orbiting Environmental Satellites (POES) have been in operation for more than three decades and are the primary source for monitoring weather across the globe. POES utilizes a near-circular, sun-synchronous orbit and views the entire surface of the Earth every one to two days. AVHRR is a broadband scanner aboard these satellites, sensing in the visible (Channel 1), near-infrared (Channel 2), and thermal infrared (Channel 3, Channel 4, and Channel 5) portions of the electromagnetic spectrum at a spatial resolution of 1000 m. Currently, NOAA satellites 14, 15, 16, and 17 are operational (NOAA, 2003).

The MODIS instrument, aboard NASA's Terra and Aqua space crafts (launched in December 1999 and May 2002, respectively) has a higher spectral and spatial resolution than the AVHRR sensor. MODIS acquires data in 36 spectral bands between visible and thermal infrared portions of the electromagnetic spectrum at three spatial resolutions - 250, 500, and 1000 m. In addition, the satellites are equipped with Direct Broadcast (DB) capability. In other words, data are not only stored for later downloads, but they can also be broadcast in real time to ground stations equipped to receive them (NASA, 2003).

NEXRAD is a Doppler radar system, previously known as the Weather Surveillance Radar-1988 Doppler (WSR-88D). NEXRAD provides precipitation data for larger areas with better spatial and temporal resolution than conventional raingauge networks. The raw data, or Stage I output, are available in 4 km x 4 km resolution grids, with cells identified by the Hydrologic Rainfall Analysis Project (HRAP) number. Stage I data are corrected using a bias adjustment factor based on available one-hour raingauge reports. The resulting correction is available as Stage II data. Finally, Stage II data for all radars are combined into one map with ground truth data from gauge stations, and overlapping areas are averaged together. The result is multi-sensor Stage III adjusted data. In this process, the combining and averaging of overlapping data, or mosaicking, helps to compensate for the overestimation or underestimation of individual radars (Jayakrishnan 2001). More detailed information about NEXRAD products and processing algorithms can be found in Crum and Alberty (1993), Klazura and Imy (1993), Smith et al. (1996), and Fulton et al. (1998).

With these datasets, several real-time products have been developed, some of which are currently available via the internet at the Texas Weather Connection (TWC) Website (<http://twc.tamu.edu>). Among these products are a wildfire risk assessment index, a real-time crop monitoring system, and a runoff prediction map for the state of Texas.

REAL-TIME WILDFIRE RISK ASSESSMENT

Every year, thousands of hectares of grassland and forests are lost due to wildfires. According to the National Interagency Fire Center, about 4 million acres are scorched by wildfire every year (NIFC, 2003). These fires cost millions of dollars in economic loss and cause irreparable damage to the environment. Forest fire managers across the United States use fire potential or drought indices to assess wildfire risks and to alert local residents of potential fire threats. These indices are derived from weather data, such as temperature, rainfall, and vegetation condition, recorded by local weather stations. Weather data often come from sparsely located weather stations. The drought indices derived from these point source weather data are then manually interpolated across the entire state, based on expert judgment, at a coarse spatial resolution (county level). This procedure of calculating and interpolating drought indices across the entire state relies heavily on expert judgment and involves many uncertainties. Further, high spatial resolution data are often needed for effective wildfire risk assessment and control.

During the past two decades, several advances have been made in remote sensing, GIS, and computational sciences. In addition, high spatial resolution data, such as temperature and rainfall, are readily available for use in conservation and management of natural resources, and provide the means to develop fire potential indices in real time. The objective of this research is to develop a near real time fire risk index using weather data obtained from satellites carrying the NOAA-AVHRR sensor series and the NEXRAD weather radar for Texas.

Keetch-Byram Drought Index

The Keetch-Byram Drought Index (KBDI) is widely used by fire managers to monitor moisture deficiency in the deep duff and upper layers of the soil profile. It is so widely used because of its simplicity and the fact that it is the only drought index that relates the effect of drought to potential fire activity. KBDI is based on a simple single-layer water balance model and indicates the amount of moisture depleted from the soil. The theory and framework of KBDI are based on the following assumptions (Keetch and Byram, 1968):

1. The rate of soil moisture loss depends on density of the vegetation cover, antecedent moisture conditions, annual rainfall, and evapotranspiration.
2. The field capacity of soil is 8 in of available water. (Eight inches of water is chosen because in many areas of the country, it takes all summer for the vegetation cover to transpire that much water. This number is reasonably well suited for use in forest fire control.)

The four climatological parameters used to calculate KBDI include daily maximum temperature, daily rainfall, cumulative antecedent moisture deficiency, and annual average precipitation. Keetch and Byram (1968) explain in detail the mathematical formulations involved for computing KBDI. The result of this system is a number that represents the moisture deficiency

in the upper soil layer in hundredths of an inch. A scale of 0 to 800 is used to represent the moisture deficiency, with 0 being no moisture deficiency and 800 being the maximum possible moisture deficiency. These numbers are correlated with the fire potential as shown in Table 5-1.

Table 5-1. Keetch-Byram Drought Index (KBDI) and fire potential.

KBDI	Fire potential
0 – 200	Low
200 – 400	Moderate
400 – 600	High
600 – 800	Very high

In Texas, if the KBDI for a county is more than 500, countywide outdoor burn bans are imposed by the Texas Forest Service (TFS) to prevent wildfires in that county.

Current Practice

Presently, all the climatological data needed to compute KBDI are obtained from 60 ground-based weather stations across Texas. Daily weather data for these stations are collected by the National Weather Service (NWS) and are available for download via the internet (<http://iwin.nws.noaa.gov/iwin/tx/climate.html>). These daily weather data are downloaded manually from the NWS and imported into a spreadsheet to calculate daily KBDI. The KBDI derived from these point data sources are then interpolated at a county scale across the entire state based on expert judgment. Some of the uncertainties involved with this procedure are the following:

- Localized precipitation events are common in arid climatic zones. These precipitation events may not be captured by the sparsely located rain gauge stations.
- Interpolation of KBDI from weather station data across large regions could introduce errors.
- The interpolation method in use is based on human judgment. This might introduce further bias when interpolating KBDI across large areas.

With advances in spatial and computational sciences, the procedure for computing KBDI can be automated, and spatial accuracy can be considerably improved (county scale to 4km × 4km) by using GIS and remote sensing technologies.

Real-Time Methodology

The proposed methodology involves the use of remotely sensed data from AVHRR and NEXRAD for deriving weather parameters such as maximum air temperature and daily rainfall.

Maximum air temperature (T_a), needed for calculating KBDI, is derived from land surface temperature (T_s) obtained from the thermal channels of AVHRR. Land Surface Temperature (LST) is the temperature measured just a few inches above the surface of the land or vegetation. The LST can be derived using a split window algorithm from the brightness temperatures of channels 4 and 5 of AVHRR. Several split window algorithms have been developed and used to derive LST from these channels to account for the effects of atmospheric disturbances on the satellite measurements. The split window algorithm developed by Ulivieri et al. (1994) has been used in this study to derive LST from the thermal channels. As previously mentioned, LST is different from the air temperature that is measured at a standard height of 2 m. Maximum air temperature (T_a) can be obtained from the surface temperature (T_s) using an energy balance approach. But such an approach involves many variables that cannot be readily derived from satellite measurements.

According to Narasimhan et al. (2003), there is a strong linear relationship between surface temperature obtained from the satellite and the maximum air temperature measured at weather stations across the state. Hence, a simple regression approach was developed in order to derive (T_a) from (T_s). This regression model is of the form:

$$T_a(i) = m(i)\sqrt{T_s \times T_{lm}} + C(i) \quad [1]$$

where $T_a(i)$ is the estimated daily maximum air temperature for climatic zone i , T_s is the land surface temperature ($^{\circ}\text{C}$), T_{lm} is the long-term monthly maximum air temperature ($^{\circ}\text{C}$), and $m(i)$ and $C(i)$ are regression constants for climatic zone i (where $i = 1, \dots, 10$) (Table 5-2).

Table 5-2. Regression coefficients used for deriving maximum air temperature (T_a) from surface temperature (T_s).

Climatic division	$m(i)$	$C(i)$	R^2
1	0.78	5.04	0.74
2	0.88	3.46	0.80
3	0.86	4.73	0.81
4	0.9	4.82	0.83
5	0.82	2.72	0.75
6	0.86	4.12	0.78
7	0.75	7.47	0.72
8	0.86	5.31	0.78
9	0.81	5.99	0.71
10	0.81	6.55	0.75

Daily precipitation, again needed for calculating KBDI, was obtained from Stage III NEXRAD weather radar. Precipitation is the most sensitive parameter in the estimation of KBDI. As previously mentioned, localized precipitation events are very common in arid climatic zones. These precipitation events may not be captured by the sparsely located raingauge stations.

Currently, NEXRAD provides the best estimates of precipitation over large areas with high spatial resolution ($4\text{km} \times 4\text{km}$).

Since outdoor burn bans and distribution of fire personnel and resources across the state depend on KBDI estimates, accurate estimation of KBDI is essential. Hence, by using remotely sensed temperature and precipitation estimates obtained from AVHRR and NEXRAD, respectively, accurate estimation of KBDI is possible at a high spatial resolution.

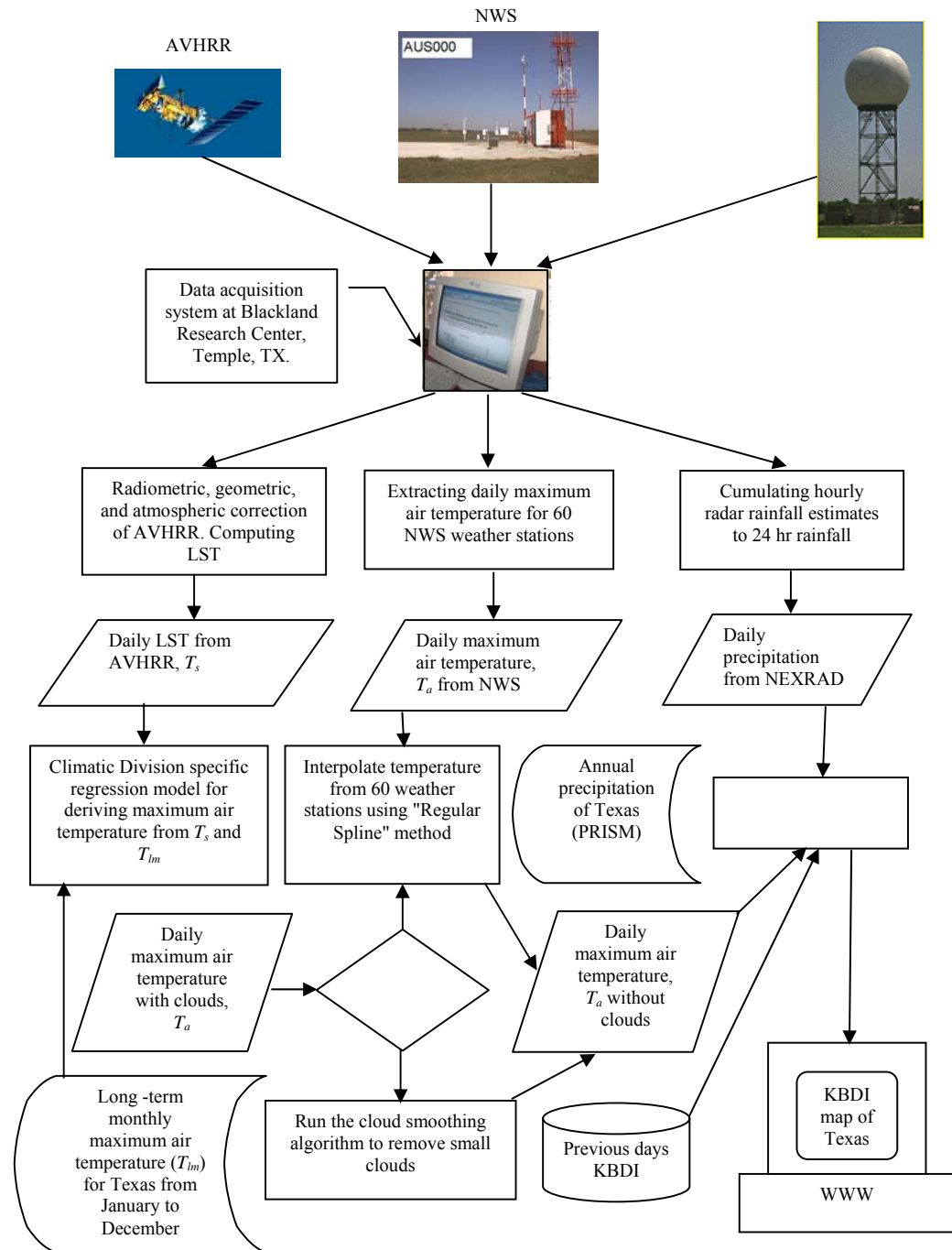
Development of Real-Time System

A real-time system (Fig. 5-1) has been developed for estimation of daily KBDI from remotely sensed data using Arc Macro Language (AML) scripts in ESRI's ArcInfo software. The satellite receiving system located at the Blackland Research Center (BRC), in Temple, TX, acquires daily raw AVHRR data from NOAA-14 and NOAA-15 satellites. An automatic data processing system has been developed using PCI Geomatics' remote sensing software for radiometric, geometric, and atmospheric corrections and computing NDVI and LST. In addition, algorithms developed by various researchers have been refined and are used for cloud detection (Chen et al., 2002). During cloudy days (cloud cover $> 30\%$), it may not be possible to get maximum air temperature estimates from the AVHRR satellites. On these days, maximum air temperature measured at 60 NWS weather stations across Texas is interpolated using a "Regular Spline" method, available in the ArcInfo system. The resulting maximum air temperature is used as a replacement for the satellite data during cloudy days. An automatic data-capturing algorithm is used to obtain the daily maximum air temperature from the 60 NWS stations.

Stage III NEXRAD data are collected and archived by the NWS. The Stage III data, obtained from the NWS River Forecasting Center (RFC) in Fort Worth, TX, through a cooperative arrangement, is in a Hydrologic Rainfall Analysis Project (HRAP) grid system, whereas the rest of the data are in a regular grid system. Hence, the precipitation data are remapped to the regular grid system using the ArcInfo. Once all of the input data are prepared, KBDI is computed using AML scripts, again, in ArcInfo. This entire system is completely automated and no longer requires manual data processing. Once the KBDI information is processed, it is distributed to forest fire managers across Texas through the World Wide Web (WWW) at <http://twc.tamu.edu>.

Summary

A real-time system has been developed for estimation of a fire potential index (KBDI). The use of GIS and remote sensing technologies overcomes the uncertainties involved in the computation of the KBDI index. The spatial accuracy of KBDI estimates has also been improved (county scale to $4\text{km} \times 4\text{km}$) due to the use of real-time, and readily available, remotely sensed data and GIS (Fig. 5-2 and Fig. 5-3). Efforts are also underway for the development of a new fire potential index by incorporating NDVI estimates with that of soil moisture deficit. NDVI gives a measure of greenness/dryness of vegetation. Because this plays an important role in the ignition or spread of wildfire, it can give a better estimate of fire potential at any given place.



NWS - National Weather Service, NEXRAD - Next Generation Weather Radar, LST - Land Surface Temperature

Fig. 5-1. A real-time system for computing the Keetch-Bryam Drought Index (KBDI) using remotely sensed data and geographic information systems (GIS).

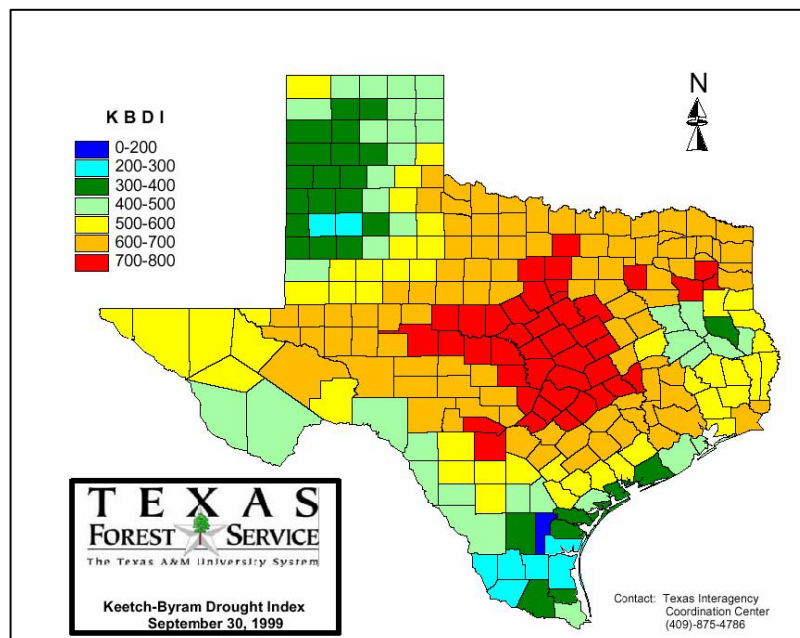


Fig. 5-2. Keetch-Byram Drought Index (KBDI) for 30 Sept. 1999 computed by conventional methods (Courtesy of TFS).

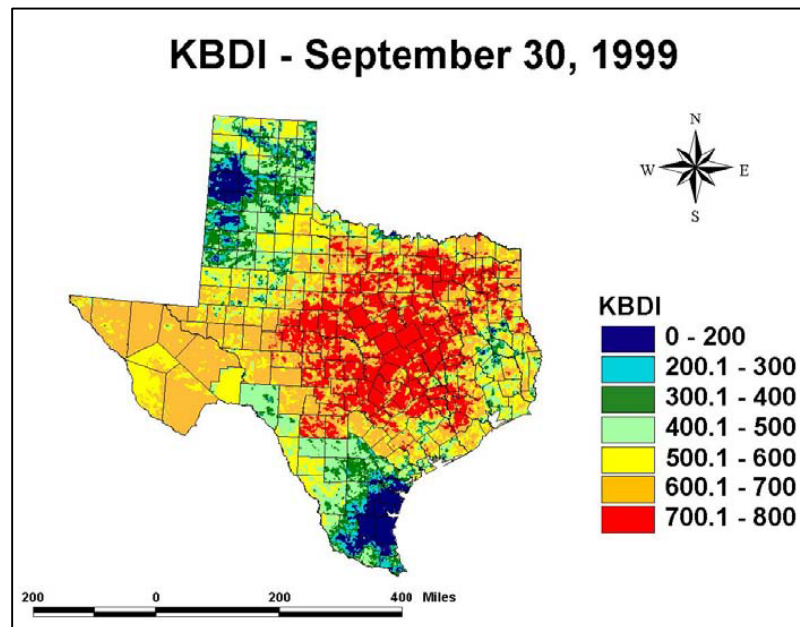


Fig. 5-3. Keetch-Byram Drought Index (KBDI) at a resolution of 4km × 4km computed using remotely sensed data.

REAL-TIME CROP MONITORING

Vegetation indices (VIs) based on visible and near-infrared reflectance values are primarily acquired for vegetation studies. The Normalized Difference Vegetation Index (NDVI) is the most widely used VI for vegetation research and can be used to detect change, estimate biomass, and map land cover (Jakubauskas et al., 2002; Maselli et al., 2000; Chen et al., 1999). Most crop growth studies involve the utilization of a temporal series of NDVI values derived from the NOAA-AVHRR sensor series (Dabrowska-Zielinska et al., 2002; Rasmussen, 1998). The multitude of spectral bands in the MODIS instrument provides another data resource for near real time agricultural studies. Besides NDVI, the MODIS instrument provides the Enhanced Vegetation Index (EVI), with improved sensitivity in high biomass regions and improved vegetation monitoring through a de-coupling of the canopy background signal and a reduction in atmospheric influence (Terrestrial Biophysics & Remote Sensing Lab, 2003). The EVI contains self-correcting atmospheric and soil calibration factors and quality control diagnostics, and is derived from the visible (0.62-0.67 μm), near-infrared (0.841-0.876 μm), and blue (0.459-0.479 μm) reflectance data suggested by Huete et al. (1994). It is defined by the following equation:

$$EVI = G \times \frac{\rho_{NIR} - \rho_{red}}{\rho_{NIR} + C_1 \times \rho_{red} - C_2 \times \rho_{blue} + L} \quad [2]$$

where ρ is the atmospherically corrected (for Rayleigh and ozone absorption) surface reflectance data, L is the canopy background adjustment, and C_1 and C_2 are the aerosol resistance coefficients. The blue band is used to correct for aerosol influences in the red band. The EVI values vary between -1.0 and +1.0. Negative EVI values indicate the presence of clouds, snow, or water, and positive EVI values are positively correlated to the abundance of green vegetation.

Daily coverage of the earth surface is a strong advantage of MODIS data, but cloud contamination limits the data usage for environmental monitoring (Ohring and Clapp, 1980). Cloud detection is strongly recommended for real-time data such as those from AVHRR and MODIS (Gutman et al., 1994; Cihlar, 1996; Chen et al., 2002). The maximum value compositing (MVC) method is widely used to minimize the effects of cloud contamination on MODIS data (Holben, 1986). The MVC method retains the highest VI value for a given pixel over a pre-defined compositing period since the presence of clouds, smoke, haze, snow, and ice in a pixel reduces VI values. The 36-channel high spectral resolution MODIS data are used to produce the 16-d EVI and NDVI composite products at spatial resolutions of 250, 500, and 1000 m.

Crop Monitoring Study

Several vegetation monitoring studies have been conducted using NDVI, based on the assumption that NDVI and leaf area index (LAI) are closely correlated to the fraction of photosynthetically active radiation (PAR) intercepted by canopies (Hatfield et al., 1984; Shanahan et al., 2001). Sorghum (*Sorghum bicolor*) and corn (*Zea mays*), two of the major crops in Mexico, are planted along the east and west coasts of Mexico, respectively. Sorghum is primarily planted between January and February and is harvested in June. Corn is planted in November and harvested in May of the next year. The NDVI composite data from AVHRR images have been used to monitor corn growth stage and to estimate corn yield in Mexico starting in 1999 (Baez-Gonzalez et al., 2002) to ensure food security. Since the MODIS instrument provides real-time

vegetation information at finer resolutions (250 and 500 m) than AVHRR, the objective of this study was to assess the suitability of the EVI temporal profiles at different resolutions for sorghum and corn monitoring in Mexico. All remote sensing procedures were done in PCI Geomatics and ERDAS systems.

For this research, 16 sorghum and 16 corn locations were randomly selected from a series of field samples for 2002 provided by scientists of the National Research Institute of Forestry, Agriculture, and Livestock Production (INIFAP). Moreover, each studied location was verified using LANDSAT-7 Enhanced Thematic Mapper (ETM+) images acquired in February and May 2002 for sorghum and maize, respectively. The sorghum fields had maximum LAI values at the end of April and beginning of May, and the corn fields reached maximum LAI values between February and March. The longitude and latitude of each location were used to extract EVI values from the MODIS data. A series of 16-d EVI composite data at different resolutions were downloaded from NASA GSFC DAAC (<http://modis.gsfc.nasa.gov/data/dataproducts.html>) for the period from the end of 2001 to the middle of 2002 for the crop monitoring study.

Results and Discussion

All 16 sampled sorghum locations had maximum EVI values occurring between the middle of April and the beginning of May, coincident with the time of maximum leaf area index (LAI) for the sorghum fields (Alma Baez-Gonzalez, personal communication; March 2003). The EVI temporal profiles for 500m MODIS pixels (EVI_500m) were similar to EVI profiles for 1000-m MODIS pixels (EVI_1000m) for sorghum growth, with maximum EVI values occurring at the same time (Fig. 5-4). Most EVI temporal profiles for 250-m MODIS pixels (EVI_250m) had maximum values that were either 16 d earlier or later than the EVI_500m and EVI_1000m data. Only three out of 16 locations had maximum EVI values occurring at the same time period for all three pixel resolutions. The EVI difference between the EVI_1000m and EVI_500m data was less than that between the EVI_500m and EVI_250m data. The EVI_500m data usually had maximum values that were similar to or greater than those of the EVI_1000m data. Maximum values of the EVI_250m data were more variable. Six EVI_250m data out of 16 had lower maximum values compared to the EVI_500m data.

Eastern Mexico has several large areas of sorghum fields. Each area is divided into many small parcels of agricultural land that are rectangular in shape. Although all of the parcels were planted with sorghum, planting time and farming practice differed between parcels. In addition, a couple of urban areas were adjacent to or within agricultural areas. The TM images revealed different spectral responses for agricultural parcels of land next to each other. The EVI_1000m data were most likely to cover more than one parcel, while the EVI_250m data were almost certainly composed of a single parcel or homogeneous land-cover type. The EVI_500m may cover one or more parcels of land, depending on the parcel sizes. Five out of the 16 samples had parcel sizes less than 250m × 250m, and four out of the 11 remaining samples had parcel sizes less than 500 m × 500 m. The remaining seven samples had parcel sizes less than 1000m × 1000m. The EVI_250m data represented real-time information well, similar to field conditions of sorghum growth for every monitoring site in Eastern Mexico. The EVI_1000m data probably presented combined field situations for the monitoring spot and its neighbor parcels. The quality of EVI_500m data was between that of EVI_250m and EVI_1000m data.

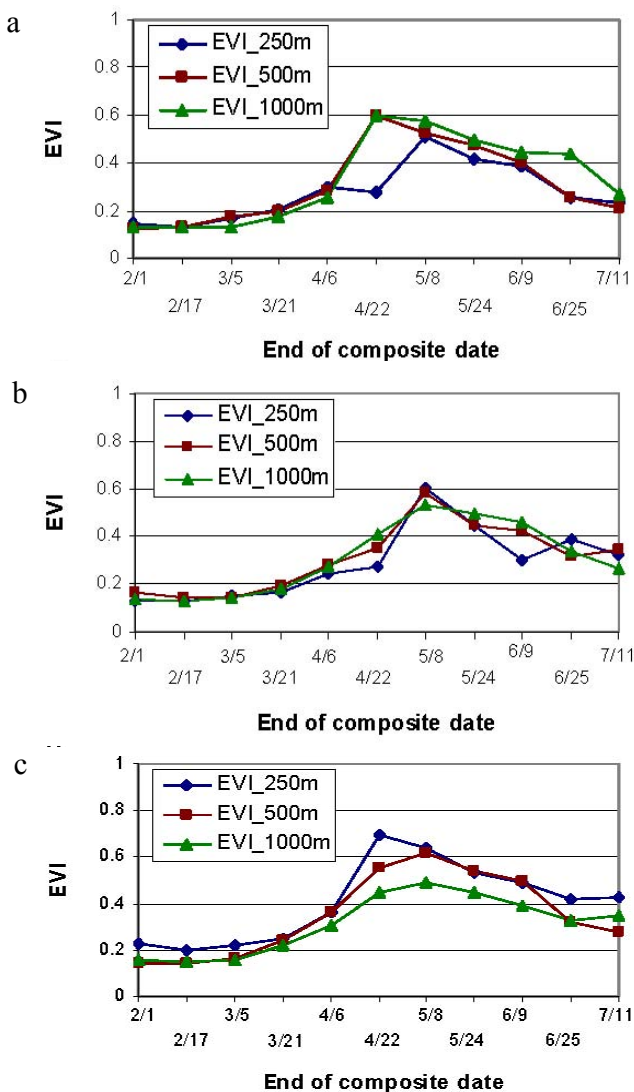


Fig. 5-4. EVI temporal profiles for sorghum fields from MODIS data at three spatial resolutions at different locations (a, b, c) in Tamaulipas in Eastern Mexico in 2002.

The EVI temporal profiles for sorghum (Fig. 5-4) and corn fields (Fig. 5-5) had different patterns. The EVI values for corn fields reached a plateau between 75 and 110 d after planting and declined when the corn started to mature. The period of 75 to 110 d after planting included the growing stages of silking, doughing, and denting. The EVI profiles for sorghum fields reached a peak when the sorghum started heading, around 85 d after planting, and declined immediately when sorghum started changing colors (senescing). The EVI profile for corn included a plateau because corn experiences a slower reduction in LAI and radiation use efficiency than sorghum as part of senescence after reaching maximum EVI (Kiniry et al., 1992).

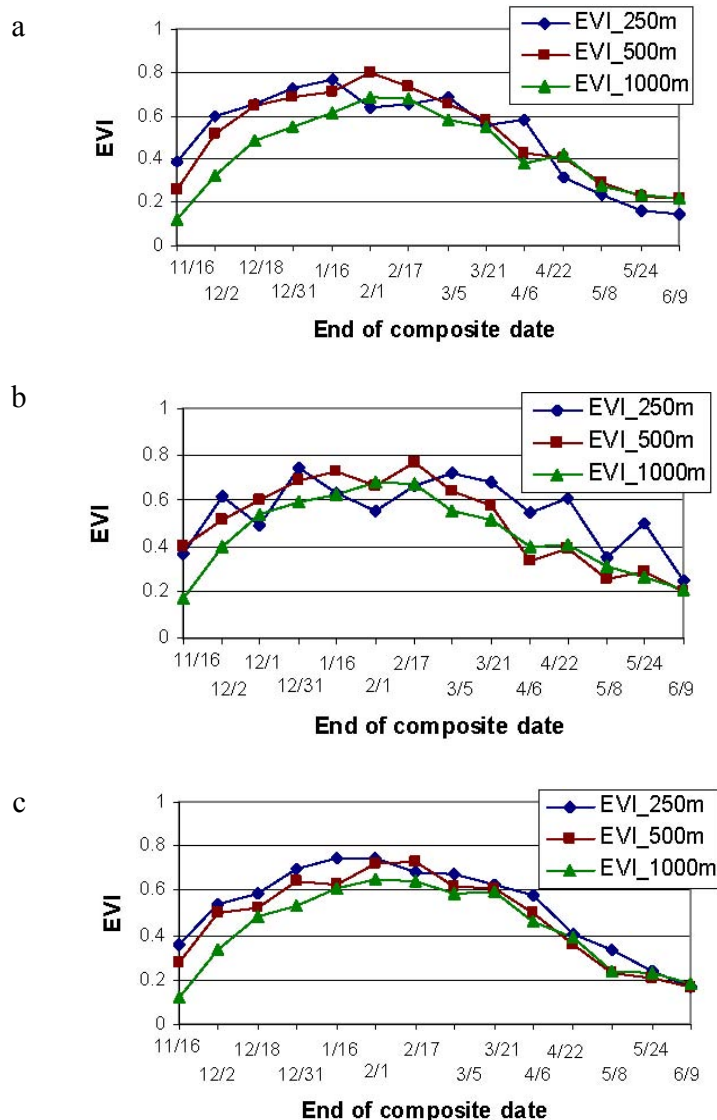


Fig. 5-5. EVI temporal profiles for corn fields from MODIS data at three spatial resolutions at different locations (a, b, c) in Sonora in Western Mexico from 2001 to 2002.

The EVI_1000m data for corn had very similar behaviors for each sampled location, reaching the maximum plateau from the end of January to the end of February, when the leaf area index reached maximum values as well. Irregular up-and-down behaviors occurred frequently in the EVI_250m data for corn. These data usually had the largest EVI values before reaching the silking stage. The EVI_500m data for corn always had greater EVI values than the EVI_1000m data before silking, but both EVI values were very similar when the corn reached maturity. The EVI profiles for sorghum demonstrated the opposite behavior. At all three resolutions, these data had very similar values before reaching the maximum level, and then the EVI values diverged when the data declined.

Clouds were visible in the 16-d EVI composites acquired between November and March. Moreover, visible cloud shadows frequently appeared in the EVI composites, although the cloud contamination had been effectively removed by maximum value compositing (MVC). It was apparent that the 16-d composite period may not be long enough for obtaining cloud-free information. Chen et al. (2003) recommended that cloud detection be applied to the individual scene before producing composite data. Overall, the EVI_250m data for sorghum behaved more closely to crop conditions as known to exist in the fields than the EVI_250m data for corn. The main reason was that the EVI composite data were less cloud-contaminated in the sorghum season, from February to June. Cloud and cloud shadow effects were more significant for the EVI_250m data than EVI_1000m data if the clouds and cloud shadows did not contaminate the entire pixel of 1000 m × 1000 m.

Summary

Although the Normalized Difference Vegetation Index (NDVI) has been successfully applied to several agricultural studies, published research studies have concluded that NDVI values were responding to the vegetation canopy background. The Enhanced Vegetation Index (EVI) derived from the Moderate Resolution Imaging Spectroradiometer (MODIS) was improved, with increased sensitivity for biomass estimation in dense vegetation canopies, through a de-coupling of the canopy background signal and a reduction in atmospheric and soil reflectance influence. In this study, the MODIS EVI data at all three spatial resolutions provided information on sorghum growth stage consistent with actual crop conditions as reported in the fields. Our results showed that the MODIS EVI 250m composite data were not as reliable as the 500m and 1000m data for corn monitoring because of frequent cloud contamination occurring during the first three months of the growing season. Moreover, the MODIS EVI value difference among the three resolutions was attributable to the proportion of crop fields within the pixel. Overall, this study exhibited that MODIS EVI composites can be used to support real-time crop monitoring in Mexico.

REAL-TIME RUNOFF ESTIMATION

The purpose of this third study was to evaluate variations of the Natural Resources Conservation Service (NRCS) curve number (CN) method for estimating near real-time runoff for naturalized flow, using high-resolution radar rainfall data in Texas. The CN method is an empirical method for calculating surface runoff, which has been tested on various systems over a period of many years. Many of the findings of previous studies indicate the need to develop variations of this method to account for regional and seasonal changes in weather patterns and land cover that might affect runoff. This study seeks to address these issues, as well as the inherent spatial variability of rainfall, in order to develop a means of predicting runoff in near real time for water resource management. In the past, raingauge networks provided data for hydrologic models. However, these networks were generally unable to provide data in real time or capture the spatial variability associated with rainfall. Radar networks, like NEXRAD, which are widely available and continue to improve in quality and resolution, can accomplish these tasks.

Methodology

Ten watersheds of varying size in four river basins throughout different agro-climatic regions of Texas were used in this study in order to account for the wide variety of hydrologic conditions throughout the state (Table 5-3). These areas were chosen based on the dominant land use, soil hydrologic group, and streamgauge location for validation and calibration of model results.

Table 5-3. Description of watershed study areas chosen for analysis.

Watershed	USGS Streamgauge	Stream Name	Major Land Resource Area	Drainage Area (km ²)	Rainfall Range (mm)	Major Land Cover Characteristics
Trinity-1	8042800	West Fork Trinity River	Texas North Central Prairies	1769	550 - 750	56% herbaceous rangeland; 17% shrubland; 13% deciduous forest
Trinity-2	8065800	Bedias Creek	Texas Claypan	831	750 - 1075	76% improved pasture and hay
Trinity-3	8066200	Long King Creek	Western Coastal Plains	365	1025 - 1350	80% forested; 15% improved pasture and hay
Red-1	7311600	North Wichita River	Rolling Red Plains	1399	500 - 750	33% herbaceous rangeland; 40% row crops; 18% shrubland
Red-2	7311783	South Wichita River	Rolling Red Plains	578	500 - 750	60% herbaceous rangeland; 28% shrubland
LCR-1	8144500	San Saba River	Edwards Plateau	2940	375 - 750	71% shrubland; 21% herbaceous rangeland
LCR-2	8150800	Beaver Creek	Edwards Plateau	557	375 - 750	40% shrubland; 40% evergreen forest
LCR-3	8152000	Sandy Creek	Texas Central Basin	896	625 - 750	41% evergreen forest; 33% shrubland; 16% herbaceous rangeland
SA-1	8178880	Medina River	Edwards Plateau	850	375 - 750	60% forest; 20% shrubland; 14% herbaceous rangeland
SA-2	8178700	Salado Creek	Edwards Plateau / Texas Blackland Prairie	355	375 - 1150	50% forest; 32% urban; 10% shrub and herbaceous rangeland

Daily runoff calculations for the study sites were made using the NRCS CN method, which provided a means of estimating runoff based on land use, soil type, and precipitation. This calculation is based on the retention parameter, S , initial abstractions I_a (surface storage, interception, and infiltration prior to runoff), and the rainfall depth for the day, R_{day} (all in mm

H_2O). The retention parameter is variable due to changes in soil type, land use, and soil moisture, and is defined as Eq. [3]:

$$S = 25.4 \left(\frac{1000}{CN} - 10 \right) \quad [3]$$

Average CN values (CNII) are assigned based on the land use and soil hydrologic group from lookup tables in the Soil Conservation Service (SCS) National Engineering Handbook, Section 4: Hydrology (NEH-4). CN values for wet (CNIII) and dry (CNI) antecedent moisture conditions are calculated from this average value. A more detailed description of these calculations can be found in Neitsch et al. (2001). For the actual runoff calculation, initial abstractions (I_a) are generally approximated as 0.2 S , and the basic equation becomes Eq. [4]:

$$Q_{surf} = \frac{(R_{day} - 0.2S)^2}{(R_{day} + 0.8S)} \quad [4]$$

where Q_{surf} is surface runoff in mm, and R_{day} is rainfall depth for the day, also in mm. Runoff will occur only when $R_{day} > I_a$ (Neitsch et al., 2001). However, Ponce and Hawkins (1996) suggest that 0.2 S may not be the most appropriate number for I_a , and that it should be interpreted as a regional parameter. To test this, 0.2 S , 0.1 S , and 0.05 S were used in the runoff equation to determine the most appropriate constant for I_a in various agro-climatic regions of Texas. Stage III NEXRAD precipitation data were used as the rainfall input for the equation in order to produce runoff estimates in real time. In addition, NEXRAD is able to capture the spatial and temporal variability of rainfall more effectively than traditional raingauge networks over large areas. In such areas, rainfall contributions from heavy, localized storms can go unaccounted for based on traditional raingauge information.

Runoff estimates generated by the CN method equation were compared with U.S. Geological Survey (USGS) streamflow estimates at the watershed outlets. Because streamflow is composed of baseflow and runoff portions of flow, it was necessary to process this data through a baseflow separation filter program, such as the one outlined in Arnold et al. (1995). This process allowed for direct comparison of runoff estimates to USGS data.

Statistical analysis for this study consisted of basic regression analysis and estimation efficiency (Nash and Sutcliffe, 1970), which are commonly used in hydrologic model evaluation. The equation is calculated as:

$$COE = 1.0 - \left(\frac{\sum_{i=1}^n (O_i - R_i)^2}{\sum_{i=1}^n (O_i - O_m)^2} \right) \quad [5]$$

where COE is the coefficient of efficiency, or runoff estimation efficiency, n is the number of days of comparison, O_i is the observed streamgauge runoff for a watershed for day i , O_m is the mean observed streamgauge runoff for a watershed over all days, and R_i is the estimated runoff for a watershed for day i . When $R_i = O_i$, $COE = 1$. This would represent a good comparison between observed and estimated runoff values. Where $COE < 1$, the estimated runoff value is less

representative than the mean value for the dataset. In general, COE values greater than 0.4 are considered to be highly significant.

Results and Discussion

In this analysis, 9 out of 10 watersheds produced statistically significant runoff results using CNI with an initial abstraction coefficient of 0.1 when compared to observed runoff (Hadley, 2003). Traditionally, CNII would be used with an I_a coefficient of 0.2. Using a dry antecedent moisture condition would decrease runoff, whereas the 0.1 coefficient would slightly increase runoff by decreasing initial abstractions. These adjustments produced runoff estimates that more closely matched observed runoff than did the traditional calculations. For these nine watersheds, the combined COE was 0.70, the slope was 0.78, and the r^2 was 0.77. Based on the significance of these findings, the modified runoff equation was extrapolated to the entire state. A more detailed description of these results can be found in Hadley (2003).

Real-Time Runoff Estimation Maps

The three main datasets used to generate runoff estimates using the NRCS CN method are land-cover, soils, and precipitation data. For real-time runoff estimation, the land-cover data are obtained from the 1992 USGS National Land Cover Data (NLCD) at a 30-m resolution. In addition to land cover, the soil hydrologic group classification is needed to determine the CN value for a particular area. This information is derived from the U.S. Department of Agriculture (USDA) – NRCS State Soil Geographic (STATSGO) database, which was obtained at a 250-m resolution. The final input needed for this calculation is the rainfall depth for the day. Because rainfall is the driving factor in runoff, it is altogether necessary to obtain the most accurate rainfall input available. In this case, the Stage III NEXRAD radar rainfall data are used. These data are better able to capture the spatial and temporal variability of rainfall than traditional raingauge networks and are available at a 4-km resolution. Furthermore, as more detailed input data become available, they can be easily substituted for these existing datasets.

With the use of ESRI's ArcInfo software and AML scripts, real-time runoff maps are generated daily. The land-cover and soils data are used to assign the CN value from a lookup table. This value is then converted to the CNI, or dry antecedent moisture condition, value and used with the 0.1 I_a coefficient and the daily NEXRAD rainfall data to calculate surface runoff. The result is a daily runoff map that is posted on the internet for public use. In addition, using the DEM flow direction map to summarize runoff estimation will allow routing of stream flow into river reaches in order to estimate stream flow in real time.

Summary

The goal of this study was to develop a near real time method for generating runoff estimates using the NRCS CN method. This was successful, based on the statistical significance of the runoff estimates as compared with observed USGS streamflow. Providing access to such information via the internet will prove useful in all types of watershed and water resource management, including reservoir operation. In addition, as NEXRAD rainfall data are replaced

with forecast information, it will be possible to translate this methodology into a tool that could be used for flood prediction and mitigation.

CONCLUSIONS

The research products discussed herein use readily available remote sensing and radar-based real-time data to provide decision-making tools to natural resource managers. Many more real-time applications could be developed by combining ground- and radar-based weather station data as well as information from various remote sensing platforms and rendering the raw and processed data through the internet. Similar research works are in progress to develop additional real-time systems for applications, such as crop growth monitoring using Growing Degree Days (GDD), Potential EvapoTranspiration (PET), and severity indices for crop diseases such as Sorghum Ergot and Wheat Karnal Bunt. Developing such tools would help action agencies, such as TFS, TWDB, USDA, and river authorities make time-sensitive decisions that could have significant impact on society.

ACKNOWLEDGMENTS

The authors would like to thank several groups for their support and contributions. Dr. Alma Delia Baez-Gonzalez and Dr. Mario Tiscareño-Lopez at Laboratorio Nacional de Modelaje y Sensores Remotos, Campo Experimental Pabellón, INIFAP provided locations of corn and sorghum as well as Landsat ETM+ images for the real-time crop monitoring study. The Texas Forest Service (TFS) , the Texas Agricultural Experiment Station (TAES), and the Texas Water Resources Institute (TWRI) provided partial funding for the wildfire risk assessment study. In addition, TWRI provided partial funding for the real-time runoff prediction study.

REFERENCES

- Arnold, J.G., P.M. Allen, R. Muttiah, and G. Bernhardt. 1995. Automated baseflow separation and recession analysis techniques. *Ground Water*. 33(6):1010-1018.
- Baez-Gonzalez, A.D., P.Y. Chen, M. Tiscareño-Lopez, and R. Srinivasan. 2002. Using satellite and field data with crop growth modeling to monitor and estimate corn yield in Mexico. *Crop Sci.* 42(6):1943-1949.
- Chen, P.Y., R. Srinivasan, G. Fedosejevs, and J.R. Kiniry. 2003. Evaluating different NDVI composite techniques using NOAA-14 AVHRR data. *Int. J. Remote Sens.* 24(17):3403-3412.
- Chen, P.Y., R. Srinivasan, G. Fedosejevs, and B. Narasimhan. 2002. An automated cloud detection method for daily NOAA-14 AVHRR data for Texas, USA. *Int. J. Remote Sens.* 23(15):2939-2950.
- Chen, X.W., R. Tateishi, and C.Y. Wang. 1999. Development of a 1-km land-cover dataset of China using AVHRR data. *ISPRS J. Photogramm. Remote Sens.* 54(5-6):305-316.
- Cihlar, J. 1996. Identification of contaminated pixels in AVHRR composite images for studies of land biosphere. *Remote Sens. Environ.* 56:149-163.
- Crum, T.D. and R.L. Alberty. 1993. The WSR-88D and the WSR-88D operational support facility. *Bull. Am. Meteorol. Soc.* 74(9):1669-1687.

- Dabrowska-Zielinska, K., F. Kogan, A. Ciolkosz, M. Gruszczynska, and W. Kowalik. 2002. Modeling of crop growth conditions and crop yield in Poland using AVHRR-based indices. *Int. J. Remote Sens.* 23(6):1109-1123.
- Fulton, R.A., J.P. Breidenbach, D.J. Seo, and D.A. Miller. 1998. The WSR-88D rainfall algorithm. *Weather and Forecasting* 37:377-395.
- Gutman, G., A. Ignatov, and S. Olson. 1994. Towards better quality of AVHRR composite images over land: Reduction of cloud contamination. *Remote Sens. Environ.* 50:134-148.
- Hadley, J.L. 2003. Near real-time runoff estimation using spatially distributed radar rainfall data. M.S. thesis. Texas A&M Univ., College Station.
- Hatfield, J.L., G. Asrar, and E.T. Kanemasu. 1984. Intercepted photosynthetically active radiation estimated by spectral reflectance. *Remote Sens. Environ.* 14:65-75.
- Huete, A., C. Justice, and H. Liu. 1994. Development of vegetation and soil indices for MODIS-EOS. *Remote Sens. Environ.* 49:224-234.
- Holben, B.N. 1986. Characteristics of maximum values Composite images from temporal AVHRR data. *Int. J. Remote Sens.* 7:1417-1434.
- Jakubauskas, M.E., D.L. Peterson, J.H. Kastens, and D.R. Legates. 2002. Time series remote sensing of landscape-vegetation interactions in the southern Great Plains. *Photogramm. Eng. Remote Sens.* 68(10):1021-1030.
- Jayakrishnan, R. 2001. Effect of rainfall variability on hydrologic simulation using WSR-88D (NEXRAD) data. Ph.D. diss. Texas A&M Univ., College Station.
- Keetch, J.J., and G.M. Byram. 1968. A drought index for forest fire control. USDA-Forest Service Research Paper No. SE 38. Asheville, NC.
- Kiniry, J.R., J.R. Williams, P.W. Gassman, and P. Debaeke. 1992. A general, process-oriented model for two competing plant species. *Trans. ASAE.* 35:801-810.
- Klazura, G.E. and D.A. Imy. 1993. A description of the initial set of analysis products available from the NEXRAD WSR-88D system. *Bull. Am. Meteorol. Soc.* 74(7):1293-1311.
- Maselli, F., S. Romanelli, L. Bottai, and G. Maracchi. 2000. Processing of GAC NDVI data for yield forecasting in the Sahelian region. *Int. J. Remote Sens.* 21(18):3509-3523.
- Narasimhan, B., R. Srinivasan, and A.D. Whittaker. 2003. Estimation of potential evapotranspiration from NOAA-AVHRR satellite. *Appl. Eng. in Agric.* 19(3):309-318.
- Nash, J.E. and J.V. Sutcliffe. 1970. River flow forecasting through conceptual models. Part I – A discussion of principles. *J. Hydrol.* 10:282-290.
- National Aeronautics and Space Administration (NASA). 2003. MODIS Web: About MODIS [Online]. [4p.] Available at <http://modis.gsfc.nasa.gov/> (Downloaded 28 Oct. 2003).
- National Interagency Fire Center (NIFC). 2003. Wildland Fire Statistics [Online]. [2p]. Available at <http://www.nifc.gov/> (Downloaded 10 Nov. 2003).
- National Oceanic and Atmospheric Administration (NOAA). 2003. Office of Satellite Operation: Polar Spacecraft and Instruments [Online].[6p.] Available at <http://www.oso.noaa.gov/> (Downloaded 10 Nov. 2003).
- Neitsch, S.L., J.G. Arnold, J.R. Kiniry, and J.R. Williams. 2001. Soil and Water Assessment Tool (SWAT) theoretical documentation. Blackland Research Center, Texas Agricultural Experiment Station, Temple, TX.
- Ohring, G., and P.F. Clapp. 1980. The effects of changes in cloud amount on the net radiation at the top of the atmosphere. *J. Atmos. Sci.* 37(2):447-454.

- Ponce, V.M. and R.H. Hawkins. 1996. Runoff curve number: Has it reached maturity? *J. Hydrol. Eng.* 1(1):11-19.
- Rasmussen, M.S. 1998. Developing simple, operational, consistent NDVI-vegetation models by applying environmental and climatic information: Part II. Crop yield assessment. *Int. J. Remote Sens.* 19(1):119-139.
- Shanahan, J.F., J.S. Schepers, D.D. Francis, G.E. Varvel, W.W. Wilhelm, J.M. Tringe, M.R. Schlemmer, and D.J. Major. 2001. Use of remote-sensing imagery to estimate corn yield. *Agron. J.* 93:583-589.
- Smith, J.A., D.J. Seo, M.L. Baeck, and M.D. Hudlow. 1996. An intercomparison study of NEXRAD precipitation estimates. *Water Resour. Res.* 32(7):2035-2045.
- Terrestrial Biophysics & Remote Sensing Lab. 2003. Enhanced vegetation index (EVI) [Online]. [1 p.] Available at <http://tbrs.arizona.edu/project/MODIS/evi.php> (Updated 1 Feb. 2003). University of Arizona, Tucson, AZ.
- Olivieri, C., M.M. Castronovo, R. Francioni, and A. Cardillo. 1994. A split window algorithm for estimating land surface temperature from satellites. *Adv. in Space Res.* 14(3):59-65.

Page blank

70

CHAPTER 6

Evapotranspiration Modeling for Irrigation Purposes

Ignacio Sanchez Cohen, Ernesto A. Catalan Valencia,
and Magdalena Villa Castorena

CONTENTS

Introduction	72
Water Availability and Irrigation Needs	73
Methods for Computing Evapotranspiration	74
Combination Methods	75
Radiation Methods	77
Temperature Methods	78
Evaporation Methods	79
Comparison of Methods	79
Some Applications of ET Data	81
Using computed ET_0 for Irrigation Scheduling	81
Other Uses of Computed ET for Planning Purposes	83
Conclusions	86
References	87

INTRODUCTION

Growing more food with less water is the key to solving the world's water crisis... Only by achieving 'more crop per drop' can we hope to increase food security for the world's poor.

IWMI

Water availability is considered to be one of the most critical factors for food production, economic development, and life itself. The presence or absence of this natural resource determines the health and well-being of societies. Water shortages have led most of arid and semi-arid countries to increase food imports because the local agricultural sector is not able to produce sufficient food to satisfy the existing food demands. The increasing food demands are posing serious challenges to all sectors concerned with the allocation and use of water, particularly agriculture, which is by far the largest user of water in the world. The International Water Management Institute estimates that 118 countries have enough hydraulic resources for satisfying their water demands through 2025; nevertheless, some of these countries should build large and expensive hydraulic structures, and not all may have the economic resources to do so (IWMI, 2003).

Total availability of fresh water for humans has declined over time due to growing population and competence among different sectors, such as agriculture, industry, and domestic use. Efforts must be directed at producing more food with less water or at increasing the efficiency of use since agriculture is entering into serious conflicts with urban population and activities such as industrial development. Figure 6-1 shows this situation for Mexico and the United States. For both countries, the population growth and the per capita water availability (PCWA) follow opposite trends. With respect to PCWA figures in 1955, the PCWA declined by 63 and 33% in 1990 and is expected to decrease by 75 and 45% in 2025 for Mexico and the United States, respectively.

Agriculture currently consumes 70 % or more of the world's developed freshwater supplies. If it is considered that it takes 2000 to 5000 L of water to produce enough food to feed one person each day, it is easy to comprehend how important increasing the productivity of water in agriculture is to our future (IWMI, 2003). Table 6-1 shows an example of irrigation water use for some countries by the year 2000 according to their renewable water capacity.

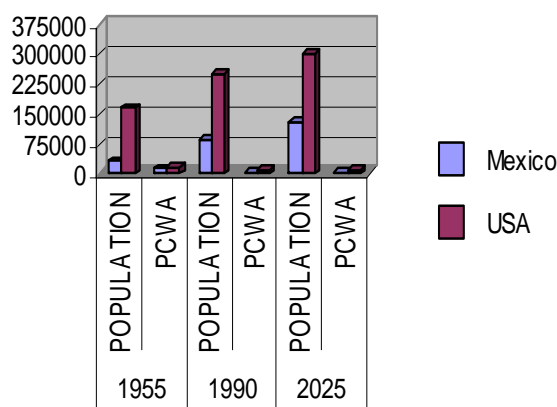


Fig. 6-1. Population and annual renewable fresh water availability for Mexico and the United States. (Data for year 2025 consider low projection. FAO, 2003) PCWA, per capita water availability.

Table 6-1. Irrigation water use for selected countries related to their renewable water resources. Adapted from FAO's Information System on Water and Agriculture (FAO, 2003).

Country	Total renewable water resources (km ³)	Irrigation water requirements (km ³)	Water use efficiency (%)	Water withdrawal (% of renewable water resources)
Bolivia	622	0.3	23	0
Brazil	8233	6.2	17	0
India	1897	303	54	29
Guatemala	111	0.4	25	1
Jordan	0.9	0.3	39	86
Mexico	457	18.5	31	13
Pakistan	223	72.1	44	73

WATER AVAILABILITY AND IRRIGATION NEEDS

The combination of two separate processes whereby water is lost from the soil surface by evaporation, on the one hand, and from the crop by transpiration, on the other hand, is referred to as evapotranspiration (ET). The growth of crops depends on how much water they transpire directly from the leaves and evaporate from soil. The reason why the term evapotranspiration is taken to be *consumptive use* is that, in practice, direct evaporation is difficult to measure separately from transpiration, so the two terms are lumped together merely for the sake of convenience (Hillel, 1997). In this way, efficient irrigation methods seek to reduce the rate of evaporation but not the rate of transpiration. Clearly, however, much of the water evaporated without entering the plant is consumed non-productively. Therefore, any method of irrigation that minimizes evaporation but not transpiration is likely to increase the efficiency of water utilization by the crop.

In planning irrigation schemes, the Moisture Availability Index (MAI) is used; it is the ratio between rainfall at 75% of probability of occurrence and potential evapotranspiration. The greater the MAI, the less is the water stress. Figure 6-2 shows the MAI for the American continent for two distinctive months. According to this figure, there is a greater likelihood of success with rain-fed agriculture schemes during summer in most of the northern and central portions of the continent.

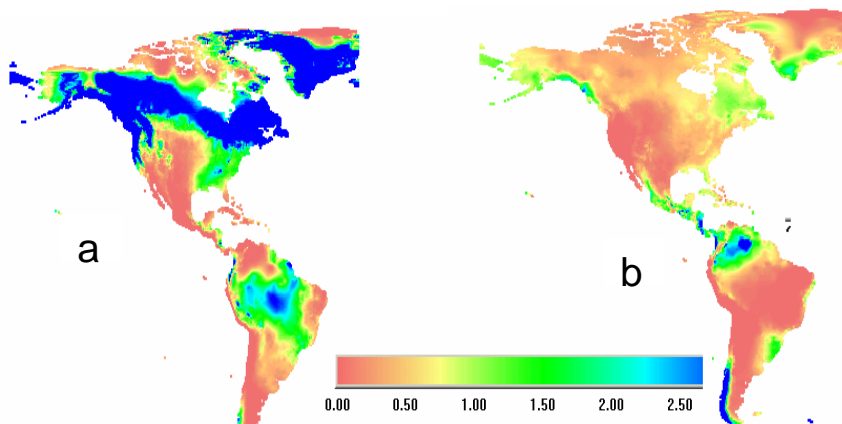


Fig. 6-2. Moisture availability index for the American continent for January (a) and August (b) computed using IWMI Atlas Synthesizer.

Also, for planning purposes, the evapotranspirative deficit ($1 - P/ET$) is used; it refers to the amount of water deficit that needs to be supplied either by rainfall (P) or irrigation in order to have potential yields. In this equation, ET may be exchanged by pan evaporation data (Ev). Even though the result of this shift in variables does not produce the same result, the overall outcome reflects the same situation, highlighting lack of adequate amount of water for supplying crop water demands. Figure 6-3 shows the evapotranspirative deficit for the irrigation districts of Mexico.

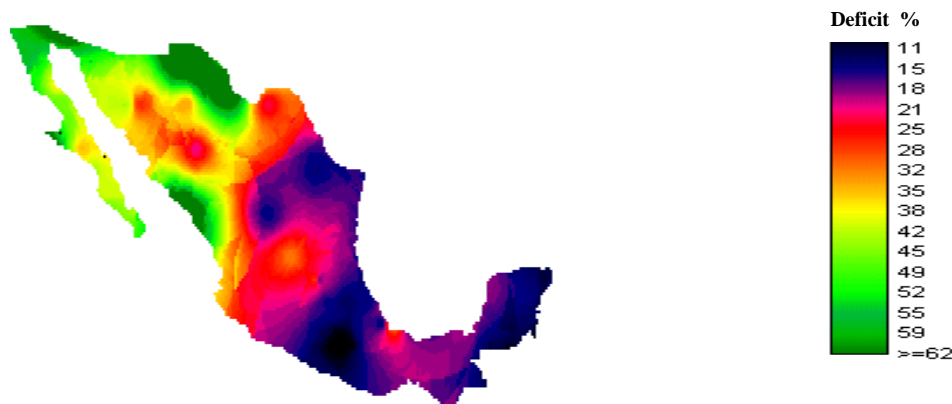


Fig. 6-3. Evapotranspirative deficit for the irrigation districts of Mexico. Interpolation procedure may reflect over-estimation of deficit in the Sierras. Source: Sanchez-Cohen et al., 2003.

METHODS FOR COMPUTING EVAPOTRANSPIRATION

Evapotranspiration data at different space scales (local, field, regional) and time steps (instantaneous, daily, seasonal) are required for many applications in agricultural and natural resource management, such as irrigation scheduling, planning the efficiency of plant water use, plant growth modeling, predicting crop yield, and for hydrologic studies (Steiner et al., 1991; Hillel, 1997). Evapotranspiration is a physical-physiological process related to water vapor transport from soil and plant to atmosphere. Available methods for measuring evapotranspiration are based on soil water balance estimation, direct measurements using lysimeters, micrometeorological methods, including portable chambers, eddy correlation or Bowen ratio, or plant physiological methods (Hatfield, 1990; Allen et al., 1990). However, in most locations, equipment needed for direct measuring of evapotranspiration is not available, and evapotranspiration must be estimated from available climatic and crop data.

A common procedure used in irrigation management programs for estimating actual evapotranspiration, ET_c , from a crop is to first estimate potential evapotranspiration (ET_p) for a reference crop and then to apply dimensionless crop and soil coefficients (Doorenbos and Pruitt, 1977; Allen et al., 1989). The ET_c is the amount of water lost from the plant and soil to the atmosphere, given the current meteorological conditions, soil water availability, and plant growth

stage. Potential evapotranspiration for a reference crop is known as reference evapotranspiration, and the crop is usually taken as well-irrigated, short clipped grass, ET_0 , or alfalfa, ET_r (Allen et al., 1990; Jensen et al., 1990). The crop coefficient represents the ratio of evapotranspiration occurring with a specific crop at a specific stage of growth to the reference crop and is determined empirically or from experimental data (Doorenbos and Pruitt, 1977; Inzunza and Mojarro, 1989; Annandale and Stockle, 1994). In order to obtain reliable estimates of ET_c from a specific crop, appropriate crop coefficients selected from literature or experimental data must be used. For example, crop coefficients originated from a grass reference crop should not be used with alfalfa reference evapotranspiration or vice versa.

Various methods with varying degrees of complexity are used for estimating either ET_0 or ET_r . All of them attempt to represent the physical laws governing the evapotranspiration process and use diverse meteorological and cropping data, such as solar radiation, air temperature, wind speed, and leaf area index. The methods or equations for estimating reference evapotranspiration fall within four general categories: 1) combination methods, 2) radiation methods, 3) temperature methods, and 4) evaporation methods (Jensen et al., 1990). The combination methods use more than one approach to arrive at evapotranspiration estimates and involve a solution of the energy balance equation ($R_n = H + LE + G$). The following is a brief description of some of the most representative methods of each category; many others are reported in literature (Rodriguez, 1986; Hatfield, 1990; Mojarro, 1990).

Combination Methods

The Penman method (Penman, 1948) is a combination equation that has the following general form:

$$\lambda ET = \frac{\Delta(R_n - G) + \gamma 6.43 W_f(e_a - e_d)}{\Delta + \gamma} \quad [1]$$

where λET is the evapotranspiration rate denoted as a rate of latent heat flux density ($MJ m^{-2} t^{-1}$), with t being the time scale for the estimation of water vapor flux, Δ is the slope of the saturation vapor pressure curve ($kPa ^\circ C^{-1}$), R_n is net radiation flux density to the plant canopy ($MJ m^{-2} t^{-1}$), G is soil heat flux density ($MJ m^{-2} t^{-1}$), γ is the psychometric constant ($kPa ^\circ C^{-1}$), e_a is the saturation vapor pressure at the current air temperature (kPa), e_d is the saturation vapor pressure at the dew point temperature (actual vapor pressure of the air, kPa), and W_f is an empirical wind function:

$$W(u) = a_w + b_w u_2 \quad [2]$$

where u_2 is wind speed (ms^{-1}) at 2 m above the ground, and a_w and b_w are empirical coefficients. Penman (1948, 1963) recommended values of 1.0 and 0.537 for a_w and b_w for clipped grass.

Some of the most known combination methods originated from modifications of the Penman equation. Two of them were based on studies conducted at Kimberly, Idaho, for alfalfa ET_r and focused on the estimation of alternative values of the wind function coefficients. The first method was the **1972 Kimberly Penman equation** for which Wright and Jensen (1972) suggested values of 1.0 and 0.0536 for a_w and b_w for alfalfa grown in coastal and humid climates, and values of 0.75 and 0.993 for alfalfa in arid and semi-arid areas. The second method was the **1982 Kimberly**

Penman equation for which Wright (1982) developed the following expressions for the estimation of the wind function coefficients using the calendar day, D, as independent variable:

$$a_w = 0.4 + 1.4 \exp \left\{ -[(D - 173)/58]^2 \right\} \quad [3]$$

$$b_w = 0.605 + 0.345 \exp \left\{ -[(D - 243)/80]^2 \right\} \quad [4]$$

Another modified Penman method is the **FAO Penman equation** that was presented by Doorenbos and Pruitt (1977) in the FAO-24 report for the estimation of grass ET₀. Basically, the modifications include a more sensitive wind function with values of 1.0 and 0.864 for the coefficients a_w and b_w, a correction factor estimated from local climatic data affecting the right side of the Penman equation, and the assumption that G=0 for daily periods.

The Penman-Monteith method (Monteith, 1981) is the most relevant Penman derived equation. It is considered as a combination equation that includes aerodynamic and surface resistance terms. This method can be used for the estimation of either grass ET₀ or alfalfa ET_r, but different values are used for leaf area index (LAI) and bulk stomatal resistances (Allen et al., 1989). The equation has the form:

$$\lambda ET = \frac{\Delta(R_n - G) + \rho c_p(e_a - e_d)r_a}{\Delta + \gamma(1 + r_c/r_a)} \quad [5]$$

where ρ is the density of air (kg m^{-3}), c_p is the specific heat of air ($\text{MJ kg}^{-1} \text{ }^{\circ}\text{C}^{-1}$), r_a is the aerodynamic resistance to vapor and heat diffusion (t m^{-1}), and r_c is the bulk stomatal (canopy) resistance (t m^{-1}). The aerodynamic resistance is estimated as:

$$r_a = \frac{\ln[(z_m - d)/z_{om}] \ln[(z_h - d)/z_{oh}]}{k^2 u_z} \quad [6]$$

with

$$z_{om} = 0.123h_c \quad [7]$$

$$z_{oh} = 0.1z_{om} \quad [8]$$

$$d = 0.67h_c \quad [9]$$

where z_m is the height of the wind speed measurement (m), z_h is the height of the air temperature and humidity measurements (m), d is the zero plane displacement height (m), z_{om} is the roughness length for momentum transfer (m), z_{oh} is the roughness length for water vapor and heat transfer (m), k is the von Karman constant for turbulent diffusion (0.41), u_z is the wind speed (m s^{-1}) at height z , and h_c is the mean height of crop canopy. The canopy resistance is approximated as:

$$r_c = \frac{r_l}{0.5 \text{ LAI}} \quad [10]$$

where r_l is an average value of minimum daytime surface (stomatal) resistance for a single leaf (approximately 100 s m^{-1} for alfalfa and grass leaves), and LAI is the canopy leaf area index.

Radiation Methods

The Jensen-Haise equation (Jensen and Haise, 1963) is a radiation method that provides estimates of alfalfa reference evapotranspiration on either monthly or 5-d time steps:

$$\lambda ET_r = C_T (T - T_x) R_s \quad [11]$$

where C_T and T_x are empirical constants valid for a specific area, T is the daily mean air temperature in $^{\circ}\text{C}$, and R_s is the solar radiation in $\text{MJ m}^{-2} \text{ d}^{-1}$. Jensen suggested the following relations to estimate C_T and T_x (Jensen et al., 1990):

$$C_T = \frac{1}{C_1 + C_2 C_H} \quad [12]$$

$$T_x = -2.5 - 1.4(e_2 - e_1) - \text{Elev}/550 \quad [13]$$

$$C_1 = 38 - (2\text{Elev}/305) \quad [14]$$

$$C_2 = 7.3 \quad [15]$$

$$C_H = \frac{5.0 \text{ kPa}}{(e_2 - e_1)} \quad [16]$$

where Elev is site elevation in m, e_2 and e_1 are the saturation vapor pressure in kPa at mean monthly minimum and maximum air temperature, respectively, of the warmest month of the year.

The **Priestley-Taylor radiation equation** (Priestley and Taylor, 1972) is another simplified method for the estimation of grass ET_0 or alfalfa ET_r . It is for use in humid sites where the advective effects of wind are minor; therefore, the aerodynamic component of the Penman equation is eliminated. In addition, the energy component of this equation is affected by a calibration coefficient $\alpha=1.26$, resulting in the following equation with all its variables previously defined:

$$\lambda ET = \alpha \frac{\Delta}{\Delta + \gamma} (Rn - G) \quad [17]$$

The FAO radiation method proposed by Doorenbos and Pruitt (1977) requires solar radiation and air temperature data for the estimation of grass ET₀:

$$ET_0 = a + b \left[\frac{\Delta}{\Delta + \gamma} Rs \right] \quad [18]$$

where solar radiation, Rs, is required in mm d⁻¹, the constant $a=-0.3$ mm d⁻¹, and b is an empirical coefficient that depends on mean relative humidity (RH_{mean}, in percentage) and mean daytime wind speed (U_d, in m s⁻¹) and can be estimated as:

$$\begin{aligned} b = & 1.066 - 0.13 \times 10^{-2} RH_{\text{mean}} + 0.045 U_d - 0.20 \times 10^{-3} RH_{\text{mean}} U_d \\ & - 0.315 \times 10^{-4} RH_{\text{mean}}^2 - 0.11 \times 10^{-2} U_d^2 \end{aligned} \quad [19]$$

Temperature Methods

The SCS Blaney-Criddle method (Blaney and Criddle, 1962) was developed in the western United States and has been applied in many places around the world. Originally, this method was created for obtaining seasonal estimates of potential evapotranspiration, ET_p, but it was later adapted for monthly (or daily as a monthly average) periods of time according to the following equations:

$$ET_p = p(0.46 T + 8.13) \quad [20]$$

$$p = 0.00304 \cos^{-1} \left[\frac{-\sin(\delta) \sin(\text{lat})}{\cos(\delta) \cos(\text{lat})} \right] \quad [21]$$

$$\delta = \text{sen}^{-1}(0.39795 \cos(0.98563(\text{DDA} - 173))) \quad [22]$$

where ET_p is obtained in mm d⁻¹ as a monthly average, p is the mean daily percent of annual daytime hours, T is daily mean air temperature as a monthly average in °C, δ is solar declination angle in degrees, lat is the latitude, and DDA is Julian day.

The FAO-24 Blaney-Criddle method for estimating grass reference evapotranspiration is the result of a revision made by Doorenbos and Pruitt (1977) of the original Blaney-Criddle method:

$$ET_0 = f_e \{ a + b[p(0.46 T + 8.13)] \} \quad [23]$$

$$a = 0.0043 RH_{\text{min}} - n/N - 1.41 \quad [24]$$

$$b = 0.82 - 0.0041 RH_{\text{min}} + 1.07 \frac{n}{N} + 0.066 U_d - 0.006 RH_{\text{min}} \frac{n}{N} - 0.0006 RH_{\text{min}} U_d \quad [25]$$

where ET_0 is in mm d^{-1} , f_c is a correction factor by altitude above sea level, a and b are two climatic calibration coefficients derived from measured ET_0 and climatic data, RH_{\min} is the minimum daily relative humidity in percentage, n/N is the ratio of possible to actual sunshine hours, and U_d is daytime wind at 2-m height, in ms^{-1} . The expression for the b coefficient is a simplified version (Cuenca, 1989) of the equation obtained by Frevert et al. (1983) from tabulated data reported by Allen and Pruitt (1986). An adjustment in grass reference evapotranspiration of a 10% upward for each 1000-m increase in elevation above sea level was suggested by Allen and Pruitt (1986).

The Hargreaves method for estimating grass reference evapotranspiration was originally presented as a radiation method by Hargreaves (1974):

$$ET_0 = 0.0135Rs(T + 17.8) \quad [26]$$

and adapted by Hargreaves and Samani (1982) for situations when solar radiation measurements are not available:

$$ET_0 = 0.0023Ra TD^{1/2}(T + 17.8) \quad [27]$$

where Rs and Ra are solar radiation and extraterrestrial radiation expressed in equivalent evaporation units (mm), respectively, and TD is the difference between maximum and minimum air temperature in $^{\circ}\text{C}$. Because Ra can be estimated for any given day and location, only maximum and minimum air temperatures require direct observation in this method.

Evaporation Methods

The pan evaporation method, the oldest and simplest approach for estimating grass ET_0 , indirectly integrates the effects of atmospheric conditions on evaporation through the following proportional relationship:

$$ET_0 = k_p E_{\text{pan}} \quad [28]$$

where E_{pan} is pan evaporation, and k_p is a required coefficient as pan evaporation is generally higher than evaporation from soil and water ponds. Numerous studies have shown that k_p depends on several factors, such as the type of pan used, the climate, and the conditions of the nearby surface around the pan, which hampers the reliability of this method (Pruitt, 1966; Doorenbos and Pruitt, 1977). Other evaporation methods, such as the FAO-24 (Doorenbos and Pruitt, 1977) and the Christiansen (Jensen et al., 1990) pan evaporation methods, focus on estimating k_p values from weather parameters and some characteristics of the pan surrounding area.

Comparison of Methods

Jensen et al. (1990) presented a comparison of 20 different methods for estimating ET_0 and ET_r against lysimeter measurements in 11 different locations. A subgroup of 15 of these methods are compared in Table 6-2 in terms of type of method or classification, data requirements, time resolution or time step, and method performance in wet and arid sites. In this study, as in many

others, the combination methods, which are based on the energy balance analysis, have shown good performance, especially the Penman Monteith equation, which has performed well in humid and arid sites and at monthly, daily, hourly, or shorter time steps (Garcia, 1986; Allen et al., 1989; Steiner et al., 1991). The main limitation of the combination methods is related to instrumentation and collection of climatic data, particularly water vapor pressure deficit and wind speed.

Table 6-2. Comparison of methods for estimating reference evapotranspiration.

Methods by classification group (Jensen et al., 1990)	Reference crop	Data required					Minimum time step	Rank of methods according to Jensen et al. (1990)	
		Air Temp.	Air Hum.	Wind Speed	Solar Rad.	Evap.		Wet sites	Arid sites
Combination									
Penman (1963)	Alfalfa Grass	✓	✓	✓	✓		Daily	3	4
Penman-Monteith (1965)	Alfalfa Grass	✓	✓	✓	✓		Hourly Daily	1	1
FAO-Penman (1977)	Grass	✓	✓	✓	✓		Daily	11	6
Kimberly-Penman (1982)	Alfalfa	✓	✓	✓	✓		Daily	5	2
Radiation									
Turc (1961)	Grass	✓	✓		✓		10 days	2	13
Jensen-Haise (1963)	Alfalfa	✓			✓		5 days	9	7
Priestley-Taylor (1972)	Alfalfa Grass	✓			✓		10 days	4	14
FAO-24 radiation (1977)	Grass	✓	✓	✓	✓		5 days	8	3
Temperature									
Thornwaite (1948)	Grass	✓					Monthly	10	15
SCS Blaney-Criddle (1962)	Alfalfa Grass	✓					Monthly	12	10
FAO-24 Blaney-Criddle (1977)	Grass	✓	✓	✓			5 days	6	5
Hargreaves (1982)	Grass	✓					10 days	7	8
Evaporation									
Type A pan evaporation	Grass					✓	Daily	15	12
Christiansen (1968)	Grass	✓	✓	✓		✓	Monthly	14	11
FAO-24 pan evaporation (1977)	Grass		✓	✓		✓	5 days	13	9

The relative performance of some of the radiation, temperature and evaporation methods in Table 6-2 does not reflect the amount of data required or the assumptions made about each method. For example, the temperature methods of Thornwaite and SCS Blaney Criddle had a similar performance as the evaporation methods of Christiansen and FAO-24 despite their differences in the amount of data required. Similarly, the performance of the temperature method of Hargreaves was comparable to that of the temperature FAO-24 and some of the radiation methods. On the other hand, the radiation method of Priestley-Taylor had a better performance in wet sites, which is congruent with the assumption of not considering aerodynamic effects, but the Jensen-Haise method showed a contrary behavior.

In general, the radiation, temperature, and evaporation methods are considered as empirical or statistical approaches because they are limited by the representativeness of the original data used to estimate the calibration coefficients (Hatfield, 1990). The reliability of these methods depends not only on the nature of each approach, but also on the amount of data used in the calibration process. Therefore, local calibration with sufficient amount of data is advisable for obtaining reliable ET estimates. Despite their limitations, these empirical methods are used because some of them are the only option for estimating ET in areas where climatic data are quite limiting.

SOME APPLICATIONS OF ET DATA

Using Computed ET_0 for Irrigation Scheduling

The main purpose of irrigation scheduling is to predict the appropriate time of irrigation and amount of water to be applied in order to satisfy crop water demand. Although several methods for irrigation scheduling have been proposed in the literature, we will focus on one of the most known methods: the soil water balance method, which has been applied in large irrigation areas and is based on the following equation:

$$\Delta W = I + P - ET_c - D \quad [29]$$

where ΔW is the change of soil water content, P is precipitation, I is irrigation, ET_c is actual crop evapotranspiration, and D is drainage or deep percolation. Each of these components must be quantified in proper space and time scales to solve the soil water balance equation. The space scale is the soil depth explored by plant roots, and the time scale is usually one day as most computational programs for irrigation scheduling use daily time steps to solve that equation (Fox et al., 1994; Ojeda et al., 1999; Catalan, 2002). The soil water content for the actual day, W_i , can be obtained in terms of a known soil water content from the previous day, W_{i-1} , and the rest of the terms of Eq. [29] estimated for the actual day:

$$W_i = W_{i-1} + I_i + P_i - ET_{c,i} - D_i \quad [30]$$

The value of W_i is compared with a critical soil water content value (W_c) each day for determining irrigation time. If W_i is less than W_c , then the crop must be irrigated the next day; if not, each term on the right side of Eq. [30] is updated for the next day. The critical soil water content is estimated as:

$$W_c = AW(1.0 - MAD) \quad [31]$$

where AW is available water in the soil profile, and MAD is a dimensionless fraction representing the portion of AW that is allowed to be depleted between two irrigation events. The quantity AW is obtained with:

$$AW = (\theta_{FC} - \theta_{PWP}) D_R \quad [32]$$

where θ_{FC} and θ_{PWP} are the volumetric soil water content at field capacity and permanent wilting point, respectively, and D_R is the plant root depth. Values for θ_{FC} and θ_{PWP} can be experimentally measured or estimated from soil texture. On the other hand, the amount of water required for irrigation (I) is computed as the difference between AW and W_c only for the day when W_i is less than W_c , but is assumed to be zero for any other day.

The precipitation term, P_i , is actually estimated as effective rain (P_e) as some part of it is lost by evaporation or runoff and is not available for plant use. Because of the complexity of its estimation, P_e is usually estimated with empirical expressions derived from statistical analysis such as that proposed by Orosky and Mockus (1964), cited by Ojeda et al. (1999):

$$P_e = K_p P \quad [33]$$

$$\frac{1}{K_p} = 1.53 \frac{P}{ET_c} + 0.8 \quad [34]$$

where K_p is an empirical coefficient, P is observed precipitation, and ET_c is actual precipitation accumulated since the last precipitation event.

As mentioned earlier, actual crop evapotranspiration, ET_c , is commonly estimated with ET_0 affected by crop coefficients which are empirical ratios of ET_c to ET_0 :

$$ET_c = K_c ET_0 \quad [35]$$

where K_c is a dimensionless crop coefficient for a specific crop at a given growth stage and soil moisture status. Crop coefficients indicate the relative capacity of a specific crop-soil surface to meet the evaporative demand of a reference crop surface determined by climate conditions (ET_0) (Jensen et al., 1990). A crop-specific K_c curve describes the variation of K_c with time throughout the crop season. Other variables such as solar thermal units and growing degree days have been used instead of elapsed time to describe K_c variations. Several sets of crop coefficients, in correspondence with different methods for estimating ET_0 , are reported in the literature (Doorenbos and Pruitt, 1977; Wright, 1982).

Deep percolation or drainage (D) will occur when soil profile water-holding capacity is overloaded. This is when $P_e - ET_c$ is greater than AW, and the value of D is computed as:

$$D = AW - P_e + ET_c \quad [36]$$

Irrigation scheduling can be performed at different degrees of approximation, depending on the type of weather data used to estimate ET_0 . Average irrigation schedules for a given crop,

location, and soil type can be obtained with daily average values of climatic variables derived from historical weather data. Table 6-3 shows approximate irrigation schedules for bean, sorghum, and wheat obtained from average climatic data for a loam soil at the irrigation district of Buenaventura in Chihuahua, Mexico. Real-time irrigation schedules can also be obtained by predicting irrigation time from real-time estimates of ET_0 . This approach requires the monitoring of actual climatic data for computing ET_0 and can be complemented with the use of sensors for the monitoring of some crop water stress indicators (Ojeda et al., 1999).

Table 6-3. Approximate irrigation schedules for some crops at Buenaventura in Chihuahua, Mexico.

Crop: Bean; Sowing date: 06/01; Crop cycle: 100 days								
Irrigation number	1	2	3	4	5	6	7	Total
Irrigation depth (cm)	12	7	7	6	6	6	6	50
Irrigation interval (days)	0	20	18	14	12	12	12	
Crop: Sorghum; Sowing date: 04/15; Crop cycle: 120 days								
Irrigation number	1	2	3	4	5	6	7	Total
Irrigation depth (cm)	14	9	9	9	8	8		57
Irrigation interval (days)	0	30	25	15	15	15		
Crop: Wheat; Sowing date: 03/01; Crop cycle: 130 days								
Irrigation number	1	2	3	4	5	6	7	Total
Irrigation depth (cm)	14	9	9	9	8	8	8	65
Irrigation interval (days)	0	32	20	16	14	14	14	

Other Uses of Computed ET for Planning Purposes

Water is one of the main inputs to agricultural production. Its scarcity reduces the rate of evapotranspiration affecting crop yield. Therefore, information about crop water needs is of crucial importance, especially when this resource is limited. Some applications of the knowledge of crop water demands are the following:

Optimal water use: Different mathematical expressions have been used to relate crop yield to evapotranspiration. One of the most known expressions is the relationship proposed by Doorenbos and Kassam (1979):

$$\left(1 - \frac{ET_c}{ET_m}\right) = Ky \left(1 - \frac{Y_c}{Y_m}\right) \quad [37]$$

where ET_c is actual evapotranspiration and depends on the magnitude of crop water use deficit for a specific crop irrigation management, ET_m is the maximum crop evapotranspiration under unlimited water supply, and K_y is a crop factor representing the rate between the relative evapotranspiration deficit and the relative crop yield deficit. Thus, the crop will yield Y_c if ET_c

occurs and will yield Y_m if ET_m occurs. This relationship indicates how much crop yield will decrease under limited water supply for crop development. Table 6-4 shows some K_y values obtained for different crops at the Lagunera Region, an arid area located in the northern Mexican states of Coahuila and Durango.

Table 6-4. Crop sensitivity to water stress.

CROP	K_y
Sorghum	1.65
Maize	(0.319) [†] -(0.225) [‡]
Beans	0.85
Maize forage	1.12

[†] First crop phenological development period (from sowing to flowering)

[‡] Second crop phenological development period (from flowering to maturity)

Studies of productivity potential: These are of crucial importance to rain-fed agriculture. Figure 6-2 shows the value of the moisture availability index (a modification of the left hand side of Eq. [37]), which is useful for determining basic criteria of potential harm to crops due to water deficit.

Global planning: For global planning purposes, ET data aid in better decision-making on irrigation systems, e.g., water allocation and management in irrigation districts. Figure 6-4 shows ET_m values for some crops under distinctive climatic regions of Mexico (characterized by different colors in the figure). Based on this information, irrigation planners may schedule irrigations for crops even on a daily basis (precision agriculture) or by some other irrigation interval.

Comparative indexes: ET data are also useful for evaluating and comparing irrigation districts or irrigation_units in terms of agronomic, hydrologic, economic and financial comparative indexes (Kloezen and Garces, 1998): For instance, Fig. 6-5 shows the relative water availability index (DRAR) for four irrigation districts of Mexico. This index is computed as:

$$\text{DRAR} = \frac{\text{TWC}}{\text{ET}_m} \quad [38]$$

where TWC is total water conveyance to the irrigation unit (irrigation + total precipitation), and ET_m is as previously defined. In general terms, a DRAR less than one means that there was a water deficit that affected crop yield. A DRAR around or equal to 1.5 means that system operation was adequate, without impact on crop yield. The greater the DRAR, the less the management requirements for success. DRAR values greater than 2.5 mean that water deficit was not an important factor to impact irrigation development. This information allows us to understand better the processes and dynamics of system management.

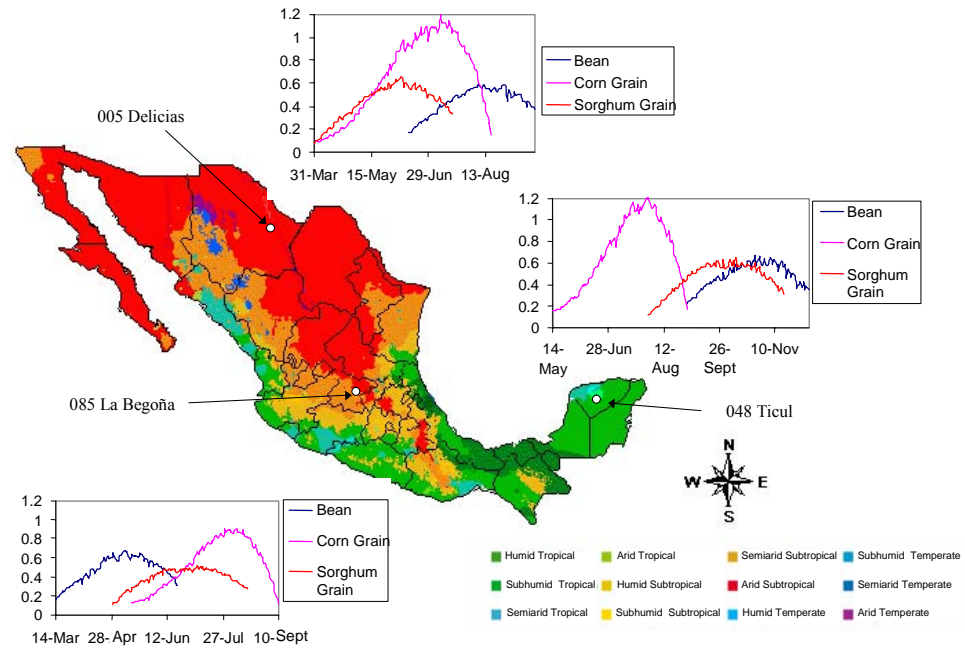


Fig. 6-4. ET_m for some crops in distinctive climatic regions of Mexico.

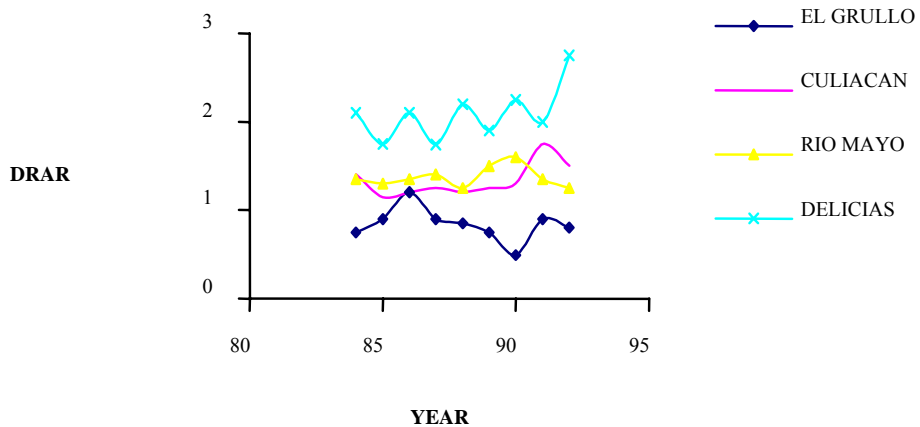


Fig. 6-5. Variation of relative water deficit (DRAR) for four irrigation districts of Mexico. Source: Levine, 1999.

Other indexes are combined with ET data to evaluate irrigation system performance. For example, the standardized gross value of production (SGVP) allows the comparison of systems irrespective of their location or the type of crops being produced; the SGVP may be computed as:

$$SGVP = \left(\sum A_i Y_i \frac{P_i}{P_b} \right) P_m \quad [39]$$

where A_i is the area cultivated with crop i , Y_i is the yield of crop i , P_i is the local price of crop i , P_b is the local price of base crop (main local crop also internationally commercialized), and P_m is the international price of base crop. Combining the SGVP with ET data allows comparing the water use productivity (WUP) of different irrigation systems, or of different crops produced at different locations. Table 6-5 shows the use of this index in the irrigation district No.17 Comarca Lagunera, Mexico. The WUP shows that corn for forage yields the most money for unitary measure of ET, followed by sorghum and chile. This procedure allows planners to decide crop patterns when water availability is scarce or rainfall is uncertain.

Table 6-5. Water use productivity (WUP) for Irrigation District No.17, Comarca Lagunera, Mexico, for year 2001.

CROP	AREA (A) (ha)	MEAN YIELD (Y) (Mg ha ⁻¹)	PRICE (P) (\$ Mg ⁻¹)	SGVP [†] (A·Y·P·P _b ⁻¹ ·P _m) (\$)	ET (cm)	WUP SGVP ET ⁻¹ (\$ cm ⁻¹)
Sorghum grain	873	3.24	150	424,200	45	9427
Sorghum (broom)	3236	4.34	130	1,825,720	55	33,195
Sorghum forage	4113	43.16	22	3,905,374	41	95,253
Corn grain	4553	3.37	160	2,455,040	76	32,303
Corn forage	8873	43.44	24	9,250,632	64	144,541
Melon	1117	22.38	129	3,224,742	97	33,245
Watermelon	889	25.76	120	2,748,120	97	28,331
Peanuts	241	1.78	1900	815,100	70	11,644
Beans	944	1.22	651	749,952	49	15,305
Tomato	485	16.20	210	1,649,970	90	18,333
Chile	997	11.23	420	4,702,320	61	77,087
TOTAL				31,751,170		

[†]The main local crop is cotton with $P_b=P_m=\$ 879 \text{ Mg}^{-1}$

CONCLUSIONS

Water accounting is a big issue in arid regions where rainfall uncertainty limits the amount of water for irrigation. The knowledge of crop evapotranspiration plays an important role in water budgets of these regions. It is clear that the method for computing ET will depend mainly on available data and the precision desired. It is not worth using a sophisticated method for computing crop water demands when results are to be used for a global water budget where precision within a 10-d period is not needed. Nevertheless, if more precision is required and the necessary equipment for doing precise measurements is available, we should use it no matter what it takes in terms of field work. Less precise (compared with the standard) methods yield ET results

that need to be critically evaluated to see if they fulfill the information requirements we are looking for.

The main use of ET data is in irrigation scheduling; hence, modeling crop water demands points mostly to this direction. For several decades, ET modelers have focused on approaches for estimating ET that demand less information; however, recent developments in instrumentation and data acquisition give ET modelers the possibility of changing this trend and focusing on more complete and precise approaches for estimating ET. Increasing the accuracy and resolution of ET modeling will allow a higher degree of control on this process and hence, better management and planning of water resources. An example of this is real-time irrigation scheduling, which has become a powerful tool for automating irrigation systems using ET information and soil data. This procedure will have a great impact as the trend in irrigation districts is to pressurize the water delivery system in the near future.

In planning irrigation schemes, irrigation planners should look for alternative crops when traditional crops demand more water than is available. This is part of an overall strategy for coping with water scarcity. In some countries such as Mexico, irrigation district managers group farmers around main water delivery canals (compact areas) in order to avoid large transects for conducting water to fields. The DRAR index thus helps planners evaluate the irrigation districts' performance by comparing water demands (ET) versus water delivered to fields by the irrigation district. This procedure highlights water conveyance efficiency.

This chapter has pointed out some of the many applications of ET data which have increasing water use efficiency as a main goal. Further research is needed in order to have a more precise ET assessment that considers actual technological developments and the growing needs for increasing water use efficiency.

REFERENCES

- Allen, R.G., M.E. Jensen, J.L. Wright, and R.D. Burman. 1989. Operational estimates of reference evapotranspiration. *Agron. J.* 81:650-662.
- Allen, R.G., R.H. Cuenca, M.E. Jensen, W.O. Pruitt, R.K. Blatchlet, J.M. Erpenbeck, E.L. Johns, J.F. Stone, R.D. Burman, R.W. Hill, P.R. Nixon, and J.L. Wright. 1990. Evapotranspiration and irrigation water requirements. In M.E. Jensen, R.D. Burman, and R.G. Allen (ed.) *Manuals and Reports on Engineering Practice No. 70*. ASCE, New York.
- Allen, R.G., and W.O. Pruitt. 1986. Rational use of the FAO Blaney-Criddle formula. *J. Irrig. Drain. Div. Am. Soc. Civ. Eng.* 112:139-155.
- Annandale, J.G. and C.O. Stockle. 1994. Fluctuation of crop evapotranspiration coefficients with weather: A sensitivity analysis. *Irrig. Sci.* 5:1-7.
- Blaney, H. F. and W.D. Criddle. 1962. Determining consumptive use and irrigation water requirements. *Tech. Bull. No. 1275*. USDA-ARS.
- Catalan, V.E. 2002. Program for farm irrigation scheduling. (In Spanish.) CENID RASPA INIFAP, Gómez Palacio, Durango, México.
- Cuenca, R.H. 1989. Irrigation systems design. An engineering approach. Prentice Hall, New Jersey, USA.

- Doorenbos, J., and A.H. Kissam. 1979. Yield response to water. Irrigation and Drainage Paper No. 33. FAO, Rome, Italy.
- Doorenbos, J., and W.O. Pruitt. 1977. Crop water requirements. Irrigation and Drainage Paper No. 24. FAO, Rome, Italy.
- Food and Agricultural Organization. 2003. FAO's information system on water and agriculture. Land and Water Development Division, FAO, Rome, Italy.
- Frevert, D.K., R.W. Hill, and C.C. Braaten. 1983. Estimation of FAO evapotranspiration coefficients. *J. Irrig. Drain. Div. Am. Soc. Civ. Eng.* 109:265-269.
- Fox, F.A., T.F. Schere, D.C. Slack, and L.J. Clark. 1994. Arizona Irrigation Scheduling (AZSCHED Version 1.1E). User's manual. Cooperative Extension, University of Arizona, Tucson, AZ.
- Garcia, H.G. 1986. Evapotranspiration of annual crops at the Lagunera Region.(In Spanish.) p. 182-208. *In* Estudios de evapotranspiracion. SARH-INIFAP-PRONAPA, Gomez Palacio, Durango, Mexico.
- Hargreaves, G.H. 1974. Estimation of potential and crop evapotranspiration. *Trans. ASAE* 17:701-704.
- Hargreaves, G.H., and Z.A. Samani. 1982. Estimating potential evapotranspiration. *J. Irrig. Drain. Div. Am. Soc. Civ. Eng.* 108:223-230.
- Hatfield, J.L. 1990. Methods of estimating evapotranspiration. p. 435-468. *In* B.A. Stewart and D.R. Nielsen (ed.) Irrigation of agricultural crops. Agron. Monogr. 30. ASA-CSSA-SSSA, Madison, WI, USA.
- Hillel, D. 1997. Small-scale irrigation for arid zones. Principles and options. FAO Development Series No. 2. FAO, Rome, Italy.
- Inzunza, M.A.I., and F.D. Mojarrro. 1989. Determining a crop coefficient for maize. (In Spanish.) Technical report. CENID RASPA-INIFAP, Mexico.
- IWMI. 2003. International Water Management Institute. Comprehensive Assessment of Water Management in Agriculture. Third World Water Forum, Kyoto, Japan. [Online] Available at <http://www.iwmi.org/assessment>. Consulted on 15 May 2003.
- Jensen, M.E. and H.R. Haise. 1963. Estimating evapotranspiration from solar radiation. *J. Irrig. Drain. Div. Am. Soc. Civ. Eng.* 89:15-41.
- Jensen, M.E., R.D. Burman, and R.G. Allen. 1990. Evapotranspiration and irrigation water requirements. Manuals and Reports on Engineering Practice No.7. Irrigation Water Requirements Committee of the Irrigation and Drainage Division, Am. Soc.Civ. Eng., Drainage Division, New York.
- Kloezen, W.H., and C. Garces-Restrepo. 1998. Assessing irrigation performance with comparative indexes: The Alto Rio Lerma Mexican irrigation district case. Research Report 21. International Water Management Institute, Colombo, Sri Lanka.
- Levine, G. 1999. Understanding irrigation performance: Relative water availability as an explanatory variable. Latin American Series No. 6. International Water Management Institute, Mexico, D.F.
- Mojarro, F.D. 1990. Evapotranspiration and crop water needs. (In Spanish.) p 181-204. *In* L.F. Flores L., A. Lagarda M., C. Godoy A., R. Jasso I., and I. Sanchez C. (ed). Metodologia de investigacion y diagnostico en Relacion Agua Suelo Planta Atmosfera. CENID RASPA-INIFAP, Gomez Palacio, Durango, Mexico.
- Monteith, J.L. 1981. Evaporation and surface temperature. *J. Meteorol.* 107:1-27.

- Ojeda B.W., E. Sifuentes I., J.M. González C., J.A. Guillen G. and H. Unland W. 1999. Real-time irrigation forecast. (In Spanish.) Centro Nacional de Transferencia de Tecnología de Riego y Drenaje, Instituto Mexicano de Tecnología del Agua, Mexico.
- Penman, H.L. 1948. Natural evaporation from open water, bare soil, and grass. Proc. R. Soc. London A193:120-145.
- Penman, H.L. 1963. Vegetation and hydrology. Tech. Communication No. 53. Commonwealth Bur. Soils, Harpenden, England.
- Priestley, C. H. B., and R. J. Taylor. 1972. On the assessment of surface heat flux and evaporation using large scale parameters. Monthly Weather Rev. 100:81-92.
- Pruitt, W.O. 1966. Empirical method of estimating evapotranspiration using primarily evaporation pans. p. 57-61. In *Evaporation and its role in water resources management*. ASAE publ. St. Joseph, MI.
- Rodriguez, Z.C. 1986. Tools for determining crop evapotranspiration. (In Spanish.) p. 73-99. In L.F. Flores and R. Jasso I. (ed.) *Lisimetrica: Estudios de evapotranspiracion*. SARH-INIFAP-PRONAPA, Gomez Palacio, Durango, Mexico.
- Sanchez-Cohen, I., J. Estrada Avalos, and G. Gonzalez Cervantes. 2003. Irrigation technology transference in the irrigation districts of Mexico. Water International 27 (4): 578-584.
- Steiner, J.L., T.A. Howell, and A.D. Schneider. 1991. Lysimetric evaluation of daily potential evapotranspiration models for grain sorghum. Agron. J. 83:240-247.
- Wright, J.L. 1982. New evaporation crop coefficients. J. Irrig. Drain. Div. Am. Soc. Civ. Eng. 08:57-74.
- Wright, J.L., and M.E. Jensen. 1972. Peak water requirements of crops in southern Idaho. J. Irrig. Drain. Div. Am. Soc. Civ. Eng. 96:193-201.

Page blank
90

CHAPTER 7

Radar Remote Sensing for Estimation of Surface Soil Moisture at the Watershed Scale

M. Susan Moran, Stephen McElroy, Joseph M. Watts,
and Christa D. Peters-Lidard

CONTENTS

Introduction	91
Semi-Empirical Approaches	94
m_s Change Detection	96
SAR Data Fusion	97
SAR Plus Radar Backscatter Models	98
Conclusions	100
Acknowledgments	102
References	102

INTRODUCTION

Knowledge of surface soil moisture at the watershed scale would be useful for such critical applications as regional resource management during times of drought or flooding. Surface soil moisture information is also a critical forcing variable in many Soil Vegetation Atmosphere Transfer (SVAT) models to estimate profile soil moisture at daily time steps. Such applications to watershed management have a common set of requirements that define the desired soil moisture product. The spatial distribution is generally required at a very fine resolution (from 10 to 100 m); the required coverage of distributed soil moisture information is on the order of 1000 to 25,000 km²; and, in most cases, the soil moisture quantization can be coarse, such as three to four levels ranging from dry to very wet.

A great deal of progress has been made in the use of spectral images from satellite sensors for surface soil moisture mapping, where surface soil moisture (m_s) is the average moisture (cm³ cm⁻³)

Table 7-1. RADARSAT, ERS, ENVISAT, and JERS configurations.

	RADARSAT	ERS SAR	ERS ENVISAT ASAR	JERS ALOS PALSAR (planned)
Incidence Angle	20-50°	23°	15-45°	10-51°
Wavelength (cm)	5.7	5.7	5.7	23
SAR band	C	C	C	L
Polarization	HH	VV	HH, VV, VH, HV	HH, VV, HH, HV, VV & VH
Resolution (m)	10-100	30	10-100	10-100

in the top few centimeters of soil over a heterogeneous volume. The greatest progress has been made with passive microwave sensors. These sensors measure the intensity of microwave emission (at wavelengths $\lambda = 1-30$ cm) from the soil, which is related to its moisture content because of the large differences in dielectric constant of dry soil (~3.5) and water (~80). This emission is proportional to the product of surface temperature and surface emissivity, which is commonly referred to as the microwave brightness temperature (T_B). The relation between T_B and m_s varies with differences in surface roughness and vegetation biomass and is further affected by the changes in dielectric constant related to soil texture. The efficacy of the measurement is a function of wavelength, where longer wavelengths ($\lambda > 10$ cm) probe deeper into the soil and have the ability to penetrate a vegetated canopy (see review by Njoku and Entekhabi, 1996).

However, the use of passive microwave measurements for soil moisture mapping at watershed scales is limited for many reasons. First, the spatial resolution is inherently coarse, on the order of tens of kilometers. Second, until just recently, the information was available only from aircraft-based sensors, resulting in limited coverage, infrequent repeat visits, and delays in product delivery. On the other hand, two satellite-based passive microwave sensors will be providing imagery later this decade. The Advanced Microwave Scanning Radiometer (AMSR-E) was successfully deployed on the NASA Aqua platform in 2003 (Njoku et al., 2003), and the Soil Moisture and Ocean Salinity (SMOS) mission is planned for launch by the European Space Agency (ESA) in 2007 (Kerr, 2001). The spatial resolution of these sensors is estimated to be 56 and 37 km, respectively.

The only satellite systems that currently meet the spatial resolution and coverage required for watershed management are active microwave sensors (see review by Moran et al., 2004). The most common imaging active microwave configuration is the synthetic aperture radar (SAR), which transmits a series of pulses as the radar antenna traverses the scene. Then, these pulses are processed together to simulate a very long aperture capable of high surface resolution (Ulaby et al., 1996). There are three operational SAR satellite systems with frequencies suitable for soil moisture: ESA ERS-1/2 C-band SAR, ESA ENVISAT C-band ASAR, and Canadian C-band RADARSAT-1/2 (Table 7-1). These SAR systems can provide resolutions from 10 to 100 m over a swath width of 50 to 500 km, thus meeting most spatial requirements for watershed management. As with passive microwave sensing, the magnitude of the SAR backscatter coefficient (σ^0) is related to m_s through the contrast of the dielectric constants of bare soil and water. Similarly, the perturbing factors affecting the accuracy of m_s estimation are soil surface roughness and vegetation biomass. Studies, particularly in the past decade, have resulted in a multitude of methods, algorithms, and models relating satellite-based images of SAR backscatter to surface soil moisture. However, no operational algorithm exists using SAR data acquired by existing spaceborne sensors (Borgeaud and Saich, 1999).

For all orbiting sensors, including the AMSR-E and SMOS missions, remote sensing alone can only provide surface soil moisture m_s , with stated depths varying from 1 to 5 cm (Ulaby et al., 1996; Oh, 2000). Most studies agree that the penetration depth for microwave sensing is between 0.1 to 0.2 times the wavelength, where the longest wavelengths (L-band) are about 21 cm. To fully meet the requirements for soil moisture information for watershed management, it will be necessary to combine the horizontal coverage and spatial resolution of remote sensing with the vertical coverage and temporal continuity of a soil moisture simulation model. Such models are generally called Soil Vegetation Atmosphere Transfer (SVAT). The advantage of SVAT models is that profile soil moisture (m_p) is estimated to several meters depth on hourly, daily or monthly timesteps. One disadvantage of SVAT models for monitoring regional soil moisture condition is that they are one-dimensional, and without remotely sensed inputs, they are rarely capable of producing a distributed map of soil moisture.

In this review, we will concentrate on approaches for estimating m_s at the scale of managed watersheds ranging in size from 1000 to 25,000 km². These include physically based approaches for m_s estimation using SAR, with particular emphasis on use of radar backscatter models and brief mention of SAR for m_s change detection and SAR data fusion. The review will finish with a synthesis of the most important research and development issues related to watershed management. For convenience, all acronyms and scientific notation are summarized in Tables 7-2 and 7-3, respectively.

Table 7-2. Summary of Acronyms.

ALOS	Advanced Land Observation Satellite
AMSR-E	Advanced Microwave Scanning Radiometer on the NASA Aqua satellite
ASAR	Advanced Synthetic Aperture Radar
ENVISAT	ENVIronment SATellite
ERS SAR	European Remote Sensing SAR
ESA	European Space Agency
GIS	Geographic Information System
HAPEX-Sahel	Hydrologic Atmospheric Pilot Experiment in the Sahel (Prince et al., 1995)
HH, VV, HV, VH	Horizontal and Vertical co-polarization
HYDROS	NASA HYDROsphere State mission
IEM	Integral Equation Model (Fung and Chen, 1992)
JERS SAR	Japanese Earth Resources Satellite SAR
LAI	Leaf area index
NASA	National Aeronautics and Space Administration
NBMI	Normalized Radar Backscatter soil Moisture Index (Shoshany et al., 2000)
NDVI	Normalized Difference Vegetation Index
PALSAR	Phased Array type L-band Synthetic Aperture Radar
RADAR	Radio Detection and Ranging
RADARSAT	RADAR SATellite
RS	Remote Sensing
SAR	Synthetic Aperture Radar
SGP	Southern Great Plains
SMOS	Soil Moisture and Ocean Salinity
SSM/I	Special Sensor Microwave/Imager
SVAT	Soil Vegetation Atmosphere Transfer
WCM	Water Cloud Model (Attema and Ulaby, 1978)

SEMI-EMPIRICAL APPROACHES

The radar backscatter, σ^o , from a vegetated surface is composed of three contributions

$$\sigma^o = \tau^2 \sigma_s^o + \sigma_{dv}^o + \sigma_{int}^o, \quad [1]$$

where σ_s^o is the backscatter contribution of the bare soil surface, τ^2 is the two-way attenuation of the vegetation layer, σ_{dv}^o is the direct backscatter contribution of the vegetation layer, and σ_{int}^o represents multiple scattering involving the vegetation elements and the ground surface (Ulaby et al., 1996). For densely vegetated targets, $\tau^2 \approx 0$ and σ^o are determined largely by volumetric scattering from the vegetation canopy. For sparsely vegetated targets, $\tau^2 \approx 1$ and the second and third terms in Eq. [1] are negligible; in that case, σ^o is determined by the soil roughness and moisture content. For bare soil, σ_s^o has a functional relation with m_s , where

$$\sigma_s^o = f(R, m_s) \quad [2]$$

Table 7-3. Summary of scientific notation.

σ^o	Radar backscatter coefficient
σ_{int}^o	Multiple scattering involving the vegetation elements and the ground surface
σ_s^o	Backscatter contribution of the bare soil surface
σ_{dv}^o	Direct backscatter contribution of the vegetation layer
σ_{dry}^o	Backscatter from vegetated terrain under completely dry soil surface conditions
σ_{wet}^o	Backscatter when the soil surface is saturated with water
$\Delta\sigma^o$	Difference between dry- and wet-season σ^o
I_{m_s}	Relative measure of surface soil moisture
θ_i	Incidence angle
K_{sat}	Soil hydraulic conductivity
m_p	Profile soil moisture
m_s	Surface soil moisture.
ρ_λ	Surface spectral reflectance in optical wavelengths
R	Surface roughness term
T_B	Microwave brightness temperature
T_R	Infrared radiative temperature
τ^2	Two-way attenuation of the vegetation layer
V	Vegetation biomass
λ	Wavelength

and R is a surface roughness term (Engman and Chauhan, 1995). Considering this, many algorithms using single-wavelength, single-polarization SAR for estimating m_s follow a standard two-step approach, where the first step is to estimate and remove the signal due to backscatter from the vegetation canopy. Thus, $\sigma^o \cong \sigma_s^o$. The second step is to determine the relation between σ_s^o and m_s , based on the assumption that the surface roughness adds a signal to the backscatter intensity that can be treated as an offset (Schneider and Oppelt, 1998). Thus, for a target of uniform R ,

$$m_s = a + b\sigma_s^o, \quad [3]$$

where a and b are regression coefficients determined primarily from field experiments, which encompass the target-invariant R and the scene-invariant SAR λ , θ_i , polarization, and calibration. Therefore, Eq. [3] is only valid for a given sensor, landuse, and soil type, and for targets when τ^2 , σ_{dv}^o and σ_{int}^o are known or negligible. Nonetheless, in some cases, it is a reasonable approach and provides an operational method for regional estimation of m_s .

For example, Quesney et al. (2000) resolved Eq.[1] to [3] to derive soil moisture information with accuracies of ± 0.04 - 0.05 ($\text{cm}^3 \text{ cm}^{-3}$) from ERS SAR measurements over an agricultural watershed in France. Based on an *a priori* vegetation classification of the site and some in-situ measurements, they selected sensitive targets where soil moisture retrieval was possible due largely to the low vegetation biomass. For these targets, a first-order radiative transfer model was used to correct the radar response for the effect of the vegetation canopy. Then, sensitive targets were classified into roughness classes based on their furrow direction as viewed by the radar beam. These classes were assumed to be homogeneous in terms of large-scale roughness contributions. Empirical relations between σ^o and corresponding in-situ measurements of m_s were determined for each class and applied to all sensitive targets in the SAR image. They concluded that the same relation between σ^o and m_s could be used from November to August (excepting the months of May and June) for wheat fields in an agricultural watershed in France.

Similarly, for a semi-arid watershed in Arizona, Moran et al. (2000) utilized the difference between dry- and wet-season SAR σ^o ($\Delta\sigma^o$) to normalize the effects of surface roughness and topography on ERS SAR measurements. This required that the images be acquired with exactly the same sensor configuration, particularly the same incidence angle. Thoma et al. (2005) improved upon this approach to minimize empiricism and used a quantitative form of $\Delta\sigma^o$ to map m_s for an entire watershed with RADARSAT for three dates in 2003. In these studies, the effects of vegetation were found to be negligible and could be ignored, supporting similar findings by Dobson et al. (1992), Lin and Wood (1993), Demircan et al. (1993), Dubois et al. (1995), and Chanzy et al. (1997). But for many locations, the vegetation was simply too dense to monitor soil moisture with only a single-wavelength data set (Wever and Henkel, 1995; Wang et al., 1996).

A great limitation of all these approaches is that the sensitivity of radar backscatter to R can be much greater than the sensitivity to m_s . For example, Herold et al. (2001) reported that the backscatter range from different roughness conditions was about 17 dB, whereas the variations caused by soil moisture were about 6 dB. Sano et al. (1998) found that SAR σ^o data were nearly insensitive to soil moisture due to the stronger influence of soil roughness. Oh et al. (1992) stated that the primary cause of backscatter variation in radar image scenes was surface roughness, and secondarily, moisture content. Thus, it is imperative that surface roughness and topography be accounted for in any operational approach.

m_s CHANGE DETECTION

An approach that may have potential for operational application is the use of single-wavelength, multi-pass SAR images for change detection, rather than absolute m_s estimation (Engman 1994). This approach is based on the assumption that the temporal variability of R and vegetation biomass (V) is generally at a much longer time scale than that of m_s , and therefore, the change in SAR σ^o between repeat passes results from the change in m_s . Thus, a multi-temporal SAR data set could be used to minimize the influence of R and V , and maximize the sensitivity of σ^o to changes in m_s . Though useful for many applications, it is notable that the assumptions do not hold for cultivated crops where R and V change dramatically over short time periods. Furthermore, images must be acquired with the same sensor configuration to avoid the need for topographic corrections due to variations in θ_i and image orientation.

Simply applied, a Normalized Radar Backscatter soil Moisture Index (NBMI) was derived from σ^o measurements at two times (t_1 and t_2) over one location where,

$$NBMI = \frac{\sigma_{t_1}^o + \sigma_{t_2}^o}{\sigma_{t_1}^o - \sigma_{t_2}^o} \quad [4]$$

(Shoshany et al., 2000). By normalizing the effects of R , soil type, and topography on SAR σ^o , such ratio techniques offer a relative soil moisture index varying from 0 to 1 related to distributed m_s variations.

Using a long backscatter series, it is possible to correlate changes in σ^o with changes in m_s over large areas. For example, Wickel et al. (2001) used 10 RADARSAT scenes over a one-month period to monitor m_s change in fields of wheat stubble in Oklahoma. They corrected all images for the difference in θ_i using an empirical approach and a modeling approach (Ulaby and Dobson, 1989), and then eliminated wheat fields with “major” temporal roughness changes. They computed a multitemporal regression of day-to-day differences in σ^o and m_s with a strong correlation of $r^2=0.89$.

Wagner and Scipal (2000) offered a variation on this approach that has been tested with some success in Canadian prairies, the Iberian Peninsula, the Ukraine, and savanna and grasslands in western Africa. Based on a multi-year series of ERS scatterometer images with spatial resolution of 50 km, a “knowledge base” about the backscatter behavior of each pixel was constructed. The behavior of σ^o related to θ_i over time was used to determine relative R and V , and to normalize σ^o to a reference θ_i of 40° at time t . For pixels of similar R and V , a relative measure of surface soil moisture (I_{m_s}) was estimated as

$$I_{m_s} = \frac{\sigma^o(40^\circ, t) - \sigma_{dry}^o(40^\circ, t)}{\sigma_{wet}^o(40^\circ, t) - \sigma_{dry}^o(40^\circ, t)} \quad [5]$$

where $\sigma_{dry}^o(40^\circ, t)$ represents σ^o from vegetated terrain under completely dry soil surface conditions and $\sigma_{wet}^o(40^\circ, t)$ represents σ^o when the soil surface is saturated with water. The values $\sigma_{dry}^o(40^\circ, t)$ and $\sigma_{wet}^o(40^\circ, t)$ were derived from the lowest and highest values of $\sigma^o(40^\circ, t)$ from six years of data. Thus, in this approach, the normalization of variations in θ_i , R and V and the estimation of I_{m_s} are all accomplished with a frequent-repeat, multi-year backscatter data series.

With SAR data, Lu and Meyer (2002) suggested a similar change detection approach with a significant variation. That is, they incorporated information from both SAR backscatter intensity and phase to perform an initial discrimination of changes in soil moisture from changes in surface roughness. With that preprocessing and an image-based estimate of σ_{dry}^o , they were able to detect changes in m_s ranging from 0.05 to 0.20 cm³ cm⁻³.

SAR DATA FUSION

The problem associated with discriminating the multiple influences of surface properties and sensor characteristics (e.g., R , V , θ_i , λ) on the relation between SAR σ^o and m_s has prompted a number of SAR data fusion studies. The majority of studies have addressed the complementarity and interchangeability of 1) active (SAR) microwave σ^o and passive microwave T_B , and 2) SAR σ^o and optical measurements, such as infrared radiative temperature (T_R) and surface spectral reflectance in visible and near-infrared wavelengths (ρ_λ).

As mentioned earlier, the greatest advantage of active over passive microwave sensing for watershed applications is the fine spatial resolution, where SAR resolution is on the order of tens of meters and passive microwave resolution is tens of kilometers. Similar passive and active microwave configurations appear to have similar sensitivities to soil moisture (Chauhan et al., 1999) and near-similar sensitivities to roughness (Du et al., 2000). Data fusion of passive and active microwave sensing has generally taken the form of using SAR σ^o for determining fine-resolution vegetation and roughness parameters and then combining these with coarse-resolution passive microwave T_B for estimation of regional soil moisture (e.g., Chauhan, 1997; Lakshmi et al., 2000). In other approaches, complementary passive microwave emissivity and SAR backscatter were fused through Bayesian logic to improve estimates of soil moisture condition (Notarnicola and Posa, 2001). Huang and Jin (1995) used passive and active microwave data to construct a mesh graph, where any point on the graph could be used to estimate soil moisture and roughness of bare soil separately.

There is great potential to determine subpixel variability of passive-derived soil moisture with the finer resolution active microwave data. In a recent study, Bindlish and Barros (2002) downscaled soil moisture estimates from a passive microwave sensor from 200 m to 40 m using a single polarization, single wavelength L-band SAR system. They concluded that integration of active and passive microwave technologies to monitor watershed scale soil moisture is an alternative worth exploring. This approach will likely receive more attention when the soil moisture products from AMSR-E and SMOS become available. Further support will be provided by the NASA HYDROsphere State (HYDROS) mission with a satellite-based, integrated passive and active L-band system with spatial resolutions of 3 to 40 km.

Microwave and optical remote sensing have been used separately for estimation of surface properties, and both measurements have distinct advantages. Several studies have focused on definition of the complementarity (independent information) and interchangeability (similar information) of optical and SAR data. Basically, the longer λ SAR bands ($\lambda > 6$ cm) have been related to thermal T_R measurements through the physical relation between surface evaporation and surface soil moisture content (e.g., Moran et al., 1997). For vegetated targets, shorter λ SAR bands (e.g. $\lambda \approx 2$ cm) have been related to optical vegetation indices (e.g., Normalized Difference Vegetation Index, NDVI) because visible, near-IR, and short- λ SAR signals are largely influenced by the crown layer of branches and foliage in the canopy (e.g., Prevot et al., 1993;

Moran et al., 1997). Other studies have taken advantage of both the complementarity and interchangeability of optical and SAR data to improve simulation model parameterization and inversion. Theoretical studies have shown that the inverse problem for m_s estimation could be achieved with an optical/SAR data set, but a unique solution would not be possible with either observation alone (Entekhabi et al., 1994; Chanzy et al., 1995). This work has been supported by field experiments with crops in France and Poland (Taconet et al., 1996; Olioso et al., 1998; and Dabrowska-Zielinska et al., 2001) and rangelands in Arizona (Wang et al., 2003).

SAR PLUS RADAR BACKSCATTER MODELS

The continuing efforts to disentangle the relative influences of R , V , and m_s on SAR σ^o have ultimately led to the use of physically based backscatter models. These models generally predict σ^o as a function of sensor configuration and surface conditions, and can thus be inverted to estimate m_s . Empirical, semi-empirical, and theoretical models have been developed for this purpose. Empirical models are generally derived from experiments to fit their data and may only apply to surface conditions and radar parameters at the time of the experiment (Dobson et al., 1985; Oh et al., 1992; Dubois et al., 1995; Wang et al., 1996).

To avoid this limitation, semi-empirical models have been developed based on a theoretical foundation with model parameters derived from (i.e., fitted to) experimental data. An example is the widely used Water Cloud Model (WCM) that represents the canopy as a uniform cloud of spherical droplets that are held in place structurally by dry matter (Attema and Ulaby, 1978). In WCM, the canopy can be represented by bulk variables such as leaf area index (LAI) or vegetation water content, and the model can be easily inverted. Simply, the backscatter coefficient is represented by Eq. [1], which is simplified to $\sigma^o = \tau^2 \sigma_s^o + \sigma_{dv}^o$ based on the assumption that σ_{int}^o is negligible. The attenuation of the vegetation layer (τ^2) and direct backscatter from the vegetation layer (σ_{dv}^o) are determined empirically by

$$\tau^2 = \exp(-2BV \sec \theta), \quad [6]$$

$$\sigma_{dv}^o = AV \cos \theta(1 - \tau^2), \text{ and} \quad [7]$$

$$\sigma_s^o = C + Dm_s, \quad [8]$$

where V could be green LAI, and A , B , C , and D are empirical parameters dependent upon canopy type and soil roughness (Prevot et al., 1993; Taconet et al., 1996; Moran et al., 1998).

Some effort has been made to examine radar backscatter on a strictly theoretical basis, though theoretical models are difficult to implement using computers, and their validity range is often limited. For instance, models based on the Kirchoff formulation are known to be applicable only to gently undulating surfaces within restrictive R/λ conditions, and those based on the small perturbation theory were developed for only slightly rough surfaces where $R < \lambda$ (Ulaby et al., 1982). The Integral Equation Model (IEM) combines the Kirchoff and small perturbation theories to address a wide range of roughness for bare soil surfaces, with an expression that is simpler to calculate and invert (Fung and Chen, 1992; Fung et al., 1992). For this reason, it has become the most widely used radar backscatter model and will be the focus of this section.

The IEM model has been found to be particularly suitable for retrieving m_s from single-wavelength, single-pass SAR σ^o . However, in all cases, an *a priori* measure of R was required (e.g., Tansey and Millington, 2001). This has led to a number of suggestions for determining distributed R information from orbiting SAR sensors. Considering that RADARSAT images can be acquired at a variety of θ_i , Colpitts (1998) combined two or more images of different θ_i with the IEM model to separate effects of m_s and R for several tillage types. Similarly, Pasquariello et al. (1997) found that IEM-retrieved estimates of m_s were greatly improved through inversion with multi- θ_i SAR imagery. Based on a theoretical analysis, Fung et al. (1996) reported that not only could angular SAR measurements be used to determine roughness parameters for IEM, this approach was preferable to direct ground measurements due to considerations of scale, heterogeneity and resolution. However, approaches based on multi- θ_i SAR imagery are limited because pixel information is integrated over different spatial domains with variations in θ_i . In a different approach, Verhoest et al. (2000) used multi-temporal data rather than multi-angular data to determine an effective roughness parameter. Thus, multi-temporal ERS-1 SAR σ^o was used to invert the IEM model to retrieve m_s from bare soil with reasonable accuracy.

As a result of these successes, there have been numerous refinements, improvements, and additions to the IEM that will certainly encourage more use of the model for m_s retrieval. To reduce the complexity of IEM application, algorithms have been developed based on fitting of IEM numerical simulations for a wide range of R and m_s conditions (Chen et al., 1995; Shi et al., 1997). The results are a look-up table of IEM simulations that serve to directly relate SAR σ^o to theoretical model predictions over bare and sparsely vegetated surfaces with known radar parameters. These simplified IEM-based algorithms require fewer parameters and are much easier to use with remotely sensed data.

Another critical refinement of IEM was the incorporation of vegetation backscatter effects into the m_s inversion algorithm. The original IEM was developed for bare soil conditions only, although the retrieval algorithm performed well for sparsely vegetated areas. Bindlish and Barros (2001) formulated an IEM vegetation scattering parameterization in the framework of the WCM (Eq. [6]-[8]). They reported that the application of the modified IEM led to an improvement in the correlation coefficients between ground-measured and SAR-derived m_s estimates from 0.84 to 0.95. The incorporation of vegetation scattering will expand IEM applications to moderately vegetated sites and improve applications in arid and semiarid regions where m_s is so low that the soil contribution may be equal to the magnitude of the vegetation contribution.

The IEM model has also been refined to include a penetration depth model. Studies have reported problems in IEM-based m_s retrieval due to an increase in the penetration depth of the incident wave when the soil moisture was low (e.g., Wiemann, 1998). As a result, modeled m_s could not be compared with ground measurements because IEM did not account for the fact that SAR beam penetration exceeded the layer where the soil moisture was measured (Wiemann, 1998). Boisvert et al. (1997) offered three approaches to refine IEM to account for variations in beam penetration depth. They reported that the correction allowed reliable comparisons among different SAR configurations and took into account the daily variations in the beam penetration with soil moisture.

The general consensus of studies using SAR σ^o with radar backscatter models is that the retrieval of m_s with single-wavelength, single- θ_i , single-pass SAR data is not possible without information about the surface roughness. The results also demonstrate the need for continuous measurement of surface roughness and fine-resolution information about surface topography, if

Table 7-4. Promising approaches using SAR sensors for m_s estimation.

Approach	Examples
Semi-empirical algorithm Generally uses SAR images of single λ , θ_l , and polarization. Requires multiple passes and/or ancillary information. Often scene- or site-dependent.	Moran et al. (2000); Quesney et al. (2000)
SAR for m_s change detection Requires multiple passes. Assumes temporal variability of R and V is at longer time scale than that of m_s . High potential for operational application.	Lu and Meyer (2002); Shoshany et al. (2000); Wagner and Scipal (2000); Wickel et al. (2001)
SAR data fusion – passive and active microwave Generally, uses active σ^o to determine fine resolution V and R, and passive T_B to estimate m_s OR downscale passive-derived m_s with fine resolution σ^o .	Bindlish and Barros (2002); Chauhan (1997); Huang and Jin (1995); Lakshmi et al. (2000); Notarnicola and Posa (2001)
SAR data fusion – microwave and optical Based on complementarity or interchangeability of optical and SAR data. Simplifies the inverse problem for m_s estimation.	Chanzy et al. (1995); Dabrowska-Zielinska et al. (2001); Entekhabi et al. (1994); Moran et al. (1997); Olioso et al. (1998); Taconet et al. (1996); Wang et al. (2003)
SAR plus microwave scattering model Empirical, semi-empirical and theoretical models available. Models are inverted to estimate m_s from σ^o . Advantage: high accuracy. Disadvantage: difficult model parameterization.	Colpitts (1998); Fung et al. (1996); Pasquariello et al. (1997); Tansey and Millington (2001); Verhoest et al. (2000); Wiemann (1998)

soil moisture is to be monitored accurately with single-wavelength SAR data. When SAR data with consistent ground truth information are available, it will be possible to test the many existing retrieval algorithms.

CONCLUSIONS

The basic conclusion of this review is that currently orbiting SAR sensors can provide surface soil moisture information with known accuracy at the watershed scale. Future research should be dedicated to refining the approaches that meet the requirements for watershed application and have the most potential for operational estimation of m_s (Table 7-4). The most robust, adaptable system will likely be based primarily on SAR images, and it will require a radar backscatter model for determining m_s and ground information for validation. However, there are many obstacles yet to be overcome for a truly operational application for watershed management.

First, the primary perturbing factors affecting the accuracy of SAR-derived m_s estimations are soil surface roughness and vegetation biomass. These, along with soil texture, are also primary inputs to SVAT models. In this review, several promising approaches for estimating these surface properties with satellite imagery were mentioned (e.g., Pasquariello et al., 1997; Colpitts, 1998; Mattikali et al., 1998; Verhoest et al., 2000). Not only are these approaches feasible, they are preferable to direct ground measurements because they offer flexibility of coverage and resolution required at the watershed scale.

Second, the accuracy of m_s retrieved from remote sensing in all wavelengths is limited by the non-linear effects of vegetation change. Vegetation biomass significantly influences surface reflectance, thermal emission, microwave emission, and radar backscatter from the soil surface. This review presents several approaches designed to minimize this effect, for example, limiting analysis to sparsely vegetated sites (Quesney et al., 2000), monitoring signal differences when vegetation is known to be static (Wickel et al., 2001), and by combining optical and SAR data (Chanzy et al., 1995). Alternatively, there are models designed to determine SAR backscatter from vegetation that have the potential to discriminate surface soil moisture (e.g., Ulaby et al., 1990; Bindlish and Barros, 2001). Despite these attempts, there is no operational algorithm or model using existing spaceborne sensors to determine the soil moisture of densely vegetated sites. This should be considered a priority research area.

Third, a common lament in nearly all soil moisture studies at the watershed scale is that consistent ground information about m_s and m_p is rarely available at the scale and frequency required for model calibration and validation. Though it is technologically feasible (Borgeaud and Flourey, 2000), no worldwide in situ soil moisture monitoring program is currently in place. Consequently, most studies have been undertaken in conjunction with inter-disciplinary field campaigns coordinated with multiple aircraft and satellite overpasses. For example, the HAPEX-Sahel campaign in 1992 provided multi-scale soil moisture measurements up to a regional area of 12,100 km² (Prince et al., 1995). Microwave images were acquired by the ERS SAR and SSM/I satellite sensors, and detailed project information can be obtained at <http://www.ird.fr/hapex/>. The Washita experiment conducted in 1992 and the Southern Great Plains (SGP) experiments undertaken in 1997 and 1999 employed a wide range of microwave instrumentation that provided useful soil moisture measurement techniques at numerous scales appropriate for watershed management (LeVine et al., 1994; Jackson et al., 1995, 2002a, 2002b; O'Neill et al., 1998; Jackson, 1999; Jackson and Hsu, 2001). Microwave images were acquired with aircraft- and satellite-based systems, as well as the Priroda sensors on the Mir Space Station. Links to these remote sensing soil moisture experiments, including data, images, and reports, are available at <http://hydrolab.arsusda.gov/rsbarc/RSofSM.htm>. Though such place-based campaigns have expanded the science of soil moisture estimation, it will be necessary to have spatially and temporally consistent ground truth information coincident with SAR overpasses to test the many existing retrieval algorithms.

Fourth, as described in Table 7-1, current SAR sensor configurations include a multitude of wavelengths, incidence angles, polarizations, resolutions, and overpass times. The SAR backscatter signal from a given target is highly sensitive to sensor configuration. This sensitivity has proven advantageous for studies based on the multi-dimensional information resulting from multi- λ , multi- θ_i , and/or multi-polarization data (e.g., Dubois et al., 1995; Wever and Henkel, 1995; Pasquariello et al., 1997; Colpitts, 1998). However, variations in sensor configuration can be devastating to studies based on the assumption that a change in σ^o is due exclusively to a

change in surface condition (e.g., Mattikalli et al., 1998; Wagner and Scipal, 2000). As a result, most studies of change detection have been limited to the use of a single SAR sensor with a fixed configuration. The accuracy of estimating soil properties (i.e., both soil moisture and texture) could be greatly increased if the differences in scattering due to sensor configuration could be normalized. In some cases, this has been resolved through the use of existing theoretical backscatter models (e.g., Wickel et al., 2001).

Fifth, an approach that has great potential for immediate operational application is the use of single-wavelength, multi-pass SAR images for change detection, rather than absolute m_s estimation. Many multi-pass approaches for estimating m_s were identified in this review (e.g., Shoshany et al., 2000; Wagner and Scipal, 2000; Wickel et al., 2001; Lu and Meyer, 2002). Though useful, these will not be reasonable at the watershed scale until the price of SAR imagery decreases from current levels.

Finally, in this review, three satellite systems were described with the explicit mission of measuring global soil moisture. The AMSR-E sensor, now in orbit aboard the NASA Aqua platform, was designed to provide soil moisture mapping at 56 km and generally demonstrate technology feasibility. The SMOS sensor, to be launched this decade by ESA, will provide improved soil moisture mapping at a spatial resolution of potentially 37 km. The NASA HYDROS will combine passive and active sensors to improve both sensitivity to soil moisture and spatial resolution (estimated to be 10 km). Through international cooperation, these missions have been designed to complement and build upon each other. Though none of these missions meets the spatial resolution requirements for watershed applications (10 to 100 m), the technology development and demonstration will certainly benefit the science of soil moisture mapping at all scales.

ACKNOWLEDGMENTS

The authors appreciate the generous support of the US Army Engineer Research and Development Center, Topographic Engineering Center.

REFERENCES

- Attema, E., and F. Ulaby. 1978. Vegetation modeled as a water cloud. *Radio Sci.* 13:357-364.
- Bindlish, R., and A.P. Barros. 2001. Parameterization of vegetation backscatter in radar-based soil moisture estimation. *Remote Sens. Environ.* 76:130-137.
- Bindlish, R., and A.P. Barros. 2002. Subpixel variability of remotely sensed soil moisture: An inter-comparison study of SAR and ESTAR. *IEEE Trans. Geosci. Remote Sens.* 40:326-337.
- Boisvert, J. B., Q.H.J. Gwyn, A. Chanzy, D.J. Major, B. Brisco, and R.J. Brown. 1997. Effect of surface soil moisture gradients on modeling radar backscattering from bare fields. *Int. J. Remote Sens.* 18:153-170.
- Borgeaud, M., and P. Saich. 1999. Status of the retrieval of bio- and geo-physical parameters from SAR data for land applications. p.1901-1903. *In Proc. Int. Geosci. and Remote Sens. Symp.*, Hamburg, Germany. 28 June-2 July 1999. IEEE, Piscataway, N.J.

- Borgeaud, M., and N. Flouri. 2000. On the soil moisture retrieval of bare soils with ERS SAR data. p. 1687-1689. *In* Int. Geosci. Remote Sens. Symp., Honolulu, HI. 24-28 July 2000. IEEE, New York.
- Chanzy, A., L. Bruckler, and A. Perrier. 1995. Soil evaporation monitoring: A possible synergism of microwave and infrared remote sensing. *J. Hydrol* (Amsterdam) 165:235-259.
- Chanzy, A., Y. Kerr, J.P. Wigneron, and J.C. Calvet. 1997. Soil moisture estimation under sparse vegetation using microwave radiometry at C-band. p. 1090-1092. *In* Proc. Int. Geosci. and Remote Sens. Symp., Singapore. 3-8 Aug. 1997. IEEE, Piscataway, N.J.
- Chauhan, N.S. 1997. Soil moisture estimation under a vegetation cover: Combined active and passive microwave remote sensing approach. *Int. J. Remote Sens.* 18:1079-1097.
- Chauhan, N., D. Le Vine, and R. Lang. 1999. Passive and active microwave remote sensing of soil moisture under a forest canopy. p. 1914-1916. *In* Int. Geosci. Remote Sens. Symp., Hamburg, Germany. 28 June – 2 July 1999. IEEE, Piscataway, N.J.
- Chen, K.S., S.K. Yen, and W.P. Huang. 1995. A simple model for retrieving bare soil moisture from radar scattering coefficients. *Remote Sens. Environ.* 54:121-126.
- Colpitts, B.G. 1998. The integral equation model and surface roughness signatures in soil moisture and tillage type determination. *IEEE Trans. Geosci. Remote Sens.* 36:833-837.
- Dabrowska-Zielinska, K., Y. Inoue, M. Gruszczynska, W. Kowalik, and K. Stankiewicz. 2001. Various approaches for soil moisture estimates using remote sensing. p. 261-263. *In* Proc. Int. Geosci. Remote Sens. Symp., Sydney, Australia. 9-13 July 2001. IEEE, Piscataway, N.J.
- Demircan, A., M. Rombach, and W. Mauser. 1993. Extraction of soil moisture from multitemporal ERS-1 SLC data of the Freiburg test-site. p. 1794-1796. *In* Int. Geosci. Remote Sens. Symp., Tokyo, Japan. 18-21 Aug. 1993. IEEE, Piscataway, N.J.
- Dobson, M.C., F.T. Ulaby, M.T. Hallikainen, and M.S. El-Rayes. 1985. Microwave dielectric behavior of wet soil: II. Dielectric mixing models. *IEEE Trans. Geosci. Remote Sens.* 23:35-46.
- Dobson, M. C., L. Pierce, K. Arabandi, F.T. Ulaby, and T. Sharik. 1992. Preliminary analysis of ERS-1 SAR for forest ecosystem studies. *IEEE Trans. Geosci. Remote Sens.* 30: 203-211.
- Du, Y., F.T. Ulaby, and M.C. Dobson. 2000. Sensitivity to soil moisture by active and passive microwave sensors. *IEEE Trans. Geosci. Remote Sens.* 38: 105-114.
- Dubois, P.C., J. van Zyl, and E.T. Engman. 1995. Measuring soil moisture with imaging radars. *IEEE Trans. Geosci. Remote Sens.* 33: 915-926.
- Engman, E.T., 1994. The potential of SAR in hydrology. p. 283-285. *In* Proc. Int. Geosci. Remote Sens. Symp., Pasadena, CA. 8-12 Aug. 1994. IEEE, Piscataway, N.J.
- Engman, E.T., and N. Chauhan. 1995. Status of microwave soil moisture measurements with remote sensing. *Remote Sens. Environ.* 51:189-198.
- Entekhabi, D., H. Nakamura, and E.G. Njoku. 1994. Solving the inverse problem for soil moisture and temperature profiles by the sequential assimilation of multifrequency remotely sensed observations. *IEEE Trans. Geosci. Remote Sens.* 32:438-448.
- Fung, A.K., and K.S. Chen. 1992. Dependence of the surface backscattering coefficients on roughness, frequency and polarization states. *Int. J. Remote Sens.* 13:1663-1680.
- Fung, A.K., Z. Li, and K.S. Chen. 1992. Backscattering from a randomly rough dielectric surface. *IEEE Trans. Geosci. Remote Sens.* 30:356-369.

- Fung, A. K., M.S. Dawson, K.S. Chen, A.Y. Hsu, S.T. Engman, P.O. O'Neill, and J. Wang. 1996. A modified IEM model for scattering from soil surfaces with application to soil moisture sensing. p. 1297-1299. *In Proc. Int. Geosci. Remote Sens. Symp.*, Lincoln, Nebraska. 27-31 May 1996. IEEE, Piscataway, N.J.
- Herold, M., J. Shi, and C.C. Schmullius. 2001. Multi-parameter airborne SAR remote sensing of soil moisture in agricultural areas. p. 2103-2105. *In Proc. Int. Geosci. Remote Sens. Symp.*, Sydney, Australia. 9-13 July 2001. IEEE, Piscataway, N.J.
- Huang, X., and Y.-Q. Jin. 1995. A simple method to estimate the soil wetness and surface roughness by using active/pассив microwave data. *Remote Sens. Environ.* 53:212-214.
- Jackson, T.J. 1999. Remote sensing of soil moisture in the southern great plains hydrology experiment. p. 1158-1160. *In Proc. Int. Geosci. Remote Sens. Symp.*, Hamburg, Germany. 28 June – 2 July 1999. IEEE, Piscataway, N.J.
- Jackson, T., A. Gasiewski, A. Oldak, M. Klein, E. Njoku, A. Yevgrafov, S. Christiani, and R. Bindlish. 2002a. Soil moisture retrieval using the C-Band polarimetric scanning radiometer during the Southern Great Plains 1999 experiment. *IEEE Trans. Geosci. Remote Sens.* 40:2151-2161.
- Jackson, T. J., A.Y. Hsu, A.M. Shutko, Y. Tishchenko, B. Petrenko, B. Kutuza, and N. Armand. 2002b. Priroda microwave radiometer observations in the SGP97 hydrology experiment. *Int. J. Remote Sens.* 23:231-248.
- Jackson, T. J. and A.Y. Hsu. 2001. Soil moisture and TRMM microwave imager relationships in the Southern Great Plains 1999 (SGP99) experiment. *IEEE Trans. Geosci. Remote Sens.* 39:1632-1642.
- Jackson, T.J., D.M. Le Vine, C.T. Swift, T.J. Schmugge, and F.R. Schiebe. 1995. Large area mapping of soil moisture using the ESTAR passive microwave radiometer in Washita'92. *Remote Sens. Environ.* 53: 27-37.
- Kerr, Y.H. 2001. The objectives and rationale of the soil moisture and ocean salinity (SMOS) mission. p. 1004-1006. *In Proc. Int. Geosci. Remote Sens. Symp.*, Sydney, Australia. 9-13 July 2001. IEEE, Piscataway, N.J.
- Lakshmi, V., J. Bolten, E. Njoku, and S. Yueh. 2000. Monitoring of large scale soil moisture from airborne PALS sensor observations during SGP99. p.1069-1071. *In Proc. Int. Geosci. Remote Sens. Symp.* Honolulu, HI, 24-28 July 2000. IEEE, Piscataway, N.J.
- Le Vine, D.M., T. Jackson, M. Kao, A. Griffis, and C.T. Swift. 1994. Status of ESTAR validation: Results from Washita-92. p. 1320-1322. *In Proc. Int. Geosci. Remote Sens. Symp.*, Pasadena, CA. 8-12 Aug. 1994. IEEE, Piscataway, N.J.
- Lin, D.-S., and E.F. Wood. 1993. Behavior of AirSAR signals during MAC-Europe'91. p.1800-1802. *In Int. Geosci. Remote Sens. Symp.*, Tokyo, Japan. 18-21 Aug. 1993, Tokyo, Japan. IEEE, Piscataway, N.J.
- Lu, Z., and D.J. Meyer. 2002. Study of high SAR backscattering caused by an increase of soil moisture over a sparsely vegetated area: Implications for characteristics of backscatter. *Int. J. Remote Sens.* 23:1063-1074.
- Mattikalli, N.M., E.T. Engman, L.R. Ahuja, and T.J. Jackson. 1998. Microwave remote sensing of soil moisture for estimation of profile soil property. *Int. J. Remote Sens.* 19:1751-1767.
- Moran, M.S., C.D. Peters-Lidard, J.M. Watts, and S. McElroy. 2004. Estimating soil moisture at the watershed scale with satellite-based radar and land surface models, *Canadian J. Remote Sensing* 30:805-826.

- Moran, M.S., A. Vidal, D. Troufleau, Y. Inoue, J. Qi, T.R. Clarke, P.J. Pinter, Jr., T. Mitchell, and C.M.U. Neale. 1997. Combining multi-frequency microwave and optical data for farm management. *Remote Sens. Environ.* 61:96-109.
- Moran, M.S., A. Vidal, D. Troufleau, Y. Inoue, and T. Mitchell. 1998. Ku- and C-band SAR for discriminating agricultural crop and soil conditions. *IEEE Trans. Geosci. Remote Sens.* 36:265-272.
- Moran, M.S., D.C. Hymer, J. Qi, and E.E. Sano. 2000. Soil moisture evaluation using multi-temporal synthetic aperture radar SAR in semiarid rangeland. *Agr. For. Meteorol.* 105: 69-80.
- Njoku, E.G., and D. Entekhabi. 1996. Passive microwave remote sensing of soil moisture. *J. Hydrol. (Amsterdam)* 184:101-129.
- Njoku, E., E. Jackson, V. Lakshmi, T. Chan, and S. Nghiem. 2003. Soil moisture retrieval from AMSR-E. *IEEE Trans. Geosci. Remote Sens.* 41:215-229.
- Notarnicola, C., and F. Posa. 2001. Bayesian fusion of active and passive microwave data for estimating bare soil water content. p. 1167-1169. *In Proc. Int. Geosci. Remote Sens. Symp.*, Sydney, Australia. 9-13 July 2001. IEEE, Piscataway, N.J.
- O'Neill, P.E., A.Y. Hsu, T.J. Jackson, and C.T. Swift. 1998. Ground-based microwave radiometer measurements during the southern great plains '97 experiment. p. 1843-1845. *In Proc. Int. Geosci. Remote Sens. Symp.*, Seattle, WA. 6-10 July 1998. IEEE, Piscataway, N.J.
- Oh, Y., F.T. Sarabandi, and F. Ulaby. 1992. An empirical model and an inversion technique for radar scattering from bare soil surfaces. *IEEE Trans. Geosci. Remote Sens.* 30: 370-381.
- Oh, Y. 2000. Retrieval of the effective soil moisture contents as a ground truth from natural soil surfaces. p. 1702-1704. *In Int. Geosci. Remote Sens. Symp.*, Honolulu, HI. 24-28 July 2000. IEEE, Piscataway, N.J.
- Olioso, A., H. Chauki, and J.-P. Wigneron. 1998. Estimation of energy fluxes and photosynthesis from thermal infrared spectral reflectances, microwave data and SVAT modeling. p. 1493-1495. *In Proc. Int. Geosci. Remote Sens. Symp.*, Seattle, WA. 6-10 July 1998. IEEE, Piscataway, N.J.
- Pasquariello, G., G. Satalino, F. Mattia, D. Casarano, F. Posa, J.C. Souyris, and T. Le Toan. 1997. On the retrieval of soil moisture from SAR data over bare soils. p. 1272-1274. *In Proc. Int. Symp. Geosci. Remote Sens.*, Singapore. 3-8 Aug. 1997. IEEE, Piscataway, N.J.
- Prevot, L., M. Dechambre, O. Taconet, D. Vidal-Madjar, M. Normand, and S. Galle. 1993. Estimating the characteristics of vegetation canopies with airborne radar measurements. *Int. J. Remote Sens.* 14:2803-2818.
- Prince, S. D., E. T. Engman, P. Sellers, Y. H. Kerr, J.-P. Goutorbe, T. Lebel, A. Tinga, P. Bessemoulin, J. Brouwer, A. J. Dolman, J. H. C. Gash, M. Hoepffner, P. Kabat, B. Monteny, F. Said, and J. Wallace. 1995. Geographical, biological and remote sensing aspects of the hydrologic atmospheric pilot experiment in the Sahel HAPEX-Sahel. *Remote Sens. Environ.* 51:215-234.
- Quesney, A., S. Le Hegarat-Mascle, O. Taconet, D. Vidal-Madjar, J.P. Wigneron, C. Loumagne, and M. Normand. 2000. Estimation of watershed soil moisture index from ERS/SAR data. *Remote Sens. Environ.* 72:290-303.
- Sano, E.E., A.R. Huete, D. Troufleau, M.S. Moran, and A. Vidal. 1998. Sensitivity analysis of ERS-1 synthetic aperture radar data to the surface moisture content of rocky soils in a semiarid rangeland. *Water Resour. Res.* 34:1491-1498.

- Schneider, K., and N. Oppelt. 1998. The determination of mesoscale soil moisture patterns with ERS data. p. 1831-1833. *In Proc. Int. Geosci. Remote Sens. Symp.*, Seattle, WA. 6-10 July 1998. IEEE, Piscataway, N.J.
- Shi, J., J. Wang, A.Y. Hsu, P.E. O'Neill, and E.T. Engman. 1997. Estimation of bare surface soil moisture and surface roughness parameter using L-band SAR image data. *IEEE Trans. Geosci. Remote Sens.* 35:1254-1266.
- Shoshany, M., T. Svoray, P.J. Curran, G.M. Foody, and A. Perevolotsky. 2000. The relationship between ERS-2 SAR backscatter and soil moisture: Generalization from a humid to semi-arid transect. *Int. J. Remote Sens.* 21: 2337-2343.
- Taconet, O., D. Vidal-Madjar, C. Emblanch, and M. Normand. 1996. Taking into account vegetation effects to estimate soil moisture from C-band radar measurements. *Remote Sens. Environ.* 56:52-56.
- Tansey, K. J., and A.C. Millington. 2001. Investigating the potential for soil moisture and surface roughness monitoring in drylands using ERS SAR data. *Int. J. Remote Sens.* 22:2129-2149.
- Thoma, D.P., M.S. Moran, R. Bryant, M. Rahman, C.D. Holifield-Collins, S. Skirvin, E.E. Sano, and K. Slocum. 2005. Comparison of four models for determining surface soil moisture from C-band radar imagery, *Water Resources Research* (accepted).
- Ulaby, F.T., R.K. Moore, and A.K. Fung. 1982. *Microwave remote sensing: Active and passive. Vol. II. Radar remote sensing and surface scattering and emission theory*. Addison-Wesley, Reading, MA.
- Ulaby, F.T., and M.C. Dobson. 1989. *Handbook of radar scattering statistics for terrain*. Artech House, Norwood, Massachusetts.
- Ulaby, F.T., P.C. Dubois and J. Van Zyl. 1996. Radar mapping of surface soil moisture. *J. Hydrol.* (Amsterdam) 184:57-84.
- Ulaby, F.T., K. Sarabandi, K. McDonald, M. Whitt and M.C. Dobson. 1990. Michigan microwave canopy scattering model. *Int. J. Remote Sens.* 11:1223-1253.
- Verhoest, N.E.C., R. Hoeben, F.P. De Troch, and P.A. Troch. 2000. Soil moisture inversion from ERS and SIR-C imagery at the Zwalm catchment, Belgium. p. 2041-2043. *In Proc. Int. Geosci. Remote Sens. Symp.*, Honolulu, HI. 24-28 July 2000. IEEE, Piscataway, N.J.
- Wagner, W., and K. Scipal. 2000. Large-scale soil moisture mapping in Western Africa using the ERS scatterometer. *IEEE Trans. Geosci. Remote Sens.* 38: 1777-1782.
- Wang, J. R., E.T. Engman, J.C. Shiue, M. Rusek, and C. Steinmeier. 1996. The SIR-B observations of microwave backscatter dependence on soil moisture, surface roughness and vegetation covers. *IEEE Trans. Geosci. Remote Sens.* 24: 510-516.
- Wang, C., J. Qi, M.S. Moran, and R. Marsett. 2003. Soil moisture estimation in a semi-arid rangeland using ERS-2 and TM imagery, *Remote Sens. Environ.* 90:178-189.
- Wever, T., and J. Henkel. 1995. Evaluation of the AIRSAR system for soil moisture analysis. *Remote Sens. Environ.* 53:118-122.
- Wickel, A.J., T.J. Jackson, and E.F. Wood. 2001. Multitemporal monitoring of soil moisture with RADARSAT SAR during the 1997 Southern Great Plains hydrology experiment. *Int. J. Remote Sens.* 22:1571-1583.
- Wiemann, A. 1998. Inverting a microwave backscattering model by the use of a neural network for the estimation of soil moisture. p. 1837-1839. *In Proc. Int. Geosci. Remote Sens. Symp.*, Seattle, WA. 6-10 July 1998. IEEE, Piscataway, N.J.

CHAPTER 8

Watershed Modeling and GIS Applications in the U.S. Using SWAT and Potential Use in Mexico

Jeffrey G. Arnold and Mauro DiLuzio

CONTENTS

Introduction	107
Literature Review	108
SWAT Model Overview	109
GIS Interfaces	111
Required Model Inputs	113
Available U.S. Databases	114
Readily Available Data for Entire U.S.	114
Data Available for Some Areas of the U.S.	114
U.S. Applications	117
Watershed Application of SWAT	117
National Application of SWAT	119
Current SWAT Development	122
Conclusions	122
References	123

INTRODUCTION

Large-area water resources development and management require an understanding of basic hydrologic processes and simulation capabilities at the river-basin scale. Current concerns that are motivating the development of large-area hydrologic modeling include climate change, management of water supplies in arid regions, large-scale flooding, and offsite impacts of land management. Recent advances in computer hardware and software, including increased speed and

storage, advanced software debugging tools, and GIS/spatial analysis software, have allowed large-area simulation to become feasible. The challenge then is to develop a basin-scale model that (1) is computationally efficient; (2) allows considerable spatial detail; (3) requires readily available inputs; (4) is continuous-time; (5) is capable of simulating land-management scenarios; and (6) gives reasonable results. The model must correctly reflect changes in land use and agricultural management on stream flow and sediment yield. Available models with these capabilities are generally limited by spatial scale. Available river-basin models generally do not link outputs to land use and management adequately to evaluate management strategies. In developing watershed models, we chose good agricultural management models to link with simple, efficient, yet realistic routing components for the purpose of capturing management effects on large river basins through long-term simulations.

The objective of this overview is to briefly describe the SWAT (Soil and Water Assessment Tool) model, GIS (Geographic Information Systems) interfaces, available U.S. datasets, model applications, and current model developments. Requirements for successful application of watershed models in Mexico are also discussed.

LITERATURE REVIEW

Integrated water management of large areas should be accomplished within a spatial scale unit (the watershed) through modeling. Integrated water management can be viewed as a three or more dimensional process centered around the need for water, the policy to meet the needs, and the management to implement the policy. Watershed modeling is fundamental to integrated management. Watershed models abound in the hydrological literature (Singh, 1989), and the state-of-the-art of watershed modeling is reasonably advanced. A majority of watershed models simulate watershed response with or without inadequate consideration of water quality. If these models are to be used for environmental or ecological modeling, they must consider water quality (Singh, 1995).

After the development of the Stanford Watershed Model (Crawford and Linsley, 1966), numerous operational, lumped, or "conceptual" models have been developed (Rockwood, et al., 1972; Sugawara et al., 1976; Hydrologic Engineering Center, 1981; Williams and Hann, 1973; Laurenson and Mein, 1983). In these models, some processes are described by differential equations based on simplified hydraulic laws, and other processes are expressed by empirical algebraic equations. More recent conceptual models have incorporated soil moisture replenishment, depletion, and redistribution for the dynamic variation in areas contributing to direct runoff. Several models have been developed from this concept, using a probability distribution of soil moisture, including the ARNO model (Moore and Clarke, 1981; Todini, 1996; Zhao, 1984) or using a topographic index, as in TOPMODEL (Beven and Kirkby, 1979; Beven et al., 1984). Jayatilaka et al. (1996) recently developed a variable source conceptual model that shows promise for incorporation into comprehensive models.

Another class of hydrological models is a differential model based on conservation of mass, energy, and momentum. Examples of differential models include SHE (Abbott et al., 1986a, 1986b), IDHM (Beven et al., 1987), and Binley et al. (1989). The SHE model simulates water movement in a basin with the finite difference solution of the partial differential equations describing the processes of overload and channel flow, unsaturated and saturated subsurface flow, interception, evapotranspiration (ET), and snowmelt. The spatial distribution of catchment

parameters is achieved by representing the basin on an orthogonal grid network. Jain et al. (1992) also concluded that the strength of differential models like SHE “lies beyond the field of pure rainfall-runoff modeling, for which purpose traditional and simpler hydrologic models often perform equally as well.”

In the early 1970s, work also began on non-point source modeling in response to the Clean Water Act. The CREAMS model (Knisel, 1980) was developed to simulate the impact of land management on water, sediment, nutrients, and pesticides leaving the edge of a field. Several field-scale models evolved from the original CREAMS to simulate pesticide ground water loadings (GLEAMS; Leonard et al., 1987) and to simulate the impact of erosion on crop production (EPIC; Williams et al., 1984).

Other efforts evolved to simulate hydrology and water quality of complex watersheds with varying soils, land use, and management. Several models were developed to simulate single storm events using a square grid representation of spatial variability (Beasley et al., 1980; Young et al., 1987). These models did not consider subsurface flow, ET, or plant growth. Continuous models were also developed (Johansen et al., 1984; Arnold et al., 1990) but generally lacked sufficient spatial detail.

SWAT MODEL OVERVIEW

The SWAT model simulates water quantity and quality in large, complex basins. SWAT predicts the impact of topography, soils, land use, management, and weather on water, sediment, nutrient (nitrogen and phosphorus), and agricultural chemical yields for large watersheds with an insufficient number of gages. To meet the design criteria, the model (1) does not require calibration (which is impossible on ungaged watersheds); (2) uses inputs that are readily available for large areas; (3) efficiently simulates hundreds of interacting subbasins using a daily time step, and (4) simulates hundreds of years in a continuous time model to assess long-term impacts. The command structure routes water, nutrients, and chemicals through streams and reservoirs and inputs measured data for point sources of water and pollutants (Fig. 8-1).

SWAT is a complex, conceptual model with spatially explicit parameterization. Major model components include weather, hydrology, soil temperature, plant growth, nutrients, pesticides, and land management. A complete description of SWAT model components is found in Arnold et al. (1998). Large watersheds are typically divided into smaller subwatersheds based on topography to accommodate channel and reservoir routing. The subwatersheds can be further subdivided into hydrologic response units (HRUs). HRUs in each subwatershed are created by overlaying soils and land use and “lumping” similar soils/land-use combinations. The water balance of each HRU is represented by four storage volumes: snow, soil profile (0-2 m), shallow aquifer (typically 2-20 m), and deep aquifer (>20 m). The soil profile can be subdivided into multiple layers. Soil water processes include infiltration, evaporation, plant uptake, lateral soil flow, and percolation to lower layers. Surface runoff and infiltration are simulated using the curve number technique or the Green and Ampt infiltration equation. Percolation from the bottom of the soil profile recharges the shallow aquifer (ground water recharge). Total ground water recharge is the sum of (1) water that passes past the bottom of the soil profile, (2) channel transmission losses, and (3) seepage from ponds and reservoirs. The model simulates potential evapotranspiration by the Hargreaves, Priestley-Taylor, or Penman-Monteith methods. Other components of the hydrologic balance include snowmelt, transmission losses from streams, and water storage and losses from ponds.

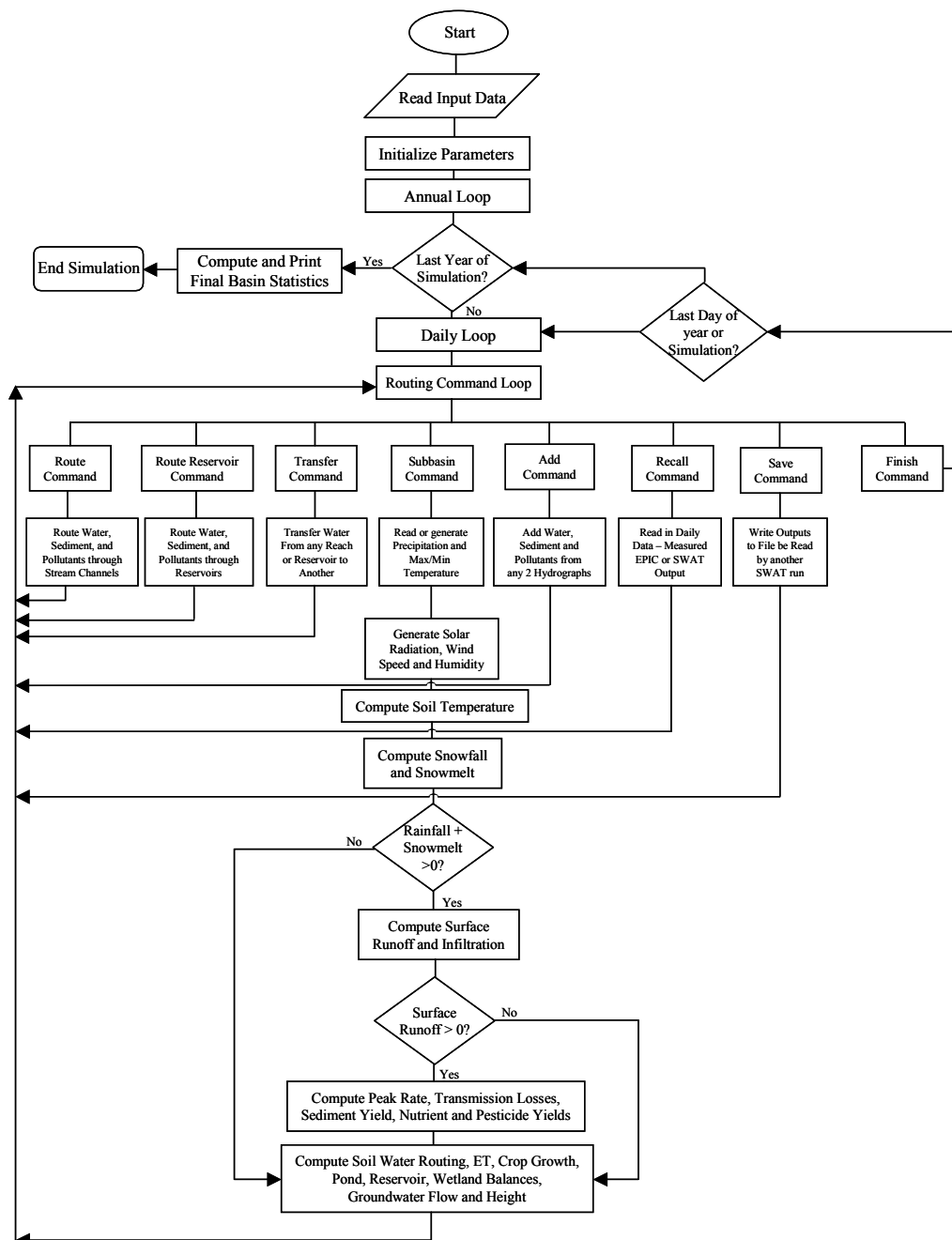


Fig. 8-1. SWAT model operational structure.

Daily precipitation, maximum and minimum air temperatures, solar radiation, wind speed, and relative humidity drive the hydrologic model. A weather generator simulates variables based on monthly climate statistics derived from long-term measured data. Weather data can differ among subbasins.

SWAT computes sediment yield for each subbasin with the Modified Universal Soil Loss Equation. Soil temperature is updated daily for each soil layer as a function of air temperature; snow, plant and residue cover; damping depth; and mean annual temperature. The model simulates crop growth with a daily time step using a simplification of the EPIC crop model which predicts phenological development based on daily accumulation of degree days, harvest index for partitioning grain yield, a radiation-use efficiency approach for potential biomass, and adjustments for water and temperature stress. Both annual and perennial crops are simulated using crop-specific input parameters. SWAT simulates nitrate losses in runoff, in percolation and in lateral subsurface flow. The model simulates organic nitrogen losses from soil erosion and an enrichment ratio. A nitrogen transformation model modified from EPIC includes residue mineralization, soil humus, mineralization, nitrification, denitrification, volatilization, fertilization and plant uptake. Phosphorus processes include residue and humus, mineralization, losses with runoff water and sediment, fertilization, fixation by soil particles and plant uptake. Pesticide transformations are simulated with a simplification of the GLEAMS model (Leonard et al., 1987) approach and include interception by the crop canopy; volatilization; degradation in soils and from foliage; and losses in runoff, percolation, and sediment. The model simulates agricultural management practices such as tillage effects on soil and residue mixing, bulk density and residue decomposition. Irrigation may be scheduled by the user or applied automatically according to user-specified rules. Fertilization with nitrogen and phosphorus can also be scheduled by the user or applied automatically. Pesticide applications are scheduled by the user. Grazing is simulated as a daily harvest operation.

SWAT simulates stream processes, including channel flood routing, channel sediment routing, nutrient and pesticide routing, and transformations modified from the QUAL2E model (Brown and Barnwell, 1987). Components include algae as chlorophyll-a, dissolved oxygen, organic oxygen demand, organic nitrogen, ammonium nitrogen, nitrite nitrogen, organic phosphorus, and soluble phosphorus. In-stream pesticide transformations include reactions, volatilization, settling, diffusion, resuspension, and burial. The ponds and reservoirs component includes water balance, routing, sediment settling, and simplified nutrient and pesticide transformation routines. Water diversions into, out of, or within the basin can be simulated to represent irrigation and other withdrawals from the system.

GIS INTERFACES

Two GIS interfaces have been developed for SWAT. The first interface was developed (Srinivasan and Arnold, 1994) using the Graphical Resources Analysis Support System (GRASS). The input interface automatically subdivides a basin (grids or subwatersheds) and then extracts model input data from map layers and associated relational data bases for each subbasin. Soils, land-use, weather, management, and topographic data are collected and written to appropriate

model input files. The output interface allows the user to display output maps and graphs output data by selecting a subbasin from a GIS map.

The next GIS interface developed for SWAT, using ArcView (DiLuzio et al, 2002), consists of three key components: (1) preprocessor generating subbasin topographic parameters and model input parameters; (2) editing input data and execute simulation; (3) postprocessor viewing graphical and tabular results. The export of data from GIS to the SWAT model and the return of results for display are accomplished by Avenue routines that are addressed directly by the interactive GIS tools, setting up parameter values via customized menus, and the automatic exchange of data.

The delineation of the watershed and the development of the watershed and subbasins database are the first steps performed by the preprocessor. The overall process for defining a flow vector grid requires the processing of a raw DEM (digital elevation model) to fill the containing pits (grid cells with no neighbor having a lower elevation) with specialized algorithms (raise the elevation of the pit until a "pour point" occurs). Once the flow direction is defined, a flow accumulation is created by counting the number of contributing cells to each cell in the grid (cells whose flow path eventually passes through the cell). Cells which are potentially part of a stream network will have a larger accumulation value, whereas cells near watershed boundaries and where overland flow dominates will have a low flow accumulation value. The definition of the subbasin outlet points is accomplished by locating the downstream edge for each branch in the stream, where the branches are controlled by the user-specified threshold on contributing number of grid cells making up the branch. Moreover, a user can interactively introduce outlet points, by clicking in correspondence of mouse cursor on the screen or importing a table of point locations (i.e., stream gauges), and eliminate any of the selecting outlets. Once the outlet locations are specified, the user defines the watershed outlet with a customized selection tool, and the subbasin delineation can be performed by a process tracing the flow direction from each grid cell until either an outlet cell or the edge of the grid is encountered.

Once watershed and subbasin boundaries are determined, all the geometric parameters of subbasins and stream reach can be determined by the raster-grid functions and stored as attributes of derived vector themes. For example, land slopes of subbasins are automatically calculated by averaging slope values of the respective grid cells; slope, length and width are calculated for the main stream channel flowing from each subbasin inlet to the subbasin outlet, and the longest stream channel extending from each subbasin outlet to the most distant point in the subbasin. Separate grid layers for land use and soil may also be overlayed with the watershed grid to calculate land-use and soil variations within subbasins. The user is provided options to use either the predominant or the no-spatial subdivision of subbasins into smaller sub-units based on the combination of all controlled percentage of land uses and soils (hydrologic response units).

A set of Avenue scripts assigned to respective buttons and tools allows the user to edit the model inputs by viewing and/or modifying any of the previously written input parameters. Additionally, the user can set up the simulation control codes (length of simulation, type of simulation, etc.), and execute the simulation, including checking the existence of all necessary input files. A set of menus and buttons allows users to display the SWAT output components in graphic and tabular formats and for each subbasin and stream reach, with a daily, monthly, and yearly time step.

The HRU extension of the interface defines the distribution and combination of the land-use and soil categories over the watershed and sub-watersheds. A set of tools allows loading and clipping land-use and soil maps (either in raster-grid or vector-shape format) on the watershed

area. The watershed clipped land-use and soil maps are reclassified into various categories which need to match the land-use categories. On the basis of the obtained distribution and combination of the HRUs, the user is provided with options to either use the predominant or subdivide into smaller sub-units based on the combination of all controlled percentage of land uses and soils, thereby reducing the total number of modeling units.

REQUIRED MODEL INPUTS

Watershed models require information related to topography, soils, land use and management, and climate. The main inputs are briefly described here.

Topographic Attributes: Basin and subbasins are determined using the Digital Elevation Model (DEM), and then areas and subbasin routing is calculated. Other inputs determined from the DEM include channel slopes and lengths, overland slopes and lengths, and location of reservoirs in the routing network. Stream channel dimensions can be estimated from regression analysis (Allen, et al. 1994).

Land-Use Attributes: The model requires a land-use type (agricultural, forest, range, urban, etc.) for each HRU. If the land use is agriculture, a multiyear cropping rotation can be input. Management operations that can be scheduled include planting and harvest, irrigation, tillage, fertilizer and manure applications, pesticide applications, and grazing.

Soils Attributes: Soil attributes are also required for each HRU. Soil physical properties include texture, bulk density, saturated conductivity, available water capacity, and organic carbon. If the curve number approach is used, a curve number is assigned to each HRU, based on land use and the hydrologic soil group.

Weather Attributes: The model requires daily precipitation, maximum and minimum temperatures, solar radiation, wind speed, and relative humidity. SWAT contains a weather generator, capable of generating daily weather series from monthly statistical averages. Daily precipitation is usually read into the model since it is critical for calibration and validation and since the generator is a point generator and does not spatially correlate precipitation. Daily maximum and minimum temperatures are input to the model when snow melt is a critical component of the hydrologic cycle. Other daily weather attributes are normally generated using the embedded weather generator.

Supplied Databases: Several databases are supplied with the model, including databases for plants, tillage, fertilizer, and pesticides. The plant database has model parameters for over 100 plant types with default data on maximum leaf area index, maximum rooting depth, maximum canopy height, energy to biomass conversion, optimum and base growth temperatures, and nitrogen and phosphorus concentrations. The tillage database has over 200 implements parameterized and contains tillage depth and mixing efficiency. The fertilizer database contains nitrogen and phosphorus contents of several common commercial fertilizers and manures. The pesticide database has properties for over 200 common herbicides and insecticides that include foliar and soil half-life, water solubility, foliar wash-off, and soil adsorption coefficient. All these databases can be modified by the user.

AVAILABLE U.S. DATABASES

Readily Available Data for Entire U.S.

Currently in the U.S., input data required to run SWAT are readily available and can be downloaded from the web (<http://www.epa.gov/OST/BASINS/gisdata.html>). The following data are available for the entire U.S.:

- (1) The Anderson level II classified land-use/land-cover layer created using the 1:250,000 scale USGS LUDA (USGS, 1990b). Land classes include agricultural, forests, range, and urban. Land area in specific crops (i.e., corn, wheat, soybeans) for each county from the National Agricultural Census Data.
- (2) The digital elevation model (DEM) for the contiguous U.S. assembled from 1:250,000 scale USGS 1° by 1°, 3 arc-second data. The horizontal cell size of this data is approximately 100 by 100 m and the vertical resolution is one meter.
- (3) The USDA-NRCS STATSGO (USDA, 1992) soil association dataset.
- (4) Statistical data from 1130 historical weather stations required for the SWAT weather generator. Daily precipitation and maximum and minimum temperatures from over 6,000 stations with 30 or more years of data.
- (5) U.S. Geological Survey daily stream flow from 15,000 gages.
- (6) Water use data from the USGS Water Use database. The database includes municipal and industrial water use and gives monthly withdrawals from surface and groundwater sources. Data on pond and reservoirs are available from the DAMS database, which is a collection of data from the National Resources Conservation that includes surface areas, volumes and spillway information from small flood control structures to large reservoirs.

Data Available for Some Areas of the U.S.

County Soils Data. Soil Survey Geographic (SSURGO) (USDA, 1995) is the most detailed level of soil mapping done by the NRCS. The database, at the county scale, includes soil maps at scales generally ranging from 1:12,000 to 1:63,360. SSURGO data are available for selected counties and areas throughout the United States and its territories. The data are archived in 7.5-min topo quad units and distributed as complete coverage for each survey area (which may consist of a county, multiple counties, or parts of multiple counties) with all adjoining 7.5-min units matched within it. The data can be downloaded from the Internet, including description and data user guide, at <http://www.ftw.nrcs.usda.gov/ssurodata.html>. The status as of 2 May 2003 shows that 1494 out of 2230 soil surveys areas are digitized and archived.

National Geospatial Datasets for Hydrology. A series of national geospatial datasets for hydrology are being constructed by the federal government in collaboration with state partners. These include (1) the National Elevation Dataset, a seamless digital elevation surface of the United States now available with one arc-second (30-m) cells, with one-third arc-second (10-m) coverage in development; (2) the National Hydrography Dataset, a complete coverage of the river networks and water bodies of the United States at 1:100,000 scale, which is being improved to 1:24,000 scale in some states; (3) the Watershed Boundary Dataset in which a four-level hierarchy of watersheds in the nation is being extended to fifth and sixth levels through a combination of automated processing of DEMs and hand digitizing; (4) the Elevation Derivatives for National

Applications in which the National Elevation Dataset is being processed to define a very dense drainage network and fine resolution set of catchments. These datasets are the basis of a national geospatial data infrastructure for hydrology in the United States. Taken in combination with real-time water resources data from about 5000 USGS monitoring stations, these represent a powerful basis for studying hydrologic processes over various scales of space and time.

The National Elevation Dataset (NED) is the result of the USGS effort to provide 1:24,000-scale Digital Elevation Model (DEM) data for the conterminous U.S. and 1:63,360-scale DEM data for Alaska, Hawaii, and the island territories, in a seamless format with consistent projection, resolution, elevation units, and horizontal and vertical datums (Gesch et al., 2002). NED has been developed by merging the highest-resolution, best-quality elevation data available across the United States into a seamless raster format. NED is regularly maintained and updated, thereby removing the need for users to repeatedly perform preprocessing steps to make the DEMs suitable for geographic information system (GIS) use.

Several NED development activities are currently underway to enhance the seamless elevation data available to users. The NED production system has been modified to produce 1/3-arc-second data, thereby maintaining the full information content of the 10-m source DEMs. Currently, 1/3-arc-second (10-m) and 1/9-arc-second (3-m) data are being produced only where there is full coverage of 10-m source DEMs for an entire 1- by 1-degree NED tile. This results in multiresolution NED products being available over certain areas. In these areas, 1-arc-second, 1/3-arc-second, and 1/9-arc-second, data are produced with the same characteristics and are “nested” spatially to facilitate easy transition between resolutions.

A second area of current research and development is the integration of source data other than standard USGS DEMs into the NED. Researchers in the USGS elevation program are actively evaluating new elevation data collection technologies, including LIDAR, IFSAR, and softcopy photogrammetry (Osborn et al., 2001). DEMs resulting from these newer production methods generally have higher resolution and accuracy than existing DEMs. To maintain the “best available” characteristic of the NED, the USGS must exploit and incorporate these new sources into the NED, especially in those areas where applications are limited by existing source data, such as low-relief coastal areas. Further information is available on the NED Web site at <http://gisdata.usgs.gov/ned/>.

The Shuttle Radar Topography Mission (SRTM) (USGS, 2003) is a joint project between the National Imagery and Mapping Agency (NIMA) and the National Aeronautics and Space Administration (NASA). The objective of this project is to produce digital topographic data for 80% of the Earth's land surface (all land areas between 60° north and 56° south latitude), with data points located every 1-arc-second (approximately 30 m) on a latitude/longitude grid. This radar system will gather data that will result in the most accurate and complete topographic map of the Earth's surface that has ever been processed. SRTM data are being processed at the Jet Propulsion Laboratory (JPL) in Pasadena, California, into research-quality digital elevation models. The data are 90-m averaged from the original 30-m data. As each continent is completed, the data are being sent to NIMA for final finishing (final editing, verification, and conformance to National Map Accuracy standards). Each continent is being processed in turn, beginning with North America, then South America, Australia, Eurasia, Africa, North and South Pacific, and North and South Atlantic. USGS hosts and distributes SRTM data for broad public access via the USGS EDC Seamless Data Distribution System - Enhanced (<http://seamless.usgs.gov>). At regular (5-6 mo) intervals, USGS may post “unfinished” 90-m continental datasets to be replaced by NIMA

validated “finished” data once received. NASA began processing mission data in April 2002 and has processed and delivered all mission data to NIMA. All international 90-m (295-ft) resolution finished data are now available to the public.

NEXRAD (Next Generation Weather Radar) based multi-sensor precipitation products are currently produced at National Weather Service (NWS) River Forecast Centers (RFCs) at a 1-h temporal and 4-km spatial resolution. NEXRAD data are derived from more than 120 weather surveillance radar, 1988-Doppler (WSR-88D) radar stations. The WSR-88D radar stations provide continuous radar coverage <3000 m above sea level, except where rising terrain obstructs the radar beam. The end result is a composite reflectivity that is converted to precipitation rates using a rainfall-reflectivity (Z-R) relationship. The rainfall rates are accumulated over time to produce hourly accumulations that are adjusted based on concurrently measured precipitation gauge data. Three stages of precipitation processing occur in the production of the digital precipitation array product. During Stage III processing, data from a number of radar sites are merged together to form a complete mosaic over a large area, and remaining identifiable errors are corrected. This is the final step in a complex process to generate the best possible quantitative estimates of precipitation, which has the potential to be used as input to hydrologic models (Shedd et al. 1992). Archiving of these products first began in 1993 with the Stage III algorithms (Fulton et al., 1998), and work to improve these algorithms continues (Seo, 2002). The grid resolution for WSR-88D radar data is often described as being on a 4 x 4 km grid. In reality, the mesh length depends on the latitude, with the grid spacing varying between approximately 3.5 and 4.5 km within the contiguous United States.

The National Land Cover Characterization project was created in 1995 to support the original Multi-Resolution Land Characterization (MRLC) initiative and fulfill the requirement to develop a nationally consistent land-cover dataset from MRLC data called National Land Cover Data 1992 (Vogelmann et al., 2001). This culminated in the September 2000 completion of land-cover mapping using a modified Anderson level II classification for the conterminous United States. In addition to satellite data, scientists used a variety of supporting information, including topography, census, agricultural statistics, soil characteristics, other land-cover maps, and wetlands data, to determine and label the land-cover type at 30-m resolution. Twenty-one classes of land cover were mapped, using consistent procedures for the entire U.S., and a subsequent accuracy assessment was performed.

USGS DEMs. The USGS produces five different digital elevation products (USGS, 1990a). Although all are identical in the manner the data are structured, each varies in sampling interval, geographic reference system, areas of coverage, and accuracy, with the primary differing characteristic being the spacing, or sampling interval, of the data. The five DEM products are as follows:

1. 7.5-Minute DEM 30- x 30-meter data spacing
2. 1-Degree DEM 3- x 3-arc-second data spacing
3. 2-Arc-Second DEM 2- x 2-arc-second data spacing
4. 15-Minute Alaska DEM 2- x 3-arc-second data spacing
5. 7.5-Minute Alaska DEM 1- x 2-arc-second data spacing

Over the years, the USGS has collected digital elevation data using a number of production strategies, including manual profiling from photogrammetric stereomodels; stereomodel digitizing

of contours; digitizing topographic map contour plates; converting hypsographic and hydrographic tagged vector files; and performing autocorrelation via automated photogrammetric systems. Of these techniques, the derivation of DEMs from vector hypsographic and hydrographic data produces the most accurate model and is the preferred method.

U.S. APPLICATIONS

Watershed Application of SWAT

The U.S. Environmental Protection Agency reported nutrient enrichment as the major cause for impairment of lakes and other water bodies in the U.S. (USEPA, 1994). EPA's water quality inventory of 1996 indicated that 40 % of the surveyed rivers, lakes, and estuaries were polluted relative to their designated uses (USEPA, 1998). To restore the quality of these water bodies, the Total Maximum Daily Load (TMDL) process was established by Section 303(d) of the Clean Water Act. A TMDL quantifies pollutant sources and maximum allowable loads of contributing point and nonpoint sources so that water quality standards are attained for uses such as for drinking water and aquatic life (USEPA, 1998). Once necessary pollutant reduction levels are identified through the establishment of TMDLs, control measures such as best management practices (BMPs) are implemented. The USEPA Office of Science and Technology has developed a framework for states to analyze impaired water bodies called BASINS (Better Assessment Science Integrating point and Non-point Sources). BASINS consists of five components: (1) national databases, (2) assessment tools, (3) utilities, (4) watershed models, and (5) post-processing and output tools. SWAT and its associated GIS interface have been integrated into BASINS and are being used in several states for TMDL analysis.

The SWAT model was applied to the 4277 km² Bosque River watershed in central Texas. This river flows into Lake Waco, which is the source of drinking water for the city of Waco. The watershed is mostly range and pasture in the upper portion while cropland is widespread in the lower portion. Manure from the 41,000 dairy cows in this watershed is applied on an area of 9450 ha. There is a strong positive correlation between elevated levels of phosphorus, the number of cows, and the total acreage of manure application fields (McFarland and Hauck, 1999). Other sources of pollution include runoff from cropland and urban areas and effluent from wastewater treatment plants.

SWAT was calibrated and validated at two USGS gaging stations in this watershed, at Hico and Valley Mills (Santhi et al, 2001). After the model was validated, several management practices were simulated to see which practices would reduce phosphorus concentrations in the river below water quality standards.

The calibrated model was used to study the long-term effects of various BMPs related to dairy manure management and municipal wastewater treatment plant loads in this watershed. Among several scenarios studied, four scenarios are discussed in this paper. Detailed description of the BMPs can be found in Santhi et al. (2002). The existing condition scenario simulates the watershed with the present dairy herd size, the present waste application fields, the average manure application rate of 13 Mg ha⁻¹yr⁻¹, the present discharge volumes from waste water treatment plants (WWTPs) with the current median concentrations for nutrients, and present urban and cropland areas. The future condition scenario reflects the projected conditions of the watershed in year 2020 with a projected dairy herd size of 67,000 cows, manure application in

waste application fields at the crop N requirement rate of 46 Mg of N $\text{ha}^{-1}\text{yr}^{-1}$, waste application field area calculated at N rate requirement, maximum permitted discharge volumes from WWTPs using nutrient concentrations defined by current median values, urban area increased by 30% to reflect the projected population growth in 2020, and cropland area at current levels (due to no increase in cropland over last two decades) (Table 8-1). Three additional WWTPs with 1 mg/l concentration of total P were input into the model as point sources along the North Bosque River to account for possible industrial future growth outside existing communities.

Table 8-1. Assumptions of BMP scenarios in the Bosque watershed.

Scenario	WWTP Flow Period	WWTP P Limit	Dairy Manure App. Rate	Reduced P in Diet	Haul off Manure
Existing	1997-98 (actual)	Median Conc.	Btw N&P Rate	No	No
Future	2020 (permitted)	Median Conc.	N rate	No	No
Scenario E	1997-98	All WWTPs at Median Conc. & Stephenville WWTP- 1mg/l	P rate	Yes	Yes
Scenario F	2020	All WWTPs with loads equal to Scenario E & Stephenville WWTP-with load equal to 1mg/l of future	P rate	Yes	Yes

BMP, best management practices; WWTP, waste water treatment plants

Several management practices on dairy manure and WWTP effluents were simulated to study the impact in reducing the mineral P loadings. Imposed dairy management practices included hauling solid manure from the watershed, applying manure at crop P requirement rate (P rate) of 6.3 Mg $\text{ha}^{-1}\text{yr}^{-1}$ (because the N rate allows more applied P than crops require), and reducing the dairy diet P to 0.4% (resulting in a 29% reduction in dairy manure P content). The concentrations of total P in WWTP effluents were reduced to 1 mg l^{-1} . Scenario E was a modification of the existing condition scenario, with additional conditions imposed on manure application rate (P rate), hauling off 38% of the manure, P diet reduction in animal feed, and 1 mg l^{-1} limits of P in WWTPs. Scenario F was a modification over the future scenario with manure applied at P rate, hauling off 38% of the manure, P diet reduction, and 1-mg l^{-1} P limits on all WWTPs.

Mineral P loadings are displayed as probability exceedance plots to analyze the effectiveness of BMPs. In these exceedance plots, annual mineral P loadings (y-axis) for the simulation period (1960 through 1998) were ordered and plotted with their associated exceedance probability values

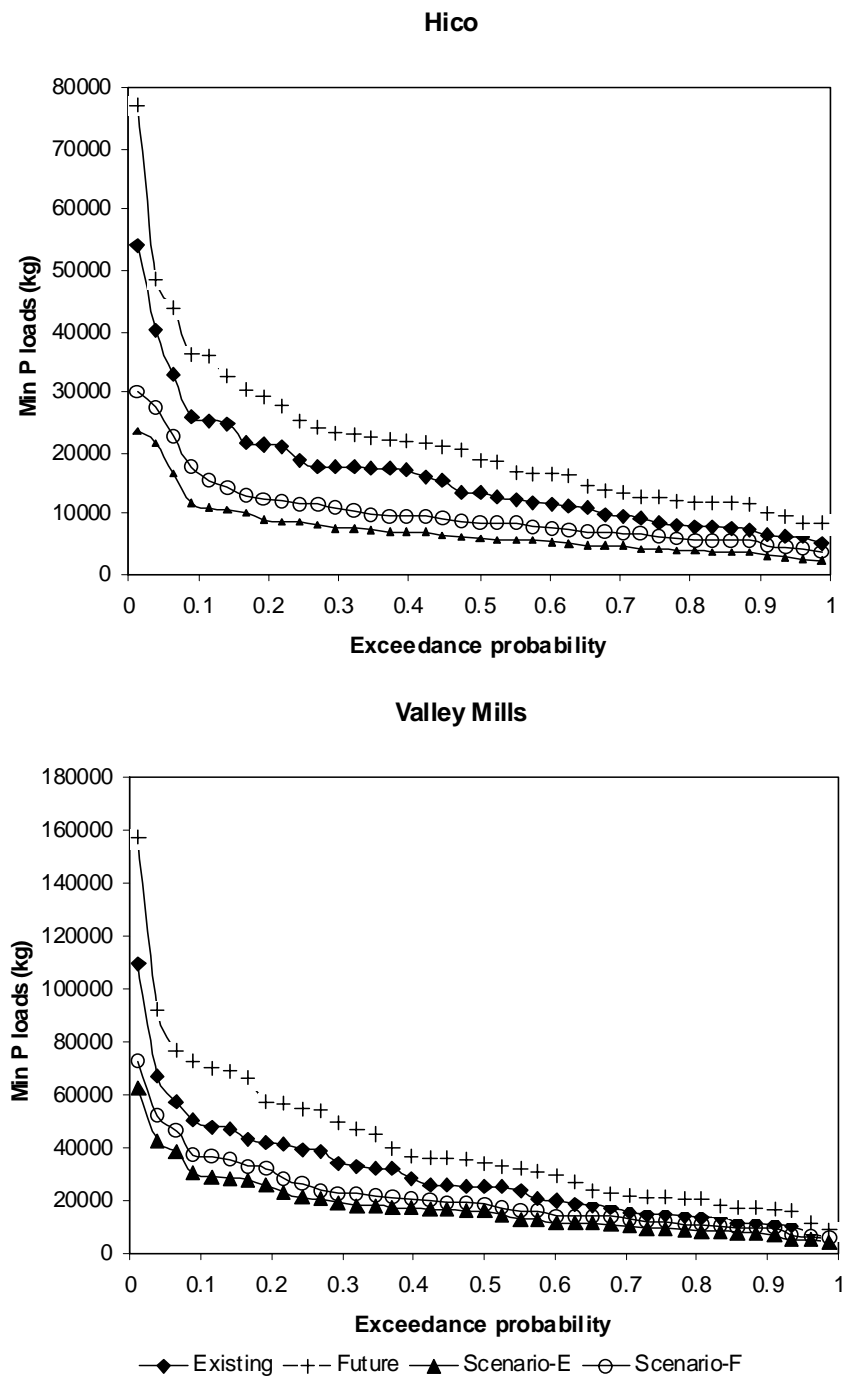


Fig. 8-2. SWAT simulated probabilities of exceeding mineral phosphorus loads at Hico and Valley Mill gages in the Bosque river watershed, Texas. Scenarios defined in text.

(x-axis) for Hico and Valley Mills (Fig. 8-2). These plots provide information on the probability of achieving a particular load of mineral P through a BMP at a particular location. Mineral P loading curves for the scenarios varied from 10,000 to 40,000 kg at 10% probability at Hico whereas it varied from 20,000 kg to 80,000 kg at Valley Mills. These curves showed loadings within 10,000 kg at Hico at 90% probability, and they showed loadings within 20,000 kg at Valley Mills for the same probability. In general, the loading curves were wider at lower probabilities, and they became closer as they reached higher probabilities. The mineral P loadings were increased by about 27% at Hico and 29% at Valley Mills in the future condition scenario as compared to the existing condition scenario. These increases were predominantly caused by projected conditions for dairy and WWTPs in the future scenario (Table 8-1). Scenario E showed reduction in mineral P loadings of about 67% at Hico and 57% at Valley Mills from the future scenario. With Scenario F, mineral P loadings were reduced 54% at Hico and 48% at Valley Mills from the future scenario. Scenario E indicated that with existing conditions, implementation of the BMPs would come closest to achieving the desired water quality goals. However, with year 2020 growth (future) conditions, more stringent controls will be required to meet the water quality goals.

National Application of SWAT

The HUMUS (Hydrologic Unit Model of the United States) project was designed to improve existing technologies for making national and river-basin scale water resource assessments, considering both current and projected future climatic characteristics, water demands, point-sources of pollution, and land management affecting non-point pollution (Srinivasan et al., 1993). The project was implemented as part of the United States Resources Conservation Act Assessment completed in 1997. The major cooperators in the HUMUS project were the USDA –ARS (United States Department of Agriculture-Agricultural Research Service and the Texas Agricultural Experiment Station, part of the Texas A & M University System.

The major components of the HUMUS system were (1) the basin-scale SWAT to model surface and sub-surface water quantity and quality; (2) a geographic information system to collect, manage, analyze, and display the spatial and temporal inputs and outputs of SWAT; and (3) relational databases used to manage nonspatial climate, soil, crop, and management data required as input to and generated as output from SWAT.

Various hydrologic and crop growth outputs from the SWAT model simulation for the entire U.S. for the HUMUS project are given in Arnold et al. (1999). The Penman-Monteith ET methodology was used in the simulation. Average annual ET generated from 20-yr SWAT model simulations had highs and lows in parts of Kansas and Nebraska (Fig. 8-3). These were due to the irrigation database used in this study. The high actual ET in most of Kansas was because the STATSGO database showed most of the state as irrigated land. With irrigation automatically triggered when plant available soil water was 50% of plant demand, irrigation of the agricultural cropland areas were greatest in parts of California, Kansas, and eastern New Mexico (Fig. 8-4). The average annual biomass production of irrigated cropland areas ranged from 25 to 32 Mg ha⁻¹. For non-irrigated cropland areas, this ranged from 21 to 25 Mg ha⁻¹. For forest land areas, values ranged from 16 to 21 Mg ha⁻¹ depending on their spatial and temporal distributions. Grains yields for irrigated land ranged from 9 to 11 Mg ha⁻¹; for non-irrigated land , grain yields ranged from 6 to 9 Mg ha⁻¹ in Midwest U.S. and 3 to 6 Mg ha⁻¹ in other grain production areas. These grain yields agreed reasonably well with state averages (Table 8-2).

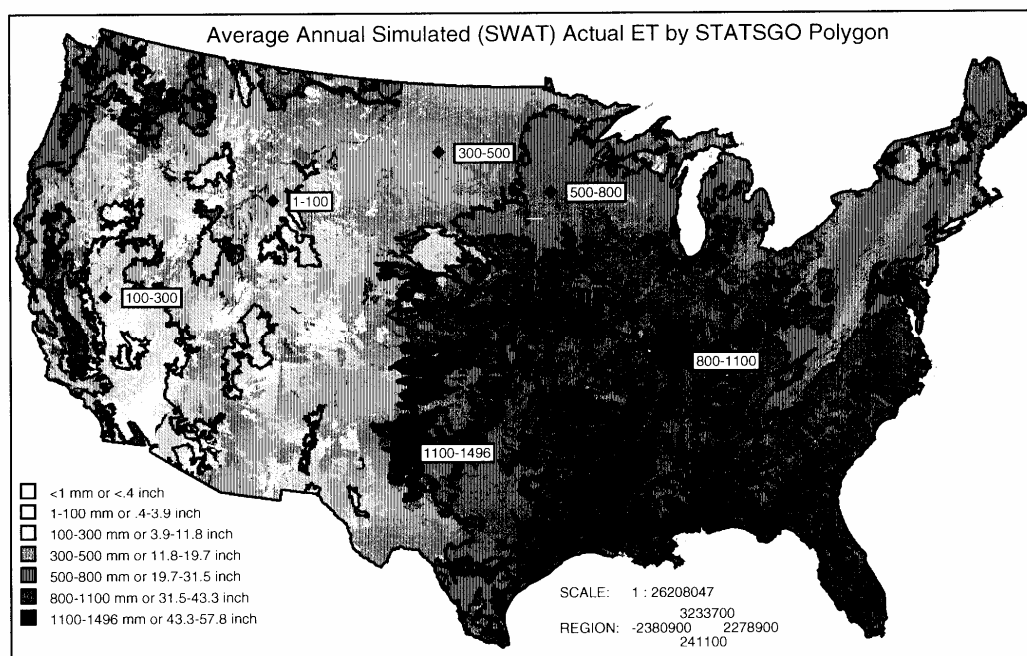


Fig. 8-3. Average annual evapotranspiration simulated by the SWAT model for the conterminous U.S.

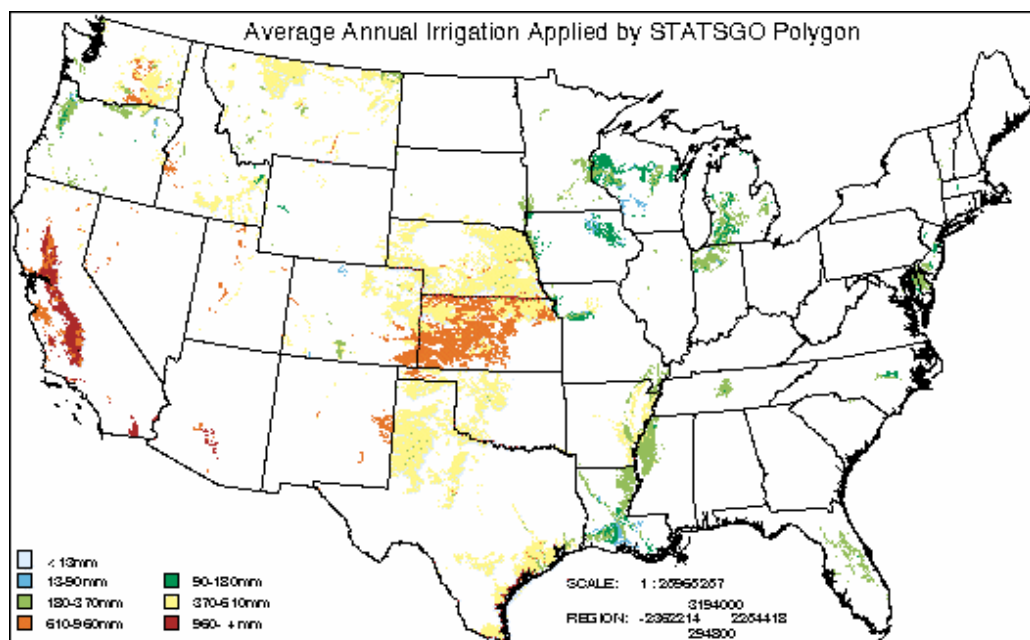


Fig. 8-4. Average annual irrigation simulated with the SWAT model based on crop water requirements.

Table 8-2. Comparison of SWAT Corn Yields vs. Ag Census and National Ag Statistics Corn Yields ($Mg\ ha^{-1}$).

State	FIPS-id	AGCENSUS (1987)	NASS (20 yr avg)	SWAT Yield
Illinois	17	6.6	6.0	6.7
Indiana	18	6.5	6.2	6.2
Iowa	19	6.6	6.2	6.6
Kansas	20	5.3	5.9	5.5
Kentucky	21	4.5	4.5	4.9
Michigan	26	4.0	4.5	2.9
Minnesota	27	5.1	4.5	3.6
Missouri	29	4.8	4.5	5.0
Nebraska	31	6.2	6.6	3.7
North Carolina	37	3.1	4.0	3.0
Ohio	39	5.7	5.6	5.8
Pennsylvania	42	4.9	4.9	2.6
South Dakota	46	3.3	3.1	3.6
Wisconsin	55	5.3	5.2	3.6

FIPS, Federal Information Processing Standard state/county code; NASS National Agricultural Statistics Service

CURRENT SWAT DEVELOPMENT

The latest version, SWAT2000, has several significant enhancements that include bacteria transport routines; urban routines; Green and Ampt infiltration equation; improved weather generator; ability to read in daily solar radiation, relative humidity, wind speed and potential ET; Muskingum channel routing; and modified dormancy calculations for tropical areas. A complete set of model documentation for equations and algorithms, a user's manual describing model inputs and outputs, and an ArcView interface manual are now complete for SWAT2000. The model has been recoded into Fortran 90 with a complete data dictionary, dynamic allocation of arrays, and modular subroutines. Current research is focusing on bacteria fate and transport, riparian zones, pothole topography and tile drains, rice fields, turf grass (golf courses), channel down cutting and widening, and macropore flow in soils. In the future, we plan to develop a programmer's manual and make the code more accessible to other scientists.

CONCLUSIONS

In the past decade, watershed models have been widely used in the U.S. due to 1) advances in computer speed and storage, 2) development of GIS, and 3) availability of national databases. Two driving forces of watershed modeling include the USEPA's need to access polluted water bodies and the NRCS's need for national assessment of the environmental impact of conservation programs. The models can be successfully applied and validated in Mexico if 1) there is sufficient need, 2) adequate databases can be developed, and 3) experimental watersheds across several ecosystems are available for validation.

REFERENCES

- Abbott, M.B., J.C. Bathurst, J.A. Cunge, P.E. O'Connell, and J. Rasmussen. 1986a. An introduction to the European Hydrological System-Système Hydrologique European 'SHE' 1: History and philosophy of a physically-based, distributed modeling system. *J. Hydrol.* (Amsterdam) 87:45-59.
- Abbott, M.B., J.C. Bathurst, J.A. Cunge, P.E. O'Connell, and J. Rasmussen. 1986b. An introduction to the European Hydrological System-Système Hydrologique European, 'SHE' 2: Structure of physically-based, distributed modeling system. *J. Hydrol.* (Amsterdam) 87:61-77.
- Allen, P.M., J.G. Arnold, and B. Byars. 1994. Downstream channel geometry for use in planning-level models. *Water Resour. Bull.* 30:663-671.
- Arnold, J.G., R. Srinivasan, R.S. Muttiah, and J.R. Williams. 1998. Large area hydrologic modeling and assessment I: Model development. *J. Am. Water Resour. Assoc.* 34(1):73-89.
- Arnold, J.G., R. Srinivasan, R.S. Muttiah, P.M. Allen, and C. Walker. 1999. Continental scale simulation of the hydrologic balance. *J. Am. Water Resour. Assoc.* 35:1037-1052.
- Arnold, J.G., J.R. Williams, A.D.Nicks, and N.B. Sammons, 1990. SWRRB: A basin scale simulation model for soil and water resources management. Texas A & M University Press, College Station, Texas.
- Beasley, D.B., L.F. Huggins, and E.J. Monke, 1980. ANSWERS: A model for watershed planning. *Trans. ASAE* 23:938-944.
- Beven, K.J. and M.J. Kirkby, 1979. A physically-based variable contributing area model of basin hydrology. *Hydrol. Sci. Bull.* 24(1):43-69.
- Beven, K.J., M.J. Kirkby, N. Schofield, and A. F. Tagg, 1984. Testing a physically-based flood forecasting model (TOPMODEL) for three UK catchments. *J. Hydrol.* (Amsterdam) 69:119-143.
- Beven, K.J., A. Calver, and E.M. Morris, 1987. The Institute of Hydrology Distributed Model (HDM). Rep. 98. Institute of Hydrology, Wallingford, United Kingdom.
- Binley, A., J. Elgy, and K.J. Beven, 1989. A physically based model of heterogeneous hillslopes. 1. Runoff production. *Water Resour. Res.* 25:1219-1226.
- Brown, L.C., and T.O. Barnwell, Jr. 1987. The enhanced water quality models QUAL2E and QUAL2E-UNCAS documentation and user's manual. EPA document # EPA/600/3-87/007. Cooperative Agreement #811883. Environmental Research Laboratory, U.S. Environmental Protection Agency, Athens, GA.
- Crawford, N.H., and R.S. Linsley. 1966. Digital simulation in hydrology: The Stanford Watershed Model IV. Technical Report No. 39. Department of Civil Engineering, Stanford University. Palo Alto, CA.
- DiLuzio, M. R. Srinivasan, and J.G. Arnold. 2002. Integration of watershed tools and SWAT model into BASINS. *J. Am. Water Resour. Assoc.* 38:1127-1141.
- Fulton, R.A., J.P. Breidenbach, D.J. Seo, and D.A. Miller. 1998. The WSR-88D rainfall algorithm. *Weather and Forecasting*. June, p. 377-395.
- Gesch, D.B., M.J. Oimoen, S.K. Greenlee, C.A. Nelson, M. Steuck, and D.J. Tyler. 2002. The National Elevation Dataset. *Photogramm. Eng. Remote Sens.* 63:5-11

- Hydrologic Engineering Center. 1981. HEC-1, flood hydrograph package –user's manual. U.S. Army Corps of Engineers, Davis, CA.
- Jain, S.K., B. Storm, J.C. Bathurst, J.C. Refsgaard, and R.D. Singh. 1992. Application of the SHE to catchments in India. Part 2. Field experiments and simulation studies with the SHE on the Kolar subcatchment of the Narmada River. *J. Hydrol.* (Amsterdam) 140:25-47.
- Jayatilaka, C.J., R.W. Gillham, D.W. Blowes, and R.J.Nathan, 1996. A deterministic-empirical model of the effect of the capillary fringe on near-stream area runoff 2. Testing and application. *J. Hydrol.* (Amsterdam) 184:317-336.
- Johansen, N.B., J.C. Imhoff, J.L. Kittle, and A.S. Donigan, 1984. Hydrological Simulation Program-Fortran (HSPF): User's manual. EPA-600/3-84-066. USEPA, Athens, Georgia.
- Knisel, W.G. 1980. CREAMS, A field scale model for chemicals, runoff and erosion from agricultural management systems. Res. Report No. 26. U.S. Dept. Agric. Conserv., U.S. Dept. of Agriculture, Washington, D.C.
- Laurenson, E.M., and R.G. Mein. 1983. RORB-Version 3: Runoff routing program – user's manual. 2nd ed. Department of Civil Engineering, Monash University, Monash, Australia.
- Leonard, R.A., W.G. Knisel, and D.A. Still. 1987. GLEAMS: Groundwater loading effects and agricultural management systems. *Trans. ASAE* 30:1403-1428.
- McFarland, A.M.S., and L.M. Hauck. 1999. Relating agricultural landuses to in-stream stormwater quality. *J. Environ. Qual.* 28: 836-844.
- Moore, R.J., and R.T. Clarke, 1981. A distribution function approach to rainfall-runoff modeling *Water Resour. Res.* 17:1367-1382.
- Osborn, K., J. List, D. Gesch, J. Crowe, G. Merril, E. Constance, J. Mauck, C. Lund, V. Caruso, and J. Kosovich. 2001. National digital elevation program (NDEP). p. 83-120. In D. Maune (ed.) Digital Elevation Model technologies and applications: The DEM user's manual. Am. Soc. Photogramm. Remote Sens., Bethesda, Maryland.
- Rockwood, D.M., E.D. Davis, and J.A. Anderson. 1972. User's manual for COSSARR Model. U.S. Army Engineering Division North Pacific, Portland, Oregon.
- Santhi, C., J.G. Arnold, J.R. Williams, W.A. Dugas, and L. Hauck. 2001. Validation of the SWAT model on a large river basin with point and nonpoint sources. *J. Am. Water Resour. Assoc.* 37:1169-1188.
- Santhi, C., J.G. Arnold, J.R. Williams, W.A. Dugas, and L. Hauck. 2002. Application of a watershed model to evaluate management effects on point and nonpoint source pollution. *Trans. ASAE* 44:1559-1570.
- Seo, D.J. 2002. About the Stage III Data [Online]. Available at http://www.nws.noaa.gov/oh/hrl/dmip/stageiii_info.htm (accessed Jan. 2003; verified 30 June 2005).
- Shedd, R.C., A. Peterlin, and L.E. Fox. 1992. WSR-88D and water management. p. 25-31. In Proc. Managing Water Resour. during Global Change, Reno, Nevada. October 1991. Am. Water Resour. Assoc., Middleburg, VA.
- Singh, V.P. 1989. Hydrologic systems. Vol. 2. Watershed modeling. Prentice Hall, Inc., Englewood Cliffs, NJ.
- Singh, V.P. (ed.) 1995. Computer Models of Watershed Hydrology. Water Resources Publications. Highlands Ranch, CO.
- Srinivasan, R., and J.G. Arnold. 1994. Integration of a basin-scale water quality model with GIS. *Water Resour. Bull.* 30:453-462.
- Srinivasan, R., J.G. Arnold, R.S. Muttiah, C. Walker, and P.T. Dyke. 1993. Hydrologic Unit

- Model for United States (HUMUS). p. 451-456. In Proc. Advances in Hydro-Science and Engineering. Nov. 1992. CCHE, School of Engineering, University of Mississippi, MS.
- Sugawara, M., E. Ozaki, I. Wantanabe, and Y. Katsuyama, 1976. Tank model and its application to Bird Creek, Wollombi Brook, Bihin River, Sanaga River, and Nam Mune. Research Note 11. National Center for Disaster Prevention, Tokyo, Japan.
- Todini, E., 1996. The ARNO rainfall-runoff model. J. Hydrol. (Amsterdam) 175:339-382.
- USDA Soil Conservation Service. 1992. State Soil Geographic Database (STATSGO) data user's guide. Publ. No. 1492. U.S. Government Printing Office, Washington, DC.
- USDA Soil Conservation Service. 1995. Soil survey geographic (SSURGO) data base. Miscellaneous Publ. No. 1527. Nat. Soil Survey Ctr. Natural Resources Conservation Service. Washington, D.C.
- USEPA. 1994. The quality of our nation's water: Executive summary of the national water quality inventory: Report to United States Congress. EPA841-R-97-008. USEPA, Washington D.C.
- USEPA. 1998. National water quality inventory: 1996 report to United States Congress. EPA841-R-97-008. USEPA, Washington D.C.
- USGS. 1990a. Digital Elevation Models: Data user's guide. National mapping program, Technical instructions, data user's guide 5. U.S. Department of Interior, Reston, VA.
- USGS. 1990b. Landuse and land cover digital data from 1:250,000 and 1:100,000 scale maps. Data user's guide 4. U.S. Department of Interior, Reston, VA.
- USGS. 2003. Shuttle radar topography mission. Mapping the world in 3-dimensions. WWW document[Online]. Available at <http://srtm.usgs.gov/> (accessed Jan. 2003; verified 30 Jun. 2005).
- Vogelmann, J.E., S.M. Howard, L. Yang, C.R. Larson, B.K. Wylie, and N. Van Driel, 2001. Completion of the 1990s national land cover data set for the conterminous United States from Landsat thematic mapper data and ancillary data source. Photogramm. Eng. Rem. Sens. 67:650-652.
- Williams, J.R. and R.W. Hann, 1973. HYMO: Problem-oriented language for hydrologic modeling – User's manual. Publ. No. ARS-S-9. USDA, Washington, D.C.
- Williams, J.R., C.A. Jones, and P.T. Dyke, 1984. A modeling approach to determining the relationship between erosion and soil productivity. Trans. ASAE 27:129-144.
- Young, R.A., C.A. Onstad, D.D. Bosch,, and W.R. Anderson, 1987. AGNPS, Agricultural Non-Point Source Pollution Model. A Watershed Analysis Tool. USDA Conservation Res. Rep. 35. Washington, D.C.
- Zhao, R.J., 1984. Watershed hydrological modeling. Water Resources and Electric Power Press, Bejing, R.O.C.

Page blank
126

CHAPTER 9

Development and Application of the Automated Geospatial Watershed Assessment Tool

Mariano Hernandez, Darius J. Semmens, Scott N. Miller, David C. Goodrich, and
William G. Kepner

CONTENTS

Introduction	128
Overview of the AGWA Tool	129
Hydrologic Models	132
KINEROS2	132
SWAT	135
Data Inputs and Parameter Estimation	138
Watershed Discretization	138
Parameter Estimation	139
Rainfall Input	139
Examples of AGWA Applications	140
Description of the Study Area and Data Sources	141
Using AGWA for Land-Cover Change Analysis	143
Introduction	143
Methods	143
Results	144
Discussion	148
Using AGWA for Land-Use Planning	148
Introduction	148
Methods	149
Results	150
Discussion	154
Summary and Conclusions	155
Acknowledgments	156
References	156

INTRODUCTION

The emphasis in natural resource management is shifting from inventory and exploitation to an integrated, broad-scale approach with the goals of maintaining diversity, balance, and long-term productivity of the environment. Accomplishing this requires an understanding of spatio-temporal processes on a detailed, integrated, and formalized level. The advent of remotely sensed and other forms of geospatial data has facilitated the study of large-scale, complex spatio-temporal processes. The need to assimilate this wealth of information when making decisions is increasing the demand for integrated computer-based tools capable of storing, manipulating, and analyzing environmental data. This chapter describes in detail the Automated Geospatial Watershed Assessment (AGWA) tool, which is an integrated hydrologic modeling toolkit developed by the USDA-ARS-Southwest Watershed Research Center in cooperation with the USEPA-National Exposure Research Laboratory-Landscape Science Program. AGWA was designed to perform watershed assessment across multiple spatial and temporal scales to facilitate scientific study and resource management. This chapter presents a detailed description of AGWA and two case studies illustrating the application of the tool. The case studies include (1) assessing the impact of land-cover and land-use change on water quantity and quality and (2) investigating the hydrologic impacts likely to result from a variety of forecasted population growth and development scenarios (alternative futures) for a semi-arid basin on the U.S.-Mexico border.

Most management decisions concerning the environment affect and are affected by the landscape. City and county planning authorities make decisions about land use and infrastructure that directly affect the landscape. Farmers make decisions about what to grow and how to grow it that affect and are affected by the landscape. Individual homeowners and business make decisions about their own behavior that affect and are affected by the landscape. Therefore, understanding and modeling the spatial patterns of landscape processes and changes over time at several different scales is critical to effective environmental management. In recognition of this, we need to develop a deeper understanding of the complex spatial and temporal linkages between and among ecological, hydrological, geomorphologic, and economic systems on the landscape and to use that understanding to develop effective and adaptive policies.

Central to environmental and ecological continua is water, which may occur as surface water, subsurface water, or groundwater. When assembled, these three types of water constitute the water continuum. The quantity and quality of these types and their variations in time and space constitute the necessary input to the integrated development and management of water resources. Integrated water management involves technology-based management and non-technology-based management. The core of technology-based management is watershed hydrology modeling (Singh, 1995).

Inherent to integrated resource management is the concept of total watershed management that is being increasingly accepted as an approach for environmental protection in general, and water resources (both quantity and quality) protection in particular. Watershed management links human activities (such as land use) within the watershed with hydrologic process and response, most commonly through the use of hydrologic models. One important outcome of this approach is that it provides a reasonable estimate of the expected water quality in the receiving stream. In other words, integrated modeling entails linking watershed conditions with water quantity and quality of the receiving body (Mankin et al., 1999).

For the decision maker, implementing simulation models and interpreting their output is complicated by the complexity of the models and by the nature of natural resource decisions that often involve conflicting objectives. Although complex simulation models aid the decision maker by predicting the outcome of particular management practice or system of practices, the abundance of information provided complicates the ability of decision makers to analyze the information and come to a decision that satisfies more than one objective. A framework that facilitates the efficient transfer of technology to user groups is thus necessary, and gives the decision maker the ability to apply the technology easily and in a repeatable and scientifically defensible manner.

In recognition of this, in June 1997, the United States Environmental Protection Agency (USEPA), National Exposure Research Laboratory (NERL), Landscape Science Program and the United States Department of Agriculture (USDA), Agricultural Research Service (ARS) entered into an Interagency Agreement for the purpose of improving ecosystem risk assessment via characterization research, process modeling, and long-term monitoring studies.

At the outset of the project, a detailed evaluation of existing hydrological models was conducted to select suitable models for multi-scale watershed assessments. It was concluded that for multi-scale modeling, it was necessary to select two models that perform successfully at small and large space-time scales. For studies to be conducted at the basin scale, the Soil Water Assessment Tool (SWAT, Arnold et al., 1994) model was selected, and for studies at the watershed or subwatershed scale, the Kinematic Runoff and Erosion Model (KINEROS2, Smith et al., 1995) model was chosen. The extensive data requirements and the difficult task of building input parameter files have long represented an obstacle to the timely and cost-effective use of such complex models by resource managers. For this reason, an intuitive GIS-based interface was developed to take advantage of the now widely available digital elevation, land-use/cover and soils datasets for the automated development of model input parameters. This interface, the Automated Geospatial Watershed Assessment tool (AGWA), was released in August 2002 (Miller et al., 2002a).

OVERVIEW OF THE AGWA TOOL

This section describes the main components of the AGWA tool, including its strengths and limitations. AGWA is an extension for the ArcView versions 3.X (ESRI, 2001). The GIS framework is ideally suited for watershed-based analysis, which relies heavily on landscape information for both deriving model input and presenting model results. AGWA is distributed freely via the Internet as a modular, open-source suite of programs and associated documentation (www.tucson.ars.ag.gov/agwa).

AGWA provides the functionality to conduct all phases of a watershed assessment for two widely used watershed hydrologic models: the Soil Water Assessment Tool (SWAT) and a customized version of the KINEmatic Runoff and erOSion model (KINEROS2). SWAT is a continuous simulation model for use in large (river-basin scale) watersheds. KINEROS2 is an event-driven model designed for small arid, semi-arid, and urban watersheds. The AGWA tool contains these models in an intuitive interface for performing multi-scale change assessment, and provides the user with consistent, reproducible results. Data requirements include elevation, land-cover, soils, and precipitation data, all of which are typically available at no cost over the internet.

Model input parameters are derived directly from these data using optimized look-up tables that are provided with the tool.

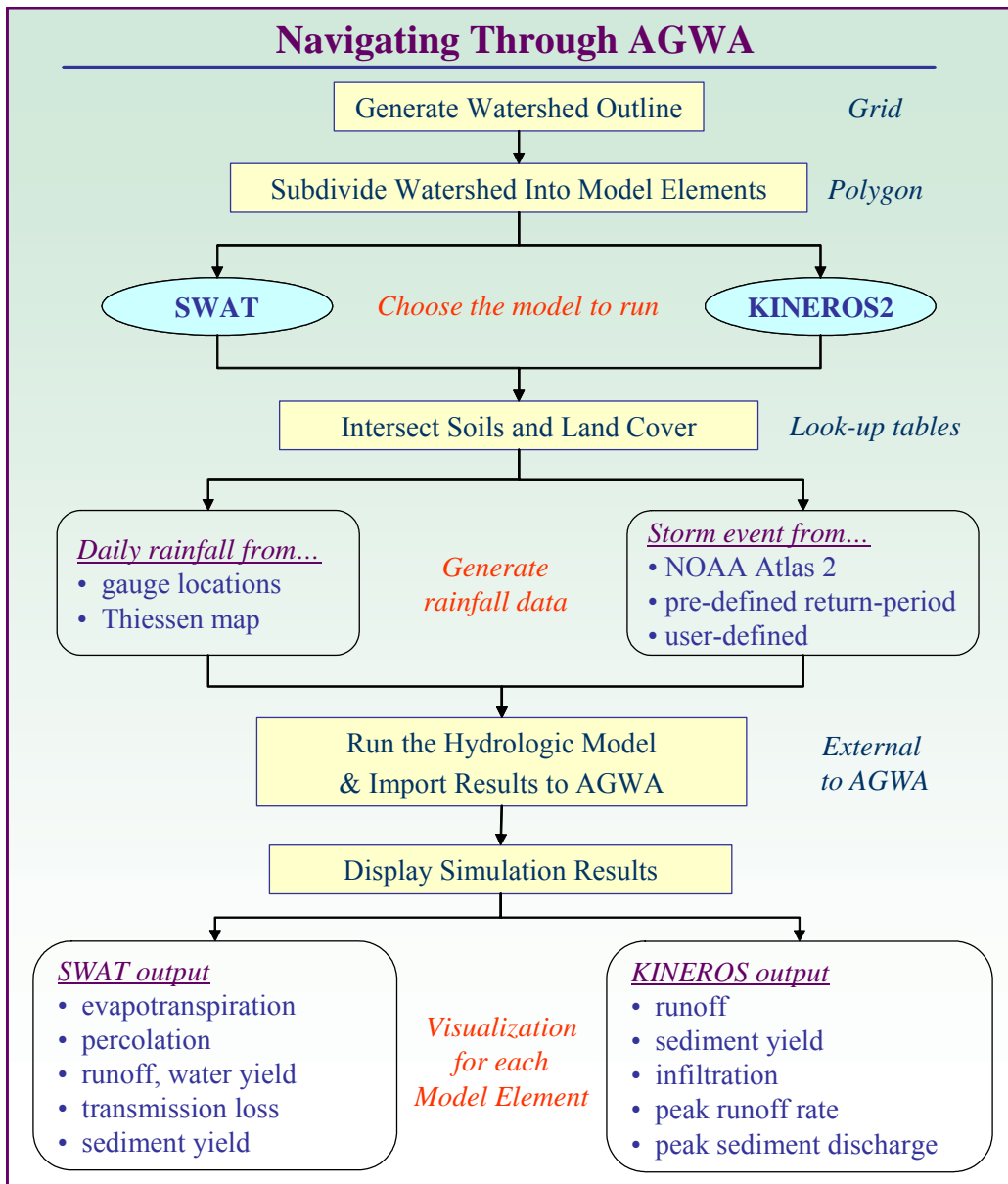


Fig. 9-1. Sequence of steps in the use of AGWA for hydrologic modeling.

The conceptual design of AGWA is presented in Fig. 9-1. A fundamental assumption of AGWA is that the user has previously compiled the necessary GIS data layers, all of which are easily obtained for the conterminous United States. The AGWA extension for ArcView adds the

'AGWA Tools' menu to the View window and must be run from an active view. Pre-processing of the DEM to ensure hydrologic connectivity within the study area is required, and tools are provided in AGWA to aid in this task. Once the user has compiled all relevant GIS data and initiated an AGWA session, the program is designed to lead the user in a stepwise fashion through the transformation of GIS data into simulation results. The AGWA Tools menu is designed to reflect the order of tasks necessary to conduct a watershed assessment, which is broken out into five major steps: (1) location identification and watershed delineation; (2) watershed subdivision; (3) land-cover and soils parameterization; (4) preparation of parameter and rainfall input files; and (5) model execution and visualization and comparison of results.

Step 1: The user first creates a watershed outline, which is a grid based on the designated outlet (pour point) of the study area. If a GIS coverage of the outlet location exists (such as would be the case for a runoff gauging station), it can be used to designate the drainage outlet. Alternatively, the user has the option of using a mouse to click on the watershed outlet. If internal gauging stations exist as a separate GIS coverage, AGWA will use them as internal drainage pour points and generate output at each of the stations. This option is particularly useful for calibration and validation of model results.

Step 2: A polygon shapefile is built from the watershed outline grid created in Step 1. The user specifies the threshold of contributing area for the establishment of stream channels, and the watershed is divided into model elements required by the model of choice. From this point onward, tasks are specific to the model that will be used (KINEROS2 or SWAT), but the same general process is followed independent of model choice.

Step 3: The watershed created in Step 2 is intersected with soil and land-cover data, and parameters necessary for the hydrologic model runs are determined through a series of GIS analyses and look-up tables. The hydrologic parameters are added to the polygon and stream channel tables to facilitate the generation of input parameter files. At this point, the user can manually alter parameters for each model element if additional information is available to guide the estimation of those values.

Step 4: Rainfall input files are built at this stage. For SWAT, the user must provide daily rainfall values for rainfall gauges within and near the watershed. If multiple gauges are present, AGWA will build a Thiessen polygon map and create an area-weighted rainfall file. For KINEROS2, the user can select from a series of pre-defined rainfall events dependent on the geographic location, choose to build his/her own rainfall file through an AGWA module, or use NOAA Atlas II return period rainfall depth grids distributed with AGWA (NOAA, 1973). Precipitation files may be created for uniform (single-gauge) or distributed (multiple-gauge) rainfall data.

Step 5: After Step 4, all necessary input data have been prepared: the watershed has been subdivided into model elements; hydrologic parameters have been determined for each element; and rainfall files have been created. The user can proceed to run the hydrologic model of choice. AGWA will automatically import the model results and add them to the polygon and stream map tables for display. A separate module controls the visualization of model results. The user can

toggle among viewing various model outputs for both upland and channel elements, enabling the problem areas to be identified visually. If multiple land-cover scenes exist, the user can parameterize either or both of the two models and attach the results to a given watershed. Results can then be compared on either an absolute or percent change basis for each model element. Model results can also be overlaid with other digital data layers to further prioritize management activities.

Hydrologic Models

Key components of AGWA are the hydrological models used to evaluate the effects of land cover and land use on watershed response. In this section, a description of the basic structure of each model is provided as well as the model's simplifying assumptions, strengths, and weaknesses. Additionally, guidelines are provided for correctly applying the hydrological models to capture the spatial heterogeneities of the watershed to represent the dominant processes at different scales. The KINEROS2 and SWAT models are able to process complex watershed representations in order to explicitly account for spatial variability of soils, rainfall distribution patterns, and vegetation.

KINEROS2

KINEROS2 is an event-oriented, physically based model describing the processes of interception, infiltration, surface runoff, and erosion from small agricultural and urban watersheds (Smith et al., 1995). In this model, watersheds are represented by subdividing contributing areas into a cascade of one-dimensional overland flow and channel elements using topographic information. The infiltration component is based on the simplification of the Richard's equation posed by (Smith and Parlange, 1978).

$$f_c = K_s \frac{e^{F/B}}{\left(e^{F/B} - 1 \right)} \quad [1]$$

$$B = G \cdot \varepsilon \cdot (S_{\max} - SI) \quad [2]$$

where f_c is the infiltration capacity (L/T), K_s is the saturated hydraulic conductivity (L/T), F is the infiltrated water (L), B is the saturation deficit (L), G is the effective net capillary drive (L), ε is the porosity, S_{\max} is the maximum relative fillable porosity, and SI is the initial relative soil saturation. Runoff generated by infiltration excess is routed interactively using the kinematic wave equations for the overland flow and channel flow, respectively stated as:

$$\frac{\partial h}{\partial t} + \frac{\partial \alpha \cdot h^m}{\partial x} = r_i(t) - f_i(x, t) \quad [3]$$

$$\frac{\partial A}{\partial t} + \frac{\partial Q(A)}{\partial x} = q_l(t) - f_{c_i}(x, t) \quad [4]$$

where h is the mean overland flow depth (L), t is the time (T), x is the distance along the slope (L), α is the $1.49 S^{1/2}/n$, S is the slope, n is the Manning's roughness coefficient, m is $5/3$, $r_i(t)$ is the rainfall rate (L/T), $f_c(x, t)$ is the overland infiltration rate (L/T), A is the channel cross-sectional area of flow (L^2), $Q(A)$ is the channel discharge as a function of area (L^3/T), $q_l(t)$ is the net lateral inflow per unit length of channel (L^2/T), and $f_{c_i}(x, t)$ is the net channel infiltration per unit length of channel (L^2/T). These equations, and those for erosion and sediment transport, are solved using a four-point implicit finite difference method (Smith et al., 1995). Unlike excess routing, interactive routing implies that infiltration and runoff are computed at each finite difference node using rainfall, upstream inflow, and the current degree of soil saturation. This feature is particularly important for accurate treatment of transmission losses with flow down dry channels. To explicitly account for space-time variations in rainfall patterns the model computes, for each overland flow element, the rainfall intensities at the element centroid are computed as a linear combination of intensities at the three nearest gauges forming a piece-wise planar approximation of the rainfall field over the watershed (Goodrich, 1991). The interpolated intensity at the centroid is applied uniformly over the individual model element.

Application of KINEROS2

In numerous modeling studies, KINEROS2 has been applied to the Walnut Gulch Experimental Watershed administrated by the USDA, Agricultural Research Service (Renard et al., 1993). This is a semi-arid watershed, with 11 nested subwatersheds that range in area from 2.3 to 148 km^2 , and an additional 13 small watershed areas ranging from 0.004 to 0.89 km^2 . Spatial variability in rainfall is assessed using a network of 85 gauges. At a small scale, Goodrich et al. (1995) and Faures et al. (1995) applied KINEROS2 to the 4.4-ha Lucky Hills LH-104 subwatershed to examine the importance of different antecedent soil moisture estimates and the effects of wind and rainfall pattern on the predicted discharges. At this scale, both studies conclude that an adequate representation of the rainfall pattern is crucial to achieve accurate runoff prediction in this environment. Goodrich et al. (1994) also looked at the sensitivity of runoff production to pattern of initial water content at the larger scale of the WG-11 subwatershed (6.31 km^2). They suggested that a simple basin average of initial moisture content will normally prove adequate and that, again, knowledge of the rainfall patterns is far more important. Michaud and Sorooshian (1994) compared three different models at the scale of the whole watershed: a lumped curve number model, a simple distributed curve number model, and the more complex distributed KINEROS2 model. The modeled events were 24 severe thunderstorms with a raingauge density of one per 20 km^2 . Their results suggested that none of the models could adequately predict peak discharge and runoff volumes, but that the distributed models did somewhat better in predicting time to runoff initiation and time to peak. The lumped model was, in this case, the least successful.

According to Syed (1999), modeling a medium-size watershed ($\sim 150 \text{ km}^2$) using the kinematic wave approximation, along with a coarse resolution DEM of the order of 80 m with vertical accuracy of tens of meter, is acceptable. For watersheds of this size, this implies that USGS level I, 30-m DEM data available throughout the continental United States is adequate. For smaller watersheds of the order of several hectares, better vertical accuracy is desired especially when using high horizontal resolution (small grid spacing) DEMs.

Watershed showing the watershed boundary and primary channel network (the pond catchment is a noncontributing area).

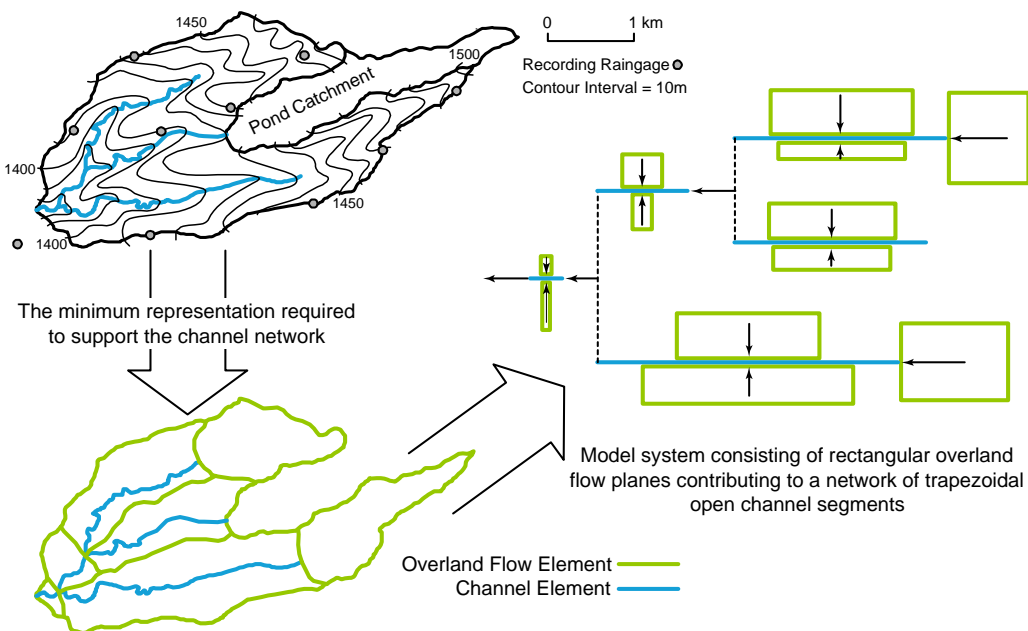


Fig. 9-2. Delineation of overland flow and channel elements in AGWA for KINEROS2 hydrologic modeling.

Limitations of the kinematic wave approximation

There is one important limitation of using the kinematic approximation to the fully dynamic flow equation; the kinematic wave equation assumes a free-overfall downstream boundary condition. Essentially the effects of any disturbance to the flow will generate a kinematic wave, but the equation can only predict the downstream movement of these waves. Thus, a kinematic wave description cannot predict the backwater effects of an obstruction to the flow for a surface flow (Beven, 2000).

Basin representation with kinematic wave elements

The contribution to the flood hydrograph from pervious and impervious areas within a single watershed is modeled in the kinematic wave method by using different types of elements as shown in Fig. 9-2. The kinematic wave elements shown are overland flow planes and a main channel. In general, watershed runoff is modeled with kinematic wave elements by taking an idealized view of the basin. Rather than trying to represent every overland flow contributing area and every possible channel, watersheds are depicted with overland flow planes and channels that represent the average conditions of the basin. Various levels of complexity can be obtained by combining different elements to represent a watershed. The simplest combination of elements that could be used to represent a watershed is two overland flow planes and a main channel. The overland flow

planes can be used to separately model the overland flow from pervious and impervious surfaces to the main channel. Flow from the overland flow planes is input to the main channel as a uniform lateral inflow. The complexity of a watershed can be modeled by combining various levels of channel elements.

The procedure for representing a watershed using overland flow and channel elements is shown in Fig. 9-2. Using topographic maps and other geographic information, a watershed is configured into an interconnected system of stream network components. The watershed is subdivided into a number of subwatersheds in order to configure the stream network. In performing the subdivision, the following are taken into account: (1) the study purpose and (2) the spatial variability of precipitation and runoff response characteristics. The purpose of the study serves to pinpoint the areas of interest and, therefore, the location of watershed boundaries. The spatial variability aids in the selection of the number of subwatersheds. Each subwatershed is intended to represent an area of the basin that, on the average, has the same hydraulic and hydrologic properties. Usually, the assumption of uniform precipitation and infiltration over a subwatershed becomes less accurate as the subwatershed size increases.

SWAT

SWAT is a river-basin, or watershed, scale model developed to predict the impact of land management practices on water, sediment, and agricultural chemical yields on large, complex watersheds with varying soils, land-use, and management conditions over long periods of time (Arnold et al., 1994). The model combines empirical and physically based equations, uses readily available inputs, and enables users to study long-term impacts.

The hydrology model is based on the water balance equation

$$SW_t = SW + \sum_{i=1}^t (R_i - Q_i - ET_i - P_i - QR_i) \quad [5]$$

where SW is the soil water content minus the 15-bar water content, t is the time in days, and R , Q , ET , P , and QR are the daily amounts of precipitation, runoff, evapotranspiration, percolation, and return flow, respectively; all the units are in mm. Since the model maintains a continuous water balance, complex basins are subdivided to reflect differences in ET for various crops, soils, etc. Thus, runoff is predicted separately for each sub-area and routed to obtain the total runoff for the basin. This increases accuracy and gives a better physical description of the water balance.

Surface runoff is estimated with a modification of the SCS curve number method (USDA, 1986).

$$Q = \frac{(R - 0.2S)^2}{R + 0.8S} \quad R > 0.2S \quad [6]$$

$$Q = 0 \quad R \leq 0.2S$$

where Q is the daily surface runoff (mm), R is the daily rainfall (mm), and S is the retention parameter. The retention parameter, S , varies (1) among watersheds because of changes in soils,

land-use, and slope and (2) with time because of changes in soil water content. The parameter S is related to curve number (CN) by the SCS equation (USDA, 1986).

$$S = 254 \left(\frac{100}{CN} - 1 \right) \quad [7]$$

The constant 254 in Eq. [7] gives S in mm. The curve number varies non-linearly from 1, dry condition at wilting point, to the wet condition at field capacity and approaches 100 at saturation.

Application of the SWAT model

SWAT is currently being utilized in several large basin projects. SWAT provides the modeling capabilities of the HUMUS (Hydrologic Unit Model of the United States) project (Srinivasan et al., 1993). The HUMUS project simulates the hydrologic budget and sediment movement for the approximately 2100 hydrologic unit areas that have been delineated by the USGS. Findings of the project are being utilized in the Resource Conservation Act (RCA) appraisal conducted by the NRCS. Scenarios include projected agricultural and municipal water use, tillage and cropping system trends, and fertilizer and animal waste use management options. The model is also being used by NOAA to estimate nonpoint source loadings into all U.S. coastal areas as part of the National Coastal Pollutant Discharge Inventory. The USEPA has incorporated SWAT into the Better Assessment Science Interacting Point and Nonpoint Sources (BASINS) interface for assessment of impaired water bodies.

Limitations of the Curve Number method

The curve number approach to predicting runoff generation has been the subject of a number of critical reviews (e.g., Hjelmfelt et al., 1982; Bales and Betson, 1982). Further work is required to clarify under what conditions the method gives satisfactory predictions. Mishra and Singh (1999) show that their generalized version of the method gives better results than the original formulation, as it should, since it has two additional fitting parameters. Hjelmfelt et al. (1982) suggest that the curve number, rather than being considered as a characteristic for a given soil-land-cover association, might better be considered as a stochastic variable. Their analysis of the annual maximum storms for two small catchments in Iowa suggested that the storage capacity parameter, S_{max} , derived for individual storms was approximately log normally distributed with a coefficient of variation on the order of 20%. The 10 and 90% quartiles of the distributions corresponded well to the modified curve numbers for dry and wet antecedent conditions, following the standard SCS procedure based on the preceding five-day rainfall. However, they found no strong correlation between curve number and antecedent condition for the individual storms, suggesting that interactions with individual storm characteristics, tillage, plant growth, and temperature were sufficient to mask the effect of antecedent rainfall alone.

Despite its limitations, the Curve Number method has been used quite widely since the tabulated curve number values provide a relatively easy way of moving from a GIS data set on soils and vegetation to a rainfall-runoff model.

Watershed showing the watershed boundary and primary channel network (the pond catchment is a noncontributing area).

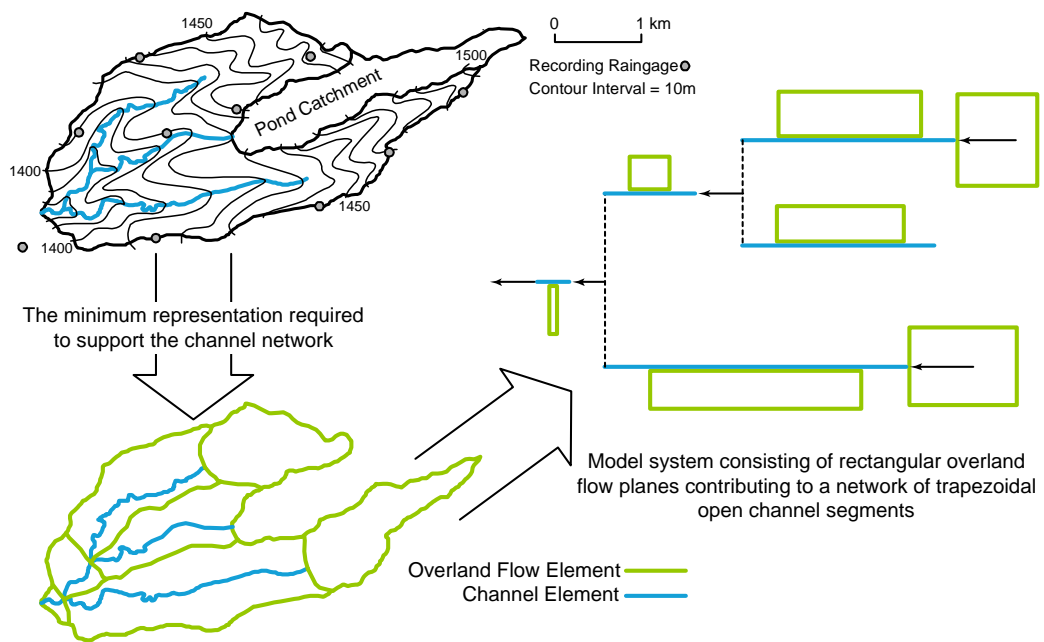


Fig. 9-3. Delineation of planes and channels in AGWA for SWAT hydrologic modeling.

Basin representation with SWAT

For modeling purposes, a watershed may be partitioned into a number of subwatersheds or subbasins. The use of subbasins in a simulation is particularly beneficial when different areas of the watershed are dominated by land uses or soils characteristically different enough to impact hydrology. By partitioning the watershed into subwatersheds, the user is able to relate different areas of the watershed to one another spatially. The number of subwatersheds chosen depends on the size of the watershed, the spatial detail of available input data, and the amount of detail required to meet the goals of the project. Figure 9-3 illustrates a watershed delineation for Subwatershed 11 of the Walnut Gulch Experimental Watershed for SWAT. The flow routing structure is delineated by linking the channels with the surrounding uplands to define the individual subwatershed and channel elements. AGWA does not split the subwatershed elements into more than one unit for SWAT (e.g., there are no separate left and right hand contributing elements to the channel element as in KINEROS2, Fig. 9-2).

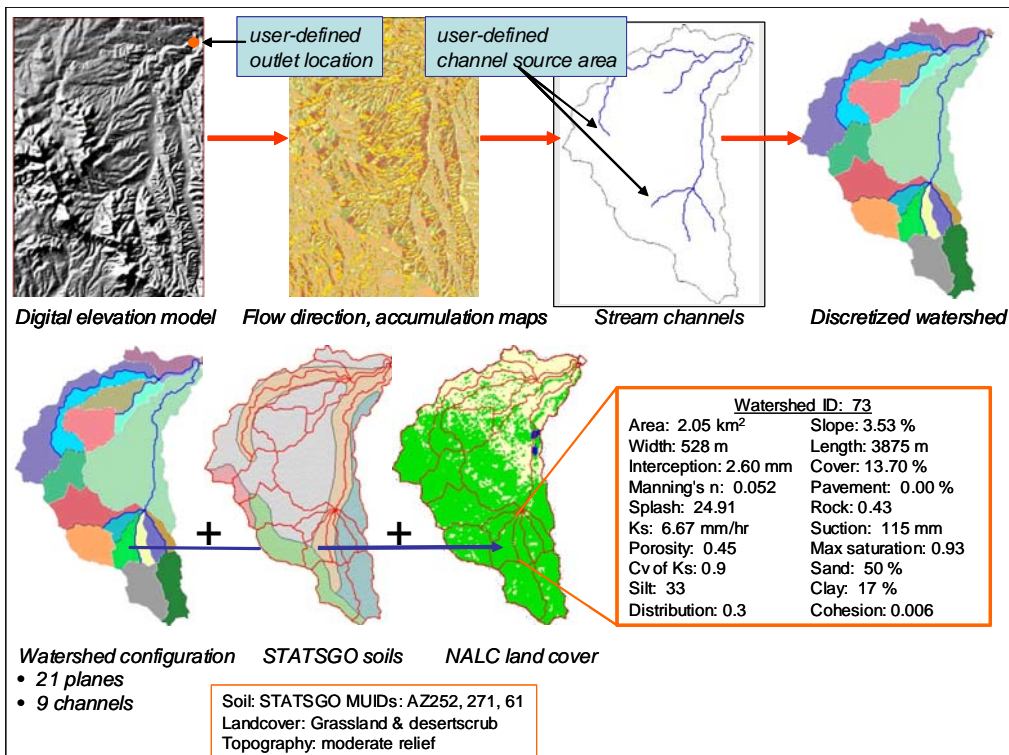


Fig. 9-4. The transformation of topography, soils, and land-cover GIS data into KINEROS2 input parameters. A DEM is used to subdivide the watershed into upland and channel model elements, each of which are parameterized according to their soil, topographic, and land-cover characteristics.

Data Inputs and Parameter Estimation

Watershed Discretization

The most widely used method, and that which is used in AGWA, for the extraction of stream networks is to compute the accumulated area upslope of each pixel through a network of cell-to-cell drainage paths. This flow accumulation grid is subsequently pruned by eliminating all cells for which the accumulated flow area is less than a user-defined threshold drainage area, called the Channel, or Contributing Source Area (CSA). The watershed is then further subdivided into upland and channel elements as a function of the stream network density. In this way, a user-defined CSA is used to define the locations and numbers of stream channels; since the watershed is subdivided into upland and channel elements as a function of the stream channels, the choice of CSA is the determining factor in the spatial complexity of the watershed discretization. This approach often creates a large number of spurious polygons and disconnected model elements due to inaccuracies in the underlying DEM. A suite of algorithms has been implemented in AGWA that refines the watershed elements by eliminating spurious elements and ensuring downstream connectivity.

Parameter Estimation

Each of the overland and channel elements delineated by AGWA is represented in either SWAT or KINEROS2 by a set of parameter values. These values are assumed to be uniform within a given element. There may be a large degree of spatial variability in the topographic, soil, and land-cover characteristics within the watershed, and AGWA uses an area-weighting scheme to determine an average value for each parameter within an overland flow model element abstracted to an overland flow plane (Goodrich et al., 2002). As shown in Fig. 9-4, the three GIS coverages are intersected with the subdivided watershed, and a series of look-up tables and spatial analyses are used to estimate parameter values for the unique combinations of land-cover and soils. SWAT and KINEROS2 require a host of parameter values, and estimating their values can be a tedious task; AGWA rapidly provides estimates based on an extensive literature review and calibration efforts. In the absence of observed data and performing a calibration exercise, these values should be used in comparative or relative assessments. Since AGWA is an open-source suite of programs, users can modify the values of the look-up tables or manually alter the parameters associated with each element.

Soil parameters for upland planes as required by KINEROS2 (such as percent rock, suction head, porosity, saturated hydraulic conductivity) are initially estimated from soil texture according to the State Soil Geographic (STATSGO) soil data following Woolhiser et al. (1990) and Rawls et al. (1982). Saturated hydraulic conductivity is reduced following Bouwer (1966) to account for air entrapment. Further adjustments are made following Stone et al. (1992) as a function of estimated canopy cover. Cover parameters, including interception, canopy cover, Manning's roughness, and percent paved area are estimated following expert opinion and previously published look-up tables (Woolhiser et al., 1990). Upland element slope is estimated as the average plane slope, while geometric characteristics such as plane width and length are a function of the plane shape assuming a rectangular shape, where the longest flow length is equal to element length. Stream channel geometric characteristics are parameterized following Miller et al. (1996), who found strong relationships between channel width and depth and watershed characteristics. Channel parameters relating to soil characteristics assume a sandy bed and all channels are assumed uniform. Channel slope is determined from a slope grid derived from the DEM.

Similar approaches are used to provide estimates for soil and land-cover parameters as required by SWAT. The most sensitive parameter of SWAT is the Curve Number, which is estimated as a function of hydrologic soil group, hydrologic condition, cover type, and antecedent moisture condition. STATSGO data provide information on soil hydrologic group, while cover type is determined from classified land-cover data. AGWA assumes a fair hydrologic condition, and antecedent moisture group II. Look-up tables following USDA-SCS (1986) recommendations are used to estimate Curve Number values for each unique combination of hydrologic group and land-cover type within a watershed element. Because the land-cover data are grids, this process occurs for each cell, and the results are area-weighted to produce a unique estimate of Curve Number for the overland flow plane.

Rainfall Input

A variety of methods are available in AGWA to create rainfall input files for KINEROS2 and SWAT. Each of these is described briefly in this section and organized according to the models for which they are designed.

KINEROS2: Either distributed or uniform precipitation input can be used with KINEROS2 and is provided in the form of storm hyetographs for one or more point locations. Data from multiple point locations are distributed across the watershed by KINEROS2 using a piecewise planar time-space interpolation technique (Goodrich, 1991). Since the spatial component of this process is computed by the model itself, it was deemed unnecessary to prepare distributed input files in AGWA. KINEROS2 rainfall input files created outside of AGWA (either uniform or distributed) can be used in AGWA without causing any problems. Methodologies for utilizing radar data to build distributed event rainfall files in AGWA are currently being investigated.

Uniform rainfall input files can be created in AGWA using one of two data sources provided with the tool or using data entered by the user. Uniform rainfall, although less appropriate for quantitative modeling of individual events, is particularly useful for relative assessment of land-cover change. Precipitation data that can be used to generate design storms in AGWA include the NOAA Atlas 2 Precipitation-Frequency Atlas of the Western United States (NOAA, 1973) and a database of return period storms from various locations. Both of these sources are provided with AGWA and are currently limited to 11 western states. Return period rainfall depths are converted to hyetographs using the USDA-SCS (1973) methodology and a type II distribution. The type II distribution is appropriate for deriving the time distribution of rainfall for most of the country, including all of the interior West. Although the NOAA Atlas 2 data can be used anywhere in the western U.S., the database can be easily edited to add data for areas where it is not provided and has the added advantage of the option to incorporate an area-reduction factor. The third option of using data entered by the user allows design storm data from any region to be used. User-defined storms are entered in the form of a hyetograph, thus providing additional flexibility in defining the time-distribution of rainfall.

SWAT: AGWA can generate either uniform or distributed rainfall input files for SWAT. The option to create distributed rainfall files uses Thiessen precipitation weighting to compute the weighted rainfall depth falling on each subwatershed for each day in the simulation period. The user is automatically routed to the dialog for creating either the uniform or distributed rainfall input based on the number of raingauges with data in a raingauge point theme that is designated by the user. If there are two or fewer gauges, Thiessen polygons cannot be generated, and a uniform rainfall input file will be created (using the gauge closest to the watershed centroid if there are two). When there are more than two gauges, a distributed input file will be written.

Although any gauge data can be used, National Weather Service gauge data are the most widely available. A point theme of raingauge locations and an unweighted daily precipitation database file are necessary to generate the input file. Missing data can be accommodated through a weighting scheme that dynamically adjusts the gauge weights according to those gauges that do have data for that day.

EXAMPLES OF AGWA APPLICATIONS

As indicated earlier, the hydrologic models in the AGWA tool have been applied on various watersheds across the United States. Sizes of these watersheds are in the range of 0.012 – 7000 square kilometers. In this section, however, we focus on two examples from the San Pedro River Basin, which traverses the U.S.-Mexico border between Arizona and Sonora. The first one involved integrating landscape assessment and hydrologic modeling for land-cover change

analysis. In this case, the AGWA tool was employed to evaluate the effects of historic land-cover change on watershed response by applying the SWAT model on the Upper San Pedro Basin to the Charleston USGS stream flow gauge and the KINEROS2 model on a small contributing subwatershed in the San Pedro River Basin. Miller et al. (2002b) demonstrated the utility of AGWA to conduct a landscape assessment analysis of the spatial distribution of land-cover changes using classified satellite imagery. Simulated watershed response in the form of runoff volume, peak runoff rate, and total sediment yield were used as indicators of watershed condition. The second example presents a scenario-based approach to regional land-use planning. This approach is particularly useful for shaping future use of land and water resources and has been used in a wide variety of geographic settings to assist stakeholders and policy makers in environmental decision-making (Schwartz 1996; Steinitz 1990). Kepner et al. (2004) demonstrated the utility of AGWA for this purpose by evaluating the spatial distribution of impacts to the hydrologic regime resulting from different land-use/cover scenarios for the Upper San Pedro River basin.

Description of the Study Area and Data Sources

The San Pedro River flows north from Sonora, Mexico, into southeastern Arizona (Fig 9- 5). With a wide variety of topographic, hydrologic, cultural, and political characteristics, the basin is a prime example of desert biodiversity in the semi-arid Southwest and an exceptional study area for addressing a range of scientific and management issues. It is also a region in socioeconomic transition, as the previously dominant rural ranching economy is shifting to irrigated agriculture and urban development (Tellman et al., 1997; CEC, 1998).

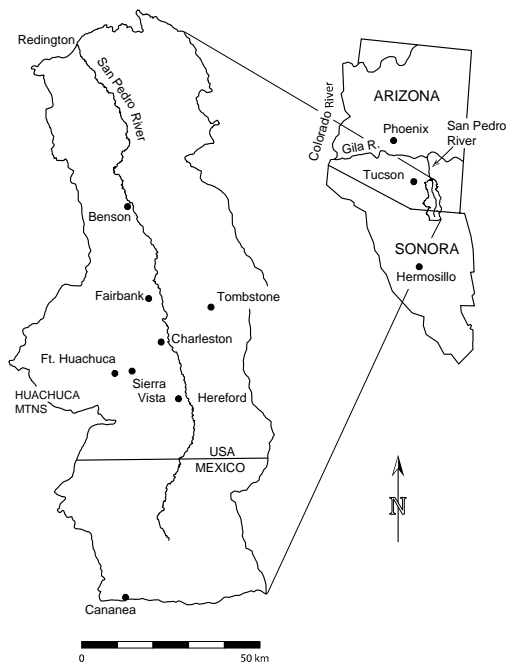


Fig. 9-5. Location of study area.

The area is a transition zone between the Chihuahuan and Sonoran deserts and has a highly variable climate with significant biodiversity. The tested watershed is approximately 7598 km² and is dominated by desert shrub-steppe, riparian, grasslands, agriculture, oak and mesquite woodlands, and at higher elevations, pine forest (Kepner et al., 2000). The basin supports among the highest number of mammal species in the world and the riparian corridor provides nesting and migration habitat for more than 400 bird species. The San Pedro River is the only unimpounded river in Arizona, and all municipal and most agricultural water is derived from groundwater sources.

For the purpose of modeling runoff from the Upper San Pedro Basin, a number of geospatial data sets were compiled that describe the landscape characteristics of the basin and are required by AGWA for modeling with KINEROS2 and SWAT. The basic input data were a USGS 30-m digital elevation model, STATSGO soil, and North American Landscape Characterization (NALC) classified satellite imagery for land-cover (Fig. 9-6a).

Standard USGS DEM data were mosaicked together, and the results were filtered using a low-pass filter to remove topographic anomalies and then filled to create a "hydrologically correct" surface, where all locations within the study area were connected to the outlet and a minimum of sinks were present. Some larger sinks within the Basin are real features, and these were retained (Fig. 9-6b).

It is recognized that STATSGO soils are overly generalized for small-scale application of rainfall-runoff modeling (Fig. 9-6c). Unfortunately, more detailed geospatial soil data are not available for the research.

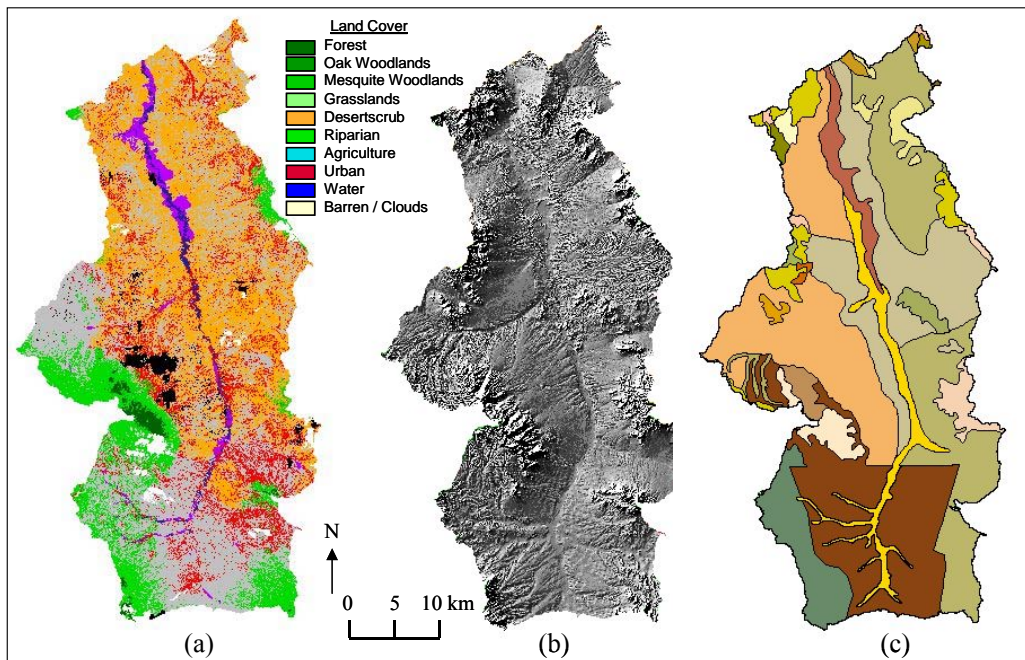


Fig. 9-6. GIS data sets for the Upper San Pedro Basin. (a) Land cover from the 1992 NALC classification, (b) topography relief map based on USGS 30m DEM data, and (c) soils data from the USDA-NRCS STATSGO.

Remote imagery was derived from the Landsat Multi-spectral Scanner (MSS) and Landsat Thematic Mapper (TM) earth observing satellites (path/row 35/38 and 35/39) (Kepner et al., 2000). Landsat-MSS satellite scenes were selected from the North American Landscape Characterization (NALC) project (USEPA, 1993). The scenes available in the NALC database (1973-92) and Landsat TM (1997) are from four pre-monsoon dates for a period approximately 25 yr (i.e., 5 June 1973, 10 June 1986, 2 June 1992, and 8 June 1997). All imagery in the database is coregistered and georeferenced to a 60 x 60 m Universal Transverse Mercator (UTM) ground coordinate grid with a nominal geometric precision of 1-1.5 pixels (60-90 m). Digital land-cover maps were developed separately for each year using 10 classes: Forest, Oak Woodland, Mesquite Woodland, Grassland, Desertscrub, Riparian, Agriculture, Urban, Water, and Barren (Fig. 9-6a) (Kepner et al., 2000).

Using AGWA for Land-Cover Change Analysis

Introduction

Hydrologic response is an integrated indicator of watershed condition, and changes in land cover may affect the overall health and function of a watershed. Such changes vary spatially and occur at different rates through time. Miller et al. (2002b) evaluated the hydrologic change both spatially, using distributed hydrologic models, and temporally, using satellite imagery acquired over 25 years. The main objective of this study was to evaluate the effects of historic land-cover change on watershed response by applying the SWAT model on the San Pedro River Basin at the Charleston USGS stream flow gauge, and the KINEROS2 model on a small contributing watershed in the San Pedro Basin. Simulated watershed response in the form of runoff volume, peak runoff rate, and total sediment yield were used as indicators of watershed condition.

Methods

The general approach used in this study was to acquire geospatial information relating to land cover, topography, and soils for the two study areas; assess the overall land-cover trends of the past quarter-century; and analyze the consequent impacts on simulated runoff.

Input parameters required by SWAT and KINEROS2 were estimated by AGWA as a function of the topographic, soil, and cover characteristics of the individual watershed response units. Look-up tables relating soil and land-cover associations to relevant hydrologic parameters (e.g., curve number, saturated hydraulic conductivity, surface roughness) were defined through literature review and calibration exercises. Hernandez et al. (2000) describe the derivation of input parameters for KINEROS2 and SWAT used in this approach.

Since KINEROS2 is an event-based model, a series of synthetic hyetographs were used as input to the model. Previously published work using long-term rainfall measurements on the Walnut Gulch Experimental Watershed were used to estimate return-period design storms as a function of watershed scale. Osborn et al. (1980) provided estimates of the 5-, 10-, and 100-yr events for both 30- and 60-min durations. These six design events provide estimates of rainfall intensity throughout the event. These estimates were determined for small watersheds, so an

adjustment was made for watershed size. It has been well demonstrated that return period-duration rainfall depths decrease as a function of watershed scale (Osborn et al., 1985).

Runoff-producing rainfall in the San Pedro Basin is dominated by summer convective thunderstorms that are locally intense and highly constrained in space. Winter rains are generally frontal and widespread with lower intensities. Runoff is produced through infiltration-excess overland flow, and winter rainfall intensities are often too low to overcome the high infiltration rates of soils within the basin. Thus, on small watersheds, the larger design storms will be driven by localized convection storms. Since these storms are localized, an adjustment factor has to be used to prevent a gross over-estimation of rainfall and the associated runoff. All six design storms were input to each of the subdivided watersheds to assess the impact of rainfall on simulation results.

In this study, the variability in rainfall through time serves as a confounding variable in the interpretation of the impacts of cover transition on hydrologic response, so it was necessary to apply the same rainfall data to each parameter set associated with different land-cover scenes. Since rainfall is held constant for each model run, changes in model results are due solely to changes in input parameters affected by land-cover change.

The SWAT model uses daily rainfall input data for multi-year simulation. Multi-year rainfall was extracted from long-term National Weather Service records and input to the SWAT model. These rainfall records represent periods in which a minimum of data were missing from the long-term records. For this effort, nine gauges that record rainfall in the San Pedro Basin contain long-term historical data for input to SWAT. A 14-yr period of record was extracted for this area.

Results

As illustrated in Fig. 9-7, significant land-cover change occurred within the San Pedro Basin between 1973 and 1997. A matrix illustrating the relative change within each cover class for the different scenes (1973 and 1997) is presented as Table 9-1.

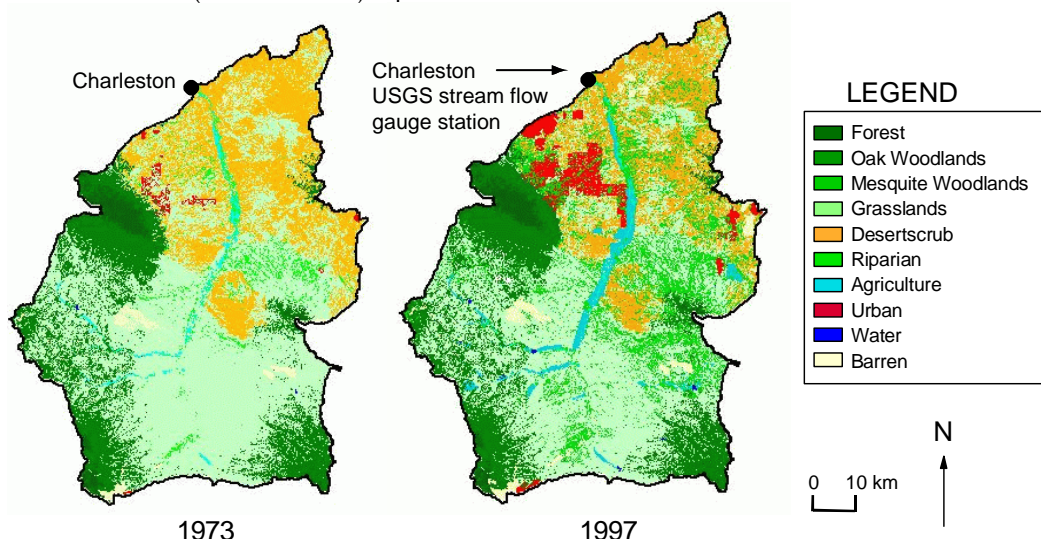


Fig. 9-7. Land-cover change within the Upper San Pedro Basin for the area drained at the Charleston USGS stream flow gauge.

Table 9-1. Percent relative land-cover change for the Upper San Pedro Watershed. A positive value in a difference column indicates an increase in area between dates (Miller et al., 2002b).

Land Cover	1973 to 1986	1986 to 1992	1992 to 1997	1973 to 1997
Forest	-0.12	-5.27	0.37	-5.04
Oak Woodland	-0.16	-4.89	1.55	-3.57
Mesquite	413.75	-1.66	-3.41	387.98
Grassland	-14.55	-0.78	-0.68	-15.80
Desertscrub	-17.83	-3.29	-2.35	-22.40
Riparian	2.16	0.42	3.70	6.38
Agriculture	31.13	29.13	-2.21	65.58
Urban	212.07	25.71	31.18	414.63
Water	11.36	14.63	23.15	57.20
Barren	62.77	-0.10	-0.34	62.05

The most significant changes were large increases in urbanized areas, mesquite woodlands, and agricultural communities and commensurate decreases in grasslands and desertscrub. This overall shift indicates an increasing reliance on ground water (due to increased municipal water consumption and agriculture) and potential for localized large-scale runoff and erosion events (due to the decreased infiltration capacities and roughness associated with the land-cover transition). The Sierra Vista subwatershed experienced significant land-cover change between 1973 and 1997, with the dominant transitions within this watershed being the declines in grasslands and desertscrub and increases in urban areas and mesquite woodlands (Table 9-2).

Table 9-2. Percent relative land-cover change for the Sierra Vista Subwatershed. A positive value in a difference column indicates an increase in area between dates (Miller et al., 2002b).

Land-cover	1973 to 1986	1986 to 1992	1992 to 1997	1973 to 1997
Forest	0	0	0	0
Oak Woodland	-0.48	-1.17	-1.47	-3.09
Mesquite	306.25	-5.98	-12.67	233.57
Grassland	-34.65	0	-9.01	-40.54
Desertscrub	-36.67	-5.38	-7.09	-44.32
Urban	302.78	19.62	36.34	556.89

Runoff was simulated with the SWAT model from the San Pedro Basin using a 14-yr continuous rainfall period with input data corresponding to the four classified satellite scenes. In general, the total annual runoff volume increased as a function of land-cover change within the basin (Fig. 9-8). The graph shows the deviation in total annual runoff results from the 1973 land-cover results. These results do not necessarily reflect observed changes in runoff volume for the time periods simulated in this study but are illustrative of the effects on hydrologic response of the transition the basin has undergone over the past quarter-century. Given that the 1973 scene serves as the base image from which landscape change is derived, annual runoff results are presented in Fig. 9-8 as the percent change from the 1973 runoff results.

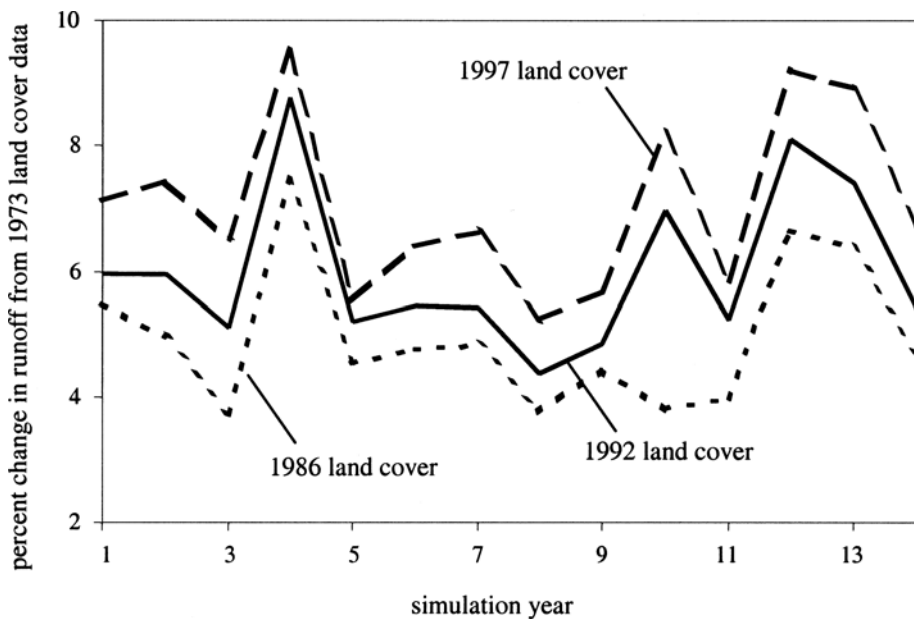


Fig. 9-8. SWAT simulation results for the Upper San Pedro Basin (Miller et al., 2002b).

Simulated runoff results show an increase in annual runoff over time commensurate with increasing urbanization and woody plant invasion. Considerable spatial variability in the observed land-cover change has implications for hydrologic modeling and assessment (Fig. 9-7, and Table 9-1).

Simulated annual runoff from the Sierra Vista subwatershed increased significantly, so the KINEROS2 model was used to investigate this area in more detail. In this approach, KINEROS2 is used to focus both temporally and spatially. SWAT is used to locate subwatersheds that are responding strongly to change over long time periods, while KINEROS2 provides more detail and analysis for return period rainfall events.

For this smaller subwatershed within the San Pedro Basin, KINEROS2 was used to simulate runoff and sediment yield for six design storms using watershed data from the classified satellite imagery, resulting in a suite of 24 simulation runs. Results for the simulation runs are given in Table 9-3, and Fig. 9-9 shows hydrographs from the two endpoint design storms, the 5-yr, 30-min event and the 100-yr, 60-min event. Note the disparity in the hydrographs resulting from the smaller event and their similarities for the larger event. The differences in simulated results decrease with increasing storm size and duration. This trend toward convergence is due to the increasing importance of storm characteristics over watershed characteristics as storm size increases. For smaller storms, changes in the watershed, especially those due to land-cover change, may radically alter the hydrologic response. However, the hydrologic response for very large storms is driven by the characteristics of the rainfall, and management may have little improvement effect. As would be expected with design storms, runoff volume and peak runoff rates increased directly with the size of the modeled events. Since erosion and sediment yield are

Table 9-3. Runoff simulation results using design rainfall events and KINEROS2 for the Sierra Vista Subwatershed (Miller et al., 2002b).

Rainfall Event	Rainfall (mm)	Runoff (mm)				Percent Change 1973 to 1997
		1973	1986	1992	1997	
5 yr, 30min	17.35	0.057	0.144	0.134	0.158	177.2
5 yr, 60min	21.08	0.185	0.339	0.367	0.498	169.2
10 yr, 30 min	22.74	1.25	1.64	1.72	1.95	56.0
10 yr, 60 min	26.44	2.07	2.47	2.55	2.79	34.8
100 yr, 30 min	31.79	7.02	7.55	7.65	7.95	13.2
100 yr, 60 min	38.33	10.2	10.7	10.8	11.0	7.8

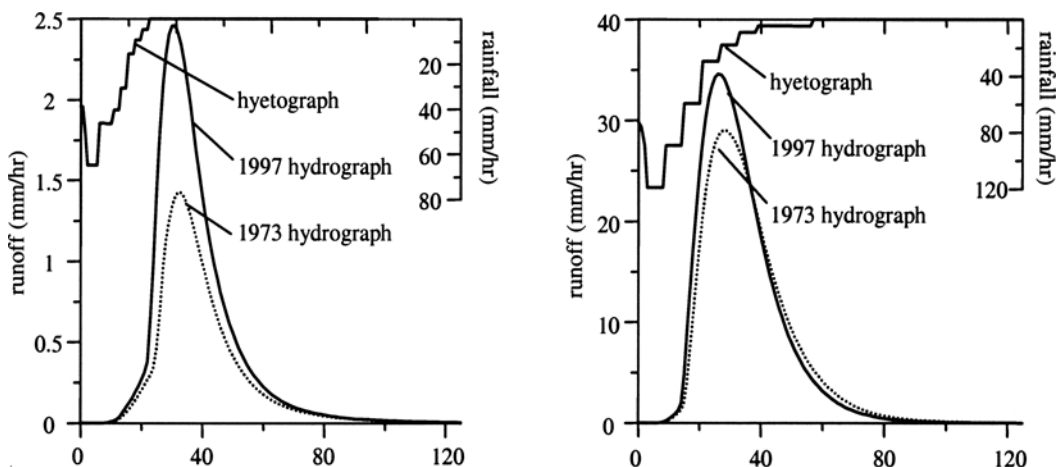


Fig. 9-9. Runoff hydrographs simulated using KINEROS2 for the Sierra Vista Subwatershed (Miller et al., 2002b).

tied closely to the energy of a given runoff event, they are subsequently determined by runoff rates and therefore increase greatly with storm size and duration. In all cases, the hydrographs produced with the 1986, 1992, and 1997 classification data were significantly larger than those produced using the 1973 data. The dominant land-cover transitions within this small watershed were from grassland and desertscrub to mesquite woodlands and urban. These transitions provide lower surface roughness values, decreased infiltration rates, and less cover, thereby reducing interceptions and exposing the surface to raindrop splash, all of which contribute to increased runoff and erosion.

The sediment yield data depicted in Table 9-4 reveal a similar response to urbanization within the watershed. Given that erosion and sediment yield are directly related to runoff velocity and volume, as runoff rates increase, the sediment likewise increases. The percent increases in sediment yield from 1973 to 1997 do not equal the percent increases in runoff for the same time periods. This apparent dissimilarity can be explained by the complexity of the spatially distributed changes within the watershed. As urbanization increases, so does the percent of impervious and paved area, which is treated in the model with a factor that reduces the erosion on those impervious areas.

Table 9-4. Sediment yield results using design rainfall events and KINEROS2 for the Sierra Vista Subwatershed (Miller et al., 2002b).

Rainfall Event	Rainfall (mm)	Sediment yield (ton)				Percent Change 1973 to 1997
		1973	1986	1992	1997	
5 yr, 30 min	17.35	2.02	18	15.2	19.2	851
5 yr, 60 min	21.08	20.8	21.9	24.1	26.9	29.3
10 yr, 30 min	22.74	212	208	248	295	39.2
10 yr, 60 min	26.44	283	423	427	449	58.7
100 yr, 30 min	31.79	1803	2070	2180	2420	34.2
100 yr, 60 min	38.33	2580	2550	2890	3090	19.8

In general, simulation results indicate that land-cover changes within the Sierra Vista watershed have altered its hydrologic response. These localized changes were associated with vegetation transition and urbanization. Reduced estimates of infiltration, percent vegetated cover, and surface roughness in conjunction with increased impervious surfaces resulted in increased simulated runoff from a variety of rainfall events.

Discussion

The Upper San Pedro River Basin has undergone a profound transition over the past several decades from a rural watershed to one with significant urban and agricultural regions. The Sierra Vista subwatershed within the Upper San Pedro Basin was chosen for more intensive research since it has undergone significant land-cover change implicated in increased runoff volumes and rates accompanied by decreased water quality due to erosion and sedimentation. These results follow the conclusions of Kepner et al. (2000), who showed that rapid urbanization in the towns within the San Pedro watershed over the past 20 years has become an important factor in altering land-cover composition and patterns.

Hydrologic modeling results indicated that watershed hydrologic response in the Upper San Pedro Basin has been altered to favor increased average annual runoff due to land-cover change during the period from 1973 to 1997, and consequently it is at risk for decreased water quality and related impacts to the local ecology. The Sierra Vista watershed within the San Pedro was modeled using design rainfall events, and the hydrographs resulting from these events showed dramatic increases in runoff volume, runoff rate, and soil loss.

Using AGWA for Land-Use Planning

Introduction

Today's environmental managers, urban planners, and decision-makers are increasingly expected to examine environmental and economic problems in a larger geographic context. To accomplish this, it is necessary to 1) understand the scale at which specific management actions are needed; 2) conceptualize environmental management strategies; 3) formulate sets of alternatives to reduce environmental and economic vulnerability and uncertainty in their

evaluation analyses; and 4) prioritize, conserve, or restore valued natural resources, especially those which provide important economic goods and services.

A scenario-based approach to regional land planning offers an organizational basis to explore decision analysis and opportunities for public resources. This approach is particularly useful for shaping future use of land and water resources, and has been used in a wide variety of geographic settings to assist stakeholders and policy makers in environmental decision-making (Schwartz 1996, Steinitz 1990). The GIS framework and automated procedures in AGWA are designed to facilitate this type of scenario-based analysis by enabling users to rapidly conduct replicate simulations for different land-use/cover scenarios and to directly compare the results of any two simulations. Kepner et al. (2004) demonstrated the utility of AGWA for this purpose by evaluating the spatial distribution of impacts to the hydrologic regime resulting from different land-use/cover scenarios for the Upper San Pedro River basin along the U.S.-Mexico border.

Methods

Baseline digital data for the year 2000 were obtained from the San Pedro River Geo-Data Browser (Kepner et al., 2003). Future scenarios were derived from Steinitz et al. (2003), who developed a series of land-use/cover maps for the year 2020 based on current land management and projected census growth. For the purpose of this study, three of the 2020 scenarios were selected that reflected important contradictions in desired future policy based on stakeholder input. These scenarios are described in Table 9-5 and shown in Fig. 9-10, and basically reflect changes in population within the watershed, patterns of growth, and development practices and constraints. The Constrained scenario is the most conservation oriented, the Plans scenario reflects the most likely census predictions with zoning options designed to accommodate growth, and the Open scenario is the least conservation and most development positioned option. The Open scenario also assumes a greater than predicted population with few constraints on land development.

Table 9-5. Scenarios for future urbanization of the upper San Pedro River Basin in the year 2020.

CONSTRAINED	Assumes lower population (78,500) than presently forecast for 2020. Development is concentrated in mostly existing developed areas (i.e., 90% urban). Removes all irrigated agriculture within the river basin.
PLANS	Assumes population increase as forecast for 2020 (95,000). Development is in mostly existing developed areas (i.e., 80% urban and 15% suburban). Removes irrigated agriculture within a 1-mi buffer zone of the river.
OPEN	Assumes population increase is more than the current 2020 forecast (111,500). Most constraints on land development are removed. Development occurs mostly into rural areas (60%) and less in existing urban areas (15%). Irrigated agriculture remains unchanged from current policy except for prohibiting new expansion near the river.

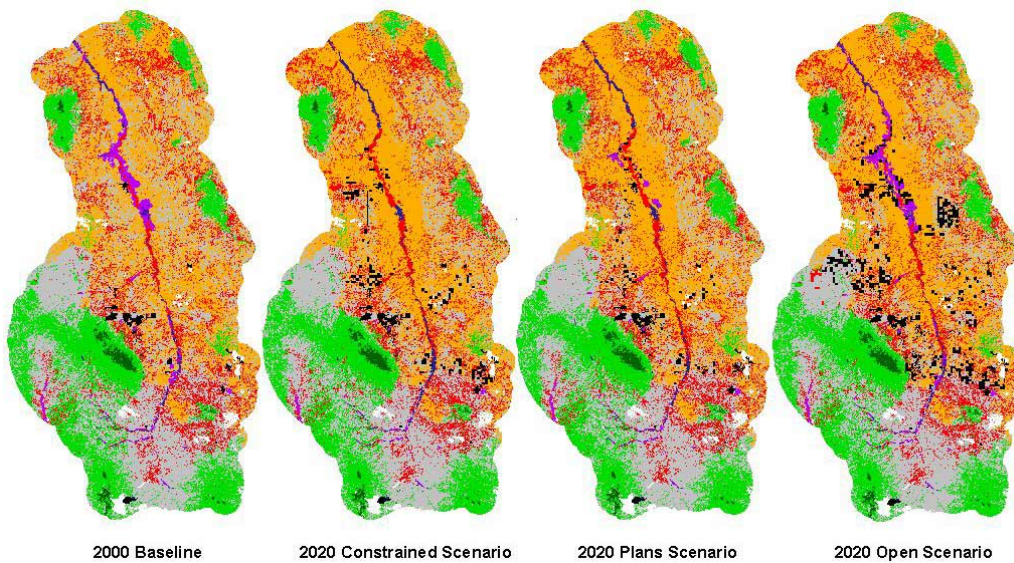


Fig. 9-10. Land-use/cover maps for the 2000 baseline and three 2020 future scenarios.

Our modeling approach involved first running SWAT using the 2000 baseline land cover to parameterize the model to determine reference condition. SWAT was run using 13 yr of continuous daily rainfall and temperature data (1960 – 1972) from a single gauge in the center of the basin. The same simulation was then performed using each of the three 2020 land-cover scenarios to develop parameter inputs. Average annual outputs from the three alternative futures were then differenced from the baseline values to compute percent change in average daily values over the 20-yr period. Output parameters compared in the analyses included surface runoff, channel discharge, percolation, and sediment yield. It is important to note that the purpose of this study was to demonstrate the utility of AGWA in alternative futures analysis. All results are presented relative to the 2000 baseline, but the model was not calibrated to permit quantitative comparisons of the hydrologic impacts. Our analyses thus focus on the relative magnitude and spatial distribution of the computed changes.

Results

A summary of the simulation results for each of the alternative futures is given in Table 9-6 and presented graphically using subwatersheds as the comparative unit in Fig. 9-11, 9-12, 9-13, and 9-14. The figures show relative departure, in percent, from the year 2000 baseline and illustrate the spatial variability of impacts on the surface water hydrology. Since soil and precipitation are held constant, differences in model output are exclusively associated with changes in land use/cover, primarily increasing urbanization and variable amounts of irrigated agriculture.

Table 9-6. Simulated average daily surface runoff, percolation, and sediment yield at the watershed outlet for the 2000 baseline conditions and predicted relative change for each of the three development scenarios from Kepner et al. (2004). Current and predicted daily groundwater overdraft for the three development scenarios from Steiniz et al. (2003).

	Baseline 2000	Simulated Percent Relative Change 2000 – 2020		
		Constrained 2020	Plans 2020	Open 2020
Surface runoff (m ³ /day)	186,538	4.3	3.7	6.9
Percolation (m ³ /day)	42,760	-2.7	-3.0	-4.6
Sediment yield (t/day)	1,042	4.4	3.7	7.0
Groundwater overdraft (m ³ /day)	131,494	-57.6	-42.1	8.1

In the case of surface runoff, the simulations show average increases over the 20-yr period commensurate with increases in urbanization, although there is considerable spatial variability of simulated hydrologic response (Fig. 9-11).

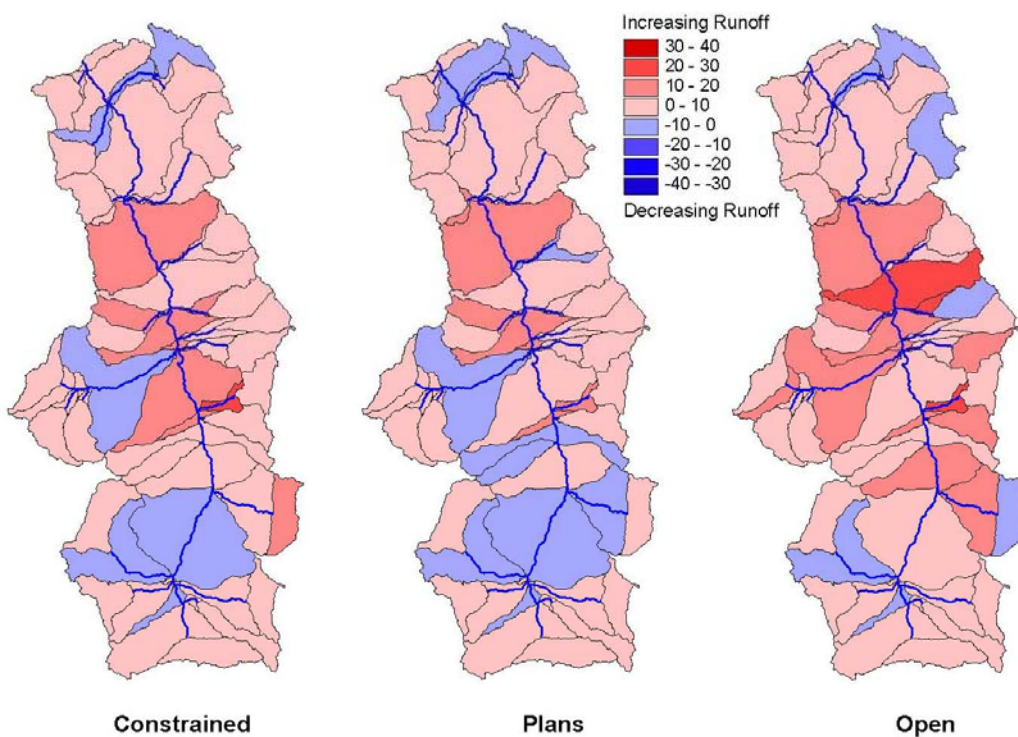


Fig. 9-11. Percent change in surface runoff, 2000 – 2020.

Most subwatersheds exhibit negative impacts (reds), but some areas do show improvement (blue), and there is substantial variation in the specific hydrologic response. The greatest change was simulated for the Open scenario with an average increase almost 7% over the 2000 baseline (Table 9-6). Simulated increases in surface runoff predominantly occur within subwatersheds located in the central portion of the watershed where the greatest development is anticipated (see Fig. 9-10).

Percent change in simulated channel discharge agrees closely with results for surface runoff. Figure 9-12 shows change in simulated mean daily channel discharge relative to the 2000 baseline for each of the three development scenarios. By mapping this model output for each reach in the model area, it is possible to visually identify reaches that are anticipated to experience the greatest changes in their hydrologic regime as a result of the land-cover/use change. Important changes in the magnitude and frequency of flooding increase the likelihood of channel scour and associated negative impacts on riparian vegetation. As such, the simulated changes to the hydrologic regime mapped in Fig. 9-12 can also be viewed as an index of riparian vulnerability to the unmitigated future development. As in the previous example, channel discharge increased most under the Open scenario, and although the results are spatially variable, the greatest impact seems to be concentrated in the subwatersheds in the central portion of the San Pedro, where most development is forecast.

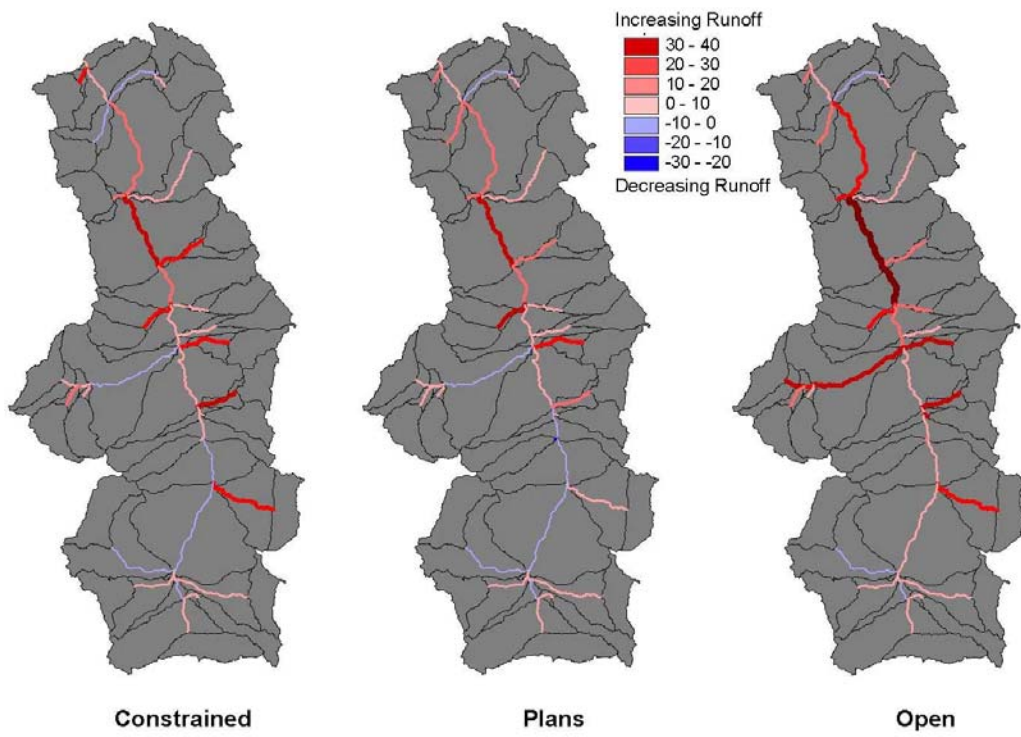


Fig. 9-12. Percent change in channel discharge, 2000 – 2020.

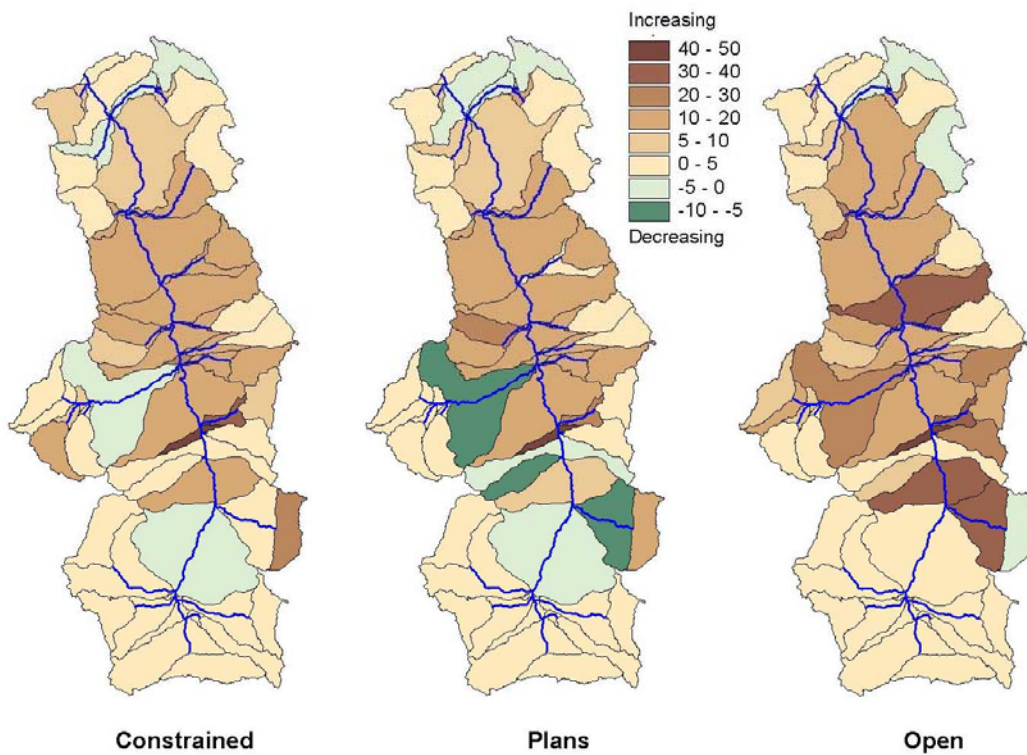


Fig. 9-13. Percent change in sediment yield, 2000 – 2020.

Sediment yield and erosion are directly related to runoff volume and velocity, and subwatersheds with the greatest increase in sediment yield (Fig. 9-13) correlate tightly with those exhibiting the greatest change in surface runoff. The Open scenario is thus expected to produce the highest sediment yields and the largest increase (7%) over the baseline conditions.

Percolation is a hydrologic measure of the water volume that is able to infiltrate into the soil past the root zone to recharge the shallow and/or deepwater aquifers. Figure 9-14 shows that although the model does predict some improvement in the watershed headwaters where human occupation is most dispersed, overall percolation is expected to decrease in all options as urban impervious surfaces are expanded. This is most apparent for the Open scenario, for which percolation is predicted to decline by 4.6% (Table 9-6), although the daily volume this would represent is trivial in comparison to the groundwater overdraft

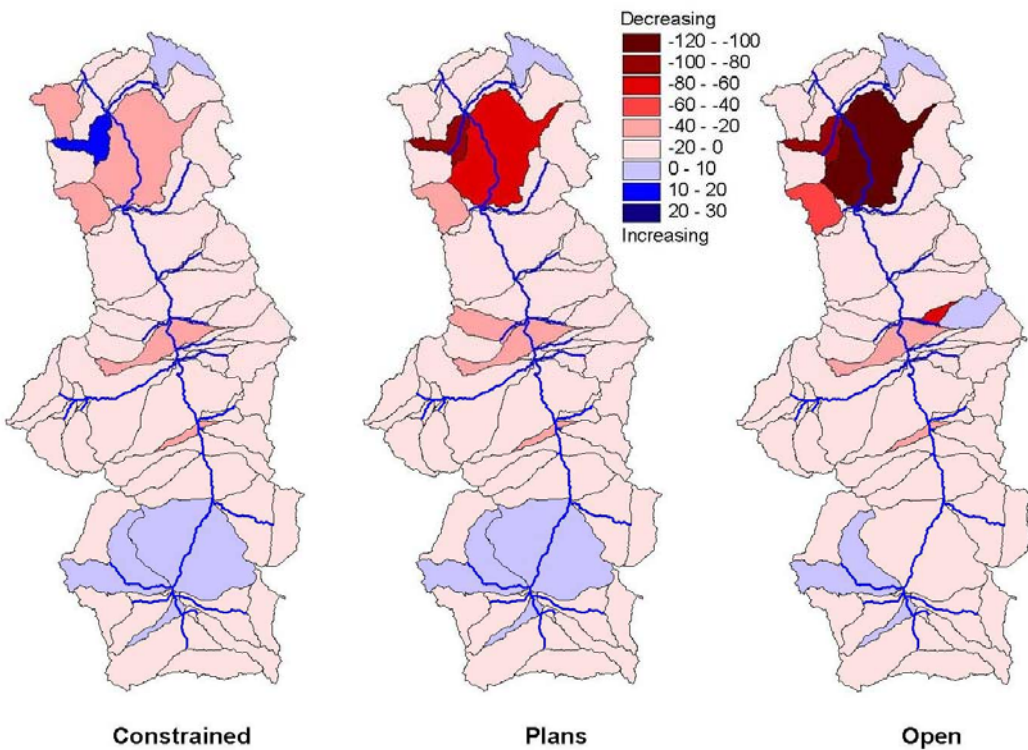


Fig. 9-14. Percent change in percolation, 2000 – 2020.

In general, under a future urbanizing environment, the model results appear to indicate that important impacts to the watershed hydrology can be expected. The most notable changes are likely to be increases in runoff, channel discharge, and sediment yield, and a reduction of surface water access to the groundwater table. This appears to agree with the results reported by Steinitz et al. (2003) who predicted changes in groundwater storage for the three 2020 scenarios (Table 9-6). In this study, the largest groundwater overdraft ($10,608 \text{ m}^3/\text{day}$ above the 2000 baseline) was predicted for the Open Scenario.

Discussion

The hydrologic responses resulting from three development scenarios for the upper San Pedro River Basin were evaluated using AGWA to demonstrate its utility in alternative futures analysis. Alternative futures research has traditionally neglected the spatially-variable impact of land-cover/use change on the surface-water hydrologic regime. With this type of assessment, however, it is possible to rapidly evaluate likely changes in surface runoff throughout a basin, as well as the cumulative downstream change as widely distributed tributary impacts are felt in the main channel. In this fashion, it is possible to assess the vulnerability of potentially sensitive areas to basin-wide development alternatives.

For the purpose of this study, negative impacts are considered to be any increase in surface runoff, channel discharge, sediment yield, and/or declines in groundwater percolation. In general,

the Open scenario has the greatest negative impact on surface water hydrology and results in greater simulated surface runoff, channel discharge, and sediment yield than the other options, especially in the downstream reaches near Benson, Arizona. Additionally, percolation and thus groundwater recharge are most reduced under this option. This scenario favors development and allows for the largest future population increase within the watershed.

The Constrained and Plans alternatives have less significant impacts to the surface-water hydrology due to the concentration of development in existing urban areas and the significant reductions in irrigated agriculture. The simulation results from these two scenarios are very similar, with most of the differences resulting from the presence or absence of agriculture in the basin. Under the Constrained alternative, the elimination of all irrigated agriculture causes the biggest reduction in groundwater pumping, but it also has the effect of producing slightly higher surface runoff and erosion than when it is present in the Plans alternative. Results thus suggest that the increased runoff resulting from additional suburban development in the Plans scenario (15% vs. 0% in Constrained scenario) is offset by the presence of agriculture, which is generally characterized by higher infiltration rates than the native desert scrub.

Areas within the San Pedro Basin are valued both for development and for conservation purposes, and this sometimes brings human values into direct conflict. Clearly policy decisions regarding both population growth and irrigated agriculture will have important impact on future water use and conservation. Scenario analyses such as this one improve our ability to make informed decisions regarding land and water resource management. By integrating spatial data and distributed modeling in natural resources management, AGWA allows stakeholders and decision-makers to assess the relative impacts of several alternative sets of options and thus provides an important tool to help make better informed choices for an improved future.

SUMMARY AND CONCLUSIONS

A GIS-based hydrologic modeling toolkit called the Automated Geospatial Watershed Assessment (AGWA) tool has been developed for use in watershed analysis. This tool has been released as an open-source suite of programs and is fully modular and customizable. AGWA automates the process of converting commonly available GIS data to input parameter files for the SWAT and KINEROS2 hydrologic models. Rainfall files for both models can be prepared within AGWA, depending on the availability of rainfall data. Results from these models, such as runoff, peak discharge, and sediment yield for each model element, are imported into AGWA and can be investigated using AGWA's visualization tools. Since the models operate at different spatial and temporal scales, they provide the ability to perform a range of analyses as tailored to specific research or management objectives.

In the absence of a calibration/validation exercise, AGWA model results are best suited for relative analysis. Given repeat classified remote sensing imagery, AGWA provides the capability to assess the spatial distribution of the impacts of land-cover change on watershed hydrologic response. In the absence of repeat imagery, AGWA may be used to identify portions of a study area that are most susceptible to change, or high-priority management zones.

The modeling capability of the AGWA tool was demonstrated by presenting two case studies. The first case study consisted in evaluating the hydrologic response of the Upper San Pedro Basin to land-cover change over several decades using the SWAT and KINEROS2 models. These models significantly differ in their representation of hydrologic processes and operate at different

temporal and spatial scales. Input parameters for these models were obtained using AGWA in conjunction with readily available topographic and soil data and a series of classified satellite images detailing land cover over the study area. The results indicate that watershed hydrologic response in the basin has been altered to favor increased average annual runoff due to land-cover change during the period from 1973 to 1997, and consequently it is at risk for decreased water quality and related impacts to the local ecology. The Sierra Vista watershed within the San Pedro was modeled using design rainfall events, and the hydrographs resulting from these events showed dramatic increases in runoff volume, runoff rate, and sediment yield. The second case study illustrated the application of the AGWA tool to evaluate the response of the San Pedro River basin to possible future urbanization scenarios in the year 2020. In general, the results appear to indicate that important impacts to the watershed hydrology can be expected. The most notable changes are likely to be increases in runoff, channel discharge, and sediment yield, and a reduction of surface water access to the groundwater table.

This chapter illustrated how the AGWA tool provides a formal specification for well-integrated, repeatable analyses that provide consistent landscape/hydrologic evaluations over time and space. Therefore, AGWA represents a powerful and flexible tool for managing resources and understanding and predicting complex and changing systems.

ACKNOWLEDGMENTS

The authors thank Lainie Levick and the Editorial Committee for their valuable comments, which led to the improvement of the manuscript.

REFERENCES

- Arnold, J.G., J.R. Williams, R. Srinivasan, K.W. King, and R.H. Griggs. 1994. SWAT: Soil_Water Assessment Tool [Online]. Available at <http://www.brc.tamus.edu/swat/> (accessed 17 May 2005). USDA Agricultural Research Service, Grassland, Soil and Water Research Laboratory, Temple, TX.
- Bales, J., and R. Betson. 1982. The curve number as a hydrologic index. p. 371-386. *In* V.P. Singh (ed.) Rainfall-runoff relationships. Water Resources Publications, Highlands Ranch, CO.
- Beven, K.J. 2000. Rainfall-runoff modelling. John Wiley & Sons Ltd., West Sussex, England.
- Bouwer, H. 1966. Rapid field measurement of air entry and hydraulic conductivity as significant parameters in flow systems analysis. *Water Resour. Res.* 2:279-238.
- Commission for Environmental Cooperation. 1998. Advisory panel report on the Upper San Pedro River initiative: Recommendations and findings presented to the Commission for Environmental Cooperation. CEC, Montreal, Canada.
- ESRI. 2001. ArcView version 3.2a software and user's manual. Environmental Systems Research Institute, Redlands, CA.
- Faures, J.M., D.C. Goodrich, D.A. Woolhiser, and S. Sorooshian. 1995. Impact of small scale spatial rainfall variability on runoff modeling. *J. Hydrol.* (Amsterdam) 173:309-326.
- Goodrich, D.C. 1991. Basin scale and runoff model complexity. Department of Hydrology and Water Resources Technical Rep. HWR91-010. University of Arizona, Tucson, AZ.

- Goodrich, D.C., J.M. Faures, D.A. Woolhiser, L.J. Lane, and S. Sorooshian. 1995. Measurement and analysis of small-scale convective storm rainfall variability. *J. Hydrol.* (Amsterdam) 173:283-308.
- Goodrich, D.C., T.J. Schmugge, T.J. Jackson, C.L. Unkrich, T.O. Keefer, R. Parry, L.B. Bach, and S.A. Amer. 1994. Runoff simulation sensitivity to remotely sensed initial soil water content. *Water Resour. Res.* 30:1393-1405.
- Goodrich, D.C., C.L. Unkrich, R.E., Smith, and D.A. Woolhiser. 2002. KINEROS2: A distributed kinematic runoff and erosion model. In Proc. Federal Inter-agency Conf. Hydrologic Modeling, 2nd, Las Vegas, NV. 28 July –1 Aug. 2002. Office of Water Quality, Reston, VA.
- Hernandez, M., S.N. Miller, D.J. Semmens, D.C. Goodrich, B.F. Goff, W.G. Kepner, C.M. Edmonds, and K.B. Jones. 2000. Modeling runoff response to land cover and rainfall spatial variability in semi-arid watersheds. *Environ. Monitoring and Assessment* 64: 285-298.
- Hjelmfelt, A.T., L.A. Kramer, and R. Burwell. 1982. Curve numbers as random variables. p. 365-370 In V.P. Singh (ed.) Rainfall-runoff relationships. Water Resources Publications, Highlands Ranch, CO.
- Kepner, W.G., D.J. Semmens, D.T. Heggem, E.J. Evanson, C.M. Edmonds, S.N. Scott, and D. W. Ebert. 2003. The San Pedro River geo-data browser and assessment tools [CDROM and online]. Available at http://www.epa.gov/nerlesd1/land-sci/san_pedro/ (accessed 17 May 2005). USEPA and USDA Agricultural Research Service (EPA/600/C-03/008 and ARS/152432).
- Kepner, W.G., C.J. Watts, C.M. Edmonds, J.K. Maingi, S.E. Marsh, and G. Luna. 2000. A landscape approach for detecting and evaluating change in a semi-arid environment. *Environ. Monitoring and Assessment* 64: 179-195.
- Kepner, W.G., D.J. Semmens, S.D. Bassett, D.A. Mouat, and D.C. Goodrich. 2004. Scenario analysis for the San Pedro River, analyzing hydrological consequences of a future environment. *J. Environ. Monitoring and Assessment* 94:115-127.
- Mankin, K.R., J.K. Koeller, and P.K. Kalita. 1999. Watershed and lake quality assessment: An integrated modeling approach. *J. Am. Water Resour. Assoc.* 35:1069-1088.
- Michaud, J.D., and S. Sorooshian. 1994. Comparison of simple versus complex distributed runoff models on a midsized semiarid watershed. *Water Resour. Res.* 30:593-605.
- Miller, S.N., D.P. Guertin, and D.C. Goodrich. 1996. Investigating stream channel morphology using a geographic information system. In Proc. ESRI User Conf., Palm Springs, CA. May 20-24, 1996. Environmental Systems Research Institute, Redlands, CA.
- Miller, S.N., D.J. Semmens, R.C. Miller, M. Hernandez, D.C. Goodrich, W.P. Miller, W.G. Kepner, and D. Ebert. 2002a. GIS-Based hydrological modeling: The automated geospatial watershed assessment tool. In Proc. Federal Inter-agency Conf. Hydrologic Modeling, 2nd, Las Vegas, NV. 28 July-1 Aug. 2002. Office of Water Quality, Reston, VA.
- Miller, S.N., W.G. Kepner, M.H. Mehaffey, M. Hernandez, R.C. Miller, D.C. Goodrich, F. Kim Devonald, D.T. Heggem, and W.P. Miller. 2002b. Integrated landscape assessment and hydrologic modeling for land cover change analysis. *J. Am. Water Resour. Assoc.* 38:915-929.
- Mishra, S.K., and V.P. Singh. 1999. Another look at SCS-CN method. *J. Hydrol. Eng.* 4:257-264.
- NOAA. 1973. NOAA Atlas 2: Precipitation frequency atlas of the Western United States. U.S. Government Printing Office, Washington, DC.

- Osborn, H.B., L.J. Lane, and V.A. Myers. 1980. Rainfall/watershed relationships for southwestern thunderstorms. *Trans. Am. Soc. Civ. Eng.* 23:82-91.
- Osborn, H.B., C.L. Unkrich, and L. Frykman. 1985. Problems of simplification in hydrologic modeling. *Hydrology and Water Resources in Arizona and Southwest* 15:7-20.
- Rawls, W.J., D.L. Brakensiek, and K.E. Saxton, 1982. Estimation of soil water properties. *Trans. Am. Soc. Agric. Eng.* 25:1316-1320, 1328.
- Renard, K.G., L.J. Lane, J.R. Simanton, W.E. Emmerich, J.J. Stone, M.A. Weltz, D.C. Goodrich, and D.S. Yakowitz. 1993. Agricultural impacts in an arid environment: Walnut Gulch studies. *Hydrological Science and Technology* 9 (1):145-190.
- Schwartz, P. 1996. *The art of the long view: Paths to strategic insight for yourself and your company*. Currency Doubleday, New York, New York.
- Singh, V.P. 1995. Watershed Modeling. p. 1-22. In V.P. Singh (ed.) *Computer Models of Watershed Hydrology*. Water Resour. Publ., Littleton, Colorado.
- Smith, R.E., D.C. Goodrich, D.A. Woolhiser, and C.L. Unkrich. 1995. KINEROS – A kinematic runoff and erosion model. p. 697-732. In V.P. Singh (ed.) *Computer Models of Watershed Hydrology*. Water Resour. Publ. Highlands Ranch, Colorado.
- Smith, R.E., and J.-Y. Parlange. 1978. A parameter-efficient hydrologic infiltration model. *Water Resour. Res.* 14:533-538.
- Srinivasan, R., J.G. Arnold, R.S. Muttiah, C. Walker, and P.T. Dyke. 1993. Hydrologic Unit Model for United States (HUMUS). p. 451-456 In *Advances in Hydro-Science and Engineering*. University of Mississippi, Oxford, MS.
- Steinitz, C. 1990. A framework for the theory applicable to the education of landscape architects (and other environmental design professionals). *Landscape J.* 9(2):136-143.
- Steinitz, C., H. Arias, S. Bassett, M. Flaxman, T. Goode, T. Maddock III, D. Mouat, R. Peiser, and A. Shearer. 2003. *Alternative futures for changing landscapes. The Upper San Pedro River Basin in Arizona and Sonora*. Island Press, Washington, D.C.
- Stone, J.J., L.J. Lane, and E.D. Shirley. 1992. Infiltration and runoff simulation on a plane. *Trans. Am. Soc. Agric. Eng.* 35 (1):161-170.
- Syed, K.H. 1999. The impact of digital elevation model data type and resolution on hydrologic modeling. PhD diss. Department of Hydrology and Water Resources, Univ. of Arizona, Tucson, AZ.
- Tellman, B., R. Yarde, and M. G. Wallace. 1997. Arizona's changing rivers: How people have affected the rivers. Water Resources Research Center Issue Paper 19. University of Arizona, Tucson, AZ.
- U.S. Environmental Protection Agency. 1993. North American Landscape Characterization (NALC). Research Brief. EPA/600/S-93/0005. USEPA, Office of Research and Development, Washington, D. C.
- U.S. Department of Agriculture, Soil Conservation Service. 1973. A method for estimating volume and rate of runoff in small watersheds. SCS-TP-149. USDA, SCS, Washington, DC.
- U.S. Department of Agriculture, Soil Conservation Service, 1986. Urban hydrology for small watersheds. Tech. Release 55. USDA, SCS, Washington, DC.
- Woolhiser, D.A., R.E. Smith, and D.C. Goodrich. 1990. KINEROS: A kinematic runoff and erosion model documentation and user manual. USDA-Agricultural Research Service Pub. ARS-77. National Technical Information Service, Springfield, VA.

CHAPTER 10

Modeling Runoff and Erosion in the Lake of Patzcuaro Watershed, Michoacan, Mexico

Luis Mario Tapia Vargas, Mario Tiscareño-Lopez, Gilberto Chavez-Leon, Ignacio Vidales Fernandez, and Luis Reyes-Muro

CONTENTS

Introduction	160
Materials and Methodology	161
Natural Rainfall Testing	162
Rainfall Simulation	163
Rill Detachment (<i>Dr</i>)	163
Interrill Detachment (<i>Di</i>)	164
Infiltration Model Adjustment	164
Dynamic and Economic Simulation Models	
for Evaluating Soil Management	165
Treatments	165
Decision Support System Simulation	166
Net Returns of Soil Management Systems	167
Decision Model	167
Weighting Alternatives	167
Erosion Simulation with GIS	168
Remote Sensing	168
Erosion Equations	168
Supervised Classification	168
Soil Management Systems Sustainability	170
Results and Discussion	170
Natural Rainfall	170
Rainfall Simulation	173
Hydrological Variables	173

Interrill Detachment (<i>Di</i>)	174
Rill Detachment (<i>Dr</i>)	175
Infiltration Model Adjustment	176
Dynamic and Economic Simulation Models	
for Evaluating Soil Management	178
GLEAMS Simulation and Calibration	178
Simulated Sediment Yield	179
DSS Model Simulation	180
Effects of Alternative Systems	181
Erosion Simulation with GIS	182
Soil Management Sustainability	184
Conclusions	185
References	186

INTRODUCTION

The continuous encroachment of agriculture and urbanization on forestlands is damaging the fragile hydrological cycle of closed Mexican watersheds such as Xochimilco, Zumpango, Patzcuaro, and Zirahuen. This problem is causing considerable environmental damage, such as increased erosion due to steep slope rainfed agriculture (McAuliffe et al., 2001). Erosion can reach up to $40 \text{ Mg ha}^{-1} \text{ yr}^{-1}$ in the Lake of Patzcuaro watershed (Gomez, 1994; Tiscareño et al., 2001). The lakes of Patzcuaro and Zirahuen are among the most important natural resources in the state of Michoacan, western Mexico. Both lakes have low nutrient levels, mainly available P and N, which limit the flourishing of algae (McAuliffe et al., 2001). However, runoff and erosion take sediments and nutrients off the agricultural hillslopes (Toledo et al., 1992) and transport them to the lake, making them available to algae. This situation is causing eutrophication of the lake and negatively affecting aquatic organisms, mainly endemic species such as the Patzcuaro White Fish (*Chiostoma estor* Jordan) and the Patzcuaro Salamander (*Ambystoma dumerilii* Dugès).

Hillslope agriculture in the Patzcuaro watershed has been practiced since ancient times (O'Hara et al., 1993), but it was mainly during the last fifty years that water surface losses reached highest level rates of up to 70 ha yr^{-1} (Tiscareño et al., 1999). Tillage practices related to maize growing, a common means of livelihood for Mexican peasants, are promoting severe soil erosion, mainly when the crop has low soil cover and rainfall has high impact energy (Tapia et al., 1999).

Best management practices such as conservation tillage, which involves no-tillage with residual soil cover, should be implemented to reduce soil erosion and runoff in agricultural slope lands. While focusing on this alternative practice, the next step is studying the problem from different points of view, evaluating its magnitude, observing different locations, modeling possible scenarios, simulating under controlled rainfall the detachment and transport of sediments, analyzing economic results, and extrapolating erosion simulation to the rest of the watershed (Fig. 10-1).

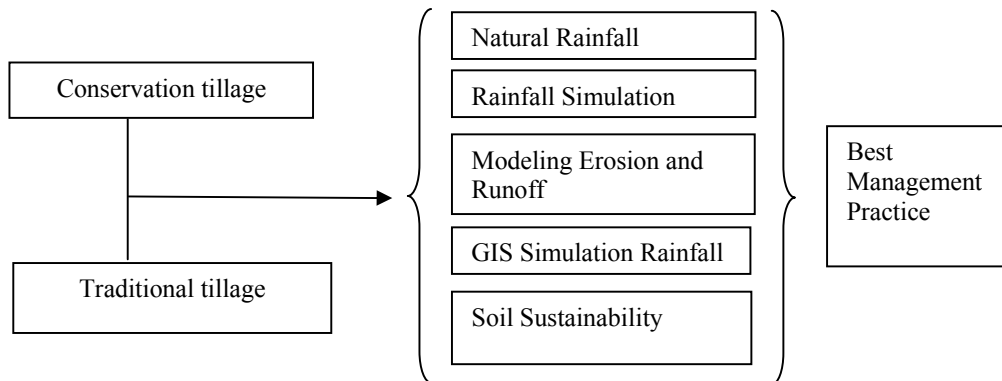


Fig. 10-1. Scheme proposed to study the effects of two soil management practices in the Patzcuaro watershed, Michoacan, Mexico.

The aim of the work presented in this chapter is to propose a soil conservation tillage management system with residual plant soil cover (CT) as an alternative to traditional tillage (TT) and to evaluate runoff and sediment output under five conditions: 1) natural rainfall, 2) rainfall simulation, 3) dynamic and economic model simulation, 4) geographic information system simulation, and 5) soil sustainability performance.

MATERIALS AND METHODOLOGY

Our experimental station is located in the town of Ajuno, within the Lake of Patzcuaro watershed, state of Michoacan, Mexico. This experimental station belongs to the Mexican National Research Institute of Forestry, Agriculture, and Livestock Production (INIFAP) and is situated at Km 17.5 of the Patzcuaro-Uruapan toll highway. The climate is temperate sub-humid, with a rainfall season from June to October (CW_2). Annual mean precipitation is 990 mm, with usually dry and cold winters. Soils are derived mainly from volcanic ashes in most of Patzcuaro watershed. The soil of the experimental station is Hydric Hapludand (Alcala et al., 2002).

We divided our work into five sections to improve reliability of comparisons. The evaluated treatments were (1) conservation tillage with residual plant soil cover (CT) and (2) prevalent traditional tillage (TT). Neither tillage nor soil movements were applied in CT. Plow-type soil movement and two cultivation machine paces were applied in TT. These two treatments were analyzed in the following sequence: 1) Natural Rainfall Testing; 2) Rainfall Simulation; 3) Dynamic Model Simulation with the Ground Water Loading Effects of Agricultural Management Systems (GLEAMS), and Economic Analysis with the Decision Support System (DSS); 4) GIS Erosion Simulation, extrapolating erosion equations to the whole watershed; and 5) Sustainability Soil Analysis, evaluating sustainability indexes of each tillage treatment.

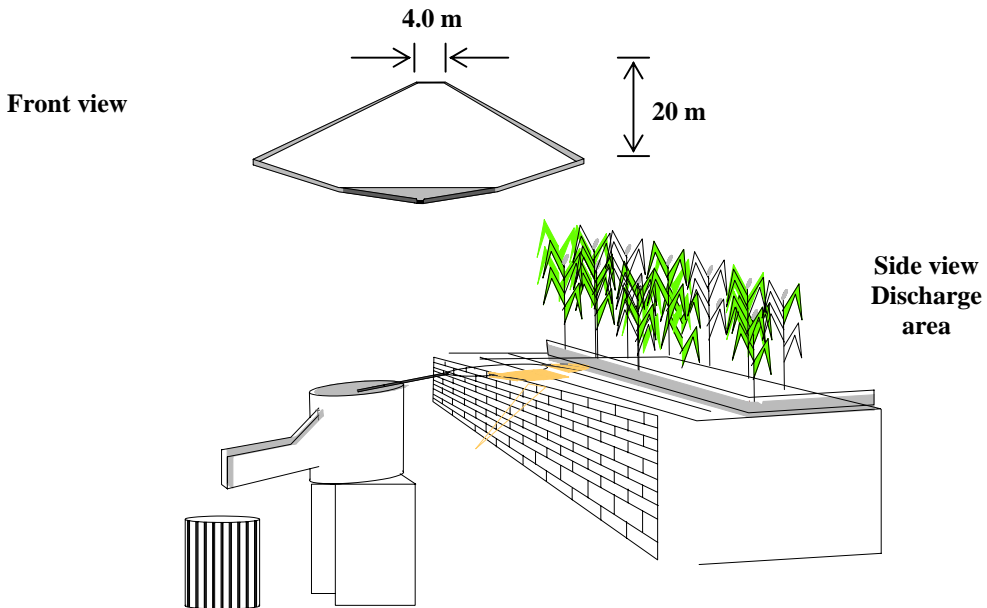


Fig. 10-2. Front and side view of the runoff plots used to evaluate runoff (Q) and sediment yield (Sy) in Patzcuaro watershed, Michoacan, Mexico.

Natural Rainfall Testing

We evaluated both treatments in two runoff plots 25 m long by 4 m wide at 9% slope each. During the last week of May 1997, a local variety of maize was sown to establish the CT and TT treatments. All management practices (weed control, fertilization, harvest) were similar in both treatments, except for the inherent practices of each treatment described earlier.

Runoff and soil erosion were measured in a collector tank at the bottom of the plot (Fig. 10-2). When runoff exceeded 450 L, a top flume on the top diverted one-eighth of the water excess to a second collector tank. Sediment concentrations in 1:1 aliquots of water runoff were used to calculate storm erosion.

Daily runoff, sediment outputs, rainfall, and EI_{30} datasets were correlated using the following equation:

$$y = a x^b \quad [1]$$

where:

$$\begin{aligned} y &= \text{runoff (mm) or sediment yields (kg ha}^{-1}\text{)} \\ x &= \text{rainfall (mm) or } EI_{30} (\text{MJ mm ha}^{-1} \text{ h}^{-1}) \end{aligned}$$

The slope of the regression equations was evaluated statistically in both treatments (CT and TT) to point out the stronger relationship between runoff and sediment yields. The parameter t was

calculated with the equation:

$$t = \frac{b_1 - b_2}{\sqrt{Sp \left[\frac{1}{SS_1} \right] + \left[\frac{1}{SS_2} \right]}} \quad [2]$$

with

$$Sp = \frac{MSE_1 - MSE_2}{2} \quad [3]$$

where

b_1 and b_2 = regression slopes for CT and TT equations, respectively.

SS_1 and SS_2 = square sum for regression model

MSE_1 and MSE_2 = mean square error equations with $n-2 + n-2$ degrees of freedom

Rainfall Simulation

In the experimental sites, rain simulation was performed on the two treatments, CT and TT, and a variable intensity rainfall simulator operated with a solenoid was used (Fig. 10-2). The rainfall simulator produced intermittent rainfall in the pre-constructed 1 x 1 m and 1 x 3 m plots. An electrical water pump, 0.75HP, 110 VAC, with a volume of $0.0007 \text{ m}^3 \text{ s}^{-1}$, supplied the water. Hydraulic energy was controlled by a valve connected to a manometer, which was usually set at 0.029 MPa; flow intensity generally was controlled by the engine speed or the water energy (Miller, 1987).

The simulation was performed on dry and wet soil (after 24 h of the dry simulation) with two replications of the same treatment in different places. Simulated rainfall was measured with pluviometers during 85 min. The evaluated variables were runoff (liters and millimeters) and soil loss (grams) on samples taken every 5 min of simulation, peak of runoff discharge (L min^{-1}), time to runoff (seconds) and to fill (seconds), and weight of samples to obtain the output of sediments rate (g s^{-1}).

Rill detachment (Dr)

On previously wet soil, an increasing flow from 5 to 35 L min^{-1} was applied on the upper limit of each tillage treatment in the simulation plot. Each run was applied individually until a steady flow was reached, which was accomplished within 6 to 8 min of application. When the steady flow was reached, a 1.0-L water sample was taken. The time of filling was measured and the sediments produced in the flow, evaluated; at the same time, the flow width, depth, and speed were measured. With this information, the hydraulic radius of the flow for each flux was determined. For all flow levels, the pair of shear stress data (τ) and the discharge of sediments was adjusted by linear regression using the following expression:

$$Dr = \tau_c + Kr \tau \quad [4]$$

where:

Dr = rill detachment ($\text{kg s}^{-1} \text{ m}^{-2}$)

τ = shear stress (Pa), obtained with the expression for uniform flow (Haan et al., 1994)

The shear stress is due to:

$$\tau = Rh * S \quad [5]$$

where:

- Rh = rill hydraulic ratio (m)
- S = rill slope (ad.)
- τ_c = critic shear stress (Pa)
- Kr = rill detachment ($s m^{-1}$)

According to Elliot et al. (1989), the slope of the regression is the value of the rill detachment coefficient (Kr), while the critic shear stress (τ_c) is the quotient of the regression constant and the slope ($\tau_c = -a/b$).

Interrill Detachment (Di)

Rainfall simulation on the tillage treatments was evaluated for each sampling time to obtain the interrill detachment coefficient (Ki) with the expression:

$$Di = \frac{Ki}{I^2 S_f} \quad (\text{kg s}^{-1} \text{ m}^{-4}) \quad [6]$$

where:

- Di = interrill detachment rate ($\text{kg s}^{-1} \text{ m}^{-2}$)
- I = rainfall intensity (m s^{-1})
- S_f = slope factor

The ratio of interrill detachment coefficient (Ki) was obtained directly from the runoff during rainfall simulations by sampling at equal periods of time (5 min), measuring the filling time of the sampling container, and computing the intensity of the rainfall period. Graphics for each treatment were generated to calculate Kr and to compute the Di value as well as the values of the different variables (τ, τ_c, Dr). Tillage effects on each treatment were compared with the magnitudes reported by Elliot et al. (1989) for some simulation sites in the U.S.A. and Mexico (Villar et al., 1999).

Infiltration Model Adjustment

Data of the runoff and rainfall ratio of the simulation events were processed to adjust the model with infiltration parameters (Hillel, 1980) under non-saturated conditions, as follows:

$$I = a\sqrt{t} + bt \quad [7]$$

where:

- I = accumulated infiltration (mm h^{-1})
- t = accumulated time (h)
- a and b = regression coefficients

Under saturated conditions, the model becomes

$$I = a + bt \quad [8]$$

Infiltration rate is obtained from

$$\frac{dI}{dt} = \frac{b}{\sqrt{t}} + a \quad [9]$$

when t tends to infinite the limit of accumulated infiltration and infiltration rate is

$$\lim_{t \rightarrow \infty} \frac{dI}{dt} = \lim_{t \rightarrow \infty} \left[\frac{b}{\sqrt{t}} + a \right] = a \quad [10]$$

where a is the steady state infiltration or saturated hydraulic conductivity. Notice that this expression is the same as that for the limit of infiltration rate. The derivation of the saturated infiltration equation yields

$$\frac{dI}{dt} = \lim_{t \rightarrow \infty} \left[\frac{bt + a}{dt} \right] = b \quad [11]$$

where b is a steady state of hydraulic conductivity when $t \rightarrow \infty$.

The steady state of hydraulic conductivity in both soil management treatments could be compared in the same way as explained earlier in the section on natural rainfall testing.

Dynamic and Economic Simulation Models for Evaluating Soil Management

Treatments

The Groundwater Loading and Evaluation of Agricultural Management Systems (GLEAMS) model and the Decision Support System (DSS) are a process-based continuous simulation set of steady-state equations using basic hydrological variables and possible soil erosion resulting from storms. In this work, two GLEAMS model components were used for simulation: the hydrological and erosion submodels. Runoff was obtained from the Natural Resource Conservation Service (NRCS). Sediment down slope was computed from the transport capacity of the flow, which is based on the continuity mass expression:

$$\frac{dq_s}{dx} = D_L + D_F \quad [12]$$

where q_s is the sediment load ($\text{kg m}^{-1} \text{s}^{-1}$) at the x point distance down slope (m), D_L the lateral inflow of sediment ($\text{kg m}^{-2} \text{s}^{-1}$), D_F the detachment or deposited sediment by the flow ($\text{kg m}^{-2} \text{s}^{-1}$).

Both terms are related to

$$D_L = 0.21 EI (s + 0.014) KCP (\Phi_p / V_u) \quad [13]$$

$$D_F = 37983 mVu \Phi_p^{1/3} (x/72.6)^{m-1} s^2 KCP (\Phi_p / V_u) \quad [14]$$

where

- EI is the Weishmeier's rainfall erosivity factor ($\text{MJ mm ha}^{-1} \text{h}^{-1}$)
- s the sine of the slope angle
- K the USLE soil erodibility factor ($\text{Mg ha h ha}^{-1} \text{MJ}^{-1} \text{mm}^{-1}$)
- C the soil loss ratio
- P the USLE contouring factor (dimensionless)
- p the peak runoff rate (mm h^{-1})
- Vu the storm runoff volume (mm) estimated above
- m the exponent in the slope-length factor
- x the distance down slope (m)

Input variables for the hydrological model were the average monthly maximum and minimum temperature, daily total rainfall, and K USLE factor based on soil texture ($0.038 \text{ Mg ha h mm}^{-1} \text{ MJ}^{-1} \text{ ha}^{-1}$). Input variables for the SLR erosion submodel were taken from the canopy crop during the growing season (Davies et al., 1990). Table 10-1 shows main input variables for the GLEAMS model.

Table 10-1. Soil input variables required for GLEAMS from experimental plots.

Variable	Conservation Tillage	Traditional Tillage
Field capacity (-0.33 bar) (mm/mm)	0.12	0.13
Withering point (-15 bar) (mm/mm)	0.07	0.07
Organic matter (%)	2.10	2.10
Bulk density (g cm^{-3})	0.99	0.99
Surface n Manning (s m^{-3})	0.07	0.02
Curve number (CN)	87	93
Soil loss rate (SLR):		
Initial	0.20	0.85
Medium	0.08	0.43
End	0.02	0.07

Decision Support System Simulation

The Decision Support System was designed to mend agricultural management systems based on potential negative effects of surface or subsurface agricultural pollutants from sediments flowing out from parcels, and farmer's net benefits (Lane et al., 1994). Three decision criteria were selected to evaluate agricultural management systems on hillslope lands of the Lake of Patzcuaro watershed. The main interest of the farmers was not only to increase economic returns but also to reduce runoff and sediment yield in the lake. Hence, the three decision criteria were (1) net benefits ($\text{US \$ ha}^{-1}$), (2) sediment yield, and (3) runoff.

One year of hydrologic data (1996) was available for the two agricultural management systems. Net returns for each treatment, total sediment yield for the whole year, and runoff and associated N losses are listed in Table 10-2. Traditional tillage (TT) net profits of $\text{US \$ 30.00 ha}^{-1}$ were above mean historical profits in the region (INEGI, 1991). Climatic data (monthly maximum, minimum, and mean temperature; daily precipitation and solar radiation) were available from a nearby (4 km) station (Santa Fe) for 1974-1991.

Table 10-2. Observed values of hydrological and crop variables in two management systems.

Treatment	Net benefits US \$ ha ⁻¹	Sediment yield Mg ha ⁻¹	Runoff cm	N runoff kg ha ⁻¹
Conventional till (TT)	141.60	3.18	8.7	7.41
Conservation till (CT)	281.30	0.27	2.1	0.69

Net Returns of Soil Management Systems

The economic program CARE, Cost and Return Estimator (Midwest Agricultural Research Associates, 1988), was used to estimate the economic returns to land and management systems from the field plots. Yields for each management system, which were assumed to be sold at current prices of 2001, were estimated with the crop growth model, with fixed and variable costs associated with each operation subtracted to calculate net returns.

Decision Model

The remaining components of the DSS are associated with the assembly of input and output information. The decision model has three sub-components: 1) the score functions and their shapes; 2) the calculation of “best” and “worst” scores; and 3) the method of ranking alternatives. Scoring functions are a means of scaling between 0 and 1 decision variables which have different units and magnitudes. This enables all the decision criteria to be compared on a common, nondimensional basis. The score functions are four basic score shapes combined with decision rules developed by Yakowitz et al. (1993).

Weighting Alternatives

Best and worst composite scores for each alternative are determined by the solutions of two simple linear programs, and these two composite scores are then aggregated to determine the preference ranking of the alternatives. For a total of m decision criteria, Yakowitz et al. (1993) give the Best or Worst composite scores as follows:

maximize (minimize):

$$\sum_{i=1}^m w(i) Sc(i, j) \quad [15]$$

subject to

$$w_1 \geq w_2 \geq \dots \geq w_m \geq 0 \quad [16]$$

$$\sum_{i=1}^m w(i) = 1 \quad [17]$$

where

w_i = weight factor based on the importance order for decision criterion i

$Sc(i, j)$ = score of alternative j evaluated for decision criterion i

The DSS allows the user to redefine an importance order for the decision variables. This feature is designed to accommodate the preferences associated with a different user's perspectives. (Hernandez et. al., 1995).

Erosion Simulation with GIS

Remote Sensing

A multi-spectral Landsat image with six bands of the TM sensor was analyzed. The image contains six bands of the electromagnetic spectrum (0.45-0.52, 0.52-0.60, 0.63-0.69, 0.76-0.90, 1.55-1.75 and 2.08-2.35 micrometers for bands 1 to 6, respectively) with a resolution of 30 x 30 m each pixel. A sub-image of 4000 columns and 2500 rows was clipped and then treated for geometric correction, georeferencing, visual improvement, and classification using GIS IDRISI for Windows (Eastman, 1992). The digital slope model (30 x 30 m) from INEGI, corresponding to the topographic charts A22, A21, A31 and A32, was included in the treatment of the image.

Erosion Equations

Two erosion equations from the GLEAMS simulation model were generated for the soil management treatments traditional tillage (TT) and conservation tillage (CT):

$$\text{TT Sediment outputs} = 1.067 e^{0.1151 S_o} \quad [18]$$

$$\text{CT Sediment outputs} = 0.168 e^{0.1227 S_o} \quad [19]$$

where:

S_o = soil slope (%)

Supervised Classification

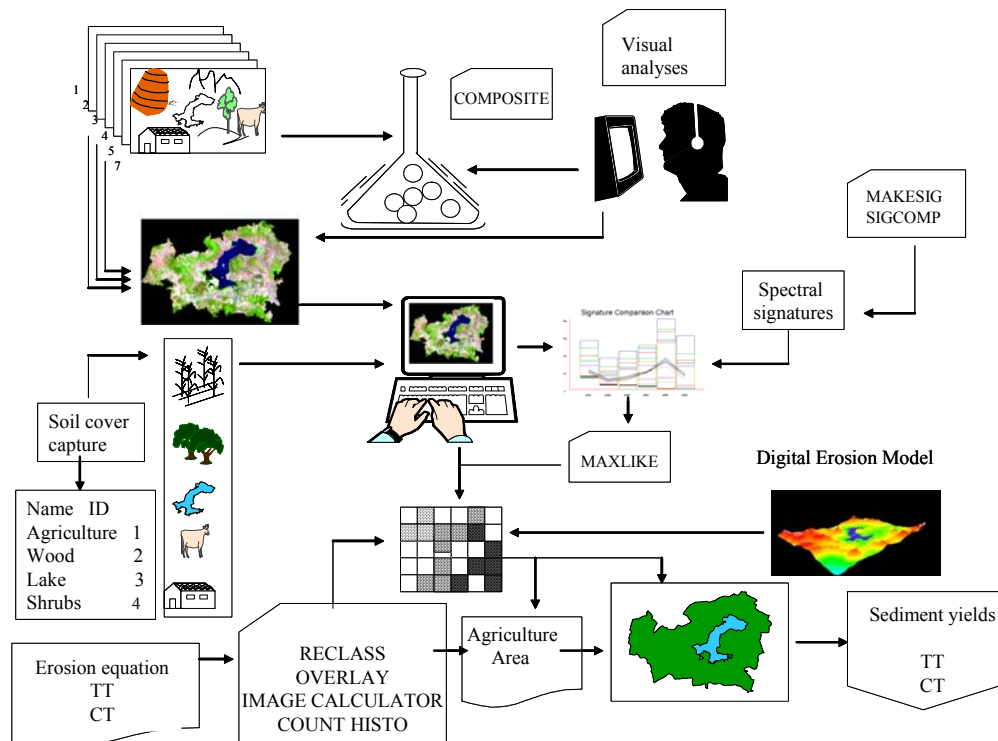
Twenty compositions in three band combinations were evaluated to select the best image composition showing sharper soil cover differences. The best band combination was 3, 4, and 5 evaluated under cathodic rays blue, green and red, respectively, with a linear saturation of 5%. Training fields were identified from field surveys or directly over the image. Field information was referenced with a global position system (GPS) receiver. Digitization of training fields was performed on GIS displays. Six main soil covers were identified by number; these covers included agricultural and forest land because they are the main sediment sources for the lake (Tiscareño et al., 2001). The remaining soil covers were used only to improve the agricultural cover in the classified image. Input information for the supervised classification of the composed image corresponding to the Patzcuaro watershed is shown in Table 10-3.

When the training fields were digitized, the spectral signatures were evaluated with the three bands of the composed image. To improve the classification of the image, the spectral signature of each band should be identified completely and separated (Chuvieco, 1986). The complete process is shown in Fig. 10-3. The composed image was classified with the maximum likelihood method which yields best results when training fields have been well-separated (Eastman, 1992).

Table 10-3. Sources of information for the supervised classification of Patzcuaro watershed

Remote sensing	Field information	GIS	Results
Rainfed agriculture	Erosion equation $Sedim = a * e^{(b * So)}$	Module analysis	Sediment outputs
Forest and shrubs	Training fields	Digital elevation model	Particle source location
Irrigated agriculture			Sediment quantification
Lake			
Cities			Treatment comparison

With the help of a geographic information system (GIS IDRISI), agricultural areas in the image were separated and revised with the digital elevation model to obtain the slope and agriculture image. This image was treated with the erosion model to generate the sediment outputs corresponding to each agricultural plot of the watershed.

**Fig. 10-3. Supervised classification steps in Patzcuaro watershed.**

Soil Management Systems Sustainability

In both treatments (CT and TT), biologic soil activity was studied at two depths (0-5 and 5-12 cm). The biologic activity was assessed with chloroform treatment, and temperature and humidity were controlled by a growth chamber (Jenkinson and Powlson, 1976).

Microbial biomass calculation (MB) was computed with the expression:

$$MB = \frac{(B - T) * PM * N}{PS} \quad [20]$$

(mg C kg⁻¹ soil)

where:

B = utilized blanch (mL)

T = utilized titrated (mL)

PM = molecular weight of HCl

N = normality of HCl

PS = soil weight (kg)

Data were analyzed and evaluated with the t test to compare mean microbial biomass of the two treatments. Organic matter (OM) and nitrate (NO_3^-) outputs were measured for each runoff event as sustainability indicators. The t test was applied to the mean of both soil treatments where each runoff event was a repetition.

RESULTS AND DISCUSSION

Natural Rainfall

In the rainfall cycle between sowing and 100% of crop soil cover (90 days), different amounts of rainfall (from 453 to 1019 mm) were registered (Table 10-4). The driest and the wettest years reached 1350 and 4330 units of EI_{30} , respectively. The maximum energy was recorded in 1998, with 1110 units of EI_{30} for 49 mm of total rainfall. For this experimental station, Santos (1995) reported 2993 EI_{30} units for a complete season rainfall in 1985. Runoff (Q), and sediment outputs (Sy) are also shown in Table 10-4. Although rainfall in 1996 and 1997 was slighter than in 1998, Q and Sy were 100% higher than in 1998. This effect was mainly found in the TT treatment. Both treatments showed consistency throughout the three years of valuation. Treatment CT could reduce from 20 to 40% the runoff with respect to TT. Sy was also higher in TT. While CT registered 0.2-0.6 Mg ha⁻¹, TT attained 2.9-3.4 Mg ha⁻¹. These amounts of Sy make a favorable difference for CT in this watershed.

Table 10-4. Hydrologic variables evaluated in runoff plots in the Lake of Patzcuaro watershed, Michoacan, Mexico.

Study year/Treatments	Hydrologic variable			
	Rainfall mm	EI_{30} MJ mm $ha^{-1} h^{-1}$	Runoff mm	Sediment outputs kg ha^{-1}
1996				
Conservation tillage	511	1835	16.3	221
Traditional tillage	511	1835	76.9	2923
1997				
Conservation tillage	453	1351	59.4	693
Traditional tillage	453	1351	90.8	3313
1998				
Conservation tillage	1019	4331	20.2	104
Traditional tillage	1019	4331	37.9	1907

The curve shape of the effect of rainfall on runoff for the period 1996-1998 clearly fits the results reported by Simmanton et al. (1973) for the studied period (Fig. 10-4). However, Q had higher magnitudes as a consequence of the three rainfall events; the other events had minimal effects on Q . The points of maximum runoff were always recorded in the TT treatment, whereas CT had slight trends. The TT performance was due to its lowest infiltration rates, which generated higher Q values than CT.

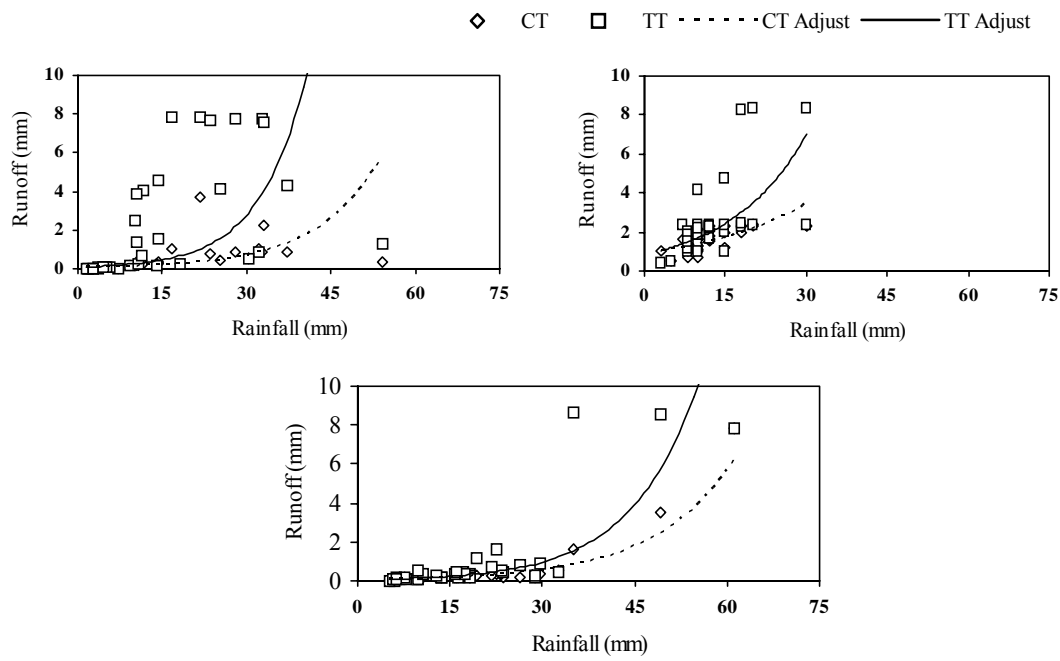


Fig. 10-4. Rainfall effects on runoff outputs (Q) in two management soil treatments, Patzcuaro Lake watershed, 1996-1998.

Treatment TT yielded higher amounts of sediment outputs (Sy) than CT (Fig. 10-5). This is prominent in the curve trend. As we found in Q , higher Sy amounts were generated in response to three major rainfall events. The rest of the rainfall events had lower EI_{30} . The maximum recorded Sy (600 kg ha^{-1}) was in TT. The importance of the vegetal residue soil cover of CT is emphasized in these maximum events with just less than 50 kg ha^{-1} of Sy . Same values of EI_{30} for both treatments produced a different effect. CT reduced Sy outputs while TT increased them. These results are in agreement with those reported by Sauer and Daniel (1987), who reported Q and Sy reductions for conservation tillage.

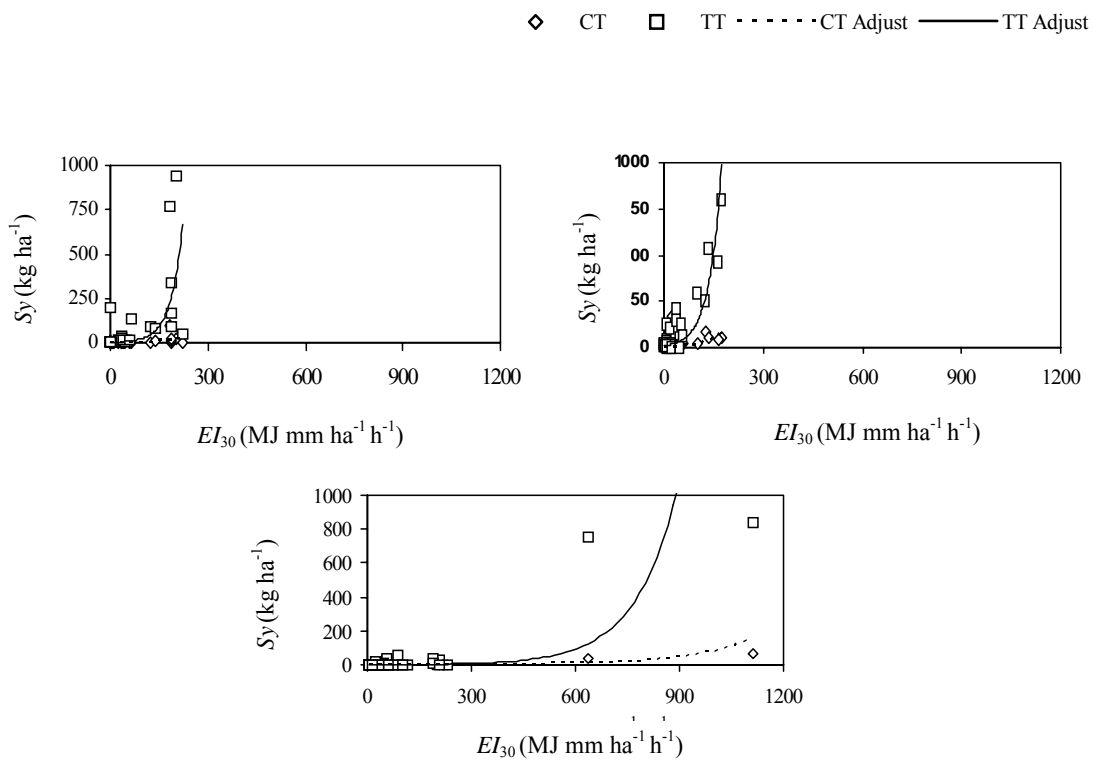


Fig. 10-5. Effect of rainfall intensity (EI_{30}) on sediment yields (Sy) in two soil management systems. Lake of Patzcuaro watershed, 1996-1998.

Square sum regression of either adjusted model or year of Q and Sy events was higher in TT than in CT (Fig. 10-4 and Fig. 10-5, Table 10- 5). In some of these annual paired results, the regression coefficients were different, showing that TT yielded more Q and Sy than CT. However, in 1997, no statistical difference was detected for Sy . In all studied years, the square sum regression of TT was two or three times higher than CT; this could make the difference between CT and TT treatments.

Table 10-5. Statistical test (*t*) for slope regression adjusted to *Q* and *Sy* annual data of conservation tillage (CT) and traditional tillage (TT) soil managements.

Year	Hydrologic Variable	Treatment	SSR	MSE	<i>t</i> _c
1996	<i>Q</i>	CT	10.9	0.094	18.7 **
		TT	21.7	0.314	
1996	<i>Sy</i>	CT	10.0	0.351	6.3 **
		TT	28.1	0.550	
1997	<i>Q</i>	CT	0.57	0.016	5.5 **
		TT	1.38	0.038	
1997	<i>Sy</i>	CT	2.39	0.900	0.4 N.S.
		TT	5.15	0.490	
1998	<i>Q</i>	CT	3.55	0.036	17.5 **
		TT	7.15	0.097	
1998	<i>Sy</i>	CT	6.82	0.674	4.3 **
		TT	21.9	0.740	

SSR: square sum regression, MSE: medium square error; *t*_c: *t* calculated; *, ** significantly different values at *p*<0.05 and *p*<0.01, respectively; NS: not significantly different at *p*>0.05.

Rainfall Simulation

Hydrological Variables

Differences between hydrological variables of rainfall simulations on both soil management treatments are clearly marked: TT yielded more runoff and soil erosion than CT; under dry simulation, runoff reached 54.3 L in TT, while in CT it was reduced by nearly 50% (Table 10-6). Great differences were observed in soil losses, with 18,800 g m⁻² in TT versus 410 g m⁻² in CT. The worst effect occurred under wet soil where both runoff and soil losses were 100% higher than in dry soil. These results confirm previous ones that showed major soil erosion susceptibility of this andisols under wet soil conditions (Tapia et al., 1999). Sediment concentration and peak runoff discharge were also higher in TT than in CT in both soil conditions. Sediment concentration was low in CT, only 2 g L⁻¹, while in TT it was 347 g L⁻¹. It is remarkable that the time to runoff was higher in dry soil condition in TT than in CT. This could have been caused by lower soil humidity content in TT.

Under natural watershed conditions, the early precipitation in June quickly moistens the soil. Ensuing July rainfall enhances soil erodibility because the soil gets wet and rainfall has great kinetic energy, more than 1000 MJ mm ha⁻¹ h⁻¹. This energy is dissipated by soil disintegration because the crop cover is still less than 30% (Tapia et al., 1999). This condition is causing large sediments to leave the hill-slope agricultural lands.

Table 10-6. Hydrological variables of two soil tillage management treatments under rainfall simulation in the Lake of Patzcuaro watershed.

Treatment	Runoff (L)	Soil loss (g m ⁻²)	Sediment concentration (g L ⁻¹)	Peak runoff Discharge (L min ⁻¹)	Time to runoff (s)
Dry simulation					
Traditional tillage	54.3	18,820	347	2.32	731
Conservation tillage	27.4	410	2	0.74	485
Wet simulation					
Traditional tillage	106.7	35,491	333	1.74	310
Conservation tillage	60.1	441	7	0.76	393

Interrill Detachment (*Di*)

In rainfall simulation, there is clearly a difference between the two soil management systems with respect to interrill detachment rate (*Di*) and runoff (*Q*) even if the registered rainfall is similar in both treatments (Table 10-7). Better physical properties are obtained by the use of CT soil management against the rainfall erosive action, which helps reduce the *Di* and the *Q* rates.

Table 10-7. Rainfall simulation results in two soil management treatments.

Treatment	Interrill detachment (g s ⁻¹ m ⁻⁴)	Rainfall (mm h ⁻¹)	Total runoff (mm)
Dry			
Traditional tillage (TT)	3.61	111.6	69.9
Conservation tillage (CT)	0.01	119.4	25.9
Wet			
Traditional tillage (TT)	7.0	101.2	100.1
Conservation tillage (CT)	0.1	124.1	60.3

The soil consistency acquired with CT allows the soil to undergo a lower erosion rate under continuous rainfall compared to a continuously tilled soil. This is due to the formation of an internal soil structure which holds more water and helps reduce the runoff and the transport of detached sediments.

On the other hand, continuous soil movement caused by TT promotes soils susceptibility to rill erosion. Norton and Brown (1992) demonstrated that as time goes on, recent tillage produces higher disintegration among rills than older tillage. This may explain what is occurring in the productive units of the watershed; the continuous movement of the soil with TT promotes soil vulnerability to rill erosion, which is the first disintegration factor that leaves the soil susceptible to removal if the flow among rills has enough capacity to transport it out of the plots. This

problem occurs in soils without structure, such as the ones on the hill slopes of Patzcuaro watershed, which can be seen in the rainfall simulation results (Table 10-6). This type of soil is highly prone to interrill disintegration, so disintegrated sediments will be available and transported out of the plot by the rill flow. The difference between the dry and wet rainfall simulation was large in interrill detachment values. The CT treatment showed how the soil reaches disintegration stability with respect to the dry simulation by maintaining low erosion values. The TT treatment, on the contrary, shows an increase in disintegration, with higher values. It was expected that when the soil was wet, it would present a lower erosion rate, as was demonstrated by Simmanton et al. (1988) and Meyer and Harmon (1992), who found a higher transport of sediments in dry rainfall simulation conditions (94.8 Mg ha^{-1}) than in wet simulation (33.3 Mg ha^{-1}). In Patzcuaro, it was found that the disintegration was higher in wet conditions, which could have resulted, as was argued by these authors, from the differences in the soil erodibility of the slope hills of Patzcuaro.

Rill Detachment (Dr)

Linear adjustment for the rill detachment data, (Dr), obtained from increasing flow simulation plots for TT and CT, shows that there is a contrasting behavior between the rill disintegration obtained with CT and with TT in large proportions (Fig. 10-6). While in CT, rates of Dr were of the order of 0 to $1.5 \text{ g m}^{-2} \text{ s}^{-1}$, in TT rates were from more than 100 to $500 \text{ g m}^{-2} \text{ s}^{-1}$. This clearly shows the superiority of CT in reducing the rill erosion and lowering the production of sediments. These effects were observed in equal inflow conditions, indicating that soil protection by conservation tillage is important in reducing erosion among and within rills.

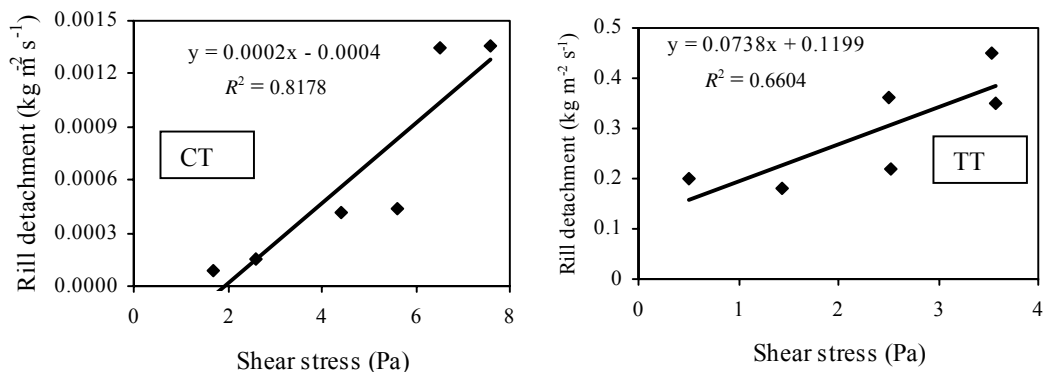


Fig. 10-6. Rill detachment (K_r) in two soil management systems of Patzcuaro watershed.

The unequal response is also partly due to the less required critical shear stress (τ_c) to produce high rates of disintegration in TT. Differences between treatments may be detected through the difference in the required values to produce rill erosion (shown in the x axis in Fig. 10-6).

Although both soils are classified the same and found in the same site, it seems like the CT soil is more mature and consolidated, as was corroborated by Norton and Brown (1992) when they evaluated the erosion differences in two soil types. This may indicate that CT confers better soil properties (according to the Dr obtained values), making CT soil behave like a more evolved and consolidated soil. Under the same simulation conditions, the parameter values for the Di and Dr differ considerably. While CT presents low values in the erosion among and within rills, TT presents high erosion rates (Table 10-8).

Table 10-8. Ki and Kr parameter values for the two tillage treatments in Patzcuaro watershed and soils of equal texture from USA and Chiapas (Mexico).

Parameter	Soil tillage management treatment			Soil from Chiapas [‡]
	Conservation tillage	Traditional tillage	Soil from USA [†]	
Dry Condition				
Ki (kg s m^{-4})	2552.0	1,262,608.0	1,170,000.00	2,901,000.00
Kr (s m^{-1})	0.0002	0.080	0.0031	0.0043
τ_c (Pascal's)	2.0	-1.6	0.24	2.7
Wet Condition				
Ki (kg s m^{-4})	19,271	3,113,579.0		

Source: [†]Norton y Brown (1992). [‡] Villar et al. (1999).

Soils under TT condition lack protection by crop residues to reduce raindrops impact, which produce high Ki values only comparable to the higher ones found by different authors in the most erodible soils of the USA (Elliot et al., 1989, Norton and Brown, 1992). The interrill erodibility coefficient as well as the erosion rill coefficient in CT presented low values, which were both lower than in TT.

The registered parameter values of Kr in Sandy-loam soils were higher than the values in CT but lower than those found in TT. This indicates the lack of structure in the Patzcuaro watershed soils, which could be corrected by the application of CT with some plant residue. However, Ki values were lower in both tillage treatments, although in wet conditions, the TT treatment became easily erosive, more than the Chiapas soil (Villar et al., 1999).

Regarding the critical shear stress in rills (t_c), the measured values were lower in both treatments than those reported for Chiapas. This indicates that less effort is required to disintegrate soil particles. However, when comparing the values of the two treatments, the CT superiority is obvious; this points out that the energy required in CT to accomplish sediment disintegration within rills is greater than that required in TT to accomplish the same. The negative value of TT is not found in natural conditions, indicating the capacity to disintegrate soil in rills of the Patzcuaro watershed.

Infiltration Model Adjustment

In the Hillel infiltration model, the importance of the hydraulic conductivity magnitude (K_s) was directly related to the treatment's ability to admit a bigger precipitation rate and to be infiltrated faster into the soil profile (Table 10-9). CT presents higher K_s than TT, indicating that it can support higher precipitation rates due to its infiltration capacity, which reduces runoff.

Table 10-9. Hillel infiltration model adjustment parameters in two tillage treatments in Ajuno, Michoacan, Mexico.

Tillage Treatments	Unsaturated soil			Saturated soil		
	K_s (mm h ⁻¹)	Regression coefficient	R^2	K_s (mm h ⁻¹)	Regression coefficient	R^2
Dry Simulation		b			a	
Traditional tillage	48.6	20.9	0.99	43.6	19.7	0.99
Conservation tillage	82.8	10.5	0.99	102.6	1.27	0.99
Wet Simulation		b			a	
Traditional tillage	22.2	8.2	0.99	21.9	5.3	0.99
Conservation tillage	64.4	36.1	0.99	76.9	20.7	0.99

Differences found in the K_s values during rainfall simulation may be directly attributed to the soil management treatment. As proposed by Jasso (1997), the soil structure may be altered by the tillage method. In this study CT improved the soil structure and consequently increased its infiltration capacity. This improvement could be made through the development of greater porosity in the top soil zone of CT, which promotes an increase in infiltration rates (Rhoton et al., 2002).

The dry and wet simulations allowed detecting K_s differences for the two soil management methods. This evaluation indicates that non-tillage management produces higher K_s values in both dry and wet conditions. CT behaves like a sponge that can absorb higher precipitation rates and maintains a high disproportion with respect to TT. Besides, hydraulic activity in CT is 100% higher than in TT in dry condition and more than 300% in wet condition. This disparity is what allows CT to show a uniform behavior, maintaining higher infiltration rates throughout the storm, while TT rapidly reduces K_s , which is reflected in lower infiltration rates and an early start of runoff.

The CT treatment showed a better performance by allowing water flow through the soil with 92.9 mm h⁻¹ under dry conditions and 37.0 mm h⁻¹ under wet conditions; TT obtained only 17.6 mm h⁻¹ and 10.9 mm h⁻¹ under dry and wet conditions, respectively (Table 10-10).

Table 10-10. Hydraulic conductivity (K_s) obtained with infiltration rate model in two soil management systems.

Treatment	Dry simulation			Wet simulation		
	K_s	b	R^2	K_s	b	R^2
TT	17.6	28.3	0.73	10.9	10.7	0.46
CT	92.9	4.9	0.36	37.0	37.8	0.85

Hydraulic conductivity recorded in CT was different from that obtained in TT under dry ($t_c=2,011.8$) and wet ($t_c=1050.1$) conditions (Table 10-11). Differences could also be detected in both soil conditions in the steady state infiltration or long-time infiltration, dry ($t_c=1,219.0$) and wet ($t_c=844.6$). In all cases, CT was significantly different from TT ($p\leq 0.01$). This shows that CT acquires better soil structure and adequate soil aggregation to improve soil infiltration capacity.

Table 10-11. Statistic comparison of hydraulic conductivity (K_s) in two soil management systems under rainfall simulation.

Treatment	K_s	SS	EMS	t_c	K_s	SS	EMS	t_c
Dry								
Traditional tillage	48.6	6316.2	0.79	2011.8**	43.6	1086.7	0.38	1219.0**
Conservation tillage	82.8	9484.5	1.36		102.6	6022.4	3.94	
Wet								
Traditional tillage	22.2	1170.9	0.24	1050**	22.0	276.9	0.21	844.6**
Conservation tillage	64.4	13,949.1	2.92		76.9	3384.1	1.93	

SS: regression square sum, EMS: error mean square, t_c : t computed $p\leq 0.01$ (*), $p\leq 0.05$ (**), respectively.

Dynamic and Economic Simulation Models for Evaluating Soil Management

GLEAMS Simulation and Calibration

The GLEAMS model predicted monthly and total seasonal runoff volume and sediment yields on hill slope fields (Table 10-12). Based on the obtained values of the coefficient of determination (R^2), estimated runoffs were linearly related to observed runoffs since the R^2 was above 0.7 for all the treatments. Runoff volume estimates for TT were underpredicted and the resulting model's proficiency (E) to predict Q was -7.4. However, CT had higher E coefficients than TT in estimating Q . This indicates a good model performance in predicting the monthly runoff volume on mulched no-tilled fields. Model proficiency to simulate Q for CT system was better than for the TT system.

Table 10-12. Linear regression coefficients and model efficiency index (E) for variables simulated by GLEAMS after local calibration.

Tillage treatment	Runoff				Sediment yield			
	<i>a</i>	<i>b</i>	R^2	<i>E</i>	<i>a</i>	<i>b</i>	R^2	<i>E</i>
	mm				$Mg ha^{-1}$			
Traditional tillage (CT)	0.80	0.44	0.99	-7.41	0.16	0.91	0.98	0.83
Conservation tillage (TT)	-0.05	1.14	0.99	0.99	0.01	0.93	0.94	0.99

The limited ability of the model to predict the monthly runoff volume for the TT plot can be attributed to a single *CN* value assigned into the model for the entire growing season. It must be kept in mind that the *CN* parameter was computed with model calibration. We have found changes in *CN* in the TT system due to crop growth and surface roughness modifications with soil cultivation. Modifications of surface roughness in TT fields subject to furrow cultivation affected the runoff volume estimated by the models.

Model predictions of total seasonal runoff for the four treatments showed slight differences between observed and simulated runoff when total seasonal amounts were considered (Table 10-13). Seasonal runoff predictions of GLEAMS are significantly better because of the unique *CN* value for the entire season.

Table 10-13. Seasonal observed (O) and simulated (S) runoff volume and sediment yields.

Tillage system	Runoff Mm		Sediment $Mg\ ha^{-1}$	
	O	S	O	S
Traditional till (TT)	85.7	86.1	3.2	3.8
Conservation till (CT)	20.9	20.6	0.3	0.3

Simulated Sediment Yield

GLEAMS' efficiency in estimating sediment yields was acceptable, considering the obtained *E* index. Some difficulties were detected in simulating *Sy* for TT since sediment yield was overpredicted (Fig. 10-7). The R^2 coefficient also indicated a linear correspondence between observed and simulated *Sy* (Table 10-13). Model inability to predict *Sy* estimates results from inaccuracies in runoff estimates. Note that runoff volume was obtained with the National Resource Conservation Service equation and later required to estimate the lateral sediment contribution (D_L) using Eq. [6] as well as the detached and deposited sediment by the flow (D_F) using Eq. [7]. This indicates that sediment yield predictions by GLEAMS are very sensitive to *Q* via *CN* calculation.

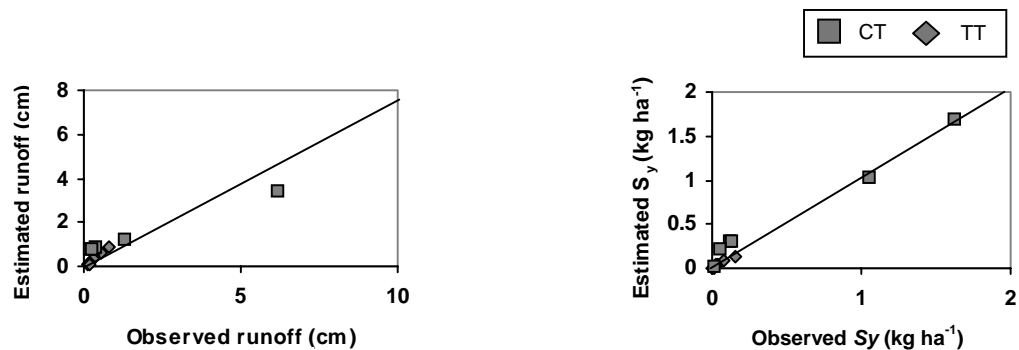


Fig. 10-7. GLEAMS simulation of runoff and sediment yield for two soil management treatments in the Lake of Patzcuaro watershed.

In general, the GLEAMS model performance was better in predicting Sy than Q . Model efficiency (E) and R^2 coefficients were higher in Sy estimation than those found in Q estimations. This situation was pointed out by Villar (1999) who found a better model efficiency for Sy than for Q in rainfed corn of Chiapas, Mexico.

An exponential fit of Sy rates against slope steepness was identified when comparing soil losses at variable slopes for CT and TT systems (Fig. 10-8). TT soil losses at 4% slope were 1.2 $Mg\ ha^{-1}$ and could reach 23 $Mg\ ha^{-1}$ at 20% slope. This indicates that CT represents a viable solution to hillslope erosion in the Patzcuaro Lake basin. However, no-tillage agriculture with the use of crop residues can hardly detain soil losses at tolerable rates in croplands located above 25% slope steepness. Thus, the model became a tool to locate points along the hillslope where soil conservation structures (e.g., terracing) need to be installed to minimize soil losses.

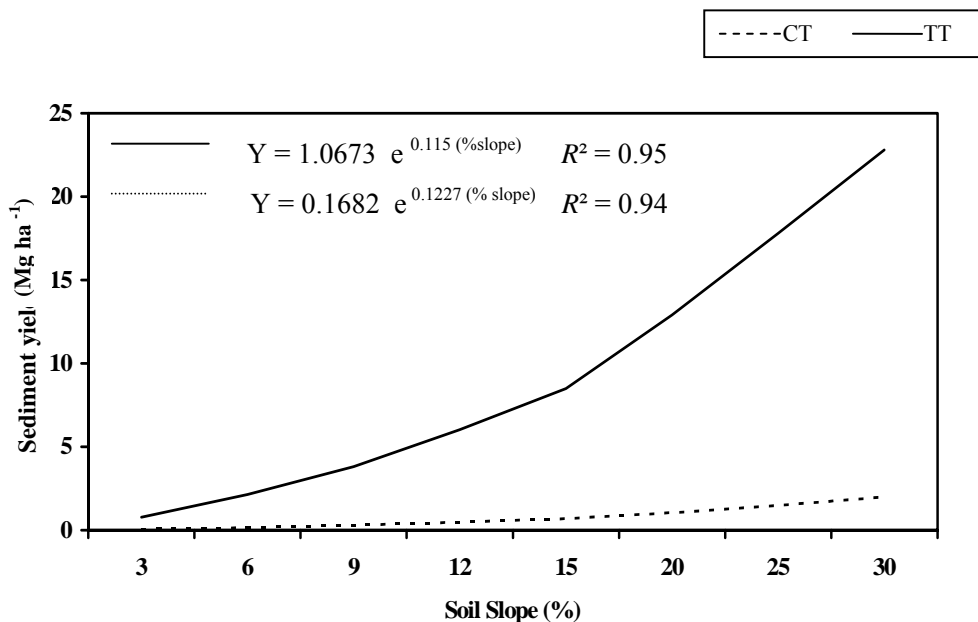


Fig. 10-8. Effect of soil slope on sediment yields in two soil managements simulated with GLEAMS for Lake of Patzcuaro watershed.

DSS model simulation

The average annual values for each decision criterion were determined for 18 yr with the GLEAMS model simulation (Table 10-14). The time series simulations of Sy and Q , runoff and net returns were underestimated for both treatments. However, long-term CT with soil residue cover estimations was better than the other soil management system, mainly in Sy . Simulation results for CT system were near to observed values. Values of underestimation were 50% for Sy and Q , while net benefits were two to ten times below the observed values. Nevertheless,

conventional tillage under 18 yr of simulation of net benefits represents the actual profits of the regional farmer based on the average regional grain yield of 1.1 Mg ha^{-1} (INEGI, 1991).

Table 10-14. Average annual values of 18-year simulation with the DSS model.

Treatment	Net benefits US \$ ha^{-1}	Sediment. Yield Mg ha^{-1}	Runoff cm
Traditional tillage (TT)	26.10	1.53	4.28
Conservation tillage (CT)	64.50	0.13	0.78

Homogeneous underestimation could lead to Sy and Q estimations that are lower than the actual values for TT treatment, but for CT treatment there is not such a situation because the model predicted better estimates of 1.5 t/ha and observed 3.2 Mg ha^{-1} Sy outputs. TT agricultural systems are the major danger to lake sedimentation. Long-term simulation results indicated that TT remained as the main source of particle outputs. O'Hara et al. (1993) estimate that up to 40% of the soil eroded in the watershed eventually reaches the lake. The 1.5-3.5 t/ha of soil erosion seems to be low compared with 5.7 t/ha obtained in other volcanic soils of Mexico (Solano et al. 1990).

Also, there is a clear difference between TT and CT in Sy simulations. The effect of soil residue cover is critical to reduce sediment losses. CT achieved the same Sy outputs (0.30 Mg ha^{-1}) reported for the pre-Hispanic age (O'Hara et al. 1993).

Effects of Alternative Systems

Net benefits (NB) as a decision variable would be ranked higher than the other variables by most regional farmers. To reflect the preferences of farmers, in the order of importance of decision variables, NB was defined as the most important decision variable (Fig. 10-9). In this scenario, the average composite score of CT treatment was higher than that of the conventional one. CT consistently scored higher than TT. The main effect that farmers seek by tillage is to maximize net profits, but it appears that no-tillage can increase crop yields and at the same time reduce erosion and offsite damages.

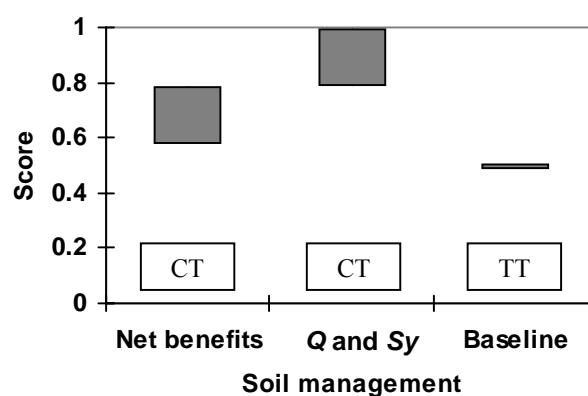


Fig. 10-9. Score index and ranking of soil management alternatives from farmer's point of view and runoff (Q) and sediment yields (Sy).

There was no difference in the ranking when greater importance was placed on sediment yield and runoff; the CT alternative was ranked above TT. The outcome using the importance order 2 was similar to farmer's importance order. The best and worst composite scores for TT system were both 0.5 because this practice scored 0.5 for all criteria. In the CT treatment, there was a 20% difference in best scores of net benefits with respect to runoff and sediment yields. The length of the bars reflects the sensitivity of the outcome to the possible weighting vectors consistent with the importance order. Major reliability for these outcomes is the measured data from experimental plots, according to Lawrence (1997). This means that the performance of the model in long-term simulations was able to separate both management alternatives, according to experimental field information utilized to feed the DSS model.

Erosion Simulation with GIS

The selected image used with the combination of bands 3, 4, and 5 in the supervised classification allowed us to easily distinguish forest, agricultural, and water body covers. The image information was completed with field and agricultural cycle knowledge for inferring possible soil cover. In the same image, a vector was digitized to separate different soil covers from training field information (Fig. 10-10). The spectral signature of each soil cover was displayed for the separation of features. Wide separation of these cover signatures means best classification results (Chuvieco, 1986).

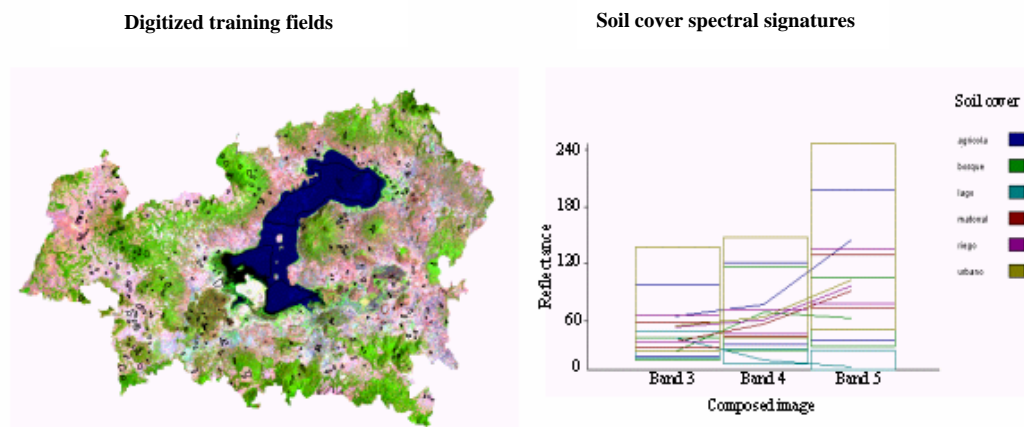


Fig.10-10. Composite image with digitized training fields and spectral signatures for the supervised classification.

Later assignation of these training fields to the whole image yielded a classified image under the maximum likelihood method (Table 10-15). Values of agricultural land were similar to those reported by Gomez (1994), but values of forest, water surface, and shrubs increased.

Table 10-15. Soil covers delimited by supervised classification in the Lake of Patzcuaro watershed.

Cluster	Soil use	Delimited area km ²	Reported area [†] km ²
1	Rainfed agriculture	336.7	359.6
2	Forest	205.3	280.1
3	Shrub and rangeland	195.9	137.4
4	Water body	80.5	125.5
5	Urban	100.9	-

[†] Source: Gomez (1994).

When the erosion equation was applied to the classified image, it clearly marked the spatial distribution and the quantification of sediment outputs from agricultural lands (Fig. 10-11). Unfortunately, agricultural lands along the lakeshore are a massive source of sediment outputs. However, conservation tillage shows less color intensity than TT in the same areas. This means that sediment outputs are less in CT than in TT (Fig. 10-11).

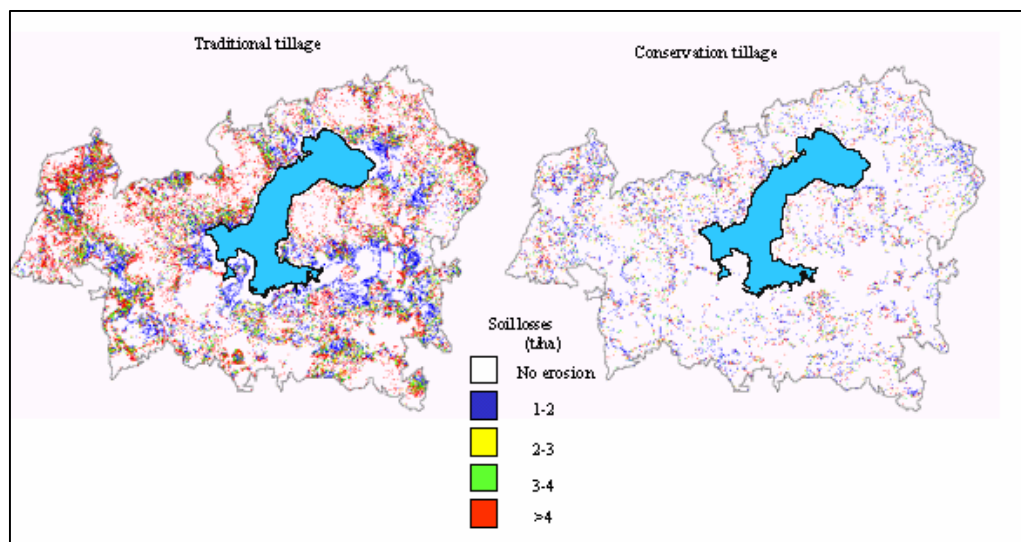


Fig. 10-11. Supervised classification of ranges of soil losses from agricultural lands in two soil management systems.

Sediment output distribution was also reduced in CT; thus, a lesser area is under erosion. In both treatments, the main erosion sources are found in the northern and eastern parts of the watershed. The erosion ranges for CT and TT and damaged surface show that no erosion area is larger in CT (84,452 ha) than in TT (67,679 ha) (Table 10-16). Erosion under CT is higher (with 16,000 ha) than in TT. Current system production (TT) affects 26.4 % of the watershed with a mean of 6.9 Mg ha^{-1} , while CT affects 8.1% of the watershed, and yields only 1.3 Mg ha^{-1} . This amount (1.3 Mg ha^{-1}) is 72% lower than the maximum permissible erosion for this kind of soils (Colegio de Postgraduados, 1991), but 6.9 Mg ha^{-1} is 383% higher.

Table 10-16. Affected soil surface by range of erosion for two management systems under supervised classification.

Soil losses Mg ha ⁻¹	Treatment	
	Traditional tillage Ha	Conservation tillage ha
0	67,679	84,452
1-2	7815	3504
2-3	3499	1374
3-4	3091	724
>4	9861	1892
Mean Mg ha⁻¹	6.9	1.3

The advantage of this supervised classification method is that the information obtained is reliable due to the correction done in the image based on field information recorded accurately (Eastman, 1992). Differences among soil covers are caused by the continuous soil use changes provoked by human activity.

Soil Management Sustainability

Microbial biomass was evaluated in the two management systems (CT and TT). Biomass concentration was higher in CT than in TT, with significant differences in the second layer (Table 10-17). In the upper soil layer, biomass ranged from 350 to 431 mg kg⁻¹ of soil, which is related to a higher activity of plants, weeds and insects (Powlson et al. 1987; Doran and Parkin, 1994). However, the deepest microbial biomass was found in CT (351 mg kg⁻¹ of soil), which may hold better soil conditions compared to TT, with only 50% of microbial biomass (156 mg kg⁻¹ of soil). These soil changes could improve soil structure and give higher permeability to withstand soil erosion and sediment transportation.

Table 10-17. Soil sustainability indicators in two tillage systems.

Treatment	Microbial biomass		Runoff water	
	0-5 cm	5-12 cm	OM	N-NO ₃
	mg C kg ⁻¹ soil		kg ha ⁻¹	
CT	429 a	351 a	3.3 a	6.2 a
TT	351 a	156 b	131.2 b	15.2 b

Values with same letter are statistically equal $p \leq 0.05$.

Nitrogen and organic matter losses were related to soil fertility. CT reduced by 2% and 40% the losses of organic matter and N-NO₃, respectively. Annual losses of organic matter in TT reached until 131.2 kg ha⁻¹ while losses of N-NO₃ were 15.2 kg ha⁻¹. Organic matter provides soil structure and better infiltration rates (Bauer and Black, 1994).

After four years (1996-1999) of continuous soil management with TT and CT systems, organic matter in CT increased in the upper layer (Table 10-18). During the first year (1996), organic matter was similar in both treatments (around 23 g kg⁻¹ soil), but in 1999, TT reduced its level by 12%, while CT increased it by 90% (43 g kg⁻¹ soil). However, organic matter diminished with soil depth in both treatments. The deepest layers had only 10% of the upper layer in CT (4 g kg⁻¹ soil) and 80% in TT (16 g kg⁻¹ soil). These values in CT are consistent with those reported by Follett and Schimel (1989), who found sudden reductions in organic matter in deep soil layers.

Table 10-18. Organic matter content (g kg⁻¹ soil) in two soil management systems.

Soil organic matter		Management system	
Depth (cm)	Year	Conservation tillage	Traditional tillage
0-5	1996	23.7 a	23.0 a
	1999	43.1 a	20.1 b
5-10	1996	19.1 a	19.7 a
	1999	16.7 a	14.3 a
10-15	1996	18.1 a	19.1 a
	1999	13.4 a	4.7 b
15-20	1996	20.4 a	21.4 a
	1999	4.7 b	16.7 a

Values with same letter are statistically equal $p \leq 0.05$.

CONCLUSIONS

Permanent dredging and restoration programs in the Lake of Patzcuaro will not have the desired effect if the sources of detachment of soil particles that cause soil erosion and sedimentation are not prevented, located, and quantified. The severity of erosion hazards imposed by cropping in steep hillslopes of the Patzcuaro watershed has been the main cause of a continuous process of depletion of local soil and water resources. Building soil conservation structures, such as checkdams, to reclaim the lake became a temporary solution to the problem. Deforestation and human activities can hardly be ended, but conservation tillage agriculture can be used and upgraded to reduce sediment outputs and pollutants from agricultural uplands of this watershed, in which corn has been grown for more than 3500 years. The conservation tillage systems evaluated in this study showed a greater impact in reducing soil erosion (>80%) and runoff (>45%) than traditional or current tillage systems that turn over the soil in hill slopes.

GLEAMS adequately predicted runoff and sediment yields from cultivated fields for a range of slope steepness. However, responses for sediment yields were much better than for runoff outputs. For the calibration stage, the model efficiency index (E) ranged from -7.2 to 0.99 for runoff and from 0.77 to 0.99 for sediment yields, indicating the advantage of GLEAMS estimates in assessing the seasonal sediment yields over the observed mean of seasonal sediments.

Rainfall simulations showed differences in runoff (TT = 69.9 mm, CT = 25.9 mm) and production of sediments in each treatment (TT = 3.61 g s⁻¹ m⁻², CT = 0.008 g s⁻¹ m⁻²). The contribution of each tillage treatment could be quantified in terms of erosion parameters, like erodibility coefficients among rills (K_t = 1,262,608 and 2,552 kg s⁻¹ m⁻⁴ for TT and CT, respectively), within rills (K_r = 0.08 and 0.0002 s⁻¹ m⁻¹ for TT and CT %, respectively) and hydraulic conductivity parameter (K_s > 60.4 and <50 mm h⁻¹ for TT and CT, respectively). This allowed making comparisons among magnitudes of the evaluated parameters as well as knowing what causes the conventional treatment to produce high rates of runoff and sediment.

The simulation with GIS allowed us to learn about the severity of soil erosion in the watershed, where more than 26,000 ha are a source of sediments with a mean of 6.9 Mg ha⁻¹ yr⁻¹. The simulation offers a way to locate, calculate and inhibit soil erosion and sediment outputs. Finally, the sustainability soil indicators indicated that CT held and increased microbian biomass by 18% with 450 g kg⁻¹ soil, while TT yielded only 370 g kg⁻¹ soil.

REFERENCES

- Alcala, M.J., S.C.A. Ortiz, and C.M.C. Gutierrez. 2002. Clasificacion de suelos de la meseta Tarasca, Michoacan. (In Spanish, with English abstract.) *Terra* 19:227-239.
- Bauer, A., and A.L. Black. 1994. Quantification of the effect of soil organic matter content of soil productivity. *Soil Sci. Soc. Am. J.* 58:185-193.
- Chuvieco, E. 1986. Fundamentos de teledeteccion espacial. Ediciones RIALP S.A., Madrid, Spain.
- Colegio de Postgraduados. 1991. Manual de conservacion del suelo y del agua. CP, Chapingo, Mexico.
- Davies, F.M., R.A. Leonard, and WG. Knisel. 1990. GLEAMS, user's manual v.1.8.55. USDA-ARS, SWRL, Tifton, GA.
- Doran, W.J., and T.B. Parkin. 1994. Defining and assessing soil quality. p. 3-21. *In* Defining soil quality for a sustainable environment. Spec. Publ. 35. SSSA, Purdue, IN.
- Eastman, R.J. 1992. IDRISI user's guide. Clark University, Worcester, MA.
- Elliot, J.W., A.N. Liebenov, J.M. Laflen, and K.D. Khol. 1989. A compendium of soil erodibility data from WEPP cropland soil field erodibility experiments 1987-88. NSERL Report 3. Ohio State University-USDA-ARS, Purdue, IN.
- Follet, R.F., and D.S. Shimel. 1989. Effect of tillage practices on microbial biomass dynamics. *Soil Sci. Soc. Am. J.* 53:1091-1096.
- Gomez, T.A. 1994. Tres niveles de erosión en la cuenca de Patzcuaro, Mich., como base para acciones y obras de conservación. (In Spanish, with English abstract) Folleto Tecnico 26. INIFAP-SARH, Uruapan, Michoacan, Mexico.
- Haan, T.C., Barfield, B.J., Hayes, J.C. 1994. Design hydrology and sedimentology for small catchments. Academic Press, San Diego, CA.
- Hernandez, M., P. Heilman, L.J. Lane, J.L. Oropeza M., and H.M. Arias R. 1995. Evaluating land management system effects on tepetate lands in central Mexico with a decision support system. p. 571-583. *In* S.A. El-Swaify (ed.) Multiple objective decision making for land water and environmental management. Lewis Pub., Washington, D.C.
- Hillel, D. 1980. Applications of soil physics. Academic Press, NY.
- Instituto Nacional de Estadistica Geografia e Informatica. 1991. VII Censo Agropecuario. Base de Datos CD. SPP, INEGI, Aguascalientes, Mexico.
- Jasso, C.C. 1997. Efecto de la labranza en la estructura del suelo y su relacion con el rendimiento de los cultivos. (In Spanish, with English abstract) p. 215-225. *In* Avances de investigacion en labranza de conservación. Libro Tecnico 1. INIFAP, Morelia, Michoacan, Mexico.
- Jenkinson, D.S., and D.S. Powlson. 1976. The effects of biocidal treatments on metabolism in soil. A method for measuring soil biomass. *Soil Biol. Biochem.* 8:209-213.
- Lane, L., J.J. Stone and D.S. Yakowitz. 1994. A multiple objective decision support system for the USDA water quality initiative. User's manual. USDA-SWRC, Tucson, AZ.
- Lawrence, P.A., J.J. Stone, P. Heilman, and L.J. Lane. 1997. Using measured data and expert opinion in a multiple objective decision support system for semi-arid rangelands. *Trans. ASAE* 40(6):1589-1597.
- McAuliffe, J., P.C. Sundt, A. Valiente-Banuet, A. Casas, and J.L. Viveros. 2001. Pre-columbian soil erosion, persistent ecological changes, and collapse of a subsistence agricultural

- economy in the semi-arid Tehuacan Valley, Mexico's 'Cradle of Maize'. *J. Arid Environ.* 47(1):47-75.
- Meyer L.D. and W.C. Harmon. 1992. Soil erosion varies during the crop year. *Trans. ASAE.* 35(2):459-464.
- Midwest Agricultural Research Associates. 1988. User's manual – Cost and return estimator. USDA-Soil Conservation Service, Contract No. 54-6526-7-268. Tucson, AZ.
- Miller, W.P. 1987. A solenoid-operated, variable intensity rainfall simulator. *Soil Sci. Am. J.* 51:832-834.
- Norton, L.D., and L.C. Brown, 1992. Time-effect on water erosion for ridge tillage. *Trans. ASAE* 35(2):473-478.
- O'Hara, S.L., F.A. Street, and T.P. Burt. 1993. Accelerated soil erosion around a Mexican highland lake caused by prehispanic agriculture. *Nature* 362:48-51.
- Powlson, D.S., P.C. Brooks, and B.T. Christensen. 1987. Measurement of soil microbial biomass provides an early indicator of changes in total soil organic matter due to straw incorporation. *Soil Biol. Biochem.* 19:159-164.
- Rhoton, F.E., M.J. Shipitalo, and D.L Linbo. 2002. Runoff and soil loss from midwestern and southeastern US silt loam soils as affected by tillage practice and soil organic matter content. *Soil Tillage Res.* 66(1):1-11
- Santos, L.E. 1995. Cuantificacion de la erosión hidrica bajo diferentes coberturas vegetales en un andosol en Patzcuaro, Mich. Tesis Profesional. UACH., Chapingo, Mexico.
- Sauer, T.J. and T.C. Daniel. 1987. Effect of tillage system on runoff losses of surface-applied pesticides. *Soil Sci. Soc. Am. J.* 51:410-415.
- Simmanton, J.R., K.G. Renard, and N.G. Sutter. 1973. Procedure for identifying parameters affecting storm runoff volumes in a semiarid environment. ARS-USDA. AGR-101. Berkeley, CA.
- Simmanton, J.R., C.W. Johnson, J.W. Nyhan, and E.M. Rommey. 1988. Rainfall simulation on rangeland erosion plots. p. 11-17. In Proc. Rainfall Simulator Workshop, Tucson AZ. USDA-ARS, Tucson, AZ.
- Solano de la Sala, T.J.A., M.M. Martínez, M.G. Anaya, and J.L.M. Oropeza. 1990. Efecto de la relación precipitación escorrentía en el proceso erosivo en diferentes usos del suelo en la cuenca del río Texcoco. (In Spanish, with English abstract.) Agrociencia serie Agua-Suelo-Clima. 1(3):25-44.
- Tapia, V. M.L Tiscareño, M.J.Oropeza, and S.B. Figueroa. 1999. Protección de suelos de ladera y erosión hidrica en la cuenca del lago de Patzcuaro, Michoacan. (In Spanish with English abstract.) Ingenieria Hidraulica en Mexico. 15(3):55-64.
- Tiscareño, M.L, A. Baez-Gonzalez,, M. V. Velasquez, K.N., Potter, J.J., Stone, M.V. Tapia, and A.R. Claveran, 1999. Agricultural research for watershed restoration in Central Mexico. *J. Soil Water Conserv.* 54:686-692.
- Tiscareño L.M., A.D. Baez G., M. Velasquez V., R. Claveran A., K. N. Potter, J.J. Stone. 2001. Estudio de caso: Labranza de conservacion para salvar el lago de Patzcuaro. In R. Claveran and F. Rulfo V. (ed.) Productividad y conservacion: Suelo y agua. Libro Tecnico 2. INIFAP, Michoacan, Mexico.
- Toledo, V., I.P. Alvarez, and P. Avila. 1992. Plan Patzcuaro 2000. Fund. Fiedrich Ebert, Mexico, D.F., Mexico.

- Villar, S.B., S.B., Figueroa, M.J., Oropeza, P.L., Landois, y H.V. Volke. 1999. Erosionabilidad de suelos y su impacto en la productividad del maiz en el tropico Mexicano. (In Spanish, with English abstract.) Agrociencia 32:199-208.
- Yakowitz, D.S., J.J. Stone, L.J Lane, P. Heilman, J. Masterson, J. Abolt, and B. Imam. 1993. A decision support system for evaluating the effects of alternative farm management systems on water quality and economics. Water Sci. Tech. 28(3-5):47-54.

CHAPTER 11

Alternative Approaches for Land Use Identification Systems Using Remote Sensing

J. German Flores-Garnica and Fabian Islas-Gutierrez

CONTENTS

Introduction	189
Pixel-Based Classification	191
Traditional Approach	193
Supervised Classification	193
Unsupervised Classification	193
Mixed Classification	194
Classification with Ancillary Data	195
Parametric Approach	196
Non-Parametric Approach	197
Spatial Analysis Methods	200
Spatial Resolution	200
Parcel-Based Classification	201
Pattern	202
Shape	203
Discussion and Conclusions	203
References	207

INTRODUCTION

Land use/cover classification, a key application of remote sensing (Carmel and Kadmon, 1998), is the process of creating thematic maps from satellite imagery. Some authors like Bauer and Steinnocher (2001) consider land use/cover classification as the main objective of satellite image processing for planning purposes. Land use/cover classification can be used to understand

the spatial behavior of a given phenomenon (Blaschke and Strobl, 2001). It is important to many organizations for many reasons, such as the constantly increasing pressure to produce better information at reduced costs (Moisen and Edwards, 1999). The following are some examples of the use of land use/cover classification: 1) defining fire burn severity in our forests; 2) classifying land use on our farms; 3) using accurate GIS data in order to make educated policy decisions; and 4) guiding organizational strategies (Visual Learning Systems, 2002). Another purpose of land use/cover classification is helping predict the dynamic changes of land use. In this sense, remotely sensed land use/cover classification has become the most credible, rapid, and effective way to monitor the conditions and changing of landscape at many scales (Luo and Hui, 1999).

Classification is a method by which categories or class identifiers are attached to the pixel, making a remotely sensed image on the basis of their characteristics (Pal and Mather, 2001). The task of land use/cover classification is a typical problem of pattern recognition where the goal is to map land use/cover from satellite images (EUROSTAT, 1995). In a land use/cover classification process, an expert tends to mirror, elucidate, quantify, and describe surface patterns (Blaschke and Strobl, 2001). Conventional land use/cover classification methods that use remote sensing mainly include traditional classification, neural network based classification, and logical reasoning classification methods based on symbolic knowledge (Luo and Hui, 1999).

When classifying land use/cover categories from aerial photos, an expert interprets mentally many factors and concepts from the image. His visual capabilities allow him to recognize and evaluate a number of characteristics in order to identify what he sees in a photograph. These image characteristics include texture, shape, pattern, size, color (tone), shadow, and association (Avery and Berlin, 1992) (Fig. 11-1).

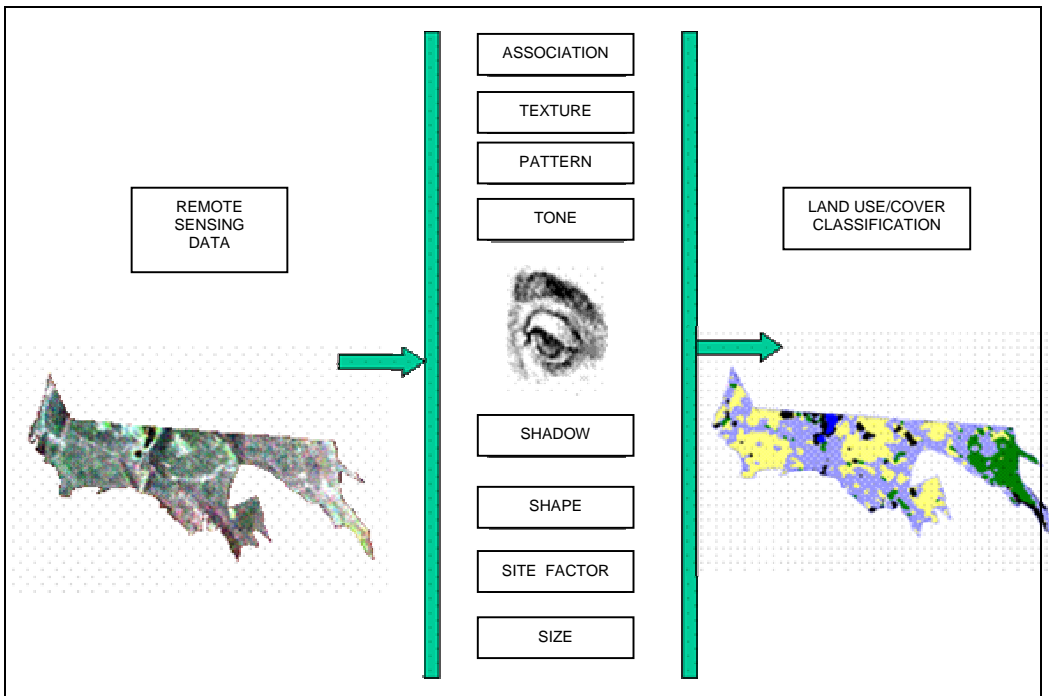


Fig. 11-1. Image characteristics considered by an expert classifier in order to define land use/cover classes from an image.

It would be ideal to have a "special software" that could classify a satellite image according to the land use/cover classes that are present on the ground, based on all these characteristics. However, this is still a dream. Although the recognition of such characteristics is relatively simple for a well-trained eye, its translation into computer algorithms is one of the most important challenges that remote sensing scientists currently face. Furthermore, this recognition would be just part of the solution because the goal in remote-sensing data processing is getting information classified into classes, such as grasslands, urban areas, deciduous tree, evergreen trees, and crops (Shine and Wakefield, 1999).

Remotely sensed data are analyzed mainly with the help of software systems that employ the multi-channel properties of satellite image data and are built on multivariate statistical approaches and GIS-type operations (Zamperoni, 1989; Jaehne, 1989). During the last 20 years, most of the classifications have been based on per-pixel spectral analysis. Throughout this period, scientists have been trying to develop alternative strategies. Eventually, it was found that a classification could be improved using ancillary data. This perspective has led to the development of various algorithms. However, per-pixel spectral information is still considered. Also, with the inclusion of more image characteristics, such as the ones mentioned earlier (e.g., texture and shape), the resulting algorithms proved to be computationally highly complicated. Currently, with the increase of computer capabilities, it is possible to develop and test various algorithms under the per-parcel approach, which considers not only the information provided by a single pixel but also the information generated by surrounding pixels. Now, image characteristics such as texture can be included in the classification procedure. This approach has been a "quantum leap" in the history of remote sensing imagery classification; it is remarkable because the new procedures tend to be as automatized as possible. In this automatization process, scientists look for algorithms that have these characteristics: speed, accuracy, simplicity, power, automation, and innovation (Visual Learning Systems, 2002).

The purpose of this chapter is to summarize two general approaches to the use of remote sensing imagery in the land use/cover classification process. However, our intention is not to discuss fully the theory of the described methods; rather, it is to give a framework that allows us to understand the perspective and sequence of some of the most used techniques.

PIXEL-BASED CLASSIFICATION

Several methods have been generated for extracting land use/cover information from remote sensing data by performing multi-spectral classification on the electromagnetic spectrum. Traditionally, most of the remote sensing data classification studies have been based on a single variable or several spectral variables (Dai, 2003). Although there have been considerable technical improvements, such as hyperspectral imagery or higher resolutions, most of the land use/cover classification studies are still based on the spectral information of each pixel (as an individual entity). This means that classification algorithms only consider, for instance, the percentage of reflectance of each pixel as the grouping criterion. In this section we discuss some of the traditional techniques under the per-pixel approach.

As mentioned earlier, technical improvements, such as satellite and computer techniques, have enabled scientists to work not only with three or seven bands, but also with a wider range of spectral classes. It is believed that the more bands, the better the classification. However, in

practice, the use of hyperspectral information has some problems, such as the calibration of the electromagnetic range represented by each band.

Current technology has resulted in a series of high-resolution remote-sensing products, which could be very helpful tools in the land use/cover classification process. However, this increase in resolution is accompanied by an increase in the spectral variability. Obviously, this variability makes the pixel grouping for classification purposes difficult.

Figure 11-2 shows the alternative sequences that could be followed when classifying land use/cover remote sensing data. It is important to point out that there is no single procedure that can be used for land use/cover classification in all possible situations. Therefore, the search for the best algorithm is an iterative process, which gives an artistic touch to imagery classification.

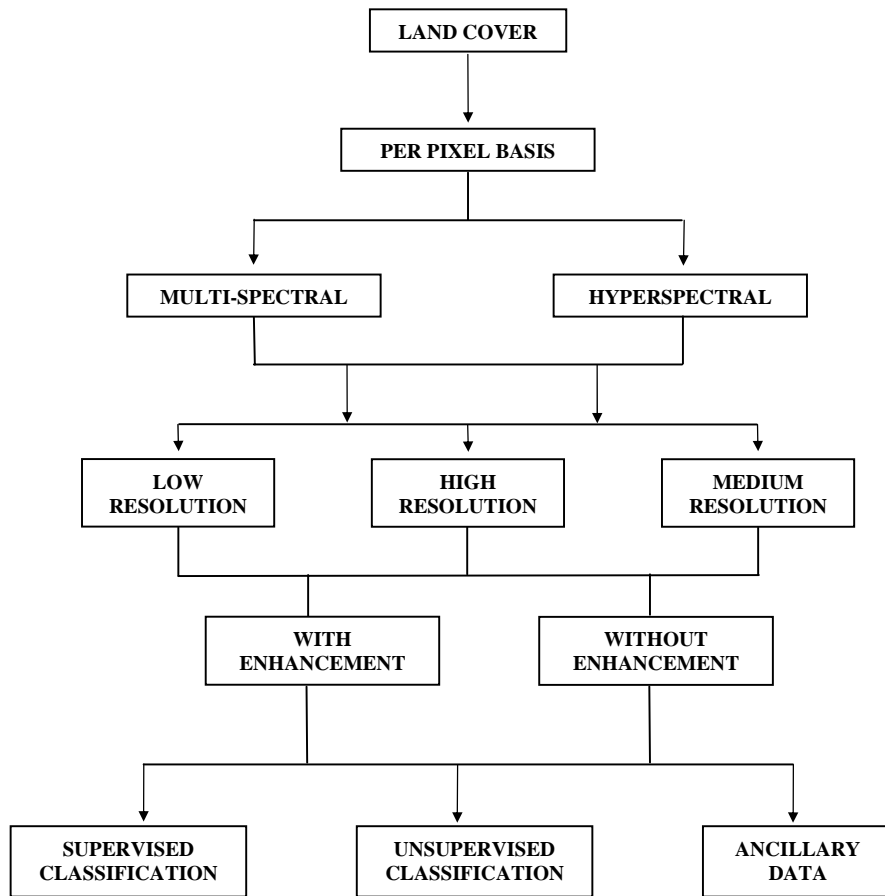


Fig. 11-2. Sequence of the land use/cover classification process of remote-sensing data using the per-pixel approach.

Traditional Approach

There are two traditional statistical approaches for land use/cover classification using remote sensing data (Lab of Landscape Ecology and Conservation Biology, 2002): 1) unsupervised and 2) supervised. In both, the task is focused mostly on two main processes: transformation and interpretation of spectral information classes of remote sensing data into land use/cover categories. The latter is performed by analysts based on their experience and knowledge of predefined land use/cover classification schemes (Dai, 2003). Mathematical and statistical analysis models are key aspects of unsupervised classification. Some of the most used methods are Iterative Self-Organizing Data Analysis Techniques (ISODATA), minimum distance methods, and maximum likelihood classification, which are based on parametric and non-parametric statistical distribution models (Luo and Hui, 1999). Assuming that data are normally distributed, both supervised and unsupervised classification approaches are based on partial data (samples or training areas). In many cases their use has resulted in an acceptable accuracy. In fact, in the last 20 years, supervised and unsupervised classification methods have been used in the majority of land use/cover classification analyses.

Supervised Classification

The maximum likelihood (ML) algorithm is one of the most used supervised land use/cover classification tools. The ML classifier is based on a probabilistic classification procedure, which assumes that each spectral class can be adequately described or modeled by a multivariate normal probability distribution in a featured space (Pal and Mather, 2001). Supervised classification assumes a prior knowledge of the land cover classes. The analyst attempts to locate samples of known land cover classes in the remote sensing scene. These sites should have pixels with similar spectral characteristics. The known sites are called training sites or training data because their spectral characteristics are used to train other pixel classification algorithms (Dai, 2003). The imagery is divided into training data, where categories are known, and test data. The choice of a good training set can have significant influence on the success of the classification approach.

In some cases, two or more land cover classes occur within the same pixel. For example, a pixel can be interpreted as containing 27% tropical forest and 73% croplands. Under these situations, the implementation of fuzzy logic in classification could help in extracting information from those mixed pixels (Dai, 2003).

Unsupervised Classification

Unsupervised procedures, such as ISODATA (Iterative Self-Organizing Data Analysis Techniques), are one of the most commonly used land use/cover classification methodologies involving remotely sensed data. Image classification is usually done in a process where individual pixels are clustered into groups or "spectral classes" by measuring the pixel's reflectance values. This is called cluster analysis or unsupervised classification. Cluster analysis is an exploratory data analysis tool for solving classification problems. Its objective is to sort pixels into groups, or clusters, so that the degree of association is strong between members of the same cluster and weak between members of different clusters.

Unsupervised classification is frequently enough to define an efficient land use classification from remote sensing data. Its major advantage is that it does not require prior knowledge on the identities of land use/cover categories. Pixels with similar spectral characteristics are grouped into clusters according to certain criteria, and then analysts assign labels for clusters and group them into land cover classes (Dai, 2003). Figure 11-3 shows the resulting classification of an area close to Guadalajara City (Jalisco, Mexico), which is mainly covered by forest (pine and oak). This unsupervised classification was good enough for the definition of first-level land use/cover categories. This first-level classification tends to identify and separate forest lands, croplands, and urban areas.

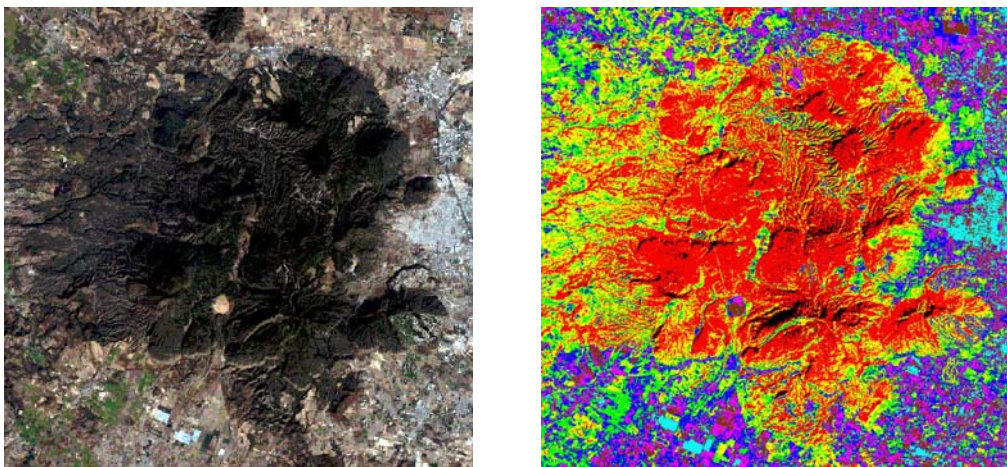


Fig. 11-3. Unsupervised land use/cover classification of an area mainly covered by forest vegetation (red), grasslands (yellow), croplands (green and purple), urban area (light blue).

Mixed Classification

Sometimes a land use/cover category is better identified through supervised classification, while another category is better classified under an unsupervised process or any other strategy. Hence, it seems logical to combine the results of two or more tested strategies. This approach is known as “mixed classification”. Some results have suggested that a mixed classification could be used to generate a better land use/cover classification (Chuvieco and Congalton, 1989). Flores and Omi (2003) report that in a fuel models mapping study, they used a mixed classification approach which considers the best classification results of both supervised and unsupervised strategies. Their study considered the following land use/cover classes: 1) Water, 2) No-Forest, 3) Fuel Model 10, 4) Fuel Model 9, and 5) Fuel Model 8. Supervised classification was better when classifying the first two classes, while unsupervised classification was better for the other classes. The mixed classification (Fig. 11-4) resulted in an average accuracy of 74.9%.

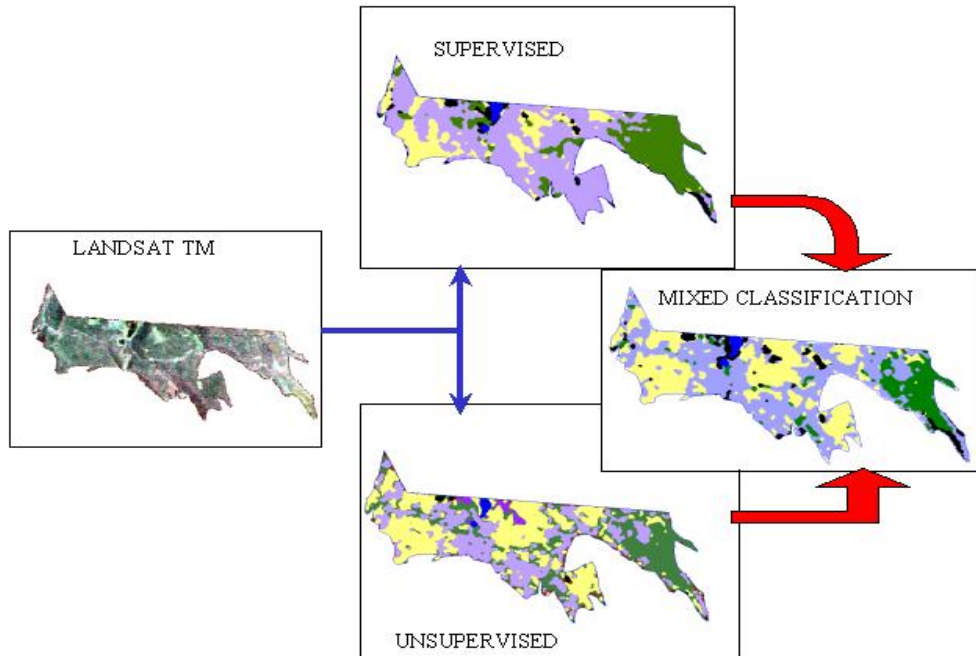
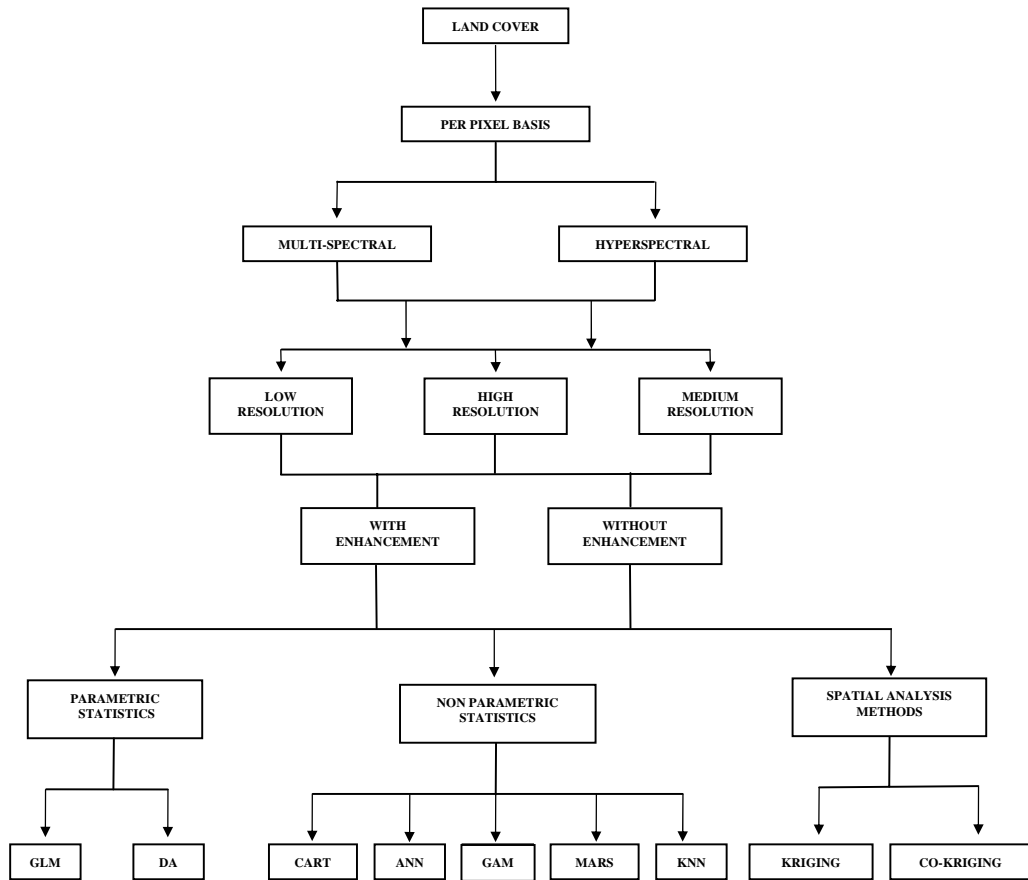


Fig. 11-4. Illustration of a mixed classification process in a study of fuel models mapping based on a satellite image (Landsat TM).

Classification with Ancillary Data

With the purpose of reducing the costs of land use/cover classification procedures, several strategies that merge satellite-based information with ground-based information have been tested (Moisen and Edwards 1999) (Fig. 11-5). The use of secondary data has also been one of the strategies to improve land use/cover classification. The objective is to analyze data of a given variable (e.g., several bands of visual satellite image data) to distinguish properties of a second variable (e.g., soil types and agricultural land-use forms) (Herzfeld, 1999). Incorporating ancillary data, such as weather, soil, altitude, aspect, etc., has resulted in an improved classification process. The information can be incorporated before, during, or after classification through geographical stratification, classifier operations, and post-classification sorting (Dai, 2003). Inexpensive maps can be produced by modeling land use/cover classes as a function of satellite-based information. Some examples of these techniques include linear models (LMs), generalized additive models (GAMs), classification and regression trees (CARTs), multivariate adaptive regression splines (MARS), and artificial neural networks (ANNs) (Moisen and Frescino, 2001).



GLM: Generalized linear model, **GAM:** Generalized additive models, **DA:** Discriminant analysis, **MARS:** Multivariate adaptor regression spline, **CART:** Classification and regression trees, **K-NN:** K-Nearest neighbor, **ANN:** Artificial neural network analysis

Fig. 11-5. Sequence of some of the methods used to include ancillary data when classifying land use/cover classes.

Parametric Approach

Linear regression derives the correlation between one group of image pixel values and a known structural parameter (samples). Then, it predicts values for the parameter in places where the parameter is not known (EUROSTAT, 1995). Linear regression methods require a linear relationship between the predicted parameter and independent variables (Lab of Landscape Ecology and Conservation Biology, 2002). Discriminant analysis is an example of this approach. This is based upon two main assumptions. The first assumption is that the distributions of all independent variables are normal (Gaussian); this encourages the use of continuous rather than discrete data in the predictive model. The second assumption, which applies only to linear analysis, is that the covariance matrixes for the different groups of observations are assumed to be equal (homoscedasticity) (Marzban et al., 1997).

Another example is the generalized linear models (GLM), which have been an important statistical development for the advancement in regression analysis (Guisan et al., 2002). GLMs are mathematical extensions of linear models that do not force data into unnatural scales, and thereby allow non-linearity and non-constant variance structures in the data (Hastie and Tibshirani, 1990). Unlike classical linear models, which presuppose a Gaussian distribution and an identity link, the distribution of a variable response in GLMs may be any exponential family distribution (Guisan et al., 2002).

Non-Parametric Approach

The non-parametric property means that non-normal, non-homogeneous and noisy data sets can be handled as well as non-linear relations between features and classes, missing values, and both numeric and categorical inputs (Quinlan, 1993). Classification and regression trees (CART), artificial neural networks (ANN), and K-nearest neighbor (KNN) use non-parametric statistical methods to create a classifier for land use/cover. In the traditional classifying approach, a common set of features is used jointly in a single decision step. An alternative approach is using a multistage or sequential hierarchical decision scheme, which allows class label rejection at intermediate stages. By this way, CART offers an effective implementation of such hierarchical classifiers (Pal and Mather, 2001).

Recently, CART, also known as recursive partitioning regression, has received more attention from land use/cover classifiers. CARTs subdivide the space spanned by the predictor variables into regions, for which the values of the variable response are approximately equal, and then estimate the variable response by a constant in each of these regions (Moisen and Frescino, 2001) (Fig. 11-6).

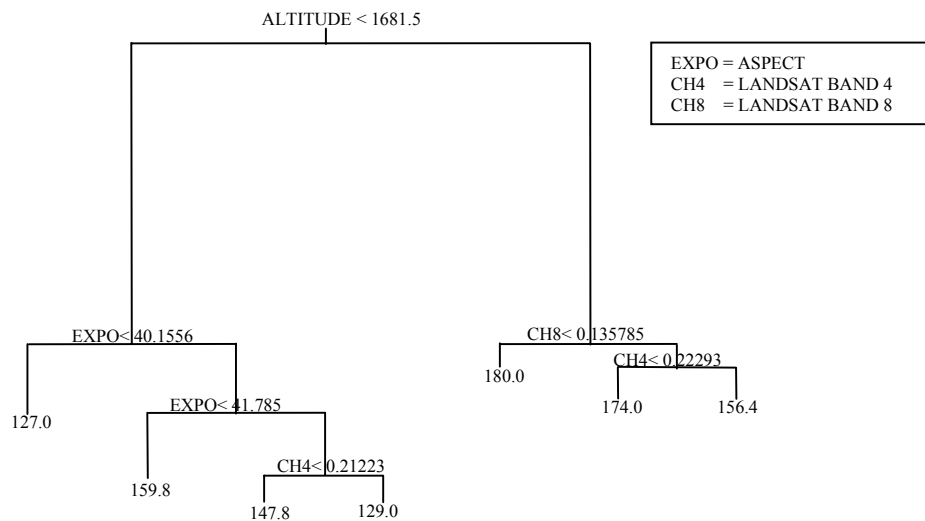


Fig. 11-6. Example of a “tree” resulting from a regression tree process, where evaporation was modeled as a dependent variable, with altitude, slope, aspect, and Landsat TM bands as independent variables.

The tree is called a classification tree if the variable response is qualitative and regression tree if the variable response is quantitative. Very few studies have assessed the use of decision trees as classifiers. However, this technique has substantial advantages for solving remote sensing classification problems due to their non-parametric nature, simplicity, robustness with respect to non-linear and noisy relations among input features and class labels, and their computational efficiency (Pal and Mather, 2001). Figure 11-7 shows an example of CART classification, based on the information of more than 13,000 reference sites. These sites were used to characterize the environmental conditions of different land use/cover classes. Among the ancillary data used in this project were 1) Landsat imagery, 2) Digital Elevation Model, and 3) climate maps. The resulting map is one of the first attempts to use CART to make a land use/cover classification at state level in Mexico. Figure 11-7 illustrates the spatial distribution of 26 land use/cover categories all over the state of Jalisco, Mexico, which represents an approximate area of 8 million ha.

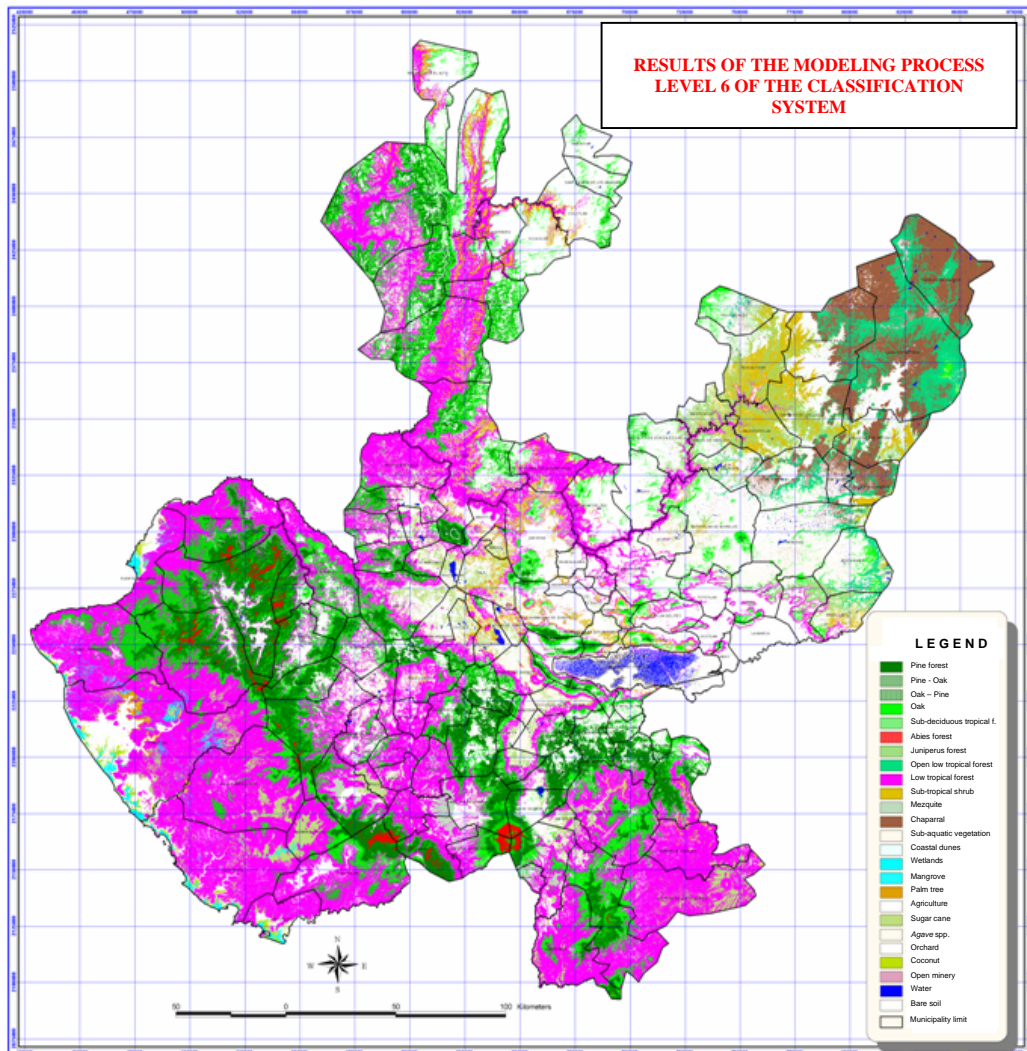


Fig. 11-7. Land use/cover classification at state level (Jalisco, Mexico), based on CART strategy, that represents 26 categories in an area of approximately 8 million ha.

Multivariate adaptive regression splines (MARS) is a flexible non-parametric regression method that generalizes the piecewise constant functions of CARTs to continuous functions by fitting multivariate splines in the regions and matching up the values at the boundaries of the regions (Moisen and Frescino, 2001). Nonlinear modeling techniques have recently become one of the major tools for land use/cover classification. Generalized additive models (GAMs) and MARS use nonlinear mathematical tools to model complex relationships between remote sensing data. GAMs are data-driven regression models that predict the value of non-linear variable response as a linear combination of non-linear functions. This kind of modeling does not require the pre-assumption of a model form and can effectively model the complex non-linear and non-Gaussian response curves, including multi-modal and asymmetric functions (Bara, 1994).

When supervised methods are used, their performances depend on how well the data match the pre-defined model. If the data are complex in structure, modeling the data in an appropriate way can become a real problem. In this case, non-parametric classification techniques such as artificial neural networks (ANN) are increasingly used (Pal and Mather, 2001). In other words, in complicated pattern recognition, a system-level view is required. Individual ANNs are seen as components in a larger satellite image analyzing system (EUROSTAT, 1995) where data diversity is large (Moshou et al. 2001). Recently, remote sensing classification methods have been based on ANN. This is because of the potentialities offered by this approach to provide "soft classifications" that are necessary to manage uncertainties, such as "mixed" pixels contained in remote-sensing data (Giacinto and Roli, 1997). Compared to statistical models, ANNs represent a relatively new approach to developing predictive models.

ANN models use design principles similar to the information-processing system of the human brain (Bharath and Drosen, 1993). ANNs-based classification methods simulate the human vision and neural processing system to get the cognition for the remote-sensing image (Luo and Hui, 1999) (Fig. 11-8). ANN models require that several architectures and training parameters be selected prior to analysis. The optimal number of hidden layers and the number of nodes per hidden layer are generally unknown *a priori* for a specific data set, and must be empirically determined through an examination of different parameter settings (Marzban and Stumpf, 1996). Moreover, training parameters must be defined before initializing the learning algorithm used by the network (Blackard and Dean, 1999).

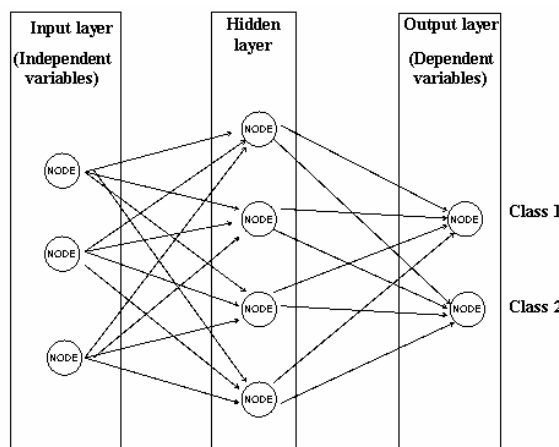


Fig. 11-8. Architecture of an artificial neural network (ANN), where lines represent connection weights (Adapted from Giroux and Dean, 2001).

Some of the approaches used for the preparation of the ANN inputs include histograms of the pixel intensities, texture parameters extracted from the image, and pixel matrixes for spatial information (Ashih, 2002). Although there is a variety of ways for constructing ANN-based models, “backpropagation networks” appear to be the most frequently used in the practice (Moisen and Frescino, 2001). This machine learning technique improves the classification accuracy of remote sensing data, according to some studies (Dai, 2003). ANN classifiers are non-parametric and, therefore, may be more robust when distribution is strongly non-Gaussian. ANN methods can generally get higher accuracy, especially in the classification of a complicated land type (Luo and Hui, 1999). They can be seen as a revolutionary new tool for different kinds of pattern recognition tasks. ANNs can utilize supervised classification procedures to classify an observation set into given mutually exclusive categories (Blackard and Dean, 1999).

Rodriguez (2000) developed an ANN to identify land cover/use in the eastern part of the state of Mexico. This model uses altitude, aspect, slope, distance to streams, geology data, edaphology data, and principal components analysis of Landsat images. With a backpropagation approach, the model showed an accuracy of 83%.

Spatial Analysis Methods

Geostatistics is a commonly used term to describe a set of techniques that model spatial variation in data and use these models to estimate or classify other data (Shine and Wakefield, 1999). Spatial data in most cases are not spatially independent; therefore, values which are spatially close show less variability than the values which are farther away from each other (Shine and Wakefield, 1999). Among the geostatistical techniques, kriging is one of the most used processes to evaluate the spatial autocorrelation of a variable. Kriging methods are based on the variogram definition, which is a spatial structure function that depends only on first-order differences, or increments, of the data considered as a realization of a stochastic process. This property is assured by the intrinsic hypothesis of these methods (Matheron, 1963). A model is fitted to match the transitive behavior typical of a regionalized variable. The advantage of geostatistical over purely mathematical algorithms is that spatial relationships are taken into account.

Spatial Resolution

Land use/cover classification had been limited in the past by the relatively coarse spatial resolution of the available data sources. However, current computer improvements have helped to enhance remote sensing technology. Spatial resolutions of satellite data have increased considerably in the last few years. Now it is possible to access information of very high spatial resolution, such as that produced by the IKONOS and Quickbird systems. This condition of higher resolution presents more alternatives for land use/cover classification. However, although for visual interpretation, a finer spatial resolution allows a better land cover classification, a new problem is created for conventional automated classification techniques. For example, due to the higher resolution of recent remote-sensing data, such as from IKONOS, an automatic or semi-automatic image detection feature based only on their spectral characteristics can become difficult (Hofmann, 2001). The reason for this is that the spectral variability of surface features increases as the spatial resolution of the sensors increases (Marceau et al, 1990) (Fig. 11-9).

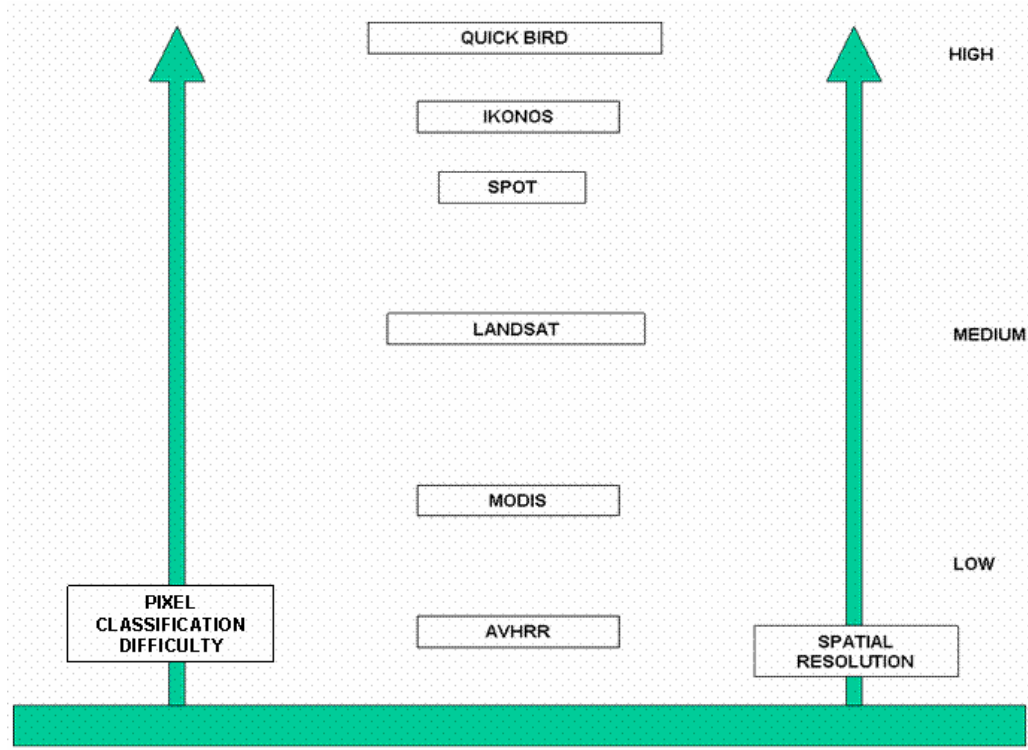


Fig. 11-9. Examples of remote sensing data sources and their corresponding relation with spatial resolution and pixel variability.

Therefore, the development of several advanced space-borne high-resolution sensors has not presented a total solution because it may decrease the classification accuracy of traditional methods on a per-pixel basis (Schiewe et al., 2001). Moreover, automated procedures to interpret high-resolution data are confronted with various problems, such as the following: 1) the lack of adequate analysis tools; 2) differentiation difficulty between features; 3) some desired map features detected only by human interpretation and knowledge (Hoffmann and Van der Vegt, 2001).

PARCEL-BASED CLASSIFICATION

Regardless of the improvements in remote sensing technology and the complexity of the various land use/cover classification algorithms, many land use/cover classifiers still continue basing their classification process on concepts developed in the 70s (Blaschke and Strobl, 2001). They still use an approach that is based on the per-pixel classification of a multi-dimensional space feature, which does not make use of any spatial concept (Blaschke and Strobl, 2001). Moreover, the pixel variability (internal) and the noise within land use classes increased (Schiewe et al. 2001). As a result of this condition, traditional classification approaches are producing too many categories or categories that are not well-defined because their clusters are built only upon spectral homogeneities (Schiewe et al. 2001). When spectral characteristics are not enough to classify land use/cover classes, the measurement of similarity level of features based on spectral

information does not guarantee the correctness of such classification (Dai, 2003). Furthermore, the most significant problem with this approach, which is usually ignored, is that a substantial proportion of the signal or reflectance apparently coming from the land area represented by a pixel comes from the surrounding pixels (Townshend et al. 2000). Therefore, semantic information necessary for image interpretation is not mostly represented in single pixels but in meaningful image objects and their mutual relations. Beyond the pure spectral information, image-objects are characterized by a number of additional features such as texture and shape which can hardly be exploited using per-pixel approaches (Hoffmann and Van der Vegt, 2001). Moreover, it is important to answer the question of "how to build meaningful objects which coincide with patterns of reality" (Blaschke and Strobl, 2001).

As an alternative, recent trends in computer technology try to recognize objects in images by first isolating components of objects and relationships between them (Sowmya and Trinder, 2000). This resulted in the per-field or per-parcel classification approach. While traditional multi-spectral algorithms consider only spectral similarities independently from their occurrence, the segmentation or per-parcel approach follows the hypothesis that neighboring image elements belong to the same category (Schiewe et al., 2001.). An image classification based on the segmentation approach holds more spectral information compared to a pixel's single values. This results in a variety of derived spectral features, such as brightness, textural features, contrast features, and contrast-related features (Hofmann, 2001). The software used for these purposes must be designed to address the labor cost and time issues of database maintenance using high-resolution imagery. At the same time, such software should be simple, affordable, accurate, fast, and excellent at capturing land cover features using data from very high resolution color and multispectral imagery to lower-resolution panchromatic data (Visual Learning Systems, 2002). Segmentation algorithms have been developed just recently for the analysis of remotely sensed data (Ryherd and Woodcock, 1996). This is the reason why related commercial software packages (e.g., Arboreal [Schiewe et al., 2001], eCognition [Definiens, 2003]) were not available before the year 2000. In these systems, the automatization degree is a key factor in avoiding manual tasks without losing quality.

Pattern

In human interpretation of image data, spectral, textural, temporal, and contextual features are four important pattern elements (Dai, 2003.). Most efforts in the development of land use/cover classification are currently focused on the idea that the computer recognizes texture patterns. One of the main reasons for developing techniques that are classified under the pixels segmentation approach is that most image data exhibit texture, a characteristic that is neglected in common per-pixel classifications (Blaschke and Strobl, 2001). The effort in various studies is focused on defining how to include neighborhood information across several spectral bands for a pixel-based analysis. This has been tried, using pre-defined boundaries, under the per-parcel classification approach (Blaschke and Strobl, 2001).

The texture approach considers the spatial information as an additional clue in characterizing and identifying land covers, in order to face the problem of reduced class separability in relation to the increased internal variance. This is an alternative for removing excess spectral detail considered as noise (Dai, 2003). In the literature, different kinds of textural features have been proposed, such as multi-channel filtering features, fractal-based features, and co-occurrence (EUROSTAT, 1995). ANNs capabilities have also been used to generate terrain textures from a

digital elevation model and remotely sensed data (Alvarez, 1995). The gray-level co-occurrence matrix (GLCM) contains the relative frequencies with which two neighboring pixels with a certain gray level co-occur in the image. In this analysis, the interpixel angles (e.g., 0°, 45°, 90°, 135°) are also considered (Dai, 2003). The approach using textural parameters performs frequently well for both gray-scale and multispectral image classification (Ashih, 2002).

Another approach in texture computation is based on the spatial correlation among pixels. This spatial dependence can be quantified and incorporated into the classifier (Shine and Wakefield, 1999). Texture is described considering local and global variability and spatial correlation. Both aspects are analyzed through the semivariogram function concept (Dai, 2003). However, too small parcels could present a problem when using the variogram as a texture measurement because this approach requires that the homogeneous regions of different texture within the image must be sufficiently large to allow robust variogram calculations (Dai, 2003).

Shape

Many of the land use/cover classes can be distinguished from each other based on their characteristic shape or structure (EUROSTAT, 1995). The main purpose of the segmentation approach should be generating meaningful objects. This means that the shape of an object on the ground is represented by a corresponding image object. This shape could be used to help land use/cover classification of remote-sensing image features by their physical properties (i.e., color, texture, and form) (Hofmann, 2001). The idea behind the shape recognition is to develop a machine learning approach to automated feature extraction that incorporates software agent technology which learns how to find land cover features based on user-specified examples (shape files). In this way, the software should provide object-specific feature-capturing technology using spatial context and advanced machine learning techniques that allow a user to control the feature extraction process, rather than using hard-coded rule bases (Visual Learning Systems, 2002).

DISCUSSION AND CONCLUSIONS

It is considered that traditional multi-spectral classification methods on per-pixel basis are no longer suited for the evaluation of high-resolution data from remote sensing. However, although the successful launching of high-resolution, multi-spectral satellite spread out the application of remote sensing, there is no essential change in the course of remote-sensing data processing (Yu et al. 2002). Moreover, the increasing variety of satellites and sensors as well as spatial resolution influences a broad spectrum of applications but does not automatically lead to better results (Blaschke and Strobl, 2001). As an alternative, region-based approaches consisting of a segmentation and classification step have begun to offer a satisfying solution. However, this implies the need for a more efficient use of spectral information in order to improve classification results. Sometimes, complex techniques show better results than traditional classification methods. For instance, Blackard and Dean (1999) reported that a feedforward artificial neural network model predicted more accurately forest cover type than did a traditional statistical model based on Gaussian discriminating analysis. One of the reasons for this may be the assumptions associated with most statistical analysis techniques (Blackard and Dean, 1999). However, ANNs, for example, do not always outperform traditional predictive models. In some cases, a traditional maximum-likelihood classifier outperformed ANN models when classifying remotely sensed crop

data (Jan, 1997). Therefore, no single classification algorithm can be regarded as a “panacea”. The reported superiority of one algorithm over the other depends strongly on the selected data set and the effort on the designing of the classifier “architecture” (Raymer et al., 2000). For instance, Shine and Wakefield (1999) found evidence that choosing testing points in supervised classification or a regular grid using geostatistically-chosen training data, based on a spatial variation scale determined from a data variogram, produces results which are comparable to those produced by analyst-chosen testing points. When using real data, in some instances, simple algorithms (such as a linear approach) perform virtually as well as the more complex models (Moisen and Frescino, 2001).

In selecting the better land use/cover classification method, we must consider the potential accuracy achieved. Accuracy variation of land use/cover classification may be attributed to various factors, such as terrain, landscape complexity, and land use patterns (Steele et al., 1998). We also have to consider the effects of topography, basically when shadow occurs. If we do not consider those factors, there may be serious consequences in the construction and application of thematic maps. Moreover, classification error matrixes are not a natural tool for analyzing precision in spatial variation (Steele et al., 1998). When thinking about the accuracy of remotely sensed land use/cover classification under an automated modeling approach, it is important to note that high scores for global performance measures do not necessarily mean that the classification will be better for management applications on the ground.

Another approach is to get the advantage of several classification methods. However, ensembles of different land use/cover classification techniques tend to be complex, and the improvement in accuracy achievement could be minor. Another solution, as shown earlier, has been the incorporation of secondary data to improve land use/cover classification. However, selecting the right combination of ancillary data sources and data analysis approaches has become critical to the generation of quality land use/cover maps (Sun, 1999). On the other hand, dimensionality reduction has been one of the alternatives to improve land use/cover classification. Raymer et al. (1997) discuss a very interesting strategy for dimensionality reduction using genetic algorithms. Essentially, this is an innovative approach to feature extraction in which feature selection, feature extraction, and classifiers training are performed simultaneously using a genetic algorithm (Raymer et al., 2000). However, this strategy has not been widely used.

In comparing the different land use/cover classification strategies, it could be said that all of them are workable in an automated environment. However, computation running time is one factor to be considered in the land use/cover classification process because methods can differ substantially. For instance, generally ANNs are slow (Moisen and Frescino, 2001), while traditional methods, such as supervised and unsupervised classification, are generally faster. Cost and labor hours are other factors to be considered when comparing and choosing a land use/cover method. Since traditional methods use more time (labor hours) to produce results, their process could result in higher cost. Figure 11-10 shows a hypothetical comparison of the costs and labor hours of three major approaches of land use/cover classification. As expected, a manual classification could imply a higher cost, mainly if we consider a long area to classify. Computer-based classification decreases costs substantially, and theoretically we could say that the per-parcel approach has more advantages in both labor and cost than the other approaches. However, we also must consider accuracy, software cost, and training cost in order to use the new technologies. For instance, texture is an important property of geographical images that can improve retrieval effectiveness and efficiency (Blaschke and Strobl, 2001). In general, when

deciding upon what land use/cover methodology to use, several criteria have to be considered (Malmberg and Miljöanalys, 2001): 1) obtaining a product of high quality; 2) creating a methodology that is repeatable; 3) time and cost efficiency in the work production; and d) independence for the operator performing the classification work.

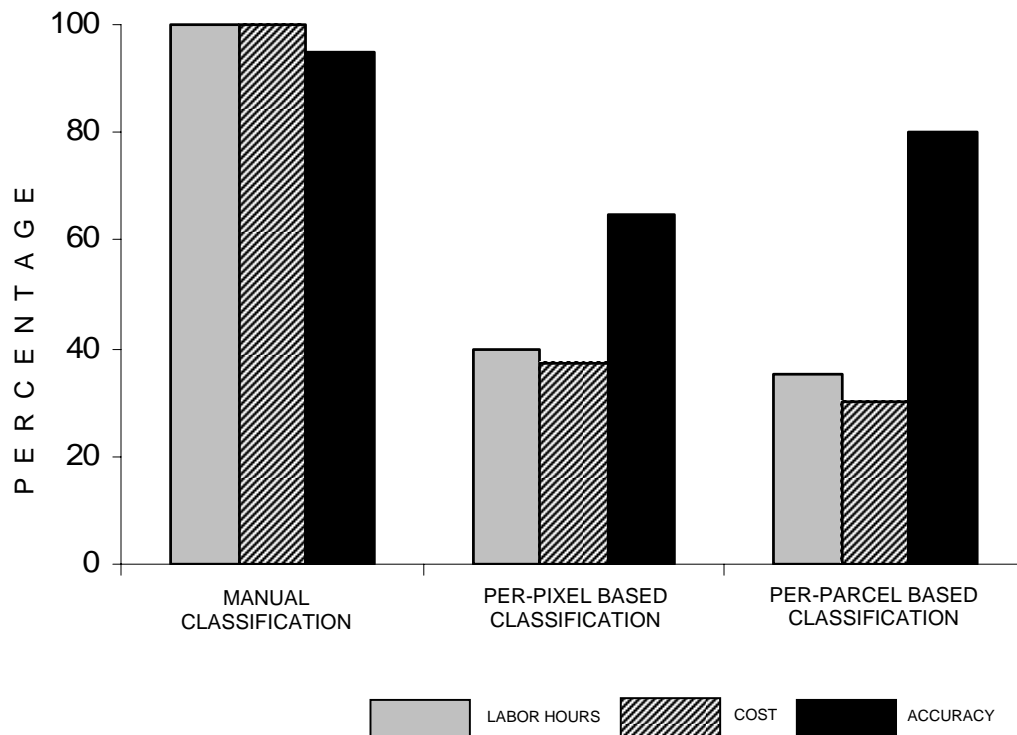


Fig. 11-10. Different classification approaches and a hypothetical comparison of their corresponding labor hours and cost.

Many land use classifiers who are in favor of a segmentation approach argue that image segmentation is intuitively appealing because human vision generally tends to generalize images into homogeneous areas first, and then to characterize these areas more carefully later (Gorte, 1998). Although there has been a lot of development in segmentation of gray tone, there has been little progress in segmentation of color or multi-band imagery (Kartikeyan et al. 1998).

It is very important to point out that there is still a lot of work to do in order to perform an automatized land use/cover classification just like the way the human brain does. This involves recognizing more characteristics than just brightness, color or texture (Fig. 6-11). Moreover, we are just starting to develop some technology in order to work at a more complex level. A reflection of this is the fact that commercial software capable of recognizing image texture, as well as another classification criterion, has not been more than four years in the market. At this stage, it is

also possible to train a computer to recognize the shape of some features. However, this new technology needs to be tested under different conditions, mainly in those areas where the limits of land use/cover classes are not well-defined. As shown in Fig. 11-11, we still need to include size as well as other classification factors.

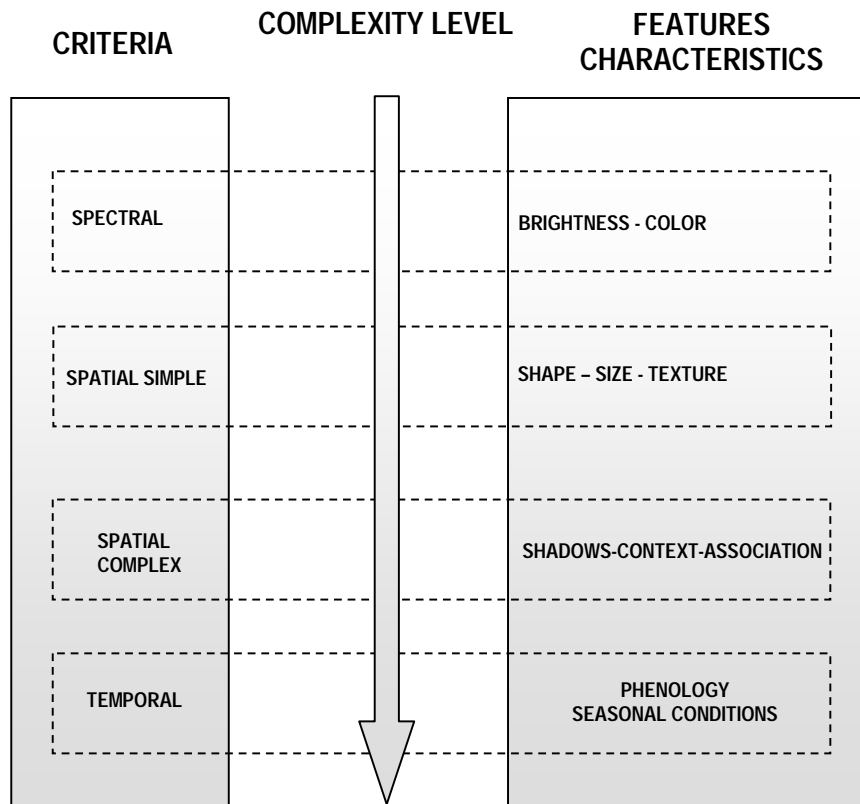


Fig. 11-11. Hierarchical organization of visual interpretation criteria (Adapted from European Commission, 1993 [Chuvieco, 2002]).

Using a more complex spatial criterion, we should develop computer systems that allow identifying not only shadows but also context and association as other factors to support a land use/cover classification process. After that, we need to consider a temporal criterion, mainly in classes that manifest certain changes due to seasonal conditions. For instance, evergreen forests do not lose their leaves, a condition that allows identifying them in any month of the year. On the other hand, some broadleaf species lose their canopy during the winter. This temporal criterion has been used to classify many land use/cover classes, mainly croplands.

Finally, perhaps land use/cover classification by remote sensing will never reach the same level of classification as that by the human eye, but current technology tends to provide a faster and more accurate land use/cover classification that will allow us to support the decision-making process with more confidence. However, the true challenge is to be able to develop the corresponding automatized processes. The people who have been working on land use/cover

classification understand that this process requires not only an adequate technical knowledge but also a valuable “artistic touch”.

REFERENCES

- Alvarez, S. 1995. Generation of terrain textures using neural networks. M.Sc. thesis. Department of Computer Science, Colorado State University, Fort Collins.
- Ashih, D. 2002. Land-use classification of aerial images using artificial neural networks. M.Sc. thesis. University of Georgia, Athens, Georgia.
- Avery, T.E. and G.L. Berlin. 1992. Fundamentals of remote sensing and airphoto interpretation. 5th ed. Prentice Hall, Upper Saddle River, New Jersey.
- Bara, T.J. 1994. GIS-based regionalization of natural landscapes using derived landcover occurrence probabilities [Online]. Available at <http://sgis.ursus.maine.edu/gisweb/spatdb/gis-lis/gi94005.html> (accessed 7 May 2005).
- Bauer, T., and K Steinnocher. 2001. Per-parcel land use classification in urban areas applying a rule-based technique. *GIS*: 24-27.
- Bharath, R., and J. Drosen. 1993. Neural network computing. Winderest/McGraw-Hill, New York.
- Blackard, J.A., and D.J. Dean. 1999. Comparative accuracies of artificial neural networks and discriminant analysis in predicting forest cover types from cartographic variables. *Comput. and Electronics in Agric.* 24:131-151.
- Blaschke, T., and J. Strobl. 2001. What's wrong with pixels? Some recent developments interfacing remote sensing and GIS. *GIS*: 12-17.
- Carmel, Y., and R. Kadmon. 1998. Computerized classification of Mediterranean vegetation using panchromatic aerial photographs. *J. Veg. Sci.* 9(3):445-454.
- Chuvieco, E. 2002. Teledetección ambiental. Ariel Ciencia, Barcelona.
- Chuvieco, E., and Congalton, R.G. 1989. Applications of remote sensing and geographic information systems to forest fire hazard mapping. *Remote Sens. Environ.* 29: 147-159.
- Dai, X. 2003. Improved classification of remote sensing data for land/cover classification [Online]. Available at <http://www.cse.psu.edu/~cg585/termPaper/Dai.pdf> (accessed 7 Apr. 2003).
- Definiens, N. 2003. eCognition-object oriented image analysis. Definiens Imaging GmbH [Online]. Available at <http://www.definiens-imaging.com/product.htm> (accessed on 15 Mar. 2003).
- EUROSTAT. 1995. Use of neural networks for improving satellite image processing techniques for land cover/land use classification. EUROSTAT Remote Sensing and Statistics Programme[Online]. Available at <http://europa.eu.int/en/comm/eurostat/research/supcom.95/16/result/> (accessed on 25 Feb. 2003; verified on 6 June 2003).
- Flores G., J. G. and Omi, P. N. 2003. Mapping forest fuels for spatial fire behavior simulations using geomatic strategies. *Agrociencia* 37: 65-72.
- Giacinto, G., and F. Roli. 1997. Ensembles of neural networks for soft classification of remote-sensing images [Online]. Available at www.diee.unica.it/~giacinto/PAPERS/EUIT97.pdf (accessed on 3 May 2003).
- Giroux, E.M., and D.J. Dean. 2001. Neural networks an alternative to statistical modeling the semivariogram analysis portion of co-kriging procedures [Online]. Available at

- http://www.cnr.colostate.edu/~denis/pubs_online/Giroux_and_Dean_2000.PDF (accessed on 17 May 2005; verified 6 June 2005).
- Gorte, B. 1998. Probabilistic segmentation of remotely sensed images. ITC Publication Series No. 63. International Institute for Geo-Information Science and Earth Observation, Enschede.
- Guisan, A., T.C. Edwards, Jr., and T. Hastie. 2002. Generalized linear and generalized additive models in studies of species distributions: Setting the scene. Ecological Modelling 157:89-100.
- Hastie, T.J., and R.J. Tibshirani. 1990. Generalized additive models. Chapman & Hall/CRC, Boca Raton.
- Herzfeld, U.C. 1999. New approaches to statistical analysis of satellite and remote-sensing data [Online]. Available at www.stat.fi/isi99/proceedings/arkisto/invited/ 81.html (accessed 21 Feb. 2003).
- Hoffmann, A., and J.W. van der Vegt. 2001. New sensor systems and new classification methods: Laser- and digital camera-data meet object-oriented strategies. GeoBIT/GIS: 18-23.
- Hofmann, P. 2001. Detecting buildings and roads from IKONOS data using additional elevation information. GeoBIT/GIS: 28-33.
- Jaehne, B. 1989. Digitale Bildverarbeitung. Springer-Verlag, Berlin.
- Jan, J.F. 1997. Classification of remote sensing data using adaptive machine learning techniques. Ph.D. diss. Department of Forest Sciences, Colorado State University, Fort Collins.
- Kartikeyan, B., A. Sarkar, and K. Majumder. 1998. A segmentation approach to classification of remote sensing imagery. Intern. J. Remote Sens. 19(9): 1695-1709.
- Lab of Landscape Ecology and Conservation Biology. 2002. Extracting forest structural information from remotely-sensed data for fire and wildfire modeling. ForestERA. Center for Environmental Sciences and Education. Northern Arizona University, Flagstaff.
- Luo Jiancheng, Z.C., and H. Lin. 1999. Geo-Interpretation model for land-cover/land-use classification. Hong Kong. November 22-25, 1999. In Proc. of: GIS Development. Land Use[Online]. Available at <http://www.gisdevelopment.net/aars/acrs/1999/ts5/ts5213.shtml>. (accessed 17 Mar. 2003).
- Malmberg, U. and M. Miljöanalys. 2001. BALANS land cover and land use classification methodology. Environmental and Climate Programme. Centre for Earth Observation, Stockholm.
- Marceau, D.J., P.J. Howarth, J.M. Dubois, and D.J. Gratton. 1990. Evaluation of the gray-level co-occurrence matrix method for land cover classification using SPOT imagery. IEEE Trans. Geosci. Remote Sens. 28(4): 513-519.
- Marzban, C., and G. Stumpf. 1996. A neural network for tornado prediction based on Doppler radar-derived attributes. J. Appl. Meteorol. 35: 617-626.
- Marzban, C., H. Paik, and G. Stumpf. 1997. Neural networks versus Gaussian discriminant analysis. AI Appl. 1(1): 49-58.
- Matheron, G. 1963. Principles of geostatistics. Econ. Geol. 58: 1246-1266.
- Moisen G.G. and T.C. Edwards, Jr. 1999. Use of generalized linear models and digital data in a forest inventory of northern Utah. J. Agric. Biol. Environ. Statistics 4: 372-390.
- Moisen, G.G., and T. Frescino. 2001. Comparing five modeling techniques for predicting forest characteristics. U.S. Forest Service, Rocky Mountain Research Station, Ogden.
- Moshou, D., E. Vrindts, B. De Ketelaere, J. DeBaerdemaeker, and H. Ramon. 2001. A neural network based plant classifier. Comput. Electron. Agric. 31(1): 5-16.

- Pal, M., and P.M. Mather. 2001. Decision tree based classification of remotely sensed data. In Proc. of: Asian Conference of Remote Sensing, 22nd, Singapore. 5-9 Nov. 2001. National University of Singapore, Singapore [Online]. Available at <http://www.crisp.nus.edu.sg/~acrs2001/pdf/046PAL.PDF> (accessed on 25 Feb. 2003; verified 6 June 2005).
- Quinlan, J.R. 1993. *C4.5: Programs for machine learning*. Morgan Kaufmann, CA.
- Raymer, M.L., P.C. Sanschagrin, W.F. Punch, S. Venkataraman, E.D. Goodman, and L.A. Kuhn. 1997. Predicting conserved water-mediated and polar ligand interactions in proteins using a k-nearest-neighbors genetic algorithm. *J. Mol. Biol.* 265: 445-464.
- Raymer, M.L., W.F. Punch, E.D. Goodman, L.A. Kuhn, and A.K. Jain. 2000. Dimensionality reduction using genetic algorithms. *IEEE Trans. of Evolutionary Comput.* 4(2):164-171.
- Rodriguez, B. E. 2000. Aplicación de redes neuronales artificiales y técnicas SIG para la predicción de coberturas vegetales. M.Sc. thesis. Universidad Autónoma Chapingo, Chapingo.
- Ryherd, S. and C. Woodcock. 1996. Combining spectral and texture data in the segmentation of remotely sensed images. *Photogramm. Eng. Remote Sens.* 62(2): 181-194.
- Schiewe, J., L. Tufte, and M. Ehlers. 2001. Potential and problems of multi-scale segmentation methods in remote sensing. *GIS* 6(1): 34-39.
- Shine, J.A. and G.I. Wakefield. 1999. A comparison of supervised imagery classification using analyst-chosen and geostatistically-chosen training sets. In Proc. of: GeoComputing 99. Fredericksburg, VA, USA. 25-28 July. Mary Washington College, Fredericksburg [Online]. Available at http://www.geovista.psu.edu/sites/geocomp99/Gc99/044/gc_044.htm (accessed on 15 Feb. 2003; verified 6 June 2005).
- Sowmya, A., and J. Trinder. 2000. Modelling and representation issues in automated feature extraction from aerial and satellite images. *J. Photogramm. Remote Sens.* 55: 34-47.
- Steele, B.M., J.C. Winne, and R. Redmond. 1998. Estimation and mapping of misclassification probabilities for thematic land cover maps. *Remote Sens. Environ.* 66:192-202.
- Sun, W. 1999. A new information fusion method for land-use classification using high resolution satellite imagery. Ph.D. diss. Doktor der Naturwissenschaften. Johannes Gutenberg-Universität, Mainz.
- Townshend, J., C. Huang, S. Kalluri, R. DeFries, S. Liang, and K. Yang. 2000. Beware of per-pixel characterization of land cover. *Intern. J. Remote Sens.* 21(4): 839-843.
- Visual Learning Systems. 2002. Using Feature Analyst™ for land cover and land use mapping. Visual Learning Systems, Inc., Missoula.
- Yu, Z., Z. Jixian, W. Guangliang, and L. Zongjian. 2002. Urban land-use classification using integrated airborne laser scanning data and high resolution multi-spectral satellite imagery. In Proc. Pecora 15/Land Satellite Information IV/ISPRS Commission I/FIEOS 2002 Conf., Denver. 10-15 Nov. 2002. Earth Data Analysis Center, Albuquerque [Online]. Available at <http://www.isprs.org/commission1/proceedings/paper/00100.pdf>. (accessed 7 Mar. 2003; verified 6 June 2005).
- Zamperoni, P. 1989. *Methoden der digitalen Bildverarbeitung*. Braunschweig, Wiesbaden.

Page blank

210

CHAPTER 12

Working Smarter: Research and Decision Support Systems in Mexican Agriculture

**Philip Heilman, Jeffry Stone, Ignacio Sanchez Cohen,
Hilario Macias Rodriguez, and Roy S. Mann**

CONTENTS

Introduction	212
Literature Review	213
Methodology	215
Discussion	221
Conclusions	230
Acknowledgments	232
References	232

INTRODUCTION

Because technological improvements make workers more productive in manufacturing, wages rise. And they rise not only for manufacturing workers but also for postal workers, teachers, and other service workers... But the technology of personal services is not easily changed. Since it still takes one person to drive a truck and one teacher to teach a class, the cost of these services is forced to rise.

Baumol and Blinder

Agricultural research institutions will face many challenges in the 21st century. The importance of producing food and fiber is recognized, and agriculture plays a critical role in rural employment and environmental management. However, agriculture is a mature sector, and research institutions are unlikely to see large budget increases while national budgets are limited. At the same time, research budgets consist largely of salaries for researchers and support personnel. As it takes one person to perform an experiment, budgets are subject to the “cost disease of personal services” identified by Baumol and Blinder (1991, p.7). For many agricultural research institutions, salary costs are increasing faster than budgets, leading to consolidation and reorganization.

In response, agricultural research institutions try to do more with less. There are essentially two options: work harder or work smarter. In the short run, it is possible to make improvements by working harder, but in the long run, organizations are more likely to make sustained progress by “working smarter”. The information technology revolution provides a potential source of tools that could help agricultural research institutions work smarter by increasing both the productivity of the agricultural research institutions and the agricultural systems they serve. Computer programs designed explicitly to help people work smarter by making better decisions are called Decision Support Systems (DSS). These tools are clearly no panacea, but in the right situations, they can provide significant benefits. Over time, as the cost of information technology infrastructure continues to decrease, the benefits of providing DSS technology will exceed the cost in more situations, and the role of DSS in agriculture will grow.

This chapter argues that DSS, defined as computer-based information systems designed to help participants in Mexico’s agricultural system make better decisions, can play an effective role in improving Mexican agriculture. If agricultural research institutions have a track record of improving efficiency and can point to additional opportunities to improve the agricultural sector, those research institutions can justify a growing budget.

On the other hand, developing Decision Support Systems is expensive and not trivial or easy. Information technology is its own field and requires a different skill set than most agricultural scientists have acquired. To some extent, this is because DSS are an integrator of information and a producer of “secondary” data rather than a generator of primary or source information. Furthermore, skills are required in both computer science and management information systems, so that the software developed is computationally efficient, easy to use, and produces results that “make sense” to those who will use the outcomes to make decisions. The development of software often seems to be a never-ending endeavor, and the time required to anticipate potential problems, maintain and support large software projects is often beyond the scope of research projects.

The theme of this book is that advances in remote sensing and modeling can be applied to improve the overall functioning of an agricultural system. Remote sensing provides a synoptic

view of the state of the earth's surface. Simulation models estimate what will happen in the future under different climate and management scenarios. Both remote sensing and modeling over large areas involve the manipulation of massive amounts of data. A DSS can complement remote sensing and modeling by integrating the information and providing the link with decision-makers. DSS can help convert data from remote sensing and models into knowledge that describes the likely results of alternative courses of action, and apply that knowledge in a framework that helps decision-makers.

DSS can have other, less apparent, benefits to agricultural research institutions in addition to directly helping decision-makers. One such benefit is to provide a mechanism to integrate and apply separate technical specialties. Specialization is a key factor in achieving research progress, but it is often difficult to connect research results from disparate fields. As decision support requires looking at the "big picture" there is a natural impetus for integration. A second benefit is that the application of a DSS will reveal crucial knowledge gaps. Stakeholders are naturally interested in paying for, or working through the political process to fund, research that will address those key knowledge gaps.

The objective of this chapter is to describe how research institutions in Mexico can use DSS to apply remote sensing and modeling to improve agriculture. It will also provide some suggestions for lowering the cost of developing DSS. If successful in developing and applying decision support technology, agricultural research institutions will be better able to demonstrate the contribution of their research and consequently be in a stronger position to argue for increasing budgets that will ensure a continuing and strengthened institutional presence.

LITERATURE REVIEW

There is a large and growing literature on decision support systems. As described by Power (2003), much of the initial research was designed to automate report generation with mainframe computers. Influential early books on DSS include those by Keen and Morton (1978) and Bonczek et al. (1981). Holsapple and Whinston (2001), Turban and Aronson (2000), and Marakas (2003) capture the current status and concepts of DSS, while Power (2004) provides a good introductory survey. Most of the early applications were designed to resolve business problems, although at least one early application focused on water quality issues (Bonczek et al., 1976).

Power (2004) defines a DSS as "a class of computerized information system that supports decision-making activities. DSS are interactive computer-based systems and subsystems intended to help decision makers use communications technologies, data, documents, knowledge and/or models to complete decision process tasks." It is worth emphasizing that to live up to its name, a DSS should support decision-making rather than make decisions. Often the types of decisions that DSS are designed to address take advantage of the ability of computers to manipulate large amounts of data, but also rely on a decision maker's judgment. Depending on the time frame and the scope for system manipulation, decisions can be classified as operational, tactical, and strategic. In an agricultural context, an operational decision would be how much fertilizer, pesticide, or irrigation water to apply at a given time in a growing season; a tactical decision would be to select a crop within a rotation; and a strategic decision would be to shift from conventional to organic production (Matthews and Stephens, 2002).

Complementing the development of computer systems, the last few decades have seen significant progress in the development and application of decision theory. Primarily as an

outgrowth of the field of operations research, decision theory has become much easier to apply to very complex decisions. One of the key advances has been the development of approaches to making decisions with multiple objectives. Keeney and Raiffa (1993), March (1994), and Hammond and Keeney (1999) have written good introductory books on decision theory with application to multiple objective decision-making. Beinat and Nijkamp (1998) present a number of applications of multiobjective theory to land management. Other examples of multiple objective decision-making in natural resources include the application of Saaty's (1990) Analytic Hierarchy Process, or AHP, to natural resources (Schmoldt et al., 2001) and for watershed management (de Steiguer et al., 2003), and DEFINITE by Janssen and van Herwijnen (1994).

Since the early 1990s, many natural resource applications of DSS have been developed. Compilations of such examples are described in El-Swaify and Yakowitz (1998), AWRA (2001, 2002a, 2002b), Lawrence and Robinson (2002), and Rizzoli and Jakeman (2002). Decision support for natural resources is similar to business applications in that they consist of an interface to frame the problem and to define appropriate decision criteria and feasible options, database and links to models, knowledge bases, or multiobjective decision components. While business DSS are often designed around databases, natural resource DSS often also include spatial databases in a Geographical Information System (GIS) format. Malczewski (1999) provides advice and examples of GIS approaches that directly incorporate multiobjective decision-making. Increasingly, natural resource DSS also include simulation models to assess the possible effects of alternative decisions on the natural system. Shenk and Franklin (2001) advise on the process of developing simulation models for natural resources, while Singh (2003) provides a discussion of the many issues in hydrologic modeling that are central to natural resource decision-making. Motivated by the lack of widespread application of crop models, Matthews and Stephens (2002) discuss the integration of crop models in agricultural decision support to produce improved outcomes. Similarly, Ahuja et al. (2002) describe a number of modeling efforts with a systems approach emphasizing model links to both field experiments and a DSS. McCown et al. (2002) highlight many of the problems experienced by DSS efforts focused on farmers.

A significant difference between natural resource DSS and business DSS is the longer term, provisional nature of natural resource decisions because of the general lack of knowledge about the system being managed. Often there are so many uncertainties associated with natural resource decisions that a tentative decision is made with the understanding that additional information will be collected, and the decision will be reviewed later in the light of new information. When decision makers collect data to test a working hypothesis while implementing a decision, the approach is called "adaptive management". The emphasis with this approach is on "learning by doing" or continual learning about the system being managed. Walters (1986, 2001) provides a good discussion of adaptive management and its role in decision-making and responding to monitoring when there is insufficient time to collect more information, and the risk of trial and error is unacceptable. The implication of adaptive management for decision support is that decisions are not made just once, but rather are continuously refined as part of an ongoing process.

Watersheds provide a good example of a natural resource area in which information for decision-making is typically inadequate. A watershed is a very complex system that is generally poorly understood. Newson (1997) and Brooks et al. (2003) provide good introductions to many watershed management issues. Davenport (2003) discusses watershed planning, and Loucks (1995) addresses DSS issues related to water resources planning. Typically, only some of the system inputs and outputs have been measured. A simulation model is the logical way to

understand system interactions, extrapolate from limited data sets, determine which processes need further research, and estimate the effects of alternative management systems. Because of the complexity of watershed processes, a DSS can be a useful complement to a watershed simulation model. According to the National Research Council (1999, p. 134), “given the difficulties of using and interpreting complex natural resource simulation models and data at the watershed scale, it is necessary that we develop decision tools to assist decision makers in watershed management programs and to facilitate transfer of simulation modeling technology.”

METHODOLOGY

Bakos (1998, p. 52) noted the early difficulty in harnessing information technology (IT) to improve efficiency: “Amidst the phenomenal IT revolution, several economists have been puzzled to find only modest growth in productivity reflected in the official statistics of the United States economy. The recognition of this ‘productivity paradox’ is often attributed to Nobel-winning economist Robert Solow, who famously quipped in 1987 that computers can be seen ‘everywhere except in the productivity statistics’.” Technological advances have continued to increase the power and reduce the cost of computers since Solow wryly noted the apparent failure of IT to increase productivity. Siegele (2003) argues that the IT revolution is maturing, with a shift in focus from rapid technological advance to the application of IT to solve everyday problems.

Earlier technological revolutions, such as railroads and electrical power, also underwent similar periods of limited application until standards were accepted and methods were developed to harness the potential of those technologies. Railroads allowed a huge geographic change in production and consumption by facilitating the transportation of goods. Electricity facilitated the restructuring of factories to support mass production. Information technology has an equal or greater potential to increase productivity, but that potential improvement will not be realized without a similar re-organization of parts of the economic system. Although the earlier technological revolutions substantially increased productivity, these were periods of wrenching change, and there were economic losers as well as winners.

How can agricultural systems be reorganized to take advantage of IT advances to improve decision-making? One obvious place to start is by looking at the decisions currently made in agriculture and asking where better information could lead to better decision-making. Figure 12-1 shows a very simple model of an agricultural system. For example, agricultural producers grow corn, which is processed into tortillas, which are in turn sold to consumers. Fertilizers and pesticides applied to the corn crop and oil used to lubricate a mill that grinds corn can be washed into streams and cause negative offsite effects by polluting streams and impacting key aquatic habitats. Within each box, there are a number of decisions that must be made, even if only implicitly. A farmer using the same management system year after year is essentially assuming that the system is sustainable, but it might be possible to assess the sustainability of those agronomic practices, as well as their offsite effects using a DSS. For example, is there a significant risk of losing topsoil through accelerated erosion or a risk of lowering water table?

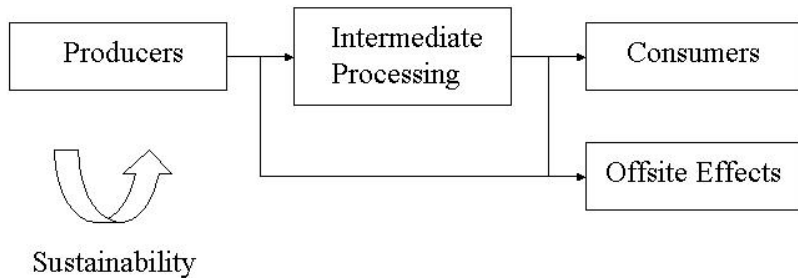


Fig. 12-1. A simple model of the agricultural system.

Even with the very simple model of cause and effect within an agricultural system in Fig. 12-1, one can imagine roles for a number of DSS focused on producers. For example, producers interested in diversifying production could use a GIS tool to make the strategic decision of identifying new crops that could be grown in a particular microclimate. Operational and tactical decisions could be made with the International Consortium for Agricultural Systems Applications' Decision Support System for Agrotechnology Transfer, DSSAT (ICASA, 2004). The DSSAT is an internationally used DSS that allows researchers to model the response to management for many crops.

Other DSS that consider the interaction of producers, intermediate production, and consumers include the International Food Policy Research Institute's Dynamic Research Evaluation for Management, or DREAM program (IFPRI, 2003). DREAM is designed to evaluate the economic impacts of agricultural research and development, particularly innovations, such as new varieties of crops. Lastly, INIFAP's *Laboratorio Nacional de Modelaje y Sensores Remotos* (National Laboratory of Modeling and Remote Sensing) is working on a DSS to provide predictions of crop yields in their *Sistema de Predicción de Cosechas* (System of Crop Yield Prediction). This information, when combined with knowledge of existing stocks and demand from consumers, could provide crucial decision support on prices, imports, exports, and local supply problems to national-level policy makers in Mexico.

The rest of this chapter will focus on an example of a DSS to address natural resource management issues, primarily sustainability and offsite effects at the watershed scale. For decades, the foundation of technical assistance for sustainability in agriculture has been the control of sheet and rill erosion on sloped areas of cultivated fields. The approach is conceptually straightforward. The Universal Soil Loss Equation (USLE) or the Revised Universal Soil Loss Equation (RUSLE) is used to estimate erosion on a hillslope (Wischmeier and Smith, 1978; Renard et al., 1997). The USLE and the RUSLE are empirical models of the form:

$$A = RKLSCP \quad [1]$$

A is soil loss in tons per acre; R is a rainfall-runoff erosivity factor; K is a soil erodibility factor; L is a slope length factor; S is a slope steepness factor; C is a cover-management factor; and P is a support practice factor. Essentially, the model captures the driving processes that cause hillslope erosion within a simple single equation that can be easily communicated. With the USLE and an estimate for the maximum acceptable soil loss, known as a soil loss tolerance, or T factor,

soil conservationists had a powerful tool for identifying fields that needed conservation practices, as well as the range of alternative farming practices that would lead to acceptable levels of erosion. Erosion at a rate less than T , by definition, should lead to sustainable levels of crop production, at least as far as soil quantity is concerned. To illustrate, annual soil loss on a field with a suspected soil erosion problem would be calculated for the current management system. If T were exceeded, the $RKLS$ factors would be held constant, and smaller C and P factors corresponding to alternative management practices could be applied until annual erosion was less than T . Some practices, such as installing terraces, would affect the LS factors as well. As soil conservationists gained experience under local conditions with the USLE, it became the standard tool, in part because of the ease with which it could be explained to farmers to support voluntary efforts to reduce erosion. Perhaps more important, however, was the overall simplicity of the approach, which was a conscious design decision. Laflen and Moldenhauer (2003, p. 39) relate discussions about the design of the USLE with Walt Wischmeier to that effect:

It was clear from the writings that the scientists well understood the erosion processes, and the fact that these interactions were present. Walt indicated that the reason these were ignored in the USLE was that a technology was needed at the field level, and it could not be too complicated. It had to be delivered in manuals and field guides. If they had tried to incorporate these interaction effects (for example erodibility and climate), the technology would have been so complicated, using dozens of tables and charts, it would not have been used. It was this focus on providing technology for the user that made the USLE, and the group that developed it, so successful.

Although simple and powerful, the USLE is limited to predicting soil detachment but not transport and deposition. Soil eroded from an agricultural field could be deposited within concentrated flow areas or along the field boundaries. The USLE is not designed to address sediment delivery issues, though sediment delivery ratios or more sophisticated models can estimate the quantity of sediment entering watercourses. Nor does the USLE address the movement of nutrients and pesticides from farm fields to water bodies. Such issues require a field-scale simulation model. Nevertheless, RUSLE is still used today as the primary simulation model for conservation planning and implementation of government programs related to soil erosion. Moving beyond the USLE to consider other resource problems in addition to erosion will require a much more sophisticated approach capable of assessing many resource considerations.

The Conservation Technology Information Center (2005) has proposed more comprehensive, though still simple, approach to conservation. They promote the “Core 4” concept consisting of 1) conservation tillage, or tillage that leaves at least 30% residue cover at planting, 2) a crop nutrient management plan, 3) a comprehensive approach to weed and pest management that minimizes the application of agricultural chemicals, and 4) strips of permanent vegetation in sensitive areas in and around fields known as conservation buffers. Additional residue cover from conservation tillage coinciding with periods of high storm activity will reduce runoff, protect the soil surface, and increase organic matter near the surface. By reducing surface runoff and the concentration of pollutants in the runoff water, and with buffer strips to remove some of the remaining pollutants, there is a great potential to improve water quality.

In the United States, the Soil Conservation Service had long recognized that a producer should have a conservation plan that addresses management impacts on all resources. To emphasize the fact that the agency considered all natural resources, the agency changed its name in the early 1990s to the Natural Resources Conservation Service, or NRCS. At roughly the same

time, the NRCS introduced a method known as the Conservation Practices Physical Effects, or CPPE, matrix (NRCS, 2003). The goal was to ensure that conservationists and producers looked broadly across all potential resource problems when formulating management systems.

The CPPE is used in the NRCS conservation planning process. During a resource inventory in the field, a conservationist will look for any of dozens of potential resource problems depending on the land use. These problems are grouped under the corresponding headings of Soil, Water, Air, Plant, Animal, and Human and are known collectively as SWAPA+H. Each potential resource problem has a quality criterion to indicate when it should be considered a problem. Once resource problems have been identified, management systems that resolve those problems are formulated.

Using observed data, simulation models, and expert opinion, one can prepare a table, such as Table 12-1, describing the effect of each alternative on a number of criteria of interest. Such a table could be simple or detailed depending on the decision makers' willingness to consider the complexities inherent in a given decision. Natural resource decisions typically involve tradeoffs, and a multiobjective approach is normally used if a table such as Table 12-1 can be created.

Table 12-1. The effect of management on decision criteria (to be quantified).

	Current Management System	Alternative 1	Alternative 2
1. Economic Returns	?	?	?
2. Sustainability			
Soil Erosion	?	?	?
Water Table	?	?	?
3. Offsite Effects			
Fertilizers	?	?	?
Pesticides	?	?	?

A number of multiobjective approaches have been proposed. The approach used in this research was first proposed by Wymore in 1988, adapted to natural resource decision-making in Lane et al. (1991), and implemented as the Water Quality Decision Support System, WQDSS (SWRC, 1994). An application of this method to water quality problems in agriculture is described in Heilman et al. (2004). The WQDSS has also been used for other applications, including shallow land burial systems for low-level nuclear waste (Paige et al., 1996), targeting farms for planning (Heilman et al., 1997), and rangeland planning (Lawrence et al., 1997). Imam (1994) addressed modeling and uncertainty issues.

The Queensland Department of Natural Resources and Mines, in association with the National Heritage Trust in Australia and under an International Memorandum of Understanding with the USDA-ARS, contracted with Netstorm, Inc. to implement the decision-making component of the WQDSS in the multi-platform Java language (Lawrence and Shaw, 2002). The new software is a generic, multiobjective decision-making tool called the Facilitator and incorporates the hierarchy tree of decision criteria by Yakowitz and Weltz (1998). This application pulls information from various sources to build the effects matrix that quantifies the impacts of the options on each decision criterion.

Because agricultural research institutions face similar challenges around the world, there is significant potential to address those challenges by developing DSS with shared or "open source"

software that will allow for customization for particular needs while sharing much of the burden of writing the rest of the code for the project. Heilman et al. (2002) describe the open source effort to be used in further development of the Facilitator. The Java language source code can be accessed through the <http://facilitator.sourceforge.net/> URL if modifications are needed.

Applications of the Facilitator have focused on planning for water infrastructure development in Queensland (Lawrence et al., 2000; Robinson et al, 1999), although the Facilitator has also been used to evaluate farming systems, floodplain management, farm forestry, animal production, project evaluation, and regional and watershed community strategy prioritizations. The Facilitator was designed for making strategic decisions where the problems are complicated enough to require a structured approach, and technical support is available to follow up on key issues affecting the decision. The three steps to make a decision using the Facilitator are 1) create a table of the effects of each alternative on each criterion by defining the decision variables or criteria, the management alternatives to be considered, and quantifying the effects of the alternatives on the criteria; 2) use available data, models, and expert opinion to score all values in the table to eliminate units and normalize elements to a scale of 0.0 to 1.0, with 1.0 being as good as possible; and 3) rank the decision variables in order of importance, graphically examine the results, and select the alternative(s) to implement or study in more depth. Lawrence et al. (2001) describe a richer conceptual framework of the many considerations and processes that lead to the definition of the alternatives and decision criteria within the decision analysis.

When performing the first step with the Facilitator, decision makers are responsible for excluding unacceptable alternatives. In the second step, decision makers select score functions for each decision variable from among the following choices: more is worse, more is better, a desirable range, or an undesirable range. The “more is worse” score function is used for a variable like the quantity of pollutants leaving a field or decline in groundwater levels, while net returns or grain yield are examples of decision variables that would be scored using a “more is better” score function. In some situations, surface runoff may constitute a “desirable range” where reducing the amount of runoff will reduce the transport of pollutants, yet some runoff is still desirable.

The third step assumes a simple additive value function of the form:

$$V(w, v) = \sum_i w_i v_i \quad [2]$$

to calculate an overall value, V , as the sum of the products of a weight, w , associated with each decision variable, or criterion, i , and the score, v , for that decision variable. Although conceptually simple, the approach can be difficult to apply because decision makers find it difficult to assign weights. Yakowitz et al. (1993) developed a method that eliminates the need for decision makers to specify a weight for each decision variable. Instead, the decision makers rank the decision variables in order of importance, and software calculates the range of possible weighting combinations for the decision variables. This method calculates a range of values representing the alternative, rather than a scalar value that quantifies the overall value of the alternative.

The method developed by Yakowitz has an intuitive appeal to decision makers. Suppose there are n criteria, which the decision-maker has ranked in importance. Let V_{ij} be the score of alternative j evaluated with respect to criterion i in the importance order. If w_i indicates the unknown weight factor associated with criterion i , the highest (lowest) or best (worst) additive composite score for alternative j , consistent with the importance order, is found by solving the following linear program described for the weights w_i :

$$\begin{aligned}
 & \max(\min) V_j = \sum_{i=1}^n w_i v_{ij} \\
 & \text{subject to } \sum_{i=1}^n w_i = 1 \\
 & w_1 \geq w_2 \geq \dots \geq w_n \geq 0.
 \end{aligned} \tag{3}$$

In both cases (maximizing or minimizing), the first constraint normalizes the sum of the weights to 1, while the second requires that the solution be consistent with the importance order and restricts the weights to be nonnegative. The solution to the two programs yields the full range of possible composite scores given the importance order. Any weight vector consistent with the importance order will produce a composite score that falls between the best and worst composite scores. Yakowitz et al. (1993) also showed that the best and worst composite scores could be calculated in closed form, as the maximum or minimum composite score can be calculated by solving the following k problems, starting at the highest ranked criterion and adding criteria until they have all been considered:

$$v_{kj} = \frac{1}{k} \sum_{i=1}^n v_{ij} \tag{4}$$

The best or worst composite score for alternative j is then selected from the results as:

$$\begin{aligned}
 BestScore = BV_j &= \max_k \{v_{kj}\}, \\
 WorstScore = WV_j &= \min_k \{v_{kj}\}
 \end{aligned} \tag{5}$$

A later study (Yakowitz and Weltz, 1998) improved the weighting algorithm by incorporating a hierarchical importance ordering, so that a number of sub-objectives could be grouped under categories, such as “erosion” and “water level” being grouped under “sustainability”. The hierarchy approach also addressed issues of bias caused by having too many criteria of one type (for example, environmental) compared to other considerations (for example, economic, social, cultural).

The multiobjective decision-making component is only a part of a DSS. Developing a DSS customized to a particular country’s institutions, customs, terminology and readily available data will probably require the development of additional software components. In recent years there has been significant progress in developing tools to manage the development of large-scale software projects. An impediment to the development of many software systems has been the inability of users to clearly articulate their needs. Users often do not have a good feel for what is possible, so while trying out prototype systems, they request changes that result in major design changes to support enhanced functionality. Such major design changes are costly and greatly slow the development effort, as developers are reluctant to revise systems in the face of frequently changing requirements. Many of the new tools are designed to support a more systematic definition of user requirements, allow for more meaningful interaction between users and the developer, provide additional flexibility in the design of software systems, and so ultimately speed the development of useful systems.

The first step in developing software is to define requirements. What will the software do? This is done iteratively. The best approach is to begin defining in general terms what the software

will be designed to accomplish. Once that is done, another layer of specificity is added as many times as is needed to unambiguously describe the task that the computer code must accomplish.

One recently developed tool that speeds this process is the Unified Modeling Language (UML). UML should significantly increase the speed and flexibility of development by modeling the user interactions that software systems will have to support (Rumbaugh et al., 1999), including the concept of "use cases" to describe interaction with users (Armour and Miller, 2001). Leffingwell and Widrig (2000) also provide instructive advice on how to manage the overall process of defining software requirements. Clemens et al. (2003) describe an approach to documenting a software project that will support a flexible, modular approach. Once the software has been designed, a number of languages and development environments can make programmers more productive. One tool to support incremental development of software by large distributed teams of developers is the Concurrent Version System (CVS). Teams of programmers in different locations can work on small pieces of large projects, sharing and tracking each other's contributions.

Agricultural research institutions should implement DSS when the expected benefits are likely to exceed the costs. Obviously not all benefits and costs can be foreseen or quantified, but the issues that are good candidates for the development of a DSS are likely to share similar characteristics. Problems cannot be too complex. The problems must be salient enough to attract attention, but not so contentious that politicians feel compelled to resolve the issue without consideration of technical merits. A DSS is more likely to provide substantial benefits if economies of scale can be realized by applying the same system multiple times for different locations, or as part of an ongoing process over time. Lastly, a DSS is more likely to be used if only a few decision makers need to be trained.

DISCUSSION

Watersheds are a natural unit for managing surface water quality and quantity. Many natural processes are integrated across a watershed, and upstream impacts on downstream water users are obvious. Often forestry, grazing, or cropped agriculture is the most prevalent land use in the headwaters, and municipal and industrial uses for water dominate in the urban areas downstream. Because many people are involved, there is an obvious potential to provide significant net benefits if watershed management can be improved.

An example of a watershed needing a planning effort is Hydrologic Region 36 (Fig. 12- 2) in the States of Durango and Coahuila in north central Mexico. This 92,000 km² watershed drains the eastern side of the Sierra Madre Mountains into a large closed basin known as La Laguna. Precipitation ranges from 200 mm annually at the lower elevations to about 600 mm annually in the Sierras, with significant variability in all areas. The watershed characteristics and associated land uses can be divided into three regions: the upper section of the watershed on the flanks of the Sierras is very rough, primarily forested, with some grazing; the central section of the watershed is less steep and drier, primarily used for grazing; the lower section of the watershed is flat and takes advantage of the water in the Nazas and Aguanaval rivers for the cities of Torreon in Coahuila and Gomez Palacio and Ciudad Lerdo in Durango, as well an extensive area of irrigated agriculture.

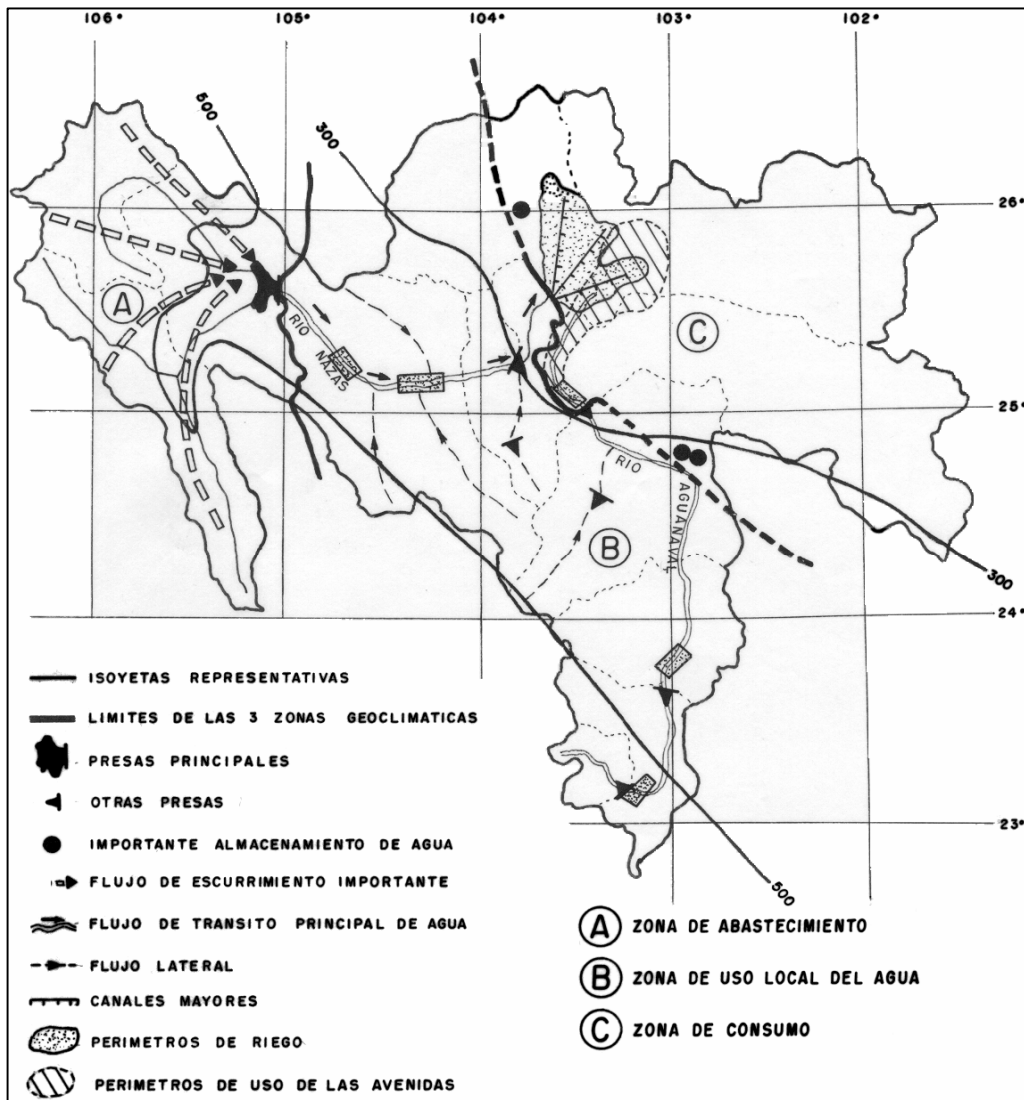


Fig. 12-2. Map of Hydrologic Region 36 showing the forested, water producing zone (A), the grazing, water for local use zone (B), and the irrigated, water consuming zone (C).

Field trips to inventory some of the common resource problems in the watershed were undertaken using a modified form of the SWAPA+H method for identifying resource problems. A one-page checklist of problems was developed for each of the three major regions and a rapid inventory performed. Table 12-2 shows the checklist for irrigated agricultural areas (in Spanish), and Table 12-3 summarizes the resource problems identified across the watershed (in English). The severity of the problems varied, but examples of most resource problems related to a particular land use could be found.

Table 12-2. Field checklist for irrigated agricultural resource problems.

Recurso	Consideración	Problema	Localidad	SI - Nota
SUELO	Erosión	a. Laminar b. Eólica c. Flujo Concentrado d. Cárcavas e. Cárcavas temporales f. Inducida por riego		
	Condición	a. Encostramiento b. Compactación		
AGUA	Cantidad	a. Exceso de escurrimiento b. Salidas inadecuadas c. Uso ineficiente d. Azolve		
	Calidad	a. Sedimentos b. Contaminación – pesticidas c. Contaminación – orgánicas d. Contaminación – patógenos e. Contaminación – nutrientes f. Salinidad g. Metales pesados h. Hábitat acuático		
AIRE	Calidad	a. Partículas en suspensión		
PLANTAS	Manejo	a. Manejo de nutrientes b. Maleza		
ANIMALES				
Fauna Silvestre	Hábitat	a. Alimento b. Agua c. Protecciones		

A true watershed planning approach in Hydrologic Region 36 would include the effects of clearing upland forest vegetation on runoff volume and peak runoff rates in the rangeland and irrigated sections of the watershed. Grazing practices in the central portion of the watershed play a role in determining how quickly the Lázaro Cárdenas and Francisco Zarco reservoirs will fill with sediment. Lastly, the lower portion of the watershed is clearly influenced by the water quantity and quality coming from the upper portions of the watershed, and the urban areas in turn affect the upper portions of the watershed by consuming wood, livestock products, and through recreation.

Table 12-3. Identified resource concerns in the Río Nazas and Río Aguanaval watersheds of Hydrologic Region 36.

Resource†	Category	Specific Resource Concern‡	Irrigated Land	Rangeland	Forest Land
Soil	Erosion	Sheet and Rill		X	X
		Concentrated Flow		X	X
		Classic Gully		X	X
		Wind	X		
		Irrigation Induced	X		
	Condition	Soil Tilth	X		
		Compaction	X		
		Contaminants, Organic Wastes (P)	X		
Water	Quantity	Water Management	X	X	X
		Restricted Capacity, Lakes and Reservoirs		X	X
	Quality	Groundwater cont., Pesticides (P)	X		
		Groundwater cont., Nutrients and organics (P)	X		
		Groundwater cont., Salinity (P)	X		
		Groundwater cont., Pathogens (P)	X		
Air	Quality	Airborne Sediments	X		
Plants	Condition	Ecological Condition (productivity)		X	X
		Health and Vigor		X	
Animal Wildlife†	Habitat	Food	X	X	X
		Cover and Shelter	X	X	X
Animal Livestock	Habitat	Food		X	X
		Water, quantity and quality		X	X
	Management	Population/Resource Balance		X	X
		Animal Health (P)		X	

† Specific wildlife species not defined.

‡(P), Potential problem identified; cont., contamination.

For simplicity, this example focuses on the decision-making of the irrigated portion of the lower region. A further simplification is to only consider surface water. Groundwater is commonly used in this irrigated area, although the quantities and distribution of pumping are not well understood. Few irrigation pumps are metered, and groundwater and surface water are regulated by different sets of laws. Efforts have been made to quantify groundwater use through methods like remote sensing and estimating the quantities of water pumped through the electricity bills, but most producers are not forthcoming about groundwater use, so the situation is unclear, although estimates indicate that withdrawals may significantly exceed recharge.

This irrigation district is officially called the Comarca Lagunera or Distrito de Riego 017, (Fig. 12-3). The basis of this example is a report on the consolidation and development of District 017 by the Comisión Nacional del Agua (2003). DR 017 consists of 20 Civil User's Associations, 17 of which are along the Río Nazas and 3 along the Río Aguanaval. There are 224,000 ha in the district, of which 93,000 are irrigated. The district consists of almost 38,000 members; 85% of the members belong to the collective landholding organizations, or ejidos, with the remainder considered small landholders.

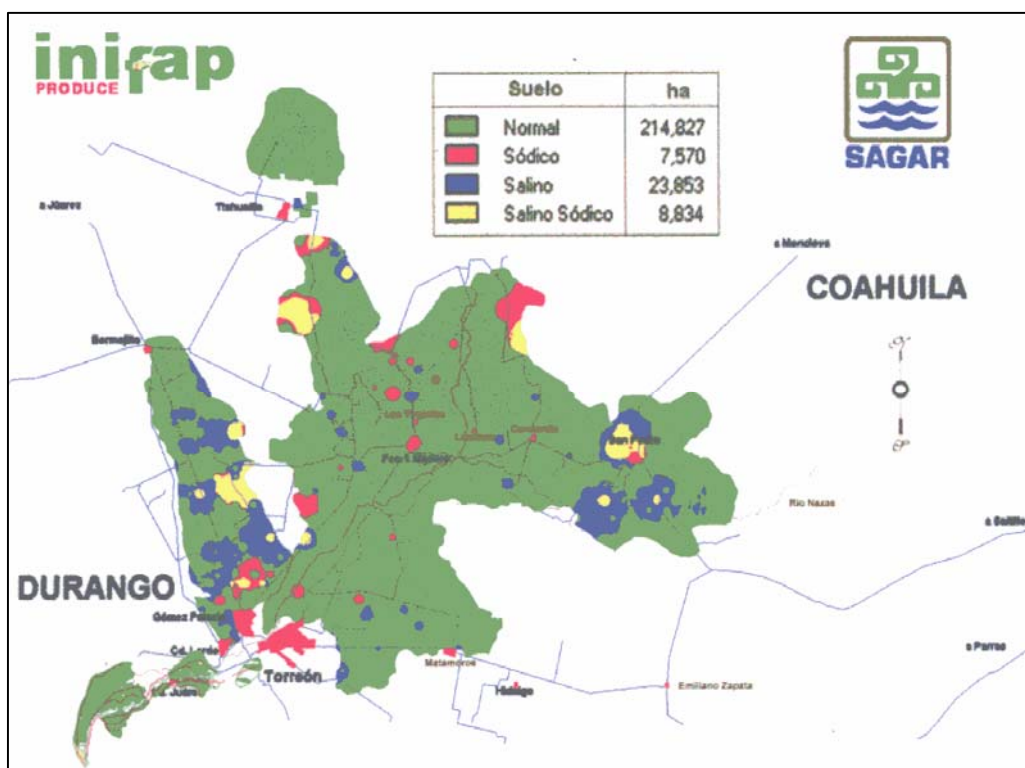


Fig. 12-3. Map of Irrigation District 017 showing the normal, sodic, saline and sodic and saline areas in the district.

Almost 2500 km of canals are used to distribute an authorized annual water volume of just over a million cubic meters. The quality of the water used is classified as poco contaminado, or slightly contaminated, in Mexico's national water quality index, and is fit for human consumption.

Based on the quantity of water stored in the two dams on October 1 each year, legal constraints, and minimum requirements for conservation and ecology, the quantity of water to be released is determined and divided among the User's Associations. Farmers then decide which crops to plant based on their allocation of water. The main crops are cotton, vegetables, and forages. Because of the varying supply of water and fluctuating prices, the area planted with each crop varies significantly each year. One trend has been toward increasing forage production, especially alfalfa, for the production of milk, as the region has developed into a major milk supply center. On the other hand, the area planted in cotton, corn, and beans has declined due to lower relative prices, although cotton prices and planned acreage may now be rising.

From the point of view of individual agricultural producers, the major problem is that water is available only to irrigate a few hectares, which is not large enough to provide a good income. Consequently, many producers are leaving agriculture. The government has a subsidy program to help producers called PROCAMPO. There has been a trend of smaller producers selling their rights to a year's allocation of water to larger producers, with or without the PROCAMPO subsidy. Such sales raise long-term concerns about inequality in water use.

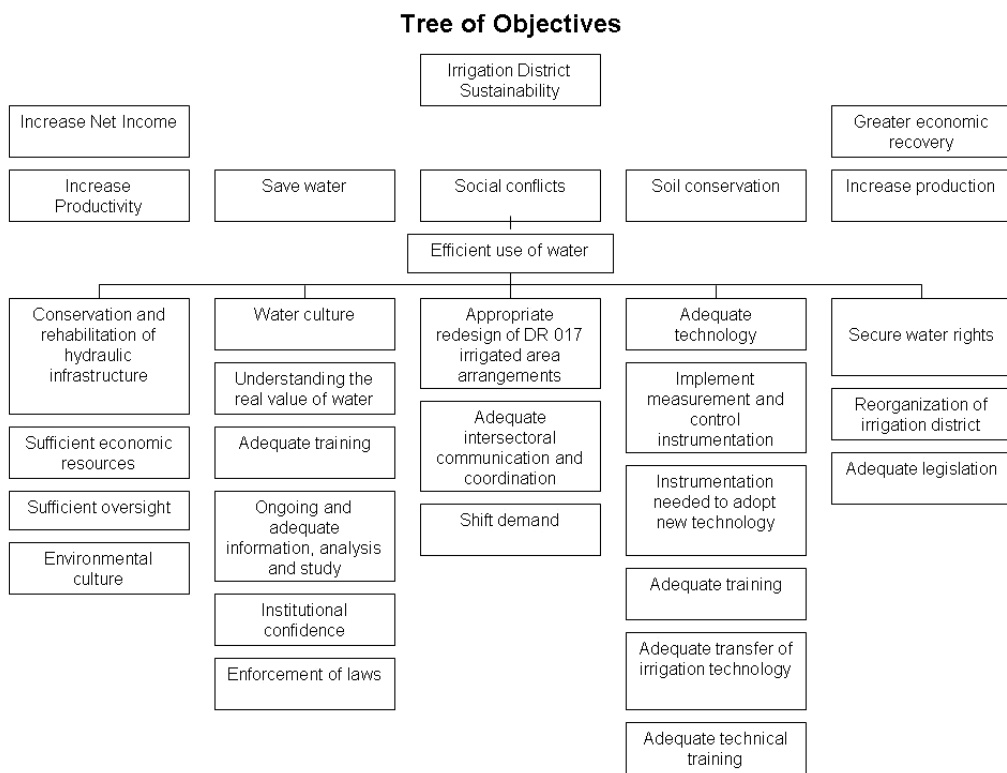


Fig. 12-4. Objective tree for Irrigation District 017.

From the point of view of the Irrigation District, there is a substantial problem with the efficiency of the system delivering water from the dams to the irrigated areas. Estimates of efficiency indicate that 63% of the water is lost between the dams and application on irrigated fields. Part of the problem is that, as there is not enough water to irrigate the whole district, water must be transported long distances to individual irrigated fields, rather than short distances to compact areas that are completely irrigated. A further complicating factor is the shift in responsibility for managing the canal network from the central government to the user groups. This shift has exacerbated planning and maintenance problems for the network of canals.

Finally, from the point of view of municipal and industrial water users, there is growing concern that agriculture uses a lot of water, but does not contribute economically in proportion to the amount of water consumed. If there is a shortage of water, the cities are entitled to use water first. Urban water planners realize that unless agriculture becomes more water-efficient, water may soon be less available and costlier for urban areas.

Given this background, the *Comisión Nacional del Agua* (C.N.A.), or National Water Commission, organized a study to determine what should be done to improve the management of DR 017. Specialists from a number of different agencies were brought together to define and document the problem. After creating a tree that identified a number of problems, a similar tree that defined objectives corresponding to each problem was created, as is shown in Fig. 12-4. For example, "Low Net Income" is identified as a problem (CNA 2003, p. 35). The corresponding

objective is “Increase Net Income” (CNA 2003, p. 37). Figure 12-4 is a translation into English of the tree of objectives. The tree shows the overall goal is the sustainability of the irrigation district. This goal is divided into five objectives: increase net income, save water, avoid social conflicts, conserve soil, and increase economic recovery. The key objective of reducing social conflicts will require the efficient use of water. Because of the focus on water use efficiency, additional objectives contributing to that objective are also listed.

Representatives of the Ministry of Agriculture and DR 017 were invited to several decision support sessions using the Facilitator. A Spanish language interface to the Facilitator was created for these sessions. The representatives differed somewhat from the experts in the CNA study by wanting to focus on four objectives: increase the productivity of irrigation water, improve the distribution of wealth, increase the transportation efficiency, and increase the global efficiency of water in the irrigation system. In the context of the objectives shown in Fig. 12-4, these objectives focus on reducing social conflicts by solving the technical problem of the efficient use of water, and avoiding increased concentration of wealth.

The alternatives that the representatives of DR 017 considered also differed from the wider perspective in the CNA study. The DR 017 representatives focused on alternatives that were primarily under the control of the irrigation district, rather than specifying actions for the governmental water-related agencies. The alternatives considered include:

- Changing the cropping pattern to less water demanding crops
- Changing to winter forage crops to reduce evapotranspiration
- Training members of the irrigation district in water conserving technology
- Rehabilitating the hydraulic infrastructure
- Shrinking the irrigated area and introducing a water market
- Varying the price of water according to the amount in reservoirs
- Baseline – Continuing with current management

Using the understanding of the participants, Table 12-4 was created to show the English and Spanish names for the criteria and alternatives, and to describe the anticipated effect of each alternative on the objectives. Effects were estimated on a scale of 0.0 to 1.0, with 1.0 being as high as possible (maximum benefit / minimum impact). Since the estimates were directly generated as scores, there was no need to use a score function to eliminate units. If the baseline situation continued, the effect would be a score of 0.5 for each of the four alternatives. All other alternatives equaled or exceeded the baseline score of 0.5 for each objective. Often, when setting up a decision like this, there will be an economic objective, such as the cost to implement, for which alternatives with environmental benefits will have higher costs and thus lower scores than the baseline. Changing the cropping pattern, producing winter forage crops, and restructuring the district and implementing a water market all had positive effects for most objectives. The three alternatives deemed to have the greatest potential to achieve the stated goals were irrigation efficiency training, rehabilitation of hydraulic infrastructure, and varying the price of water.

Using the scores in Table 12-4, a number of importance orders ranking the four objectives were tried. These importance orders allow an opportunity for multiple stakeholders within the watershed to express their concerns or preferences for which decision criteria are most important to them. The Facilitator software allows these scenarios to be rapidly calculated and compared. In addition, the DSS tool calculates all possible combinations of weights that are consistent with the importance order of the criteria.

Table 12.-4 Irrigation District 017 estimates of management effects (scores) on objectives.

	Current Management System (Situación Actual)	Change Cropping Pattern (Cambio Patrón de Cultivos)	Produce Winter Forage Crops (Cambio a Cultivos de Invierno)	Irrigation Efficiency Training (Capacitación a Usuarios del Riego)	Rehabilitate Hydraulic Infrastructure (Rehabilitación de Infraestructura Hidráulica)	Water Market and District Restructuring (Compactación y Mercado de Agua)	Vary Water Price (Precio del Recurso)
Productivity of Water (Productividad del Agua de Riego)	.5	.7	.75	.8	.85	.7	.88
Income Distribution (Mayor distribución de la Riqueza)	.5	.6	.5	.5	.6	.75	.7
Conduction Efficiency (Incremento en la Eficiencia en Conducción)	.5	.5	.6	.6	.88	.6	.8
Global Efficiency (Incremento en la Eficiencia Global)	.5	.7	.8	.87	.8	.6	.87

The results of composite scores (weights * effects scores) are shown as a horizontal bar, where the minimum composite score defines the left side of the bar, and the right side of the bar is defined by the maximum composite score. Figure 12-5 shows one importance order selected, with the resulting outcomes shown as a graphic in Fig. 12-6. In this example, increasing the global efficiency of water used for irrigation was the highest ranked objective, so the two alternatives that scored 0.87 for that objective, irrigation efficiency training and varying the water price, were the preferred alternatives. The horizontal bar representing the range of possible overall scores for varying the water price (Precio del recurso) is much narrower than the horizontal bar for training water users (Capacitación a usuarios del riego) because the minimum score for the income distribution goal with the varying the water price alternative was 0.7, but only 0.5 for the training alternative.



Fig. 12-5. Importance order (hierarchical ordering) within the Facilitator's Spanish language interface.

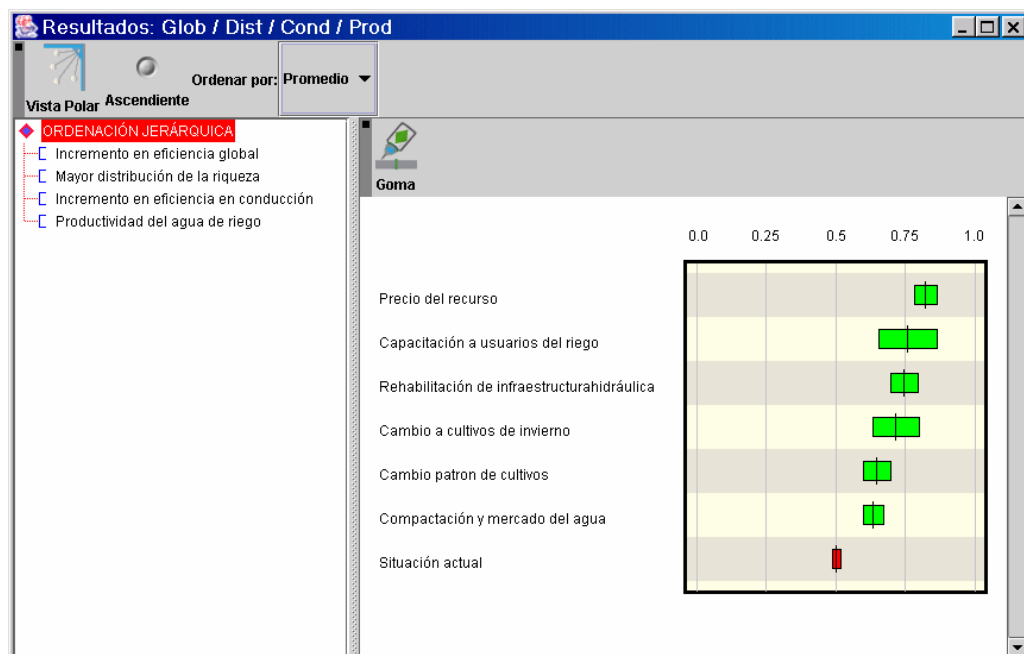


Fig. 12-6. Ranking of alternatives within the Facilitator's Spanish language interface.

Given the objectives, alternatives, estimated effects in Table 12-4, and several importance orders defined by the representatives of the irrigation district, the alternatives that tended to score the highest were varying the price of water and rehabilitating the hydraulic infrastructure. The alternatives that did the worst of those considered, though still scoring higher than the baseline situation, were changing the cropping pattern and shrinking the irrigated area and introducing a water market.

The irrigation district has not made a final decision on which alternative to implement. The application of the DSS is still an ongoing process, and there is an effort underway to improve the estimates of the effects of the alternatives on the objectives. The ALMANAC simulation model will be used to assess water savings resulting from a change to winter cropping. Economic studies to assess the response to varying the price of water and the feasibility of rehabilitating the infrastructure are also underway. A linear programming study has already shown that changing the cropping pattern could almost double income per cubic meter of water used and still save millions of cubic meters of water per year (Sanchez Cohen et al., 2003). Perhaps most encouraging has been the informal discussion with some of the other groups in Hydrologic Region 36 and their expressed willingness to work within the political system to help find additional funding to quantify decision variables.

To summarize the DR 017 example, watersheds are one area where a multiobjective DSS can make a contribution because of the need to integrate information from many sources. A DSS can frame a decision in a way that leads to the definition of critically important research questions. Generally, decisions involving natural resources are complex, and making decisions on one issue (e.g., economic) in isolation from other important considerations (social, environmental, institutional) may lead to decisions that are inconsistent with the principles of ecologically sustainable development. Whatever natural system must be managed will probably require an assessment of current condition that can benefit from remote sensing, as well as an understanding of how the components of the system interact, which can be provided through the application of simulation models. Ultimately, however, one would like to link all available information, such as natural resource inventories, simulation model results, and expert opinion, to both make decisions and guide future research.

CONCLUSIONS

Economic pressures, especially the rising cost of salaries for agricultural researchers, will continue to force agricultural research institutions to reassess their objectives. In the long run, successful responses to these economic pressures are likely to include efforts to help both the agricultural research institution and the agricultural sector as a whole to "work smarter". Working smarter implies providing more and better information in a way that leads to better decisions.

Because there is a significant economy of scale in applying DSS technology, the decisions that are likely to be supported initially will be those relating to either policy or the management of large areas. To design a DSS, one has to determine who the decision-makers are, what decisions are to be made, and what information is needed to make those decisions. One can then identify the information to be collected by remote sensing and appropriate field inventory procedures. There are few areas in the world where adequate information at the landscape scale exists to support informed decision-making. Consequently, there will have to be an effort to understand and describe the physical factors across the landscape. Based on the demand for specific information,

simulation models are chosen because of their ability to describe physical or biological systems and quantify the effects of management on key system outputs. Easy-to-use interfaces, data and time requirements can also be key determinants of which model to use. DSS complement remote sensing and simulation modeling by identifying the critical application areas needing focus.

Developing DSS technology is not a panacea and there are risks in implementing decision support technology. A very real risk is the possibility of outright failure. After investing in the development of a DSS, it may turn out that an unforeseen design flaw, a change in agricultural markets, lack of interest, political change, or some other factor prevents the DSS from being applied. In a case like that, the time and resources devoted to the DSS could have been put to a better use, particularly if the research institution has had to hire new personnel with information technology skills. Another potential source of failure is that even with user involvement in the decision-making process, implementing decisions may be problematic if significant institutional change is required.

The falling cost of hardware and the development of improved approaches to design and implement software systems imply that the real question is when, not whether, DSS technology will play a significant role in Mexican agriculture. Focusing initially on applications that other agricultural research institutions have already developed can reduce the risk of failure. The District 017 example showed the potential benefit of cooperating on an international effort that required implementing a Spanish language DSS interface, but not the full cost of developing the software. Not only is the cost of developing and implementing a DSS substantially reduced if other agricultural research institutions are working on similar tools, but experiences gained from previous applications can be shared. Other agricultural research institutions face similar economic pressure and thus have an interest in cooperating in the development of DSS products. Currently, a limited number of such cooperatively developed tools exist, although the number is likely to grow.

The DR 017 example also shows how a DSS, particularly a multiobjective DSS, could help coordinate disciplinary research that links agronomic, hydrologic and economic specialties. Perhaps the most significant contribution of a DSS to an agricultural research institution is to help it "fish" those projects of most immediate application out of the sea of potential research projects. A critical additional benefit is the realization by client groups that those key research gaps exist. Such groups may be willing to fund smaller scale research projects or work within the political system to find funding for larger projects.

Decision support technology can also help the agricultural sector as a whole work smarter. From society's point of view, a basic question is how much money should be allocated to agricultural research. An economist would respond that the appropriate investment is the amount that maximizes the net returns. Of course, assessing returns to agricultural research is problematic. Benefits are uncertain and may be realized far in the future, prices are highly variable, etc. At some initial (low) level of investment, the overhead of running an agricultural research institution exceeds the return from research, and the institution fails to generate positive net benefits. At higher levels of investment, benefits of additional research activities exceed the combined overhead and research costs to provide positive net benefits. Funding should increase for activities with a greater potential until the net benefits equal those of other projects, and similarly, funding should decrease for projects without much potential. Finally, at some level of investment, there are no longer additional projects that provide the same returns, so net returns decline. In a watershed DSS application, some of the benefits would be realized as improvements in water quality and quantity rather than agricultural income.

This chapter has essentially argued that advances in information technology are creating the potential to create much greater net benefits from agricultural research. If an agricultural research institution can help the agricultural sector work smarter by considering more options, applying better science, focusing research on the most critical problems, and especially by realizing economies of scale in addressing common problems, then a greater investment in agricultural research is justified. To apply DSS technology will take careful thought and significant effort, but it can be a useful tool to help both agricultural research institutions, and the agricultural sectors they serve, to work smarter.

ACKNOWLEDGMENTS

We gratefully acknowledge the help of a number of researchers at INIFAP CENID RASPA, including Guillermo Martínez Rodríguez, Rodolfo Jasso Ibarra, and Ignacio Orona Castillo.

REFERENCES

- Ahuja, L., L. Ma, and T. Howell. 2002. Agricultural system models in field research and technology transfer. Lewis Publishers, Boca Raton, FL.
- American Water Resources Association. 2001. Proc. Conf. Decision Support Systems for Water Resources Management, Snowbird, Utah. 27-30 June 2001. AWRA, Middleburg, VA.
- American Water Resources Association. 2002a. J. American Water Resources Association 38(2):337-586.
- American Water Resources Association. 2002b. J. American Water Resources Association 38(4):895-1155.
- Armour, F., and G. Miller. 2001. Advanced use case modeling. Addison-Wesley, NY.
- Bakos, Y. 1998. Economics and technology: The productivity payoff of computers. Sci. 281(5373): 52.
- Baumol, W.J., and A.S. Blinder. 1991. Economics: Principles and policy. 5th ed. Harcourt, Brace Jovanovich, NY.
- Beinat, E., and P. Nijkamp (ed). 1998. Multicriteria analysis for land-use management. Kluwer Academic Publishers, Boston, MA.
- Bonczek, R.H., C.W. Holsapple, and A. Whinston. 1976. Implementation of a decision support system for regional water quality processing. Paper 570. Krannert Graduate School of Management, Purdue University, West Lafayette, IN.
- Bonczek, R.H., C.W. Holsapple, and A. Whinston. 1981. Foundations of decision support systems. Academic Press, NY.
- Brooks, K.N., P.F. Ffolliott, H.M. Gregesen, and L.F. DeBano. 2003. Hydrology and the management of watersheds. Iowa State University Press, Ames, Iowa.
- Clemens, P., F. Bachmann, L. Bass, D. Garlan, J. Ivers, R. Little, R. Nord, and J. Stafford. 2003. Documenting software architecture: Views and beyond. Addison-Wesley, NY.
- Comisión Nacional del Agua. 2003. Consolidacion y desarrollo del Distrito de Riego 017, Comarca Lagunera. Comisión Nacional del Agua, Lerdo, Durango, Mexico.

- Conservation Tillage Information Center CTIC. 2005 Core 4: Conservation for agriculture's future [Online]. Available at <http://www.ctic.purdue.edu/Core4/Core4.html> (accessed 14 June, 2005; verified 1 July 2005). CTIC, W. Lafeyette, IN.
- Davenport, T.E. 2003. The watershed project management guide. Lewis Publishers, Boca Raton, FL.
- De Steiger, J.E., J. Duberstein, and V. Lopes. 2003. The analytic hierarchy process as a means for integrated watershed management. p. 736-740. In K.G. Renard et al. (ed.) Proc. First Interagency Conf. Res. in the Watersheds, Benson, AZ. 27-30 Oct. 2003. USDA-ARS, Tucson, AZ.
- El-Swaify, S.A., and D.S. Yakowitz (ed.) 1998. Multiple objective decision-making for land, water, and environmental management: Proc. Int. Conf. Multiple Objective Decision Support Systems (MODSS) for Land, Water and Environmental Management, 1st, Honolulu, HI. 23-27 July 1995. Lewis Publishers, Boca Raton, FL.
- Hammond, J.S., and R.L. Keeney. 1999. Smart choices: A practical guide to making better decisions. Harvard Business School Press, Boston, MA.
- Heilman, P., G. Davis, P. Lawrence, J. L. Hatfield, and J. Huddleston. 2002. The Facilitator - An open source effort to support multiobjective decision-making. p.253-258. In Proc. Int. Environ. Modeling and Software Society, Lugano, Switzerland. 24-27 June 2002. University of Lugano, Lugano.
- Heilman, P., J.L. Hatfield, M. Adkins, J. Porter, and R. Kurth. 2004. Field scale multiobjective decision-making: A case study from western Iowa. J. American Water Resources Association 40(2):333:346.
- Heilman, P., D.S. Yakowitz, and L.J. Lane. 1997. Targeting farms to improve water quality. Applied Mathematics and Computation 83:173-194.
- Holsapple, C.W., and A.B. Winston. 2001. Decision support systems: A knowledge-based approach. Thomson Learning/Delmar Publishers, Stamford, CT.
- International Consortium for Agricultural Systems Applications. 2004. DSSAT: Decision support system for agrotechnology transfer [Online]. Available at <http://www.icasa.net/dssat/> (accessed 14 June 2005; verified 1 July 2005). International Consortium for Agricultural Systems Applications, Honolulu, HI.
- International Food Policy Research Institute. 2003. Dream: A tool for evaluating the effects of agricultural R & D [Online]. Available at <http://www.ifpri.org/dream.htm> (accessed 14 June 2004; verified 1 July 2005). International Food Policy Research Institute, Washington, DC.
- Imam, B. 1994. Nonlinear uncertainty analysis of multiple criteria natural resource decision support systems. Ph.D. diss. University of Arizona, Tucson.
- Janssen, R., and M. van Herwijken. 1994. Definite: A system to support decisions on a finite set of alternatives. Kluwer Academic Publishers, Dordrecht, Netherlands.
- Keen, P.G.W., and M.S. Morton. 1978. Decision support systems: An organizational perspective. Addison-Wesley, Reading, MA.
- Keeney, R.L., and H. Raiffa. 1993. Decisions with multiple objectives: Preferences and value tradeoffs. Cambridge University Press, New York.
- Laflen, J.M. and W.C. Moldenhauer. 2003. Pioneering soil erosion and prediction: The USLE story. World Assoc. of Soil and Water Conserv. Spec. Publ. 1. Funny Publishing, Bangkok, Thailand.

- Lane, L.J., J.C. Ascough, and T. Hakonson. 1991. Multiobjective decision theory - Decision support systems with embedded simulation models. pp. 445-451. In Proc. Irrigation and Drainage, Honolulu, HI. 22-26 July 1991. ASCE, New York.
- Lawrence, P.A., and J. Robinson (ed.) 2002. In Proc. Int. Conf. on Multiple Objective Decision Support Systems for Land, Water and Environmental Management (MODSS '99), 2nd, Brisbane, Australia. 1-6 July 1999. Report QNRM02143. Queensland Dep. of Natural Resources, QLD, Australia. Available at <http://www.coastal.crc.org.au/modss/conference99.asp> (accessed 14 June 2005; verified 1 July 2005).
- Lawrence, P.A., and R.J. Shaw. 2002. A framework for evaluating options for improved irrigation management. pp 1-15. In Proc. Int. Conf. on Multiple Objective Decision Support Systems for Land, Water and Environmental Management (MODSS'99), 2nd, Brisbane, QLD, Australia. 1-6 July 1999. Report QNRM02143. Queensland Dep. of Natural Resources, QLD, Australia. Available at <http://www.coastal.crc.org.au/modss/conference99.asp>. (accessed 14 June 2005; verified 1 July 2005).
- Lawrence, P.A., J. Robinson, and R. Eisner. 2001. A decision environment: Going beyond a decision framework to improve the effectiveness of decision making in natural resource management. p. 1613-1618. In Ghassemi F. et al. (ed.) Int. Congr. Modeling and Simulation (MODSIM 2001), Canberra, ACT, Australia. 10-13 Dec. 2001. Modelling and Simulation Society of Australia and New Zealand, Perth.
- Lawrence, P.A., R.J. Shaw, L.J. Lane, and R. Eisner. 2000. Participatory multiple objective decision making processes: Emerging approaches with new challenges. p. 1-11 In Marshall Flug et al.(ed) Proc. Watershed Management and Operations Management 2000, Fort Collins, CO. 20-24 June 2000. ASCE, New York.
- Lawrence, P.A., J.J. Stone, P. Heilman, and L.J. Lane. 1997. Using measured data and expert opinion in a multiple objective decision support system for semiarid rangelands. Trans. ASAE 40:1589-1597.
- Leffingwell, D., and D. Widrig. 2000. Managing software requirements: A unified approach. Addison Wesley, NY.
- Loucks, D.P. 1995. Developing and implementing decision support systems: A critique and a challenge. Water Resources Bulletin 31:571-582.
- Malczewski, J. 1999. GIS and multicriteria decision analysis. John Wiley and Sons, NY.
- Marakas, G.M. 2003. Decision support systems in the 21st century. 2nd ed [Online] Available at <http://myphlip.pearsoncmg.com/cw/mpbookhome.cfm?vbookid=403> (accessed June 14, 2005; verified 1 July 2005). Prentice Hall, Upper Saddle River, NJ.
- March, J.G. 1994. A primer on decision making. Free Press, NY.
- Matthews, R., and W. Stephens (ed.) 2002. Crop-soil simulation models: Applications in developing countries. CABI Publishing, NY.
- McCown, R. L., Z. Hochman, and P. S. Carberry. 2002. Probing the enigma of the decision support system for farmers: Learning from experience and from theory. Agric. Syst. 74:1-10.
- National Research Council. 1999. New strategies for America's watersheds. National Academy Press, Washington DC.
- Natural Resources Conservation Service. 2003. Iowa's Field Office Section V, Iowa eFOTG, National CPPEs [Online]. Available at <http://www.nrcs.usda.gov/technical/efotg/> (accessed 24 Dec. 2003; verified 1 July 2005). USDA-NRCS, Washington, DC.

- Newson, M. 1997. Land, water and development: Sustainable management of river basin systems. Routledge, NY.
- Paige, G.B., J.J. Stone, L.J. Lane, D.S. Yakowitz, and T.E. Hakonson. 1996. Evaluation of a prototype decision support system for selecting trench cap designs. *J. Environ. Qual.* 25:127-135.
- Power, D.J. 2003. A brief history of decision support systems. Version 2.8 [Online]. Available at <http://DSSResources.COM/history/dsshistory.html> (accessed 31 May 2003; verified 12 Jan. 2004).
- Power, D.J. 2004. Decision support systems web tour. Version 4.3 [Online]. Available at <http://dssresources.com> (accessed 15 June 2002; verified 12 Jan. 2004).
- Renard, K.G., G.R. Foster, G.A. Weesies, D.K. McCool, and D.C. Yoder. 1997. Predicting soil erosion by water: A guide to conservation planning with the Revised Universal Soil Loss Equation (RUSLE). USDA Agric. Handbook 703. U.S. Gov. Print. Office, Washington, DC.
- Rizzoli, A.E. and A.J. Jakeman (ed.) 2002. Integrated assessment and decision support: Proc. Biennial Meeting Int. Environmental Modeling and Software Society, 1st, University of Lugano, Switzerland. 24-27 June 2002. University of Lugano, Lugano.
- Robinson, J., P.A. Lawrence, R.J. Shaw, L. Cogle, K. Rose, and R. Lait. 1999. Development and outcomes from a multiple objective decision support system for the Cattle Creek Catchment. Dep. of Natural Resources, Mareeba, QLD, Australia.
- Rumbaugh, J., I. Jacobson, and G. Booch. 1999. The unified modeling language reference manual. Addison-Wesley, NY.
- Saaty, T.L. 1990. How to make a decision: The analytic hierarchy process. *European Journal of Operational Res.* 48: 9-26.
- Sanchez Cohen, I., E. Catalan Valencia, M. Rivera Gonzalez, and M.A. Vuelvas Cisneros. 2003. Optimizacion del ingreso neto y productividad del agua en los Distritos del Riego del pais. CENID RASPA INFAP. Ciudad Lerdo, Durango, Mexico.
- Schmoldt, D.L., J. Kangas, G.A. Mendoza, and M. Pesonen. 2001. The analytic hierarchy process in natural resource and environmental decision making. Kluwer Academic Publishers, Boston, MA.
- Shenk, T.M., and A.B. Franklin. 2001. Modeling in natural resources management: Development, interpretation, and applications. Island Press, Washington, DC.
- Siegele, L. 2003. The IT industry. *The Economist*. 8 May. London, U.K.
- Singh, V.P. 2001. Water Resources L.L.C. editor profile: Vijay Singh [Online]. Available at <http://www.wrpllc.com/authors/singh.html> (accessed 31 May 2003; verified 12 Jan. 2004). Water Resource Publications, Highlands Ranch, CO.
- Southwest Watershed Research Center. 1994. A multiple objective decision support system for the USDA water quality initiative: Reference manual, version 1.1. USDA-ARS, Tucson, AZ.
- Turban, E., and J.E. Aronson. 2000. Decision support systems and intelligent systems. 6th ed. Available online at <http://cwx.prenhall.com/bookbind/pubbooks/turban2/> (accessed 14 June 2005; verified 1 July 2005). Prentice Hall, Upper Saddle River, NJ.
- Walters, C. 1986. Adaptive management of renewable resources. The Blackburn Press, Caldwell, NJ.
- Walters, C. 2001. Adaptive management of renewable resources. The Blackburn Press, Caldwell, NJ.

- Wischmeier, W., and D. Smith. 1978. Predicting rainfall-erosion losses. USDA Agric. Handb. 537. USDA-Science and Education Administration, Washington, D.C.
- Wymore, A.W. 1988. Structuring system design decisions. p. 704-709. In C. Weimin (ed.) Systems science and engineering. Proc. Int. Conf. on Systems Science and Engineering (ICSSE), Beijing, China. 25-28 July 1988. Int. Academic Publishers, Beijing, China.
- Yakowitz, D.S., L.J. Lane, and F. Szidarovsky. 1993. Multi-attribute decision making: Dominance with respect to an importance order of attributes. Appl. Mathematics and Computation 54:167-181.
- Yakowitz, D.S., and M. Weltz. 1998. An algorithm for computing multiple attribute additive value measurement ranges under a hierarchy of the criteria: Application to farm or rangeland management decisions. p. 163-177. In E. Beinat and P. Nijkamp (ed.) Multicriteria analysis for land use management. Kluwer Academic Publishers, Boston.

INDEX

- Absorption, ozone, 59
Actual evapotranspiration (AET), 33, 41, 74, 83
Adaptive management, 214
Advanced Land Observation Satellite (ALOS), 92, 93
Advanced Microwave Scanning Radiometer on the NASA Aqua Satellite (AMSR-E), 92, 93, 97, 102
Advanced Synthetic Aperture Radar (ASAR), 92, 93
Advanced Very High Resolution Radiometer (AVHRR)
 broadband scanner, 52
 NDVI composite image, 18, 59
 NDVI data for yield prediction, 18, 22
 resolution
 spatial, 18, 22, 23, 201
 temporal, 18
 weather data, 53–55, 56
Aerial photographs, 190
AET, *see* Actual evapotranspiration
Agricultural Land Management Alternatives with Numerical Assessment Criteria (ALMANAC)
 background, 2–4, 3–5
 crop parameters, 5–8
 using remote sensing, 23
 water savings assessment, 230
 yield components, 8–10
Agricultural policy, 1, 15, 155, 216
Agricultural Research Service (ARS), 2, 14, 22–23, 24, 87, 120, 128, 129, 133, 218
Agricultural systems, 212–213, 215–216
Agriculture
 agrometeorological assessments, 29–43, 45–50
 hill slope/stEEP slope, 29, 160, 175, 178, 185
 irrigated
 agroclimatic modeling, 33, 41, 42
 checklist of resource problems, 223
 futures analysis, 140, 150, 155
 irrigation scheduling, 81–83
 planning in irrigation districts, 221–230
 soil erosion modeling, 169
 yield prediction with MSPC, 16, 19–22, 23
 management using DSS, 212–235
precision, 15, 23, 84
rainfed
 effect on watersheds, 160
 erosion simulation, 169, 183
 in Mexico 30, 41
 tillage practices, 160–185
Agroclimatic modeling, 29–43
Agrometeorological assessments
 ENSO-related, 29–43
 WAOB, 45–50
Agrometeorological bulletins, 45–50
AGWA, *see* Automated Geospatial Watershed Assessment tool
Alamo switchgrass, 3
Alfalfa, 75, 76, 77, 80, 225
ALMANAC, *see* Agricultural Land Management Alternatives with Numerical Assessment Criteria
ALOS, *see* Advanced Land Observation Satellite
Alternative crop(s), 2, 30, 87
Alternative futures analysis, 117–120, 148–155, 156
AML, *see* Arc Macro Language
AMSR-E, *see* Advanced Microwave Scanning Radiometer on the NASA Aqua Satellite
Ancillary data, land classification using, 195–200
ANN, *see* Artificial Neural Network
Antenna, radar, 92
Anthesis, 3, 5, 7, 17
Aquitifer, 109, 153
ArcGIS, 48, 49
ArcInfo, 56, 66
Arc Macro Language (AML), 56, 66
ArcView, 48, 112, 122, 129, 130
Arid climate, 54, 55, 72, 75, 79, 80, 84, 86, 99, 107, 129
ARNO model, 108
ARS, *see* Agricultural Research Service
Artificial Neural Network (ANN), 195, 196, 197, 199–200, 202–203, 204
ASAR, *see* Advanced Synthetic Aperture Radar
Automated Geospatial Watershed Assessment (AGWA) tool, 128–155
applications, 140–154
land-cover change analysis, 143–148

- Automated Geospatial Watershed Assessment (AGWA) tool (cont.)
 land-use planning, 148–154
 data input and parameter estimation, 138–140
 hydrologic models
 KINEROS2, 129, 131, 132–135, 138–144, 146–148, 155
 SWAT, 135–137
 sequence of steps, 130–132
- Avena sativa* L., see Oat
- AVHRR, *see* Advanced Very High Resolution Radiometer
- Backpropagation networks, 200
- Backscatter, 91–102
- Balance, water, 2, 3, 5, 53, 74, 81, 109, 111, 135
- Band(s)
 AVHRR, 52
 blue, 59
 C-band, 92
 combination, 168, 182
 infrared, 94, 97
 land classification, 168, 182, 191–192, 195, 197, 202, 205
 Landsat TM, 168, 182, 197
 L-band, 93, 97
 MODIS, 52, 59
 near-infrared (NIR), 52, 59, 94, 97
 PAR, 8, 17
 red, 59
 SAR, 92, 93, 97
 spectral, 52, 59, 168, 191, 202
 thermal infrared, 52
 visible, 56, 59, 97
- Barley, 34, 40, 41, 42, 43
- Base temperature, 3, 5, 6, 113
- Basin, 63–67, 91–102, 107–122, 128–156, 160–185, 221–230, *see also* Watershed
- BASINS, *see* Better Assessment Science Interacting Point and Nonpoint Sources
- Bean, 33, 34, 40, 41, 42, 43, 83, 84, 86, 225
- Beer's law, 3, 8
- Best Management Practices (BMPs), 117–120, 160–161
- Better Assessment Science Interacting Point and Nonpoint Sources (BASINS), 117, 136
- Biomass, plant, 8, 17, 32, 63
- Blackland Research Center, 18, 56, 57
- Blue band, 59
- BMPs, *see* Best Management Practices
- Bosque River watershed, 117–120
- Brassica napus* L., *see* Oilseed rape
- Brightness temperature, 55, 92, 94
- Budget, water, 86, 136,
- Bulk density, soil, 111, 113, 166
- Canopy light interception, 3, 4, 7, 8
- CARE, *see* Cost and Return Estimator
- CART, *see* Classification and Regression Tree
- C-band, 92
- Change detection approach, 96–97, 100, 102
- Channel, *see* Band
- Chile, 86
- Classification, land, *see* Land-use/cover classification
- Classification and Regression Tree (CART), 195, 196, 197, 198, 199
- Classification tree, 198
- Climate, *see also* El Niño Southern Oscillation
 agroclimatic modeling, 29–43
 arid, 54, 55, 72, 75, 79, 80, 84, 86, 99, 107, 129
 change in Mexico, 29–30, 32, 35–39
 causes, 30–31
 effects on crops, 29, 31, 32–34, 40–43
 parameters, 34, 53–56
 semi-arid, 15, 72, 75, 95, 99, 128, 129, 133, 141
- Cloud contamination, 18, 56, 59, 63
- Clustering, 193, 194, 201
- CN, *see* Curve number method
- CNA, *see* Comision Nacional de Agua
- Comision Nacional de Agua (CNA), 224–227
- Compaction, 224
- Composite image
 MODIS EVI, 59–63
 MODIS NDVI, 59
 MVC correction procedure, 18, 59, 63
 NOAA-AVHRR NDVI, 18, 59
 supervised land classification, 182
- Conceptual models, 108, 109
- Concurrent Version System (CVS), 221
- Conservation, soil, 216–218, *see also* Tillage
- Conservation Practices Physical Effects (CPPE), 218
- Conservation tillage (CT), 160–185, 218
- Contamination, cloud 18, 56, 59, 63
- Conventional tillage, *see* Traditional tillage
- Core 4, 217
- Corn, *see* Maize
- Correction, satellite image, 52, 56, 59, 95, 96, 99, 116, 168, 184

- Cost and Return Estimator (CARE), 167
Cover, soil, 160, 161, 168, 170, 172, 182–184
CPPE, *see* Conservation Practices Physical Effects
CREAMS model, 109
Crop
 barley, 34, 40, 41, 42, 43
 bean, 33, 34, 40, 41, 42, 43, 83, 84, 86, 225
 chile, 86
 corn, *see* Maize
 melon, 86
 oat, 34, 40, 41, 42
 onion, 40
 peanut, 86
 potato, 5, 34, 42, 43
 sorghum, 1, 3, 5, 6, 7, 9, 34, 40, 41, 42, 59–63, 63, 84, 86
 soybean, 5, 6, 7, 114
 tomato, 86
 watermelon, 86
 wheat, 2, 5–6, 9, 33–34, 42–43, 49, 67, 83, 95–96, 114
Crop, alternative, 2, 30, 87
Crop diseases, 67
Crop modeling, 1–10, 13–23, 32–34, 40–43
Crop monitoring, 45–50, 59–63
Crop parameters, 5–8, 15, 17
Crop rotation, 2, 113, 213
Crop weather bulletins, 45–50
Crop yield prediction, 8–10, 13–23, 32–34, 40–43
CT, *see* Conservation tillage
Curve number method, 63–67, 109, 113, 133, 135, 136, 139, 143, 166, 179
CVS, *see* Concurrent Version System
- DAMS database, 114
Data fusion, SAR, 97–98, 100
Datasets, watershed modeling, 114–117
Decimal code, 18
Decision criteria, 167, 168, 181, 219, 230
Decision Support System (DSS), 161, 165, 166–168, 180–182, 211–232
Decision Support System of Agrotechnology Transfer (DSSAT), 216
Decision theory, 213–214
Decision tree, 198
Decision-making, multi-objective, 214, 218–220, 230–231
DEM, *see* Digital Elevation Model
Denitrification, 111
Depletion, soil, 108, 185
Desert, 30, 141–143, 145, 147, 155
Desertification, 30
Digital Elevation Model (DEM), 112, 113, 114, 115, 116, 117, 131, 133, 138, 139, 142, 169, 198, 203
Digital slope model, 168
Discriminant analysis, 196
Distrito de Riego 017, 224, 226–231
Diversity, 128, 141–142
Doppler radar, 52, 116
DR 017, *see* Distrito de Riego 017
Drainage, 2, 22, 64, 81, 82, 115, 131, 138
DRAR, *see* Relative Water Availability Index
DREAM, *see* Dynamic Research Evaluation for Management
Drought
 Almanac validation, 1
 crop vulnerability, 1, 9
 drought indices, 46, 53
 harvest index, 3
 in Mexico, 31
 Keetch-Bryam Drought Index, 53–59
 North American Drought Monitor, 49
 soil surface moisture information, 91
 stress studies, 9, 30
Dry matter, 3, 5, 23, 98
DSS, *see* Decision Support System
DSSAT, *see* Decision Support System of Agrotechnology Transfer
Dynamic Research Evaluation for Management (DREAM), 216
- Elevation Derivatives for National Applications, 114–115
El Niño (EN), 32, 35–40, 41–43
El Niño Southern Oscillation (ENSO)
 background, 30–31
 climate deviations in Mexican states, 35–39
 Guanajuato, 36
 Jalisco, 37
 Mexico, 35
 Michoacan, 38
 Tamaulipas, 39
 early warning system, 31
 scenarios
 El Niño (EN), 32, 35–40, 41–43
 El Viejo (EV), 32
 La Niña (LN), 32, 35–40, 41–43
 Neutral (N), 32, 35, 40, 41–43
 Strong El Niño (SEN), 32
 impact on Mexican agriculture, 41–43
 El Viejo (EV), 32
Enhanced Thematic Mapper (ETM), 19, 23, 60
Enhanced Vegetation Index (EVI), 59–63

- ENSO, *see* El Niño Southern Oscillation
- Environment Satellite (ENVISAT), 92–93
- Environmental Systems Research Institute (ESRI), 56, 63
- ENVISAT, *see* Environment Satellite
- EPIC, *see* Erosion Productivity Impact Calculator
- Erosion
- equations, 168–169, 183
 - gully, 224
 - modeling, 160–185
 - rill, 174, 175, 216, 224
 - sheet, 216, 224
 - soil, 111, 160, 162, 165, 173, 181, 184, 185, 217, 218
 - wind, 224
- Erosion Productivity Impact Calculator (EPIC), 2, 23, 32–34, 111
- ERS SAR, *see* European Remote Sensing Synthetic Aperture Radar
- ESA, *see* European Space Agency
- ESRI, *see* Environmental Systems Research Institute
- ET, *see* Evapotranspiration
- ETM, *see* Enhanced Thematic Mapper
- European Remote Sensing Synthetic Aperture Radar (ERS SAR), 92, 93, 95, 101
- European Space Agency (ESA), 92, 93, 102
- Eutrophication, 160
- Evaporation, 22, 33, 73, 74, 79–81, 82, 97, 109, 197
- Evapotranspiration (ET)
- actual (AET), 33, 41, 74, 83
 - computation methods, 74–81
 - combination methods, 75–77
 - evaporation methods, 79
 - radiation methods, 77–78
 - temperature methods, 78–79
 - data applications, 81–82, 83–86
 - definition, 73
 - modeling, 72–87
 - potential (PET), 3, 5, 33, 40, 41, 42, 67, 73, 75, 78, 109
- EVI *see* Enhanced Vegetation Index
- Facilitator, 218–219, 227, 229
- FAO radiation method, 78
- Feed, animal, 118
- Fertility, soil, 29, 184
- Fertilizer, 2, 15, 113, 136, 213, 215, 218
- Field-scale model, 1–10, 109, 217
- FIPAR, *see* Fraction of Intercepted Photosynthetically Active Radiation
- Florida Automated Weather Network, 47
- Forage, 225
- alfalfa, 225
 - maize/corn, 84, 86
 - sorghum, 86
 - winter crops, 227, 228
- Forecasts
- agricultural supply and demand, 45
 - agrometeorological, 45–50
 - ENSO, 30, 31
 - yield, 13, 14, 15, 16–23
- Fraction of Intercepted Photosynthetically Active Radiation (FIPAR), 23, 59
- Fuzzy logic, 193
- GAM, *see* Generalized additive models
- Generalized additive models (GAM), 195, 196, 199
- Generalized linear models (GLM), 196, 197
- General plant model, 1–10
- Geographic Information Systems (GIS),
- applications
 - AGWA, 129–131, 138, 139, 142, 149, 155
 - BASINS, 117
 - erosion simulation, 168–169, 182–184, 185
 - HUMUS, 120
 - KBDI, 54, 56, 57
 - land-use/cover classification, 169, 190, 191
 - natural resource modeling, 51, 53
 - SWAT, 111–113
 - WAOB, 48, 49
- Georeferencing, 143, 168
- Geostatistics, 200
- GIS, *see* Geographic Information Systems
- GLEAMS, *see* Groundwater Loading Effects and Agricultural Management Systems
- GLM, *see* Generalized linear models
- Global positioning systems (GPS), 18, 51, 168
- Glycine max* L. Merr, *see* Soybean
- GPS, *see* Global positioning systems
- Grain, 2, 3, 4, 6, 8, 9, 18, 20, 21, 34, 41, 86, 111, 120, 181
- Graphical Resources Analysis Support System (GRASS), 111
- Grass, 1, 3, 7, 75, 76, 77, 78, 79, 80, 122
- GRASS, *see* Graphical Resources Analysis Support System
- Grassland, 53, 96, 142, 143, 145, 147, 194
- Grid/gridding, 52, 56, 109, 112, 115, 116, 131, 133, 138, 139, 143, 204
- Groundwater, 114, 128, 142, 151, 153–155, 156, 219, 224

- Groundwater Loading and Evaluation of Agricultural Management Systems (GLEAMS), 109, 111, 161, 165–166, 168, 178–185
- Growing degree day models, 49
- Gully erosion, 224
- HAPEX-Sahel, *see* Hydrologic Atmospheric Pilot Experiment in the Sahel
- Hargreaves method, 79
- Harvest, 14, 22, 59, 113
- Harvest Index (HI), 2, 3, 7, 8–10, 111
- Helianthus annus* L., *see* Sunflower
- Herbicide, 113
- HI, *see* Harvest Index
- High Resolution Picture Transmission (HRPT), 18
- Hillel infiltration model, 164–165, 176–178
- Hill slope/stEEP slope agriculture, 29, 160, 175, 178, 185
- Historical rankings, 47
- HRAP, *see* Hydrologic Rainfall Analysis Project
- HRPT, *see* High Resolution Picture Transmission
- HRU, *see* Hydrologic Response Unit
- Humus, 111
- HUMUS, *see* Hydrologic Unit Model of the United States
- Hydraulic conductivity, 94, 132, 139, 143, 165, 176, 177, 178, 185
- Hydrologic Atmospheric Pilot Experiment in the Sahel (HAPEX-Sahel), 93, 101
- Hydrologic model /modeling
- AGWA toolkit, 128–156
 - ARNO, 108
 - BASINS, 117, 136
 - conceptual, 108
 - CREAMS, 109
 - differential, 108–109
 - EPIC, 22, 23, 32–34, 111
 - evapotranspiration, 72–87
 - GLEAMS, 109, 111, 161, 165–166, 168, 178–185
 - HUMUS, 120
 - IDHM, 108
 - KINEROS2, 129, 131, 132–135, 138–144, 146–148, 155
 - nonpoint source, 109
 - QUAL2E, 111
 - runoff and erosion, 63–67, 142, 143–156, 160–185
 - SHE, 108–109
- Soil Vegetation Atmosphere Transfer (SVAT), 91, 93, 101
- Stanford Watershed Model, 108
- surface soil moisture, 91–102
- SWAT, 107–122, 135–137, 139–140, 140–156
- TOPMODEL, 108
- Hydrologic Rainfall Analysis Project (HRAP), 52, 56
- Hydrologic Response Unit (HRU), 109, 112–113
- Hydrologic Unit Model of the United States (HUMUS), 2, 120, 136
- HYDROS, *see* Hydrospheric States mission, NASA
- Hydrospheric States mission (HYDROS), NASA, 93, 97, 102
- Hyperspectral imagery, 191, 192
- IDHM, 108
- IDRISI, 168, 169
- IEM, *see* Integral Equation Model
- IF SAR, 115
- IKONOS, 200, 201
- Image, satellite
- ALOS, 92, 93
 - AMSR-E, 92, 93, 97, 102
 - cloud contamination, 18, 56, 59, 63
 - correction, 52, 56, 59, 95, 96, 99, 116, 168, 184
 - composite, 18, 22, 59–63, 182
 - ESA ENVISAT, 92–93
 - ESA ERS SAR, 92, 93, 95, 101
 - hyperspectral, 191, 192
 - IKONOS, 200, 201
 - JERS SAR, 92, 93
 - Landsat, 19, 23, 60, 143, 168, 195, 197, 198, 200, 201
 - MODIS, 52, 59–63, 201
 - mosaic, 19, 52, 116, 142
 - multispectral, 59, 168, 191, 202, 203
 - NASA HYDROS, 93, 97, 102
 - NEXRAD, 52, 53, 54, 55, 56, 57, 63, 65, 66, 116
 - NOAA-AVHRR, 18, 22, 52, 53–55, 56, 201
 - PALSAR, 92, 93
 - QuickBird, 200, 201
 - RADARSAT, 92, 93, 95, 96, 99
 - SAR, 95, 96, 99, 199, 102
 - spatial resolution, 16, 18, 19, 22, 23, 52, 53, 56, 59, 60–63, 92, 93, 96, 97, 102, 116, 200–201, 203
 - spectral resolution, 59, 168, 202–203

- Image, satellite (cont.)
 - SPOT, 23
 - SSM/I, 47, 93, 101
 - temporal resolution, 18, 52, 116
- Image correction, 52, 56, 59, 95, 96, 99, 116, 168, 184
- Incidence angle, 92, 94, 95, 101
- Infiltration, 22, 64, 109, 132, 133, 135, 144, 145, 147, 148, 155, 164–165, 171, 176–178, 184
- Infiltration model, 164–165, 176–178
- Information Technology (IT), 212, 215, 231, 232
- Infrared band, 94, 97
- Infrared radiative temperature, 94, 97
- INIFAP, *see* Instituto Nacional de Investigaciones Forestales, Agricolas y Pecuarias
- Insecticide, 113
- Instituto Nacional de Investigaciones Forestales, Agricolas y Pecuarias (INIFAP), 14, 16, 22–23, 60, 161, 216
- Integral Equation Model (IEM), 93, 98–99
- Intercepted photosynthetically active radiation (IPAR) 7, 15, 23, 32, 59
- Interception, canopy light, 2, 3, 4, 7, 8
- Interrill detachment, 164, 174–175
- IPAR, *see* Intercepted photosynthetically active radiation
- Irrigated farming, *see* Agriculture
- Irrigation
 - crop irrigation schedules, 82, 83
 - decision-making, 14, 74, 84, 87, 213, 224–230
 - evapotranspirative deficit, 74
 - evapotranspiration estimation, 74–81
 - indexes, 73, 74, 84–86, 87
 - Irrigation District 017, 224, 226–230
 - modeling ENSO effects, 33, 41, 42
 - needs and water availability, 73–74
 - real-time system, 83, 87
 - scheduling, 74, 81–83, 84, 87, 111
 - SWAT simulations, 111, 113, 120, 121
 - water use by countries, 72, 73
 - yield prediction for irrigated areas, 14, 19, 20, 21, 22, 23, 33
- Irrigation District 017, 224, 226–231
- ISODATA, *see* Iterative Self-Organizing Data Analysis Techniques
- IT, *see* Information Technology
- Iterative Self-Organizing Data Analysis Techniques (ISODATA), 193
- Jalisco, 31, 33, 34, 37, 40–43
- Japanese Earth Resources Satellite Synthetic Aperture Radar (JERS SAR), 92, 93
- Jensen-Haise Equation, 77
- JERS SAR, *see* Japanese Earth Resources Satellite Synthetic Aperture Radar
- KBDI, *see* Keetch-Bryam Drought Index
- Keetch-Bryam Drought Index (KBDI), 53–58
- Kimberly Penman equation, 75, 76
- Kinematic Runoff and Erosion Model (KINEROS2)
 - applications, 140–156
 - description, 129, 132–133, 133–135, 139–140
- Kinematic wave approximation, 133, 134
- KINEROS2, *see* Kinematic Runoff and Erosion Model
- K-Nearest Neighbor, 196, 197
- K-NN, *see* K-Nearest Neighbor
- Kriging, 196, 200
- Laboratorio Nacional de Modelaje y Sensores Remotos, 16, 67, 216
- LAI, *see* Leaf area index
- La Laguna basin, 221
- Land-cover change analysis, 140–141, 143–148
- Landsat, *see* Land Satellite
- Land Satellite (Landsat)
 - image, land classification, 198, 200
 - Landsat ETM+, 19, 23, 60
 - Landsat MSS, 143
 - Landsat TM, 143, 168, 195, 197
 - spatial resolution, 201
 - spectral resolution, 168
- Land surface temperature (LST), 55, 57, 92
- Landsat Enhanced Thematic Mapper, 19, 60, 23
- Landsat ETM+, *see* Landsat Enhanced Thematic Mapper
- Landsat MSS, *see* Landsat Multi-Spectral Scanner
- Landsat Multi-Spectral Scanner (Landsat MSS), 143
- Landsat Thematic Mapper (Landsat TM), 143, 168, 195, 197
- Landsat TM, *see* Landsat Thematic Mapper
- Land-use/cover classification
 - applications, 189–190
 - approaches/methods, 189–206
 - mixed, 194–195

- Land-use/cover classification (cont.)
 nonparametric, 197–200
 parametric, 196–197
 parcel-based, 201–203, 205
 per-field, *see* parcel-based
 pixel-based, 191–200
 segmentation, *see* parcel-based
 spatial analysis, 196–200
 supervised, 168–169, 182–184, 193, 194, 199, 200, 204
 traditional, 193–194
 textural, 202–203, 102, 176
 using ancillary data, 195–200
 unsupervised, 193–194, 204
- Jalisco, 198
 National Land Cover Characterization, 116
 Patzcuaro watershed, 168–169, 182–184
- Landscape Science Program, 128, 129
- Land-use planning, 141, 148–155
 La Niña (LN), 32, 35–40, 41–43
 Lasers, 15
 L-band, 93, 97
 Leaf angle, 2
 Leaf area index (LAI)
 ALMANAC simulation, 3–8
 ceptometer, 18
 decline, 6, 7, 61
 evapotranspiration estimation methods, 75, 76, 77
 maximum, 23, 60, 62, 113
 potential, 4, 6
 relationship with NDVI, PAR, 20, 23, 59
 remotely sensed, 15, 22, 23
 use in yield prediction, 14, 15–16, 18, 23
 Water Cloud Model variable, 98
- Legume, 8
 LiCor leaf area meter, 8
 LIDAR, 115
 LST, *see* Land surface temperature
- MAI, *see* Moisture Availability Index
- Maize
 crop parameters for ALMANAC, 5, 6, 7, 9
 ENSO effects on yield, 33, 40–42
 EVI temporal profiles, MODIS, 62
 INIFAP yield forecasts, 14, 16–22
 land use, 31
 planting dates, 19, 59
 production in Mexico, 19–22, 29, 31, 225
 real-time monitoring, 59–63
 sensitivity to water stress, 1, 84
 tillage in Patzcuaro watershed, 160–185
 water use productivity, 86
- Western Corn Belt, 48
 yield simulation, 33, 16–22, 122
 ALMANAC, 3
 MSPC, 16–22
 South African model, 49
 SWAT, 122
- Management, adaptive, 214
 Manning's roughness, 133, 139
 Manure, 2, 113, 117, 118
- Map(s)
 average annual evapotranspiration (SWAT), 121
 average annual irrigation (SWAT), 121
 composite image, 182
 evapotranspiration, 85
 evapotranspirative deficit, 74
 GIS datasets for Upper San Pedro basin, 142
 Hydrologic Region 36, 222
 Irrigation District 017, 225
 Jalisco land-use classification, 198
 KBDI, 58
 KINEROS2 input parameters, 138
 Mexican states, 33
 Moisture Availability Index, 73
 North American Drought Monitor, 49
 percent change in channel discharge, 152
 percent change in percolation, 154
 percent change in sediment yield, 153
 percent change in surface runoff, 151
 San Pedro River basin study area, 141
 soil, 112–113, 114, 183
 soil losses in two management systems, 183
 Western Corn Belt, 48
- Markov processes, 32
 MARS, *see* Multivariate Adaptor Regression Spline
 Maximum likelihood method, 182–183, 193
 Maximum Value Composite (MVC), 18, 59, 63
 Melon, 86
 Meteorological stations, 34, 47, 53, 54, 55, 56, 114
 Mexico State, 31, 33, 34, 35, 40–43
 Michoacan, 31, 33, 34, 38, 40–43, 160, 161, 162, 171, 177
 Microbial biomass calculation, 170, 184–185
 Microwave brightness temperature, 92, 94
 Microwave sensing, 47, 91–102
 Mixed classification, 194–195
 Model(s), *see also* Modeling
 agrometeorological, 49–50
 ALMANAC, 2–20, 23, 230
 ANN-based, 199, 200, 203

- Model(s) (cont.)
- ARNO, 108
 - BASINS, 117, 136
 - conceptual, 108
 - continuous, 109
 - CREAMS, 109
 - crop, 1–10, 13–23, 49
 - differential, 108
 - Digital Elevation Model, 112
 - EPIC, 111
 - field-scale, 2, 109
 - generalized additive models (GAM), 195, 196, 197
 - generalized linear models (GLM), 196
 - general plant, 1–10
 - GLEAMS, 111, 165
 - growing degree day, 49
 - HUMUS, 2, 120, 136
 - hydrologic, *see* Hydrologic model/modeling
 - IDHM, 108
 - infiltration, 164–165
 - Integral Equation Model (IEM), 93, 98–99
 - KINEROS2, 129, 132–133, 133–135, 139–140, 140–156
 - linear, 195, 197
 - mathematical, 193
 - MSPC, 13–23
 - nonlinear, 199
 - nonpoint source, 109
 - process-oriented, 1
 - QUAL2E, 111
 - radar backscatter, 98–100
 - radiative transfer, 95
 - regression, 49, 55, 57, 199
 - run-off and erosion, 143–147, 160–185
 - semi-empirical, 98
 - SHE, 108–109
 - single-field, 2
 - Stanford Watershed Model, 109
 - SVAT, 91, 93
 - SWAT, 107–122, 135–137, 139–140, 140–156
 - TOPMODEL, 108
 - user-oriented, 1
 - water balance, 53
 - Water Cloud Model (WCM), 98
 - watershed, 109, 109, 113, 117–120, 128
- Modeling, *see also* Model(s)
- agrometeorological, 29–43, 49–50
 - crop, 2, 13–23, 32–33, 40–43, 121, 214
 - ENSO, 32, 35–39
 - evapotranspiration, 33, 40, 72–87
 - hydrologic, *see* Hydrologic model/modeling
 - irrigation, 72–87, 121
- land-cover change, 143–148
 - land-use future scenarios, 152–155
 - phosphorus loadings, 117–120
 - real-time
 - fire potential, 53–56
 - run-off, 63–67
 - runoff and erosion, 143–147, 160–185
 - surface soil moisture, 91–102
 - using AGWA, 128–155
 - watershed, 63–67, 91–102, 107–122, 128–156, 160–185, 214–215
- Modelo de Simulacion para Prediccion de Cosechas (MSPC)
- background, 16–17
 - current development, 22–23
 - input, 8
 - field data, 18
 - satellite data, 18
 - performance in Sinaloa, 19–22
 - schematic presentation, 16
 - variables, 17–18
- Moderate Resolution Imaging Spectroradiometer (MODIS)
- advantages, 59
 - composite image
 - crop monitoring data, 59–63
 - EVI, 59–63
 - NDVI, 59
 - resolution
 - spatial, 52, 59, 60, 61, 62, 63, 201
 - spectral, 52, 59
 - temporal, 59
- Modified Universal Soil Loss Equation (MUSLE), 111
- MODIS, *see* Moderate Resolution Imaging Spectroradiometer
- Moisture, soil, 10, 49, 53, 56, 65, 82, 91–102, 133
- Moisture Availability Index (MAI), 73, 84
- Mosaic, 19, 52, 116, 142
- MSPC, *see* Modelo de Simulacion para Prediccion de Cosechas
- MSS *see* Multi-spectral scanner
- Multiobjective decision-making, 214, 218–220, 230–231
- Multispectral scanner (MSS), 143
- Multispectral imagery, 59, 168, 191, 202, 203
- Multitemporal analysis, 96, 99
- Multivariate Adaptor Regression Spline (MARS), 170, 195, 196, 199
- MUSLE, *see* Modified Universal Soil Loss Equation
- MVC, *see* Maximum Value Composite

- NALC, *see* North American Landscape Characterization
- NASA, *see* National Aeronautics and Space Administration
- NASA Hydrospheric States mission (NASA HYDROS), 93, 97, 102
- NASS, *see* National Agricultural Statistics Service
- National Aeronautics and Space Administration (NASA), 52, 60, 92, 93, 97, 102, 115–116
- National Agricultural Census Data, 114
- National Agricultural Statistics Service (NASS), 47, 122
- National Crop Yield Prediction Project (Proyecto Nacional de Prediccion de Cosechas), 14, 16, 216
- National Elevation Dataset (NED), 23, 114, 115
- National Exposure Research Laboratory (NERL), 128, 129
- National Hydrography Dataset, 114
- National Imagery and Mapping Agency (NIMA), 115–116
- National Interagency Fire Center (NIFC), 53
- National Land Cover Characterization project, 116
- National Land Cover Data (NLCD), 66, 116
- National Oceanic and Atmospheric Administration (NOAA), 18, 23, 45, 47, 52–53, 56, 59, 217–218, 131, 136, 140
- National Research Institute on Forestry, Agriculture, and Livestock Production (INIFAP), 14, 16, 22–23, 60, 161, 216
- Natural resource management, 52–67, 74, 128–129, 214–215, 216–232
- National Weather Service (NWS), 52, 54, 56, 57, 116, 140, 144
- Natural Resources Conservation Service, 3, 63, 64, 66, 114, 122, 136, 142, 165, 217–218
- NBMI, *see* Normalized Radar Backscatter Soil Moisture Index
- NDVI, *see* Normalized Difference Vegetation Index
- Nearest Neighbor (NN), *see* K-Nearest Neighbor, Neighborhood analysis
- Near-infrared (NIR), 52, 59, 94, 97
- NED, *see* National Elevation Dataset
- Neighborhood analysis, 60, 112, 191, 196, 197, 202, 203
- NERL, *see* National Exposure Research Laboratory
- Neutral years (N), 30, 32–33, 40–43
- NEXRAD, *see* Next Generation Weather Radar
- Next Generation Weather Radar (NEXRAD), 52, 53, 54, 55, 56, 57, 63, 65, 66, 116
- NIFC, *see* National Interagency Fire Center
- NIMA, *see* National Imagery and Mapping Agency
- NIR, *see* Near infrared
- Nitrification, 111
- Nitrogen, 9, 32, 109, 111, 113, 184
- NLCD, *see* National Land Cover Data
- NOAA, *see* National Oceanic and Atmospheric Administration
- Noise, *see* Sensor noise
- Nonparametric approach, 197–200
- Nonpoint source, 109, 117, 136
- Normalized Difference Vegetation Index (NDVI), 17, 18, 22–23, 56, 59, 63, 93, 97
- Normalized Radar Backscatter Soil Moisture Index (NBMI), 93, 96
- North American Drought Monitor, 49
- North American Landscape Characterization (NALC), 142, 143
- No-tillage, *see* Conservation tillage
- NRCS, *see* Natural Resources Conservation Service
- NWS, *see* National Weather Service
- Oat, 2, 34, 40, 41, 42, 43
- Oilseed rape, 2
- Onion, 40
- Optical remote sensing, 97–98, 100, 101
- Organic farmng, 213
- Organic matter, 17, 166, 170, 184, 185, 216, 217
- PALSAR, *see* Phased Array type L-band Synthetic Aperture Radar
- Pan evaporation method, 79
- Panicum virgatum* L., *see* Alamo switchgrass
- PAR, *see* Photosynthetically Active Radiation
- Parameter(s)
- climate, 34, 53–56
 - crop, 5–8, 15, 17
 - erosion, 85
 - roughness, 97, 99
- Parameterization, 98, 99, 100, 109, 131, 109, 130
- Parametric approach, 196–197
- Parcel-based classification, 201–203, 205

- Partitioning coefficients, 17–18, 22
 Pattern (land use/cover classification), 202–204
 Pattern recognition, 190, 199, 200, 202–203
 Patzcuaro watershed, 160–185
 PCI Geomatics, 56, 60
 PCWA, *see* Per Capita Water Availability
 Peanut, 86
 Penman equation, 75, 76
 Penman-Monteith equation, 76, 109
 Per Capita Water Availability (PCWA), 72
 Percolation, 81–82, 109, 111, 135, 150, 151, 153–155
 Pesticide, 109, 111, 113, 213, 215, 217, 218, 223, 224
 Pests, 32, 217
 PET, *see* Potential evapotranspiration
 Phased Array type L-band Synthetic Aperture Radar (PALSAR), 92, 93
 Phosphorus loadings, 111, 117–120
 Photogrammetry, 115, 116
 Photographs, aerial, 190
 Photosynthetically active radiation (PAR), 7–10, 15, 17–18, 22, 59
 FIPAR, 23, 59
 IPAR, 7, 15, 23, 32
 Pixel-based classification, 191–201
 Pixel variability, 201
 Plant biomass, 8, 17, 32, 63
 Plant growth simulation, *see* Crop Modeling
 POES, *see* Polar Orbiting Environmental Satellites
 Point source, 53, 109, 117, 118
 Polarization, 92, 93, 95, 100, 101
 Polar Orbiting Environmental Satellites (POES), 52
 Policy-making
 agricultural, 1, 15, 155, 216
 environmental, 141, 149
 in Mexican agriculture, 216
 water management, 108
 with AGWA, 141, 149, 155
 with DSS, 216, 230
 with land-use/cover classification data, 190
 with models, 1, 15
 Pollution, water, 117, 120
 Postprocessing, 117
 Potato, 5, 34, 42, 43
 Potential evapotranspiration (PET), 3, 5, 33, 40, 41, 42, 67, 73, 75, 78, 109
 Precision agriculture, 15, 23, 84
 Preprocessing, 97, 112, 115
 Priestley-Taylor method, 33, 77, 80, 81, 109
 Profile soil moisture, 91, 93, 94
 Proyecto Nacional de Prediccion de Cosechas,
 see National Crop Yield Prediction Project
 Pulse, 92
 Qual2E model, 111
 Quickbird system, 200, 201
 Radar antena, 92
 Radar backscatter models, 98–100
 Radar remote sensing, 15, 52–53, 55, .57, 63, 66, 67, 91–102, 115, 116, 140
 Radar Satellite (RADARSAT), 92, 93, 95, 96, 99
 Radiation-use efficiency (RUE), 3, 5–9
 Radiative transfer model, 95
 Rainfall simulation, 32, 163–165, 173–178, 185
 Rainfed farming, *see* Agriculture
 Rangeland, 64, 98, 183, 218, 223, 224
 Raster format, 112, 115
 Real-time systems, 51–67
 crop monitoring, 59–63
 runoff estimation, 63–67
 wildfire risk assessment, 53–58
 Red band, 59
 Reflectance, 18, 59, 63, 94, 97, 101, 191, 193, 202
 Reflectivity, 116
 Regression models, 49, 55, 57, 199
 Regression tree, 195–196, 197–198
 Regular Spline method, 56
 Relative Water Availability Index (DRAR), 84–85, 87
 Remote sensing (RS)
 aerial photographs, 190
 applications
 crop yield prediction, 15, 18, 19, 22, 23
 crop monitoring, 59–63
 erosion modeling, 168, 169, 182–184
 KBDI calculation, 54–58
 land-use/cover classification, 19, 168, 169, 182, 189–206
 landscape assessment, 141, 142, 143, 145, 146, 156
 soil moisture mapping, 91–102
 combined with modeling, 15–16
 definition, 202–203, 220
 imagery, *see* Image, satellite
 lasers, 15
 microwave, 47, 91–102
 optical, 97–98, 100, 101

- Remote sensing (RS) (cont.)
 radar, 15, 52–53, 55, .57, 63, 66, 67, 91–102, 115, 116, 140
 satellite systems, *see* Satellites and sensors
 seismograph, 15
 spatial resolution, 16, 18, 19, 22, 23, 52, 53, 56, 59, 60–63, 92, 93, 96, 97, 102, 116, 200–201, 203
 spectral resolution, 59, 168, 202–203
 temporal resolution, 18, 52, 116
 Residue, 111, 160, 161, 172, 176, 180, 181, 217
 Resolution
 spatial, 16, 18, 19, 22, 23, 52, 53, 56, 59, 60–63, 92, 93, 96, 97, 102, 116, 200–201, 203
 spectral, 59, 168, 202–203
 temporal 18, 52, 116
 Revised Universal Soil Loss Equation (RUSLE), 216–217
 RFC, *see* River Forecast Center
 Rill detachment, 163–164, 175–176
 Rill erosion, 174, 175, 216, 224
 Rio Aguanaval watershed, 224
 Rio Nazas watershed, 224
 River Forecast Center (RFC), 56, 116
 Rotation, crop, 2, 113, 213
 Roughness, 76, 92, 94, 95, 96, 97, 98, 99, 101, 143, 145, 147, 148, 179
 RS, *see* Remote Sensing
 RUE, *see* Radiation-use efficiency
 Runoff, 52, 63–67, 82, 108, 109, 111, 117, 130–136, 140–142, 143–148, 149–156, 160–185, 216–217, 219, 223
 RUSLE, *see* Revised Universal Soil Loss Equation
- Salinity, 29, 93, 224, 225
 San Pedro River basin, 140–148, 149–156
 SAR, *see* Synthetic Aperture Radar
 SAR bands, 92, 93, 97
 Satellites and Sensors, *see also* Image, satellite; Remote sensing
 ALOS, 92, 93
 AMSR-E, 92, 93, 97, 102
 ESA ENVISAT, 92–93
 ESA ERS SAR, 92, 93, 95, 101
 IKONOS, 200, 201
 JERS SAR, 92, 93
 Landsat, 19, 23, 60, 143, 168, 195, 197, 198, 200, 201
 Landsat ETM+, 19, 23, 60
 Landsat MSS, 143
 Landsat TM, 143, 168, 195, 197
 MODIS, 52, 59–63, 201
 NASA HYDROS, 93, 97, 102
 NEXRAD, 52, 53, 54, 55, 56, 57, 63, 65, 66, 116
 NOAA-AVHRR, 18, 22, 52, 53–55, 56, 201
 PALSAR, 92, 93
 POES, 52
 QuickBird, 200, 201
 RADARSAT, 92, 93, 95, 96, 99
 SPOT, 23
 SSM/I, 47, 93, 101
 Satellite pour l'observation de la terre (SPOT), 23
 Scattering, 94, 99, 100, 102
 Score functions, 167, 219, 227
 SCS, *see* Soil Conservation Service
 SCS Blaney-Criddle method, 78
 Sediment yield, 108, 111, 141, 143, 146–148, 150–151, 153–156, 161, 162, 166–172, 178–183, 185
 Seed, 7, 9, 10
 Seedling emergence, 5
 Segmentation, *see* parcel-based classification
 Seismographs, 15
 Semi-arid climate, 15, 72, 75, 95, 99, 128, 129, 133, 141
 SEN, *see* Strong El Niño
 Senescence, 6, 61
 Sensor noise, 201, 202
 SGP, *see* Southern Great Plains experiments
 Shape (land use/cover classification), 7, 60, 112, 139, 167, 171, 190, 191, 202, 203, 205
 SHE model, 108
 Shear stress, 163–164, 175–176
 Sheet erosion, 216, 224
 Shuttle Radar Topography Mission (SRTM), 115
 Sierra Vista subwatershed, 145–148, 156
 Silage
 corn, 34, 40, 41, 42, 43
 oat, 34, 40, 41, 42, 43
 sorghum, 34, 40, 41, 42
 Simulation models 1, 14, 16, 17, 32, 93, 98, 129, 165, 168, 178, 213–215, 217, 218, 230–231, *see also* Model(s), Modeling
 Sinaloa, 14, 19–22
 Sistema de Prediccion de Cosechas, 216
 SMOS, *see* Soil Moisture and Ocean Salinity
 Soil
 attributes for watershed modeling, 113

- Soil (cont.)
- bulk density, 111, 113, 166
 - conservation, 216–218, *see also* Conservation Tillage
 - cover, 160, 161, 168, 170, 172, 182–184
 - erodibility, 166, 173, 175, 176, 216
 - erosion, 111, 160, 162, 165, 173, 181, 184, 185, 217, 218
 - fertility, 184, 291
 - hydraulic conductivity, 94, 132, 139, 143, 165, 176, 177, 178, 185
 - loss rate, 166
 - map(s), 112–113, 114, 183
 - moisture, 10, 49, 53, 56, 65, 82, 91–102, 133
 - Soil Conservation Service (SCS), 65, 78, 80, 81, 135–136, 139, 140, 217
 - STATSGO data, 87, 111, 139, 156
 - surveys, 114
 - SWAT model, 107–122, 135–137, 139–140, 140–156
 - texture, 22, 82, 92, 101, 102, 113, 139, 166, 176
 - type, 12, 34, 64–65, 83, 95, 96, 176, 195
- Soil and Water Assessment Tool (SWAT)
- applications
 - AGWA, 140–156
 - national, (U.S.), 120–122
 - watershed, 117–120
 - available databases, 114–117
 - components, 109
 - current development, 122
 - GIS interfaces, 111–113
 - inputs, 113
 - Mexican application requirements, 122
 - operational structure, 110
 - overview, 109–111, 135–137
- Soil Conservation Service (SCS), 65, 78, 80, 81, 135–136, 139, 140, 217
- Soil Moisture and Ocean Salinity (SMOS), 92, 93, 97, 102
- Soil Survey Geographic (SSURGO), 114
- Soil Vegetation Atmosphere Transfer (SVAT), 91, 93, 101
- Solanum tuberosum*, L., *see* Potato
- Sorghum
- crop parameters for ALMANAC, 5, 6, 7, 9
 - ENSO effects on yield, 40–42
 - EVI temporal profiles from MODIS data, 61
 - growing season, 34, 59
 - irrigation scheduling, 83
 - real-time monitoring, 59–63
 - sensitivity to water stress, 1, 84
 - water use productivity, 86
- yield simulation with Almanac, 3
- Sorghum bicolor* L. Moench, *see* Sorghum
- Southern Great Plains (SGP) experiments, 101
- Southwest Watershed Research Center, 128, 218
- Soybean, 5, 6, 7, 114
- Spatial analysis, 47, 48, 108, 200
- Spatial resolution, 16, 18, 19, 22, 23, 52, 53, 56, 59, 60–63, 92, 93, 96, 97, 102, 116, 200–201, 203
- Spatial Sciences Laboratory, 14
- Special Sensor Microwave Imager (SSM/I), 47, 93, 101
- Spectral resolution, 59, 168, 202–203
- SPOT, 23
- SRTM, *see* Shuttle Radar Topography Mission
- SSM/I, *see* Special Sensor Microwave Imager
- SSURGO, *see* Soil Survey Geographic
- Stanford Watershed Model, 108
- State Soil Geographic (STATSGO), 66, 114, 120, 139, 142
- Stations, meteorological, 34, 47, 53, 54, 55, 56, 114
- STATSGO, *see* State Soil Geographic
- Steep slope/hill slope agriculture, 29, 160, 175, 178, 185
- Strong El Niño (SEN), 32
- Sunfleck ceptometer, 7
- Sunflower, 5–7
- Supervised classification, 168–169, 182–184, 193, 194, 199, 200, 204
- Surface roughness, *see* roughness
- Surface soil moisture, 91–102
- Sustainability
- assessments with DSS, 215, 216, 218, 220, 227, 230
 - soil management, 161, 170, 184, 185
- SVAT, *see* Soil Vegetation Atmosphere Transfer
- SWAPA+H (Soil, Water, Air, Plant, Animal, and Human) method, 218, 222
- SWAT, *see* Soil and Water Assessment Tool
- Synthetic Aperture Radar (SAR), 91–102
- satellite systems, soil moisture mapping
 - Canadian C-band RADARSAT-1/2, 92, 93, 95, 96, 99
 - ESA ERS-1/2 C-band SAR, 92
 - ESA ENVISAT C-band ASAR, 92
 - plus radar backscatter models, 98–100
- TAES, *see* Texas Agricultural Experiment Station
- TAMU, *see* Texas A and M University

- Temperature
air, 29, 32, 55, 56, 75, 111
anomalies, 47
base, 3, 5, 6, 113
bulletin, 46
crop weather assessment methods, 47–49
dew point, 75
GLEAMS input, 165
infrared radiative, 94, 97
KBDI parameter, 53, 54–55, 56, .57
land surface temperature (LST), 55, 57, 92
mean, 166
methods for evapotranspiration estimation, 75, 76, 77, 78, 78–79, 80, 81
microwave brightness, 92, 94
minimum,maximum, 30, 32, 34, 35–39, 54, 55, 56, 77, 79, 111, 113, 114, 165, 166
ocean surface, 30
optimum, 3, 5, 6
pattern change, 33, 34, 35–39, 43
remote sensing data, 53, 54–55, 56, 57
soil, 46, 109, 111
statistical data, 114, 150, 166
SWAT component, 109, 111, 113
Temporal resolution, 18, 52, 116
Temporal scale, 75, 81, 96, 100, 129
Texas Agricultural Experiment Station, 67, 120
Texture, soil, 22, 82, 92, 101, 102, 113, 139, 166, 176
Texture, image, 190, 191, 200, 202, 203, 204, 205
Textural approach, 102, 176, 202–203
Thematic mapper, 143, 168, 195, 197
Thermal Abnormality Index, 32
Thermal infrared band, 52
Thiessen,
 polygon map, 131, 140
 precipitation weighting, 140
Tillage
 conservation, 160–185, 218
 traditional/conventional, 161–185
Time series analyses, 47
TM *see* Thematic mapper
TMDL, *see* Total Maximum Daily Load
Tomato, 86
TOPMODEL, 108
Total Maximum Daily Load (TMDL), 117
Traditional tillage (TT), 161–185
Training fields, 168–169, 182
Transpiration, 5, 22, 32, 33, 73
Tree, objectives, 227
Triticum aestivum L., *see* Wheat
TT, *see* Traditional tillage
Type, soil, 12, 34, 64–65, 83, 95, 96, 176, 195
UML, *see* Unified Modeling Language
Unified Modeling Language (UML), 221
United States Department of Agriculture (USDA), 2, 14, 22–23, 45, 66–67, 114, 120, 128–29, 133, 135, 139–140, 142, 218
United States Environmental Protection Agency (USEPA), 117, 122, 128–129, 136
United States Geological Survey, (USGS), 64, 65, 66, 114, 115, 116, 117, 133, 136, 141, 142, 143, 144
Universal Soil Loss Equation (USLE), 111, 166, 216–217
Unsupervised classification, 193–194, 204
United States Environmental Protection Agency, 117, 122, 128–129, 136, 143
USDA, *see* United States Department of Agriculture
USEPA, *see* United States Environmental Protection Agency
USGS, *see* United States Geological Survey
USGS Water Use database, 114
USLE, *see* Universal Soil Loss Equation
Vapor pressure deficit (VPD), 5, 80
Vegetation backscatter, 94, 95, 98, 99, 101
Vegetation indices
 Enhanced Vegetation Index (EVI), 59–63
 Normalized Difference Vegetation Index (NDVI), 17–18, 22–23, 56, 59, 63, 93, 97
Vetch, 2–3
Vicia sativa L., *see* Vetch
Visual interpretation criteria, 206
VPD, *see* Vapor pressure deficit
Walnut Gulch Experimental Watershed, 133, 137, 143
WAOB, *see* World Agricultural Outlook Board
Water
 availability, 72, 73–74, 84, 86
 balance, 2, 3, 5, 53, 74, 81, 109, 111, 135
 content, soil, 33, 81–82, 135, 136
 pollution, 117, 120
 quality, 108, 109, 117, 120, 128, 148, 156, 213, 217–218, 221, 225, 231
 use, 72, 73, 74, 83, 86, 87, 114, 136, 155, 224, 225, 226–227, 230

- Water Cloud Model (WCM), 93, 98–99
 Watermelon, 86
 Water Quality Decision Support System (WQDSS), 218
 Watershed
 Bosque River, 117–120
 LAI, *see* Leaf area index
 La Laguna, 221
 modeling, *see also* Hydrologic model/modeling
 available datasets, 114–117
 management practices and mineral P loadings, 117–120
 model inputs, 113
 real-time run-off estimation, 63–67
 runoff and erosion in two tillage systems, 160–185
 soil moisture estimation using radar remote sensing, 91–102
 using SWAT model, 107–122
 using AGWA tool, 128–156
 watershed condition indicators, 141, 143
 watershed discretization, 138
 Patzcuaro Lake, 160–185
 planning with DSS, 214–215, 221–230
 Rio Nazas, 224
 Rio Aguanaval, 224
 San Pedro, 140–148, 149–156
 Walnut Gulch Experimental Watershed, 133, 137, 143
 WCM, *see* Water Cloud Model
 Weather
 agrometeorological assessments, 29–43, 45–50
 maps, 47
 models, 49, 113
 monitoring systems, 52, 55, 67, 116
 National Weather Service (NWS), 54, 56–57, 116, 140, 144
 NEXRAD, 52, 53, 54, 55, 56, 57, 63, 65, 66, 116
 observations, 47, 50
 records, 34, 83
 stations, *see* meteorological stations
 stochastic generation, 32, 111, 113–114, 120, 140
 Texas Weather Connection (TWC), 52
 Weekly Weather Crop Bulletin WWCB, 45–50
 World Meteorological Organization (WMO), 47
 Weeds, 2, 162, 184, 217
 Weekly Weather and Crop Bulletin (WWCB), 45–50
 agrometeorological data, 47
 analytical methods, 447–49
 background, 45–46
 Wheat, 2, 5–6, 9, 33–34, 42–43, 49, 67, 83, 95–96, 114
 Wildfire risk assessment, 53–58
 Wildlife, 224
 Wind erosion, 224
 WMO, *see* World Meteorological Organization
 World Agricultural Outlook Board (WAOB), 45, 47–49
 World Meteorological Organization (WMO), 47
 WQDSS, *see* Water Quality Decision Support System
 WWCB, *see* Weekly Weather and Crop Bulletin
 Yield forecasting, large-area, 13–23, 216
Zea mays L, *see* Maize